Development of Microcantilever Sensors for Cell Studies

Yifan Liu

Submitted for the degree of Doctor of Philosophy

Heriot-Watt University

School of Engineering and Physical Sciences

December 2012

Abstract

Micro- and nano- electromechanical devices such as microcantilevers have paved the way for a large variety of new possibilities, such as the rapid diagnosis of diseases and a high throughput platform for drug discovery. Conventional cell assay methods rely on the addition of reagents, disrupting the measurement, therefore providing only the endpoint data of the cell growth experiment. In addition, these methods are typically slow to provide results and time and cost consuming. Therefore, microcantilever sensors are a great platform to conduct cell culturing experiments for cell culture, viability, proliferation, and cytotoxicity monitoring, providing advantages such as being able to monitor cell kinetics in real time without requiring external reagents, in addition to being low cost and fast, which conventional cell assay methods are unable to provide.

This work aims to develop and test different types of microcantilever biosensors for the detection and monitoring of cell proliferation. This approach will overcome many of the current challenges facing microcantilever biosensors, including but not limited to achieving characteristics such as being low cost, rapid, easy to use, highly sensitive, label-free, multiplexed arrays, etc.

Microcantilever sensor platforms utilizing both a single and scanning optical beam detection methods were developed and incorporated aspects such as temperature control, calibration, and readout schemes. Arrays of up to 16 or 32 microcantilever sensors can be simultaneously measured with integrated microfluidic channels. The effectiveness of these cantilever platforms are demonstrated through multiple studies, including examples of growth induced bending of polyimide cantilevers for simple real-time yeast cell measurements and a microcantilever array for rapid, sensitive, and real-time measurement of nanomaterial toxicity on the C3A human liver cell line. In addition, other techniques for microcantilever arrays and microfluidics will be presented along with demonstrations for the ability for stem cell growth monitoring and pathogen detection.

Acknowledgements

I am deeply appreciative for the support and guidance throughout the research and thesis writing process. First and foremost, I would like to thank my supervisor Dr. Will Shu for his years of guidance, feedback, encouragement, and patience throughout my PhD. I also highly appreciate Prof. Robert Reuben for his highly valuable suggestions and help.

I would also like to thank Mr. Richard Kinsella along with the rest of the technicians in the Mechanical Engineering workshop for their constant advice and fabrication of many of the devices in this thesis. I thank Prof. Michael Schweizer and Dr. Lilian Schweizer for their patience and help for the yeast cell experiments. Also, Dr. Jon Parry and Frank Albri for their constant help during the use of the laser fabrication processes. In addition, I am grateful to Dr. Nilesh Kinase for his assistance during the mammalian cell experiments. In additional, to Mr. Mark Leonard for his help for everything in the clean room.

And other acknowledgements towards Dr. Jesus Valera for the cantilever array interferometry, Mr. Cameron Smith in stores who I've pushed too many times for rush orders, Mr. Vamsi Velidandla at Zeta Instruments for the cantilever array tests, and Helen Bradburn from Roslin Cellab for the stem cell experiments.

Lastly, and as always, I am extremely grateful towards my parents, for their continued support and encouragement throughout my life.

Declaration Statement

ACADEMIC REGISTRY
Research Thesis Submission

Name*:*	Yifan Liu		
School/PGI:	School of Engineering and Physical Sciences		
Version: *(i.e. First, Resubmission, Final)*	Final	Degree Sought (Award **and** Subject area)	PhD Mechanical Engineering

Declaration

In accordance with the appropriate regulations I hereby submit my thesis and I declare that:

1) the thesis embodies the results of my own work and has been composed by myself
2) where appropriate, I have made acknowledgement of the work of others and have made reference to work carried out in collaboration with other persons
3) the thesis is the correct version of the thesis for submission and is the same version as any electronic versions submitted*.
4) my thesis for the award referred to, deposited in the Heriot-Watt University Library, should be made available for loan or photocopying and be available via the Institutional Repository, subject to such conditions as the Librarian may require
5) I understand that as a student of the University I am required to abide by the Regulations of the University and to conform to its discipline.

* *Please note that it is the responsibility of the candidate to ensure that the correct version of the thesis is submitted.*

Signature of Candidate*:*		Date:	

Submission

Submitted By *(name in capitals):*	YIFAN LIU
Signature of Individual Submitting:	
Date Submitted:	

For Completion in the Student Service Centre (SSC)

Received in the SSC by *(name in capitals):*			
Method of Submission *(Handed in to SSC; posted through internal/external mail):*			
E-thesis Submitted (***mandatory for final theses***)			
Signature:		Date:	

Table of Contents

Nomenclature

A	**Cross sectional area of strain gauge**
E	**Young's modulus**
i_A i_B	**Directional currents in a PSD**
k	**Spring constant**
L	**Length of cantilever beam**
L_{PSD}	**Length of PSD**
m	**Suspended mass**
R	**Resistance of strain gauge**
s	**Distance from cantilever tip to PSD**
t	**Thickness of cantilever beam**
v	**Poisson ratio**
Δd	**Cantilever bending**
$\Delta \sigma$	**Surface stress**
ρ	**Resistivity of strain gauges**

Abbreviations

AFM	**Atomic force microscope**
CAD	**Computer aided design**
CCD	**Charge coupled device**
CMRR	**Common mode rejection ratio**
DAQ	**Data acquisition**
DNA	**Deoxyribonucleic acid**
EBEAM	**Electron beam**
LDH	**Lactate dehydrogenase**
MEMS	**Microelectromechanical**
NEMS	**Nanelectromechanical**
NP	**Nanoparticle**
PBS	**Phosphate buffered solution**
PEEK	**Polyether-ether-ketone**
PDMS	**Polydimethylsiloxane**
PID	**Proportional, integral, derivative**
PMMA	**Poly(methyl methacrylate)**
PSA	**Prostate specific antigen**
PSD	**Position sensitive device**
SC	**Synthetic complete**
SEM	**Scanning electron microscope**
SLS	**Standard linear solid**
SPR	**Surface plasmon resonance**
VCSEL	**Vertical cavity surface emitting lasers**
VISA	**Virtual instrument software architechture**
YEPD	**Yeast extract peptone dextrose**

List of Publications

Y. Liu, L. Schweizer, W. Wang, R.L. Reuben, M. Schweizer, W. Shu. Label-free and Real-time Monitoring of Yeast Cell Growth by the Bending of Polymer Microcantilever Biosensors, *Sensors and Actuators B: Chemical,* **178**, 621-626 (2013).

Y. Liu, N. Kanase, V. Stone, W. Shu, Integrated Microfluidics with Microcantilever Biosensor Arrays for Real-time Nanotoxicity Measurements, *Biosensors and Bioelectronics* (Submitted)

W. Wang, **Y. Liu**, W. Shu, Static Mode Microfluidic Cantilever System, *Lab on a Chip* (Submitted)

Y. Liu, J. Valera, W. Wang, A. Moore, W. Shu. High Throughput Alternative for DNA Microarrays, *Biosensors and Bioelectronics* (In submission)

Y. Liu, A. Daniels, W. Wang, W. Shu. Microcantilevers with Integrated Microfluidics for Rapid Disease Diagnosis, *Lab on a Chip* (In submission)

W. Wang, **Y. Liu**, W. Shu. Paper Based Microfluidic Timing Device for Biochemical Reaction Kinetic Assay, *Lab on a Chip* (In submission)

W. Wang, **Y. Liu**, D. Liu, W. Shu. DNA Detected with Double Sided Polymer Based Microcantilevers, *Journal of the American Chemical Society* (In submission)

M. Kersaudy-Kerhoas, F. Amalou, **Y. Liu**, M.P.Y. Desmulliez, W. Shu. A Clamp and Play Plug-less Microfluidic Chip for Full-scale Bioprocess Automation, *The Royal Society of Chemistry* (Accepted 2011)

Y. Liu, W. Wang, W. Shu. Nanomechanical Cantilever Sensors: Theory and Applications, *Nanosensors: Theory and Applications in Industry, Healthcare, and Defense.* (2010)

Y. Liu, T. Lim, J. Ritchie, W. Shu, Tactile Microsensor Arrays for Virtual Reality, *ISAGA 2009 Conference* (2009)

J.D. Shephard, D. Varadam, W. Wang, **Y. Liu**, J.P. Parry, D.P. Hand, W. Shu. Direct Writing Large Arrays of Microcantilevers for bio-MEMS Devices, *Proceedings of LAMP2009 Conference* (2009)

Chapter 1 Introduction

1.1 Background

Micro- and nano- electromechanical (MEMS and NEMS) devices such as microcantilevers have paved the way for a large variety of new possibilities, such as the rapid diagnosis of diseases and a high throughput platform for drug discovery. These devices integrate miniaturized mechanical, electronic, and optical components through microfabrication. Microcantilevers and other devices of a miniature scale can be used for accurate sensing in either gaseous or liquid environments. After it is exposed to chemical vapors or biological molecules, the microcantilever device incur either deflection or changes in its resonant frequency. The ability to rapidly identify biological species such as DNA, bacteria, viruses, proteins, etc. is critical to diagnosis and treatment of many diseases. Even though current methods of detection that use labels such as fluorescent or radioactive tags are highly accurate, using NEMS and MEMS sensors that do not require any labeling will save a large amount of time and cost in analysis.

The majority of current biodetection schemes rely on the identification of certain biological or chemical biomarkers associated to a specific condition or disease such as specific protein molecules and gene sequences. This requires linking the receptor molecules with labeling molecules such as fluorescent markers, radioactive species, enzymes, or quantum dots (Ramachandran *et al*., 2005) that bind to the target biomarker. Labeled detection has many significant downsides in addition to the extra time and cost required. One major concern is that while receptor-analyte bindings are highly specific, non-specific binding to other molecules is always an issue. As new developments continue to find new biomarkers, in many cases the labeling techniques and the labels themselves have to constantly be updated, and current techniques already have problems labeling extremely small molecules (Cooper *et al*., 2003). Another concern is that through the use of labels, the labeled molecules may be affected, such as experiencing reduced mobility or misfolding, in addition to uncertain labeling efficiency and often being incompatible with live cell studies (Perkel, 2009). In addition, label-free detection allows for exceptionally sensitive devices and high levels of multiplexing and can be integrated with highly specific biomarkers for selective detection, without compromising sensitivity (Shu *et al*., 2008, Arntz *et al*., 2003).

Advances in this field have created sensors that use the transduction of mechanical energy, such as microcantilevers with tips in an atomic force microscope imaging (AFM, Binnig *et al*., 1986). The two methods for operation are either static or dynamic mode. In static mode, when the tip comes in contact with a surface, its deflection in response to differences in topography can be precisely measured. On the other hand, in dynamic mode, the cantilever tip becomes resonantly excited and is then measured for resonant frequency changes when the interaction between the tip and sample surface changes. The main difference between an AFM and other cantilever applications, such as the optical deflection method that will be explained later, is that the AFM requires the tip to come into physical contact with the surface of the analyte. Many new developments have since demonstrated the versatility of these techniques.

Microcantilever sensors have been shown to exhibit similar physical attributes to those in an AFM. Sensing using a microcantilever is usually performed by measuring the amount of deflection in the cantilever beam due to forces created by either mass loading or differential surface stresses. These sensors are able to be microfabricated into different shapes and sizes, along with the ability to form large arrays, which gives rise to a wide range of applications.

Understanding cell proliferation during the life cycle of a cell in response to various stimuli is very important for many biomedical applications including infectious diseases, drug discovery/testing, and public health. Conventional methods to monitor cell viability utilize optical, fluorescent, or electrical techniques; while cell viability and cytotoxicity assays are typically performed through chemically labeled assays such as MTT (3-(4,5-Dimethylthiazol-2-yl)-2,5-diphenyltetrazolium bromide, Lewinski *et al*., 2008) and MTS (3-(4,5-dimethylthiazol-2-yl)-5-(3-carboxymethoxyphenyl)-2-(4-sulfophenyl)-2H-tetrazolium, Xu *et al*., 2004), Alamar Blue, etc. These cell cultures and viability assays assess the cytotoxicity of any substance, taking advantage of in-vitro assessments of the substance to determine if it inhibits cell growth. In particular, these experiments are currently widely used for drug testing and/or discovery, because cells produce more representative responses to drugs than molecular assays and are a better method than animal testing (El-Ali *et al*., 2006, Yang *et al*., 2008). Conventional cell assay methods rely on the addition of reagents or labelling, disrupting the measurement,

therefore providing only the endpoint data of the cell growth experiment. In addition, these methods are typically slow to provide results and time and cost consuming. Also, microcantilever sensors haves the ability to be rapidly and potentially low-cost (after the initial equipment costs such as coating chambers and lasers). Therefore, microcantilever sensors are a great platform to conduct cell culturing experiments for cell culture, viability, proliferation, and cytotoxicity monitoring, providing advantages such as being able to monitor cell kinetics in real time without requiring external reagents, in addition to being low cost and fast, which conventional cell assay methods are unable to provide.

1.2 Aim and objectives

The overall aim of this thesis is to develop and test different types of microcantilever biosensors for the detection and monitoring of cell proliferation. This approach will overcome many of the current challenges facing microcantilever biosensors, including but not limited to achieving characteristics such as being low cost, rapid, easy to use, highly sensitive, label-free, multiplexed arrays, etc.

This work has 4 main research objectives:

- To develop microcantilever biosensors for probing cell proliferation, cell-drug interactions, and cell-nanoparticle interactions.

- To investigate whether cell growth can be monitored in real-time on the surface of polymer based microcantilever sensors.

- To develop cantilever arrays for large scale assays, including portable sensor arrays and multiplexed readout schemes.

- To implement and carry out experimental work and validate the microcantilever biosensor systems.

1.3 Structure of the thesis

This thesis will be presented in 8 chapters:

Chapter 1 presents the background of this thesis and explains the motivation and objectives of the work.

Chapter 2 summarizes the fundamentals of microcantilever biosensor technologies and the current methods developed in the field. It also presents several remaining challenges in microcantilever research, including but not limited to, the challenges that current biosensor platforms face.

Chapter 3 describes the methodology and experimental details of all the projects. This will include aspects of design, calibration, and initial testing phases.

Chapter 4 reports the first example of growth-induced bending of polymer cantilevers for simple real-time cell growth measurement. Saccharomyces cerevisiae yeast cells were used as a model system to study the cell growth on microcantilever sensors.

Chapter 5 presents a whole cell based polymer microcantilever biosensor array for rapid, sensitive, and real-time measurement of nanomaterial toxicity on the C3A human liver cell line.

Chapter 6 summarizes the readout techniques of microcantilever biosensor arrays, including work done in designing and fabricating the cantilever array chips.

Chapter 7 includes the work in building autonomous microfluidic systems with integrated microfluidic pumps, and the construction of portable cantilever array systems using electronic readout chips. This will include analysis of results after experiments in stem cell growth monitoring and pathogen detection.

Chapter 8 draws conclusions resulting from this research and recommendations are made for future work.

1.4 References

Arntz, Y., Seelig, J.D., Lang, H.P., Zhang, J., Hunziker, P., Ramseyer, J.P., Meyer, E., Hegner, M., Gerber, C., Label-free protein assay based on a nanomechanical cantilever array. *Nanotechnology*., **14**, 86-90 (2003).

Binnig, G., Quate, C.F., Gerber, C., Atomic Force Microscope. *Phys. Rev. Lett*. **56(9)**, 930-933 (1986).

Cooper, M.A., Label-free screening of bio-molecular interactions. *Anal. Bioanal. Chem.* **377**, 834-842 (2003).

El-Ali, J., Sorger, P.K., Jensen, K.F., Cells on chips. *Nature*. **442**, 403-411 (2006).

Elrick, M.M., Walgren, J.L., Mitchell, M.D., Thompson, D.C., Proteomics:recent applications and new technologies. *Bas. Clin. Pharmacol. Toxicol*. **98**, 432-441 (2006).

Perkel, J.M., Who needs labels? Macromolecular interactions sans labels. *Science,* **19**, 1561-1565 (2009).

Ramachandran, N., Larson, D.N., Stark, P.R.H., Hainsworth, E., LaBaer J., Emergin tools for real-time label-free detection of interactions on functional protein microarrays. *FEBS J.* **272**, 5412-5425 (2005).

Shu, W., Laurenson, S., Knowles, T.P.J., Ferrigno, P.K., Seshia, A.A., Highly specific label-free protein detection from lysed cells using internally referenced microcantilever sensors. *Biosensors and Bioelectronics*, **24**, 233-237 (2008).

Yang, S.T., Zhang, X., Wen, Y., Microbioreactors for high-throughput cytotoxicity assays. *Curr. Opin. Drug. Discov. Devel.* **11**, 111-127 (2008).

Chapter 2 Microcantilever Sensors: Theory and Applications

2.1 Introduction

Microcantilever-based sensors offer many applications for a wide range of novel sensors in the detection of various analytes in a liquid, gaseous, or vacuum media. These sensors offer high sensitivity, low cost, fast response, and high specificity without the need for pre-analysis labeling. Derived from atomic force microscopy (AFM) (Binnig *et al*., 1986), which is capable of imaging a surface with nano-scale resolution by measuring the tiny force between a sharp tip of a suspending cantilever and the surface, free-standing microcantilever sensors do not require a sharp tip or a sample surface; instead, it is used to sense a biochemical reaction taking place on the cantilever surface by measuring its nanomechanical response (Turner *et al*., 1989). One detection principle is to directly translate molecular interactions on one side of a cantilever surface into mechanical bending. The cantilever bending is modulated by the surface stress arising as a result of specific interactions between molecules immobilized on the cantilever surface with those present in the analyte. On the other hand, molecular adsorption on cantilever surfaces can also be detected by monitoring the resonant frequency changes of cantilever sensors induced by the mass change. Both of the responses can be precisely detected using either optical or electronic methods that are routinely used for AFM imaging technique. In this chapter, an extensive discussion on modes of operation, fabrication, signal readout techniques, and microfluidics will be presented, followed by a collection of recent progress and applications of such microcantilever sensors for biosensing applications.

The major advantages of microcantilevers sensors include label-free detection, small size, rapid response, high sensitivity, and the ability for high-throughput and multiplexed detection of various substances. Microcantilever sensors detect molecular binding on the cantilever surface through its nanomechanical motion, without the need for fluorescent or radioactive labeling. The signal transduction of microcantilever sensors is rapid because the small-scale devices have relatively high mechanical self-resonance frequencies in solution. Hence, the microcantilever platform is well suited to real-time monitoring of biomolecular interaction events on a sub-millisecond timescale (Krecmer *et al*., 1997). In addition, the cantilevers are constructed using standard batch-

compatible microfabrication processes and are easily scalable into arrays to allow high-throughput measurements for multiple target analytes.

2.2 Operation Principles

Microcantilever sensors can be operated either in static mode (Rudiger *et al*., 1997) or in dynamic mode (Thundat *et al*., 1994). As illustrated in Figure 2-1, in the static mode, molecular interactions on the cantilever surface are translated into a cantilever bending as a result of changes in the surface stress. In dynamic mode, the change of resonant frequency of the cantilever is monitored.

Figure 2-1: The static mode (left) and the dynamic mode (right) of a microcantilever sensor.

Dynamic mode operation allows direct measurements of molecular adsorption on the cantilever surfaces by providing quantitative analysis of mass changes. It is a highly sensitive approach where the detection of a single cell (Ilic *et al*., 2000, 2001) and a single DNA molecule (Ilic *et al*., 2005) has been demonstrated in air and vacuum environments respectively. However, due to the damping effect, dynamic mode measurements have poor sensitivity operating in liquid environments and hence limit its applications for many biosensing applications. Dynamic mode devices can be shown by the microcantilever fundamental resonance frequency, f_0, by:

$$f_0 = \frac{1}{2\pi}\sqrt{\frac{k}{m}} \qquad (2.1)$$

Where k is the sprint constant and m is the suspended mass. When a foreign mass Δm is added onto the original mass m on the cantilever beam, the frequency change can be shown by:

$$\Delta f = f - f_0 = -\frac{1}{2}\frac{\Delta m}{m} f_0 \qquad (2.2)$$

Therefore, knowing the resonant frequency of the sensor before and after a particular analyte binding allows the calculation of the amount or mass of the bound analyte. An increase in resonated mass produces a negative resonant frequency shift, while a decrease in mass causes a positive frequency shift. While the previous equations are a reasonable estimate of the resonance frequency, it can only be used in situations where the cantilever is weakly dampened. For increased accuracy of calculations, the dissipation of resonant energies must be taken into consideration.

Static mode operation meanwhile, measures the mechanical bending of a cantilever beam caused by a surface stress change. Molecular interactions on one side of a microcantilever surface will induce the surface stress change. The relationship between the bending and the surface stress change can be related using the Stoney equation (Stoney 1909):

$$\Delta z = \frac{3(1-\nu)L^2}{Et^2}\Delta\sigma \qquad (2.3)$$

where Δz is the cantilever bending amplitude, $\Delta\sigma$ is the surface stress change ν is the Poisson's ratio, E is the Young's modulus, and L and t are the length and the thickness of the cantilever respectively. It is clear from this equation that, for a given cantilever with fixed mechanical (ν and E) and geometrical (L and t) values, the cantilever bending is proportional to the surface stress change. This means the performance or the sensitivity of the sensor is determined by the mechanical and geometrical properties of the cantilever itself. For example, the sensitivity of the sensor or the bending response to a given biochemical reaction or the surface stress change is proportional to the square of cantilever length (L^2), inversely proportional to the Young's modulus *(E)*, and the square of cantilever thickness (t^2). Consequently, by increasing the cantilever length, reducing the Young's modulus (making softer cantilevers, e.g. using polymers), and fabricating thinner cantilevers will lead to enhanced sensitivity. However, all these efforts to increase sensitivity are constrained by the limits of compromising mechanical stability of the device as well as new challenges for fabricating tiny suspending cantilever beams without significantly changing the original shape of the cantilever.

2.3 Preparation of Microcantilever Sensors

2.3.1 Device fabrication

Currently, most of the commercially available microcantilevers are made of silicon, silicon nitride, and silicon oxide, which are routinely micro-fabricated for use in AFMs. Polymer microcantilevers have also been fabricated in order to exploit its lower Young's modulus and hence higher sensitivity (Calleja *et al*., 2003, 2005). In general, microcantilever sensors are fabricated in clean rooms and require multiple steps of depositing and etching processes. A typical MEMS fabrication procedure of a silicon microcantilever sensor is illustrated in Figure 2-2, which involves either bulk micromachining or surface micromachining processes (Waggoner *et al*., 2007). The bulk micromachining creates the suspending cantilever beam by etching away the bulk of the silicon wafer (Figure 2-2a), while the surface micromachining makes use of a sacrificial layer deposited on the wafer surface and releases the cantilever structures by selectively etching away the sacrificial layer from the surface (Figure 2-2b).

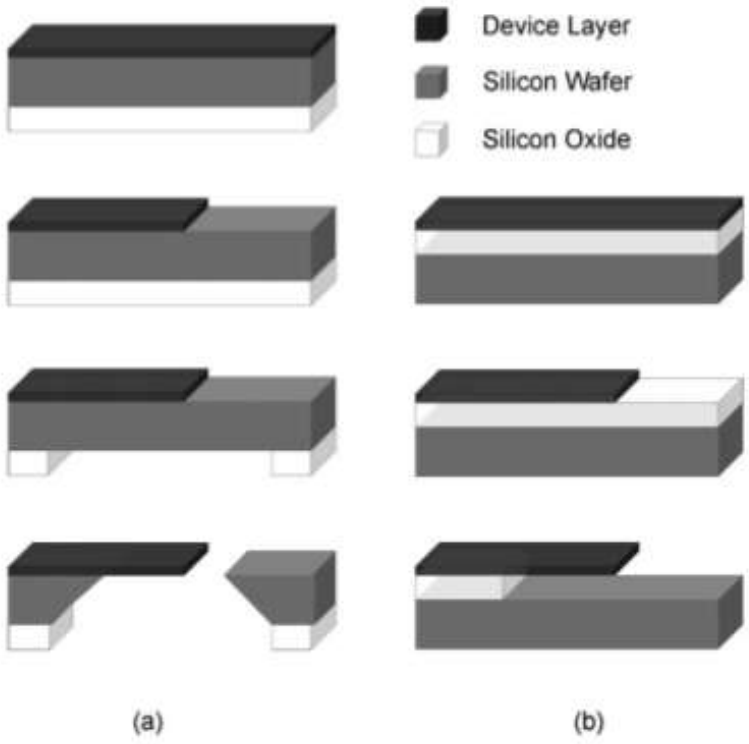

Figure 2-2: Schematic illustration of (a) bulk and (b) surface micromachining processing steps for microcantilever devices. (Figure adapted from Waggoner *et al*., 2007)

A typical silicon microcantilever sensor array fabricated by IBM Zurich Research Lab in Switzerland (Baller *et al*., 2000) has eight rectangular shape levels, each of 500 μm length, 100 μm width, and 1 μm thickness (Figure 2-3). These dimensions give rise to a low spring constant of about 0.02 N/m, with a resonant frequency of 4 kHz in air and a correspondingly fast millisecond time response (Krecmer *et al*., 1997).

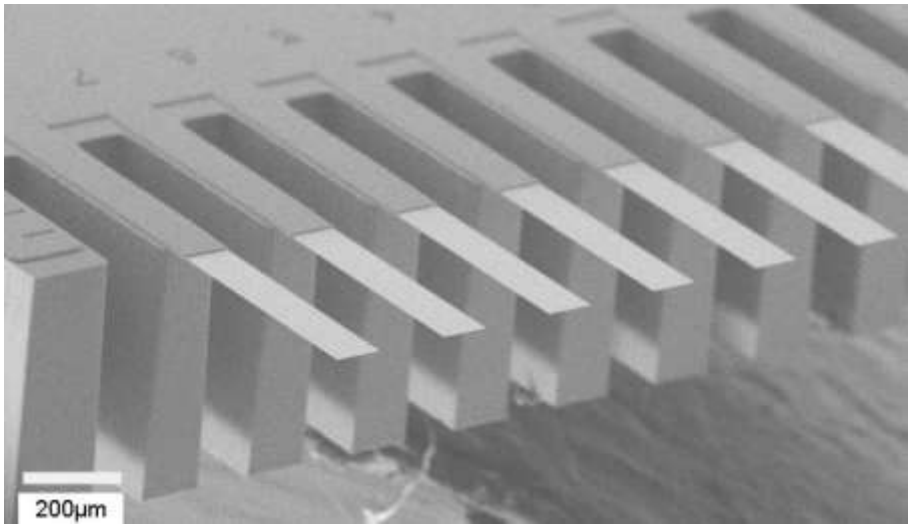

Figure 2-3: SEM image of a microcantilever sensor array. (Figure adapted from Baller *et al*., 2000)

Alternatively, direct fabrication of microcantilevers can be done using laser micromachining techniques. Both polymeric (Zhang *et al*., 2004, Shephard *et al*., 2009) and metallic (Wang *et al*., 2007) microcantilevers were fabricated using lasers of different power and wavelengths. The main advantage of the laser micromachining method is its fast speed and low cost, enabling rapid prototyping for microcantilever sensor designs.

2.3.2 Surface Functionalization Techniques

Microcantilever sensor arrays enable multiple reactions to be probed simultaneously via monitoring the bending of each cantilever beam at the same time. To probe a specific biochemical reaction, the surface of each cantilever needs to be coated or functionalized with a layer of specific chemical or biological molecules. The quality of the functionalization will directly influence the performance of the sensor signal. As the cantilever sensors are fabricated using MEMS techniques, any pre-existing functionalization prior to the cantilever fabrication will not be able to survive the harsh

depositing and etching processes. Therefore the surface functionalization of cantilevers is normally undertaken after the sensor is fabricated. For static or free-standing bending mode, the functional layer has to be coated on one side of the cantilever surface only otherwise the surface stress changes generated by both sides of one cantilever with the same coatings will cancel each other and lead to no bending signal. For this reason, one side of the cantilever surface is first coated with a chemically distinct layer from the other side. For example, a layer of 20nm gold (with 2nm of Cr as adhesive layer) is sufficient to create a uniform metallic surface on one side of a silicon cantilever. The gold surface is usually chosen because it can form a chemical bond with the sulfur group to facilitate further functionalization by thiolated molecules (e.g. thiolated DNA or proteins).

One of the main challenges in microcantilever biosensor research is to reliably and efficiently functionalize each side by coating microcantilever beams on an array with different bio/chemical molecules. One method to achieve this is through microcapillaries (McKendry *et al*., 2002, Bietsch *et al*., 2004). Microcapillaries are relatively simple to use and suitable for functionalizing cantilevers in small quantities. In addition, the incubation time is easily controlled for functionalization using microcapillaries. Figure 2-4 shows the setup for functionalizing individual cantilevers with different chemicals (Shu, 2008). Micromanipulators with translational stages precisely position a microcapillary tube filled with chemicals over a cantilever sensor. The capillary tubing will let the cantilever sensor insert inside it and bring it in contact with the chemical solution to incubate for a certain period of time for functionalization.

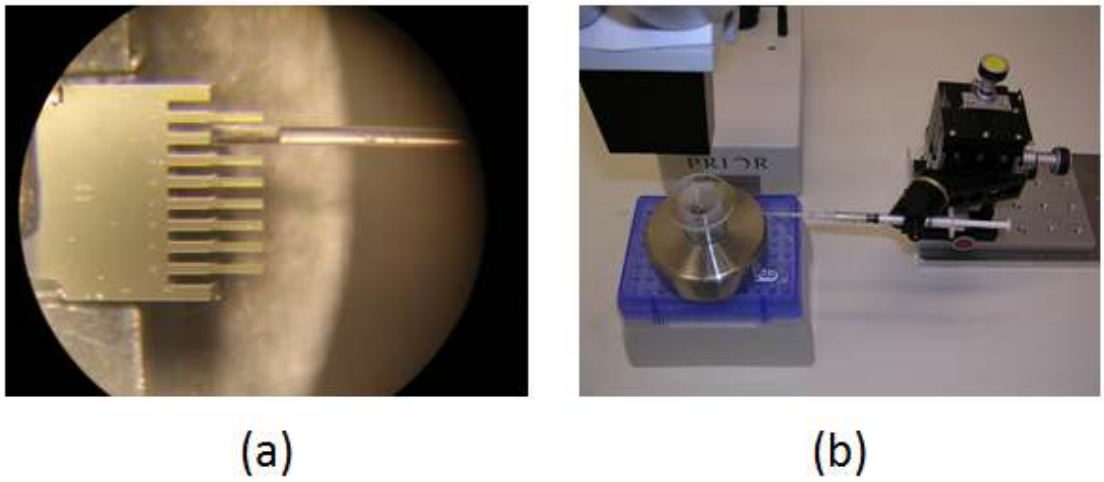

Figure 2-4: Capillary functionalization: (a) Optical image of microcapillary tube on a microcantilever sensor for functionalization. (b) Overview of the stup including microscope, micromanipulator with syringe, and cantilever holder. (Figure adapted from Shu, 2008)

In Figure 2-4a, there is an air bubble towards the end of capillary tubing, which is a common problem during functionalization. One way to remove it and allow the chemical solution to come into direct contact with the sensor is to carefully push the syringe connected to the microcapillary and observe the air bubble being driven out under the microscope. If the force of pushing the syringe is too strong, the chemical solution may be pushed all the way out of the capillary tip and flow to the substrate of the cantilever, causing cross-contamination of other cantilever sensors. To avoid the cross-contamination, an array of capillaries filled with different chemical solutions can be used to simultaneously functionalize the cantilever array as shown in Figure 2-5.

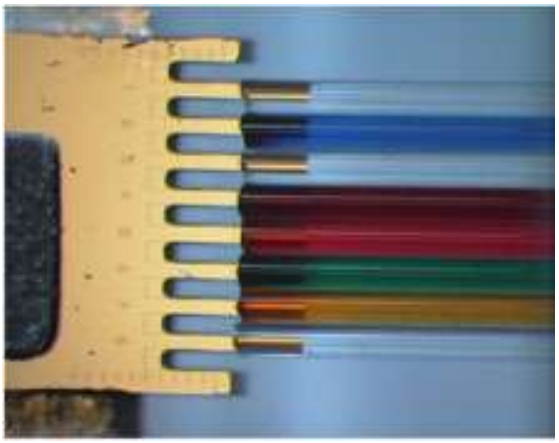

Figure 2-5: Functionalization of a cantilever array using an array of glass microcapillaries. (Figure adapted from Bietsch *et al.*, 2004)

Another efficient method of functionalizing large microcantilever array is to use a chemical inkjet printing technique (Bietsch *et al*., 2004a, 2004b), which can be used to fabricate high density DNA and protein microarray. The functionalization of self-assembled monolayers, polymer solutions, and DNA samples has been demonstrated with comparable performance on cantilever sensors. Using this method, the microcantilever sensors can be batch functionalized at the wafer level. Aside from its speed, inkjet printing has an additional advantage over the capillary method that only one side of a cantilever will be coated preventing the contamination of the backside. The main challenge for the inkjet printing method, however, is to reproducibly functionalize the flexible suspended beams with often a curved shape. The need to precisely align the nozzle for the 3-dimensional and dynamic cantilever structures presents new challenges for its future development.

2.4 Readout Techniques

Readout techniques are a vital aspect of any cantilever system. Real-time measurements and high accuracy in the sub-nanometer range is required. There are many techniques available for reading microcantilever sensor outputs such as optical, piezoresistive, piezoelectric, capacitive, and electron tunneling. Any of these techniques result in sufficient accuracy that can be used for different purposes, each with its own advantages and disadvantages. But the most commonly used readout techniques are the optical and piezoresistive/piezoelectric methods.

2.4.1 Optical

Optical readout techniques are one of the most common readout techniques for the detection of bending in cantilever beams. A laser diode is focused on the very tip of the beam, which effectively acts as a mirror from the gold coating on the surface. The reflected laser beam is reflected and read by a position sensitive detector (PSD). This method is shown in Figure 2-6.

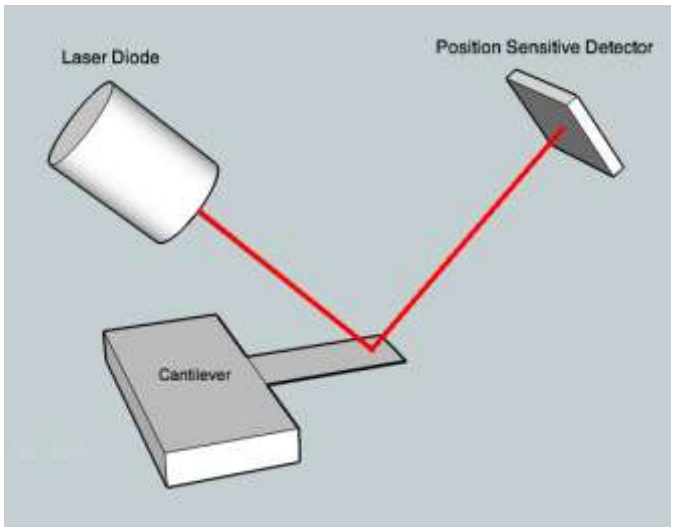

Figure 2-6: Optical detection method to detect deflection of microcantilever sensors.

In order to detect the deflection of the cantilever beam, it requires calibrating and a reading of the position of the laser reflection in the PSD as the cantilever deflects. Different electronics and/or calculations are needed to calculate physical bending in terms of nano- or micro- meters.

An advantage of the optical detection method is that it allows detection to sub-nanometer ranges (Waggoner *et al.*, 2007). Other advantages include not having electrical connections to the microcantilever, linear response, ease of use/setup, and reliability. As with all readout schemes, there are also disadvantages. Having an optical detection system with a liquid environment requires an additional precise temperature control system for the components. The laser diode, cantilever, and PSD parameters will all vary with temperature. But the main disadvantage is that this method requires external devices that require precise and continuous alignment; therefore, portability suffers and costs are increased. In addition, optical scheme readouts are limited to clear and low opacity liquids, which reduces the laser reflection or changes the liquid's

refractive index. Lastly, it is difficult to implement arrays of cantilevers to be read out by the optical detection method. It would either require multiple lasers or a sequential on-off switching solution. Even with its disadvantages, the optical readout method is one of the best and most common detection schemes, primarily because of its significant advantages.

2.4.2 Piezoresistive / Piezoelectric

Piezoresistive readout methods work by detecting changes in the resistivity of the material of the cantilever, as a stress is applied (Baselt *et al*., 1997, Minne *et al*., 1995, Tortonese *et al*., 1993, Yu *et al*., 2002). When a piezoresistive material such as doped silicon incurs a strain, its resistivity changes and can then be measured by external electronics. A DC biased and balanced Wheatstone bridge with identical resistors is generally used to measure this resistance change as shown in Figure 2-7. One of the main advantages of piezoresistive readouts is that the readout electronics can be integrated onto the same chip as the cantilever beam; therefore, arrays of cantilevers are easier to fabricate than with the optical deflection method. Also, the piezoresistive method works in liquid media of any opacity. The main disadvantage is that there is more built-in noise, which negatively affects the sensitivity and resolution of the detection scheme (Yu *et al*., 2002). Furthermore, because of the electrical connections, care needs to be taken to isolate them from any liquid media. Fabrication of the cantilever devices can also be a challenge, since there are technological limits when attempting to fabricate thin, yet sensitive cantilevers, and which incorporate built-in electronics.

Piezoelectric readout methods require cantilevers to be coated with a piezoelectric material, such as zinc oxide. Transient charges are produced due to a piezoelectric effect when the cantilever beam deflects from mass loading or surface stresses. The disadvantages of a piezoelectric readout method are similar to that of the piezoresistive, in that they require electrical connections to function. Readout signal values are also very limited, and require the piezoelectric material to be very thick, which reduces the sensitivity of the cantilever beam significantly.

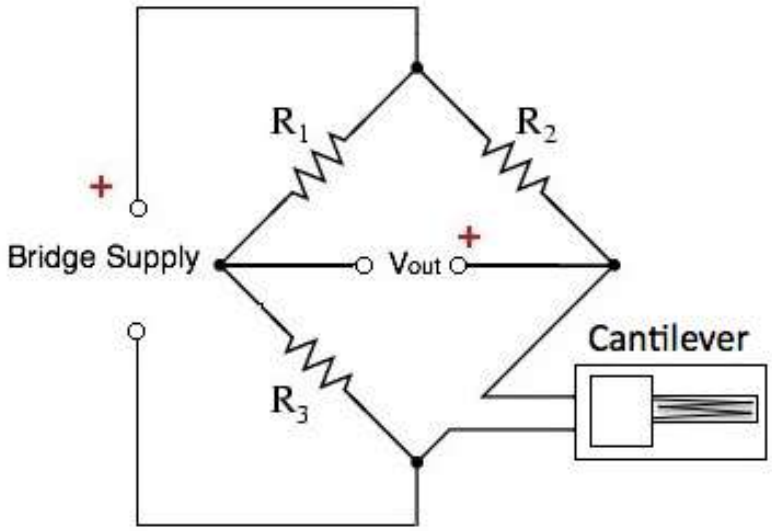

Figure 2-7: Quarter-bridge Wheatstone bridge circuit.

2.4.3 Sensor Arrays

A major advantage of microcantilever sensors is that they can be made into arrays for more accurate detection or simultaneous detection of multiple analytes. However, simultaneous readout of the signal from an array of cantilever sensors is challenging. Lang *et al*. (1998) created a setup employing an optical beam bending technique for simultaneous readout of an array of eight cantilever beams. The novelty of this setup involves the use of fiber optical ribbons which transfer the light from LEDs, as well as transferring the reflection from the cantilever beam into an array of detectors. The array of optical beams is switched on sequentially while the bending signals of the cantilevers are recorded. Up to eight biochemical reactions can be monitored simultaneously. Cantilever array systems allow for few or many of the cantilevers to be used as reference sensors, to minimize environmental noise. However, the main disadvantages of this approach include the bulky optical instrument and the requirement for precise alignment of the laser beams onto each cantilever sensor, limiting portable applications. Other optical readout methods including phase-shifting interferometric microscopy (Kelling *et al*., 2009), interferometric profiling (Reed *et al*, 2009), and on-chip optical waveguides (Lechuga *et al*., 2006).

2.5 Biosensing Applications

Over the last decade, microcantilever biosensors have found uses on probing a wide range of biological interactions and systems in both liquid and solid interfaces. The ability to sense real-time binding events as well as conformational changes of biomolecules in a label-free fashion makes the microcantilever sensor attractive, not only for biosensing applications but also as a potentially powerful tool in understanding the dynamics of biomolecular interactions.

Fritz *et al*. (2008) first demonstrated the use of microcantilever sensors for DNA hybridization reactions. An array of microcantilevers was used and the bending of each cantilever was monitored optically (Lang *et al*., 1998). Synthetic 5'thio-modified oligonucleotides with different base sequences were covalently immobilized on the gold-coated side of each cantilever as illustrated in Figure 2-8. The binding of DNA molecules in liquid onto the complementary oligo coated cantilever surface was found to induce a surface stress change and a measurable bending signal of the cantilever sensor. By measuring the differential bending signal or comparing the signal difference between cantilever sensors coated with differently sequenced oligos, a single mismatch between two 12-mer DNA molecules can be detected. This discovery opens up new applications of microcantilevers for label-free detection of single nucleotide polymorphisms (SNPs), which is important for applications in genomics research and early disease diagnosis. Hansen *et al.* (2001) revealed that the magnitude and even the direction of cantilever bending were dependent on the number and location of mismatches of the DNA. It was shown that the bending was larger for DNA targets having two mismatches than that of having one mismatch due to the increase in the repulsion forces as the mismatch number increases. Using microcantilever sensor arrays, McKendry *et al*. (2002) further showed that ultrasensitive DNA hybridization measurements can be performed to detect DNA in the order of femtomoles of DNA on a cantilever for the concentration of 75 nM in solution. Extensive research efforts on improving the sensitivity and performance for DNA hybridization detection has led to the development of microcantilever sensors using new and improved optical (Yue *et al*., 2004, Alvarez *et al*., 2005, Helm *et al*., 2005, Lechuga *et al*., 2006, Reed *et al*., 2009, Kelling *et al*., 2009) and electronic (Shekhawat *et al*., 2006, Hammelgaard *et al*., 2006) readout techniques, cantilever materials (Calleja *et al*., 2005, 2006), and receptors (Peng *et al*., 2007, Cha *et al*., 2009, Su *et al*., 2003).

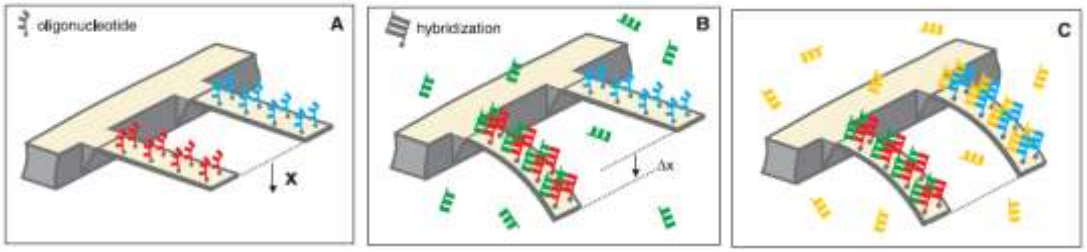

Figure 2-8: Schematic of DNA hybridization experiments with microcantilever sensor arrays. Each cantilever is functionalized with a different oligonucleotide base. (a) Initial functionalization with no cantilever deflection. (b) After exposure to the complementary oligonucleotide (green), hybridization occurs with the cantilever that has the matching oligonucleotide (red), causing a deflection in the cantilever. (c) After exposure to a second complementary oligonucleotide (yellow), hybridization occurs with the complementary sequence (blue), and the second cantilever shows deflection. (Figure adapted from Fritz *et al.*, 2000)

For probing DNA hybridization reactions, the bending of the microcantilever sensors were found to be sensitive to a range of parameters including the change of DNA entropy, ionic strength of the solution, the length of oligo, surface packing density, and hydration forces (Wu *et al*., 2001, Alvarez *et al*., 2004, Hagan *et al*., 2002, Martens *et al*., 2008). Many of the parameters can be altered when the conformation of DNA molecules changes. Harnessing this effect, microcantilever sensor arrays have been used to probe nano-scale DNA conformational changes triggered by pH changes (Shu *et al*., 2005). By direct tethering a non-classical i-motif oligos on cantilever surfaces (Liu *et al*., 2003), the well-defined conformational changes of the DNA motor molecules between the open to close states can be mechanically probed in real time without using any fluorescent tags. The surface stress changes associated with the conformational changes was found to be much larger than that of DNA hybridization (Shu *et al*., 2005), suggesting that conformation changes of ligand molecules tethered microcantilevers can be harnessed to enhance the bending signal of microcantilever sensors. Similar effects have been found in synthetic polymer brushes grafted on microcantilever sensors where the conformational changes of the polyelectrolyte polymer brushes induced large microcantilever bending triggered by external stimuli (Nehal *et al*., 2006, Valiaev *et al*., 2007, Zhou *et al*., 2006, 2008).

The research of microcantilever sensors for label-free protein detection has been driven by the potential applications for rapid identification of disease biomarkers and the creation of portable and low-cost point of care devices. Moulin *et al*. (1999) reported the non-specific adsorption of proteins on cantilever surfaces and observed the adsorption of different types of proteins can bend the microcantilever in different directions. The observed surface stress changes were slow processes and therefore attributed to the conformational changes of proteins on gold coated surfaces. By coating one side of the microcantilever with a protein recognition layer, specific antigen-antibody binding can be monitored for disease biomarkers. The fundamental study of the activity, stability, lifetime, and re-usability of monoclonal antibodies to myoglobin covalently functionalized onto microcantilever surfaces was carried out by Grogan *et al*. (2002), and found the immobilized antibody layer can remain active and relatively stable for up to 7 weeks. This study shows that microcantilever based biosensors has great potential applications to be used as label-free immunoassays. Arntz *et al*. (2003) reported a multiple antibody coated cantilever microarray to detect multiple proteins in parallel. The label-free detection of two cardiac biomarker proteins (creatin kinase and myoglobin) was demonstrated against unspecific proteins background in buffer solution. The reported sensitivity of the myoglobin detection was shown to be less than 20 μg mL^{-1} or 1 μM. The same group (Bachmann *et al*., 2005) later showed that the sensitivity of protein detection can be significantly enhanced to detect a concentration as low as 1 nM by using smaller antibody receptor (e.g. protein fragments) coated on microcantilever surfaces. The enhanced sensitivity was attributed to improved orientation of the surface bound antibodies. One in-depth study of the antibody/antigen interaction on microcantilevers was carried out by studying biotin-streptavidin binding reactions and comparing the surface stress changes generated by the binding of streptavidin onto biotin ligands with different linker structures (Shu *et al*., 2007). The study showed the bending signal or the sensitivity of the microcantilever sensors was dependent on the thickness of the biotin monolayer, pointing to the influence of electro-static interactions between the bound proteins and the gold coated microcantilever surface on the surface stress changes. In order for microcantilever biosensors to be used as immunoassays in a clinically relevant setting, the sensor platform should not only be sensitive enough to detect clinically relevant protein concentrations, but also to be able to detect specific antibody-antigen interactions against complex biological environments (i.e. blood). Wu *et al*. (2001) first investigated the specific detection of

two forms of prostate-specific antigen (PSA), biomarker associated with prostate cancer using microcantilever sensors functionalized with anti-PSA antibodies. The sensor platform was able to detect a wide range of concentrations of PSA from 0.2 ng/mL to 60 mg/mL in a background of a mixture of blood proteins (human serum albumin and human plasminogen) at 1 mg/mL as shown in Figure 2-9.

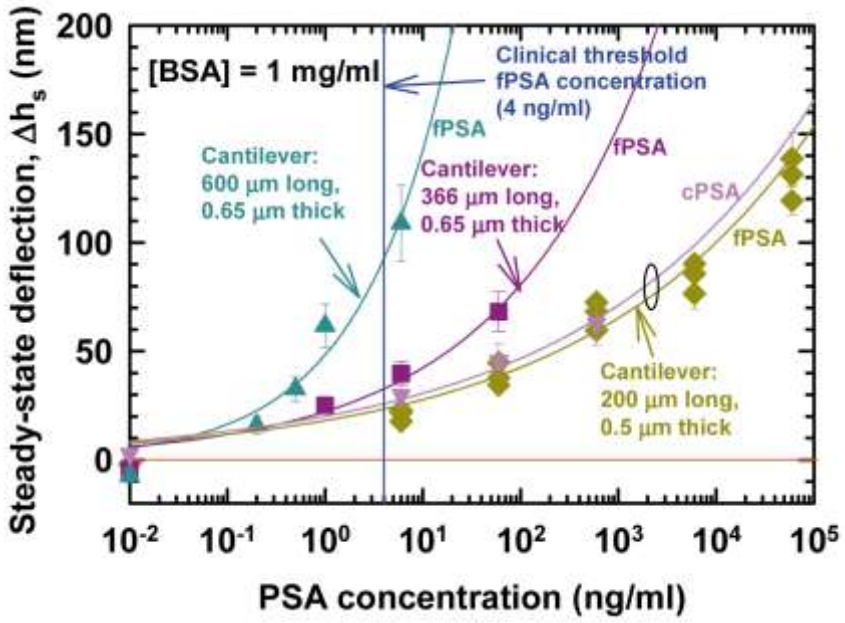

Figure 2-9: Steady-state cantilever deflections as a function of fPSA and cPSA for different cantilever geometries. Longer cantilevers produce larger bendings for the same concentration, essentially translating into higher sensitivity. (Figure adapted from Wu *et al*., 2001)

Most of the specific protein detection using microcantilever sensors has relied on the use of antibodies. In contract, the use of artificial protein binding ligands based on DNA (Savran *et al*., 2004) and peptide (Shu *et al*., 2008) aptamers were also reported. Specific detection of a protein biomarker (CDK2 at 80 ng/mL) was achieved in a complex biological environment (e.g. cell lysate) (Shu *et al*., 2008). In addition to protein binding, the aggregation of protein molecules on the surface to form insoluble protein fibrils was first studied using microcantilever sensors by Knowles *et al*. (2008). The results from the self-referenced single cantilever were found consistent with that of multiple cantilever arrays. In contrast to the relatively short time constant of protein binding reaction on surfaces (<1 hr.), the formation of protein aggregates continuously bend the microcantilevers for over 18 hrs. Ndieyira *et al*. (2008) presented a novel

approach for investigating the mechanisms of drug-target binding interactions on multiple cantilever arrays. The group demonstrated the first quantitative differential nanomechanical investigation of the antibiotic drug vancomycin with mucopeptide analogues present in the "hospital superbugs". The binding strength between the vancomycin antibiotic and the mucopeptide analogues covalently functionalized on cantilever surfaces can be determined by measuring the differential deflection as shown in Figure 2-10. This study opens up microcantilever biosensors for investigating drug-target interactions, and could speed up the discovery of new antibiotics.

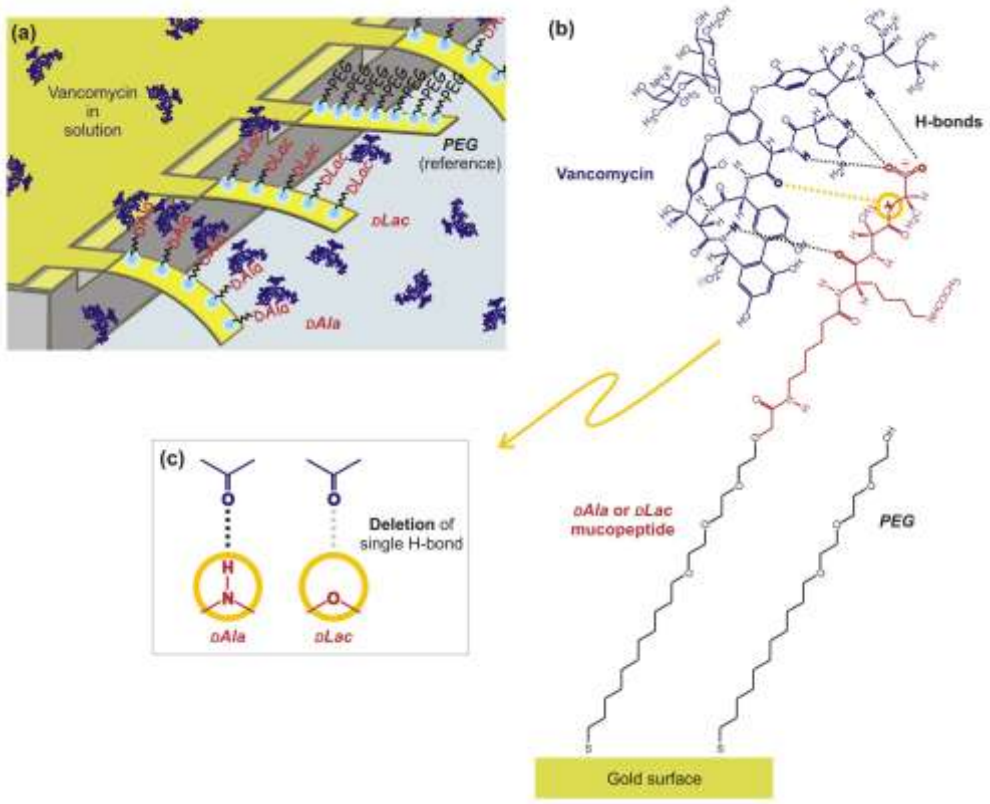

Figure 2-10: Detection of vancomycin-mucopeptide interactions on cantilever arrays. (a) Schematic diagram to show cantilevers coated with DAla (vancomycin sensitive), DLac (vancomycin resistant) or PEG (reference) alkanethiol SAMs. (b) The chemical binding interaction between vancomycin and DAla. (c) The deletion of a single H bond in mutated DLac mucopeptides gives rise to drug resistance. The binding pocket of vancomycin is represented schematically and the grey dotted line represents the deleted hydrogen bond and electrostatic repulsion between the oxygen lone pairs of electrons. (Figure adapted from Ndieyira *et al.*, 2008)

Microcantilever sensors have also been demonstrated for the whole-cell detection of micro-organisms. The rapid and sensitive detection of pathogenic bacteria at the point of care is extremely important. Antibodies specific to a certain bacteria or cells are coated on the surface of the microcantilevers, allowing for extremely high selectivity and specific binding to certain strains of pathogens. So far, most of the pathogen detection has been demonstrated using dynamic mode by monitoring frequency changes of microcantilevers associated with the mass loading (Ilic *et al*., 2000, Gupta *et al*., 2004, Gfeller *et al*., 2005, Nugaeva *et al*., 2007). Due to the damping effect and therefore the reduction of the quality factor in liquid environments, most of the studies were performed in air or humid air environments. This problem can be overcome by monitoring the higher modes of vibration instead of the fundamental mode, enhancing the sensitivity of microcantilever sensors for at least two orders of magnitude (Ghatkesar *et al*., 2007, Braun *et al*., 2009). Alternatively, a millimeter-sized piezoelectric cantilever can be used to probe cell binding with high sensitivity (Yi *et al*., 2003, Campbell *et al*., 2007, Maraldo *et al*., 2007a, 2007b). On the other hand, a novel approach using microcantilevers with embedded micro-channels was first demonstrated by Burg *et al*. (2007). This method eliminates the effect of damping by flowing the analyte inside the micro-channel of suspended microcantilevers, and is able to detect and measure the weight of individual live bacteria (Bryan *et al*., 2009).

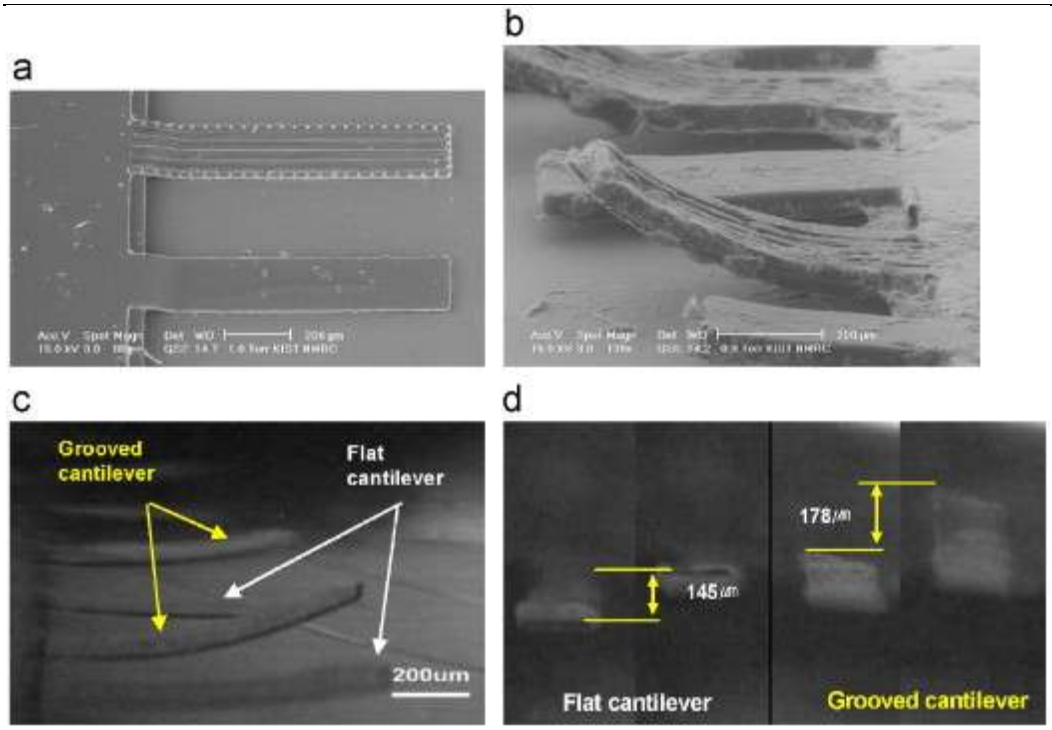

Figure 2-11: Images of flat and grooved microcantilevers: (a) Fabricated PDMS flat and grooved microcantilever, (b) SEM image of the hybrid organic–inorganic flat and grooved microcantilevers, (c) and (d) still images from video recordings of the vertical motion of the 200×1000 μm hybrid microcantilevers. (Figure adapted from Kim *et al.*, 2008)

On the other hand, Antonik *et al*. (1997) first proposed the use of microcantilever sensors for probing the nanomechanical responses of living cells cultured on one side of the cantilever surface. Even if the cells were deposited on one side of the cantilever surface, the living cells were found to grow on both sides of the cantilever surface, which emphasize the need to inhibit the growth on one side by treating the surface. The response of cells to toxins was observed by monitoring the deflection of cantilevers within several seconds of injection. Park *et al*. (2005) later showed that polymer microcantilever sensors can probe real-time contraction forces generated by mice heart muscle cells. The integration of muscle cells on grooved structured cantilever were found to generate more bending than on the flat surfaces as shown in Figure 2-11 (Park *et al*., 2007, Park *et al*., 2008, Kim *et al*., 2008, Kima *et al*., 2008). The forces generated by the living cells on the microcantilever structures have been harnessed to create cell-powered mechanical motors (Xi *et al*., 2005). The integration of skeletal muscle with silicon cantilever arrays has led to the development of serum-free cell-based sensor platform (Mainak *et al*., 2006, Das *et al*., 2007). This system not only allows real-time

and high-throughput measurement of a variety of physiological properties of the myotubes, but also could be developed as a powerful biomechanical platform for probing other complex tissues and biological circuits (Wilson *et al*., 2007).

2.6 Microfluidics and Microcantilever Arrays

Many biosensing applications on microcantilever sensors have been discussed in the above sections, but the integration of microfluidics with microcantilever arrays allow for a higher throughput biodetection. In addition, the integration of microcantilever sensor arrays into microfluidic channels reduces the amount of analyte sample required for the detection (Thaysen *et al*., 2001). Several optical detection methods have been incorporated into microfluidic systems, such as SPR and colorimetric assays (Hosokawa *et al*., 2004, Park *et al*., 2006, Puleo *et al*., 2008, Sato *et al*., 2008). They have been used in microchannel assays for antigen-antibody binding for bacteria and virus detection (Liu *et al*., 2005, Lucas *et al*., 2007, Zhang *et al*., 2006), sensing single molecules (Agrawal *et al*., 2006, Stavis *et al*., 2005, Yeh *et al*., 2004), DNA experiments (Ho *et al*., 2006, Medintz *et al*., 2003), etc.

Cantilever based arrays with microfluidic channels have been demonstrated previously (Aubin *et al*., 2007, Lechuga *et al*., 2006). For example, a portable biosensor system was shown to be able to detect nucleic acid hybridization (Lechuga *et al*., 2006). This system incorporates 20 cantilevers with a polymer based microfluidic system with an array of 20 vertical cavity surface emitting lasers (VCSELs) and corresponding photodetectors to readout the signal for sub-nanometer resolution. Easier experiments such as detecting changes in solvents, temperature, viscosity, and pH (Quist *et al*., 2006) has been demonstrated along with flow rate detection (Lien and Vollmer, 2007). A unique approach includes fabricating a microfluidic channel on the top of a microcantilever, which paves the way for applications such as mass-based flow cytometry and direct detection of pathogens (Burg *et al*., 2007). Perez *et al*., (2002) first incorporated a microfluidic channel on a cantilever itself, and demonstrated the ability to weigh and analyze biomolecules, single cells, and single nanoparticles in fluid.

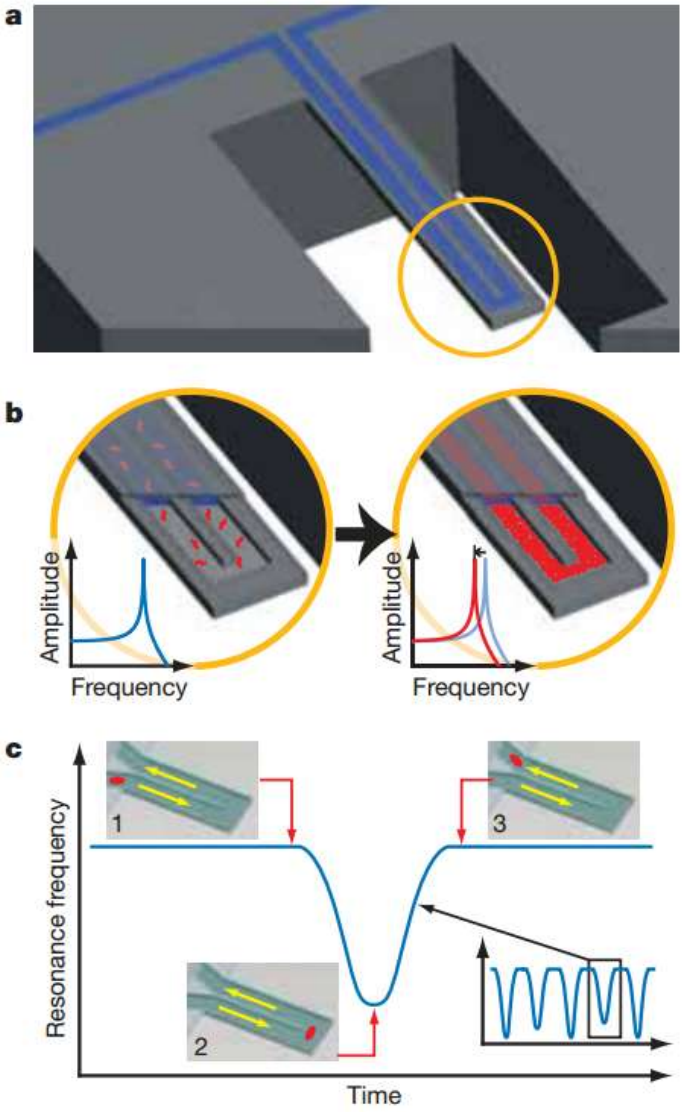

Figure 2-12: a) A microcantilever sensor with a microfluidic channel within. B) Both bound and unbound molecules increase the mass of the channel, but bound species accumulate inside the device. c) Particles flow through the channel unbound, but signals depend on the position of particles along the channel. (Figure adapted from Burg *et al*., 2007)

The majority of research demonstrated with the combination of microfluidics and microcantilever arrays were conducted on silicon based cantilevers. Raorane *et al*., (2008) demonstrated a gold coated cantilever array to measure the activity and inhibition of a model protease. The system consisted of 4-6 cantilevers per microfluidic well, and readout was one well at a time through an optical readout method of an expanded spot size laser to reflect off the gold coated cantilevers into a CCD camera to be monitored. Yue *et al*. (2008) used a similar readout system with a 2D cantilever array

for antibody-antigen binding assays involving PSA. Each chip had 80-120 reaction wells and each well has a microfluidic chamber with 4-8 cantilevers exposed to the same solution. The limit of detection was found to be 1 ng/mL. Dielectrophoresis was also used to trap cells and measure single cancer cell contractile force mechanics for cancer research with piezoresistive cantilevers in a PDMS microfluidic channel (Yue *et al*., 2011). Similarly, Park *et al*., (2008) captured live cells in microfluidic channels through dielectrophoresis, cultured the cells on the cantilever surface, and monitored cell growth through changes in cantilever resonance frequencies. Polymer SU-8 based microcantilever arrays meanwhile have been integrated with microfluidic channels for surface stress studies (Johansson *et al*., 2006). These were in an array of 4 cantilevers with a piezoresistive readout scheme. Noeth *et al*., (2011) fabricated SU-8 chips with holes built into the chip to act as filters to simultaneously count and separate particles from a liquid in a microfluidic chamber. Deflection of the cantilever was caused when a particle is too large to pass through the filter hole, and the higher flow resistance increases cantilever surface pressure and causes bending. This was tested with known bead sizes and filter holes with an optical PSD system. All the cantilever systems with integrated microfluidics have been demonstrated with either silicon based cantilevers, or piezoelectric/piezoresistive based systems. None of the systems have demonstrated cantilever array readouts with polymer cantilevers utilizing static mode deflections.

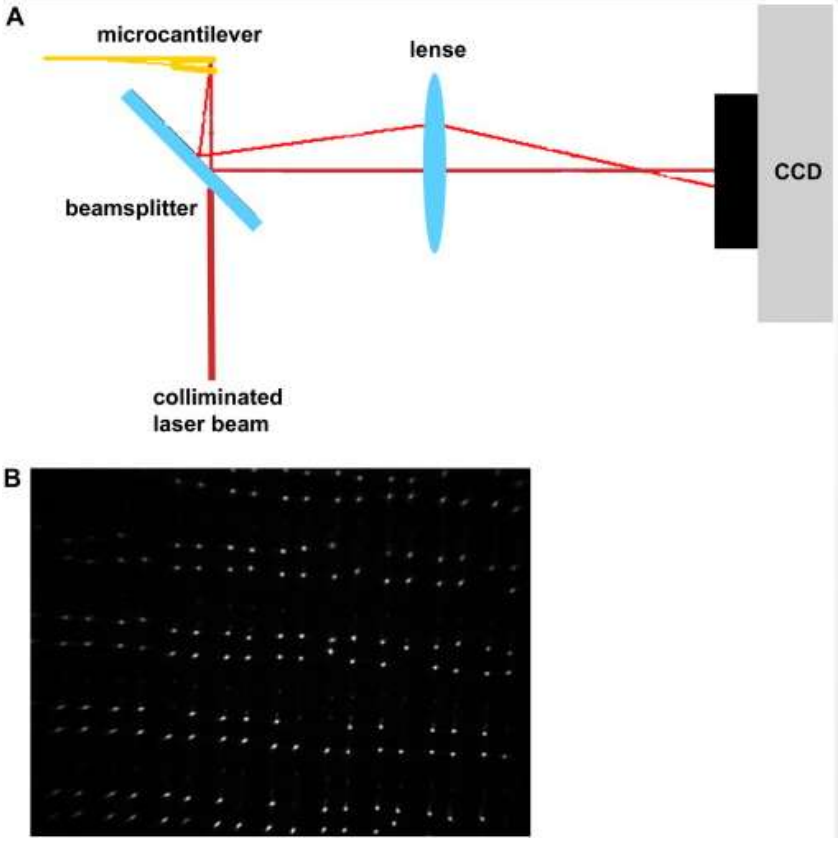

Figure 2-13: A) Schematic of a CCD optical readout scheme for microcantilever arrays. B) CCD image of a cantilever array, each spot represents a single cantilever. (Figure adapted from Biswal *et al*., 2007)

2.7 Challenges in Cantilever Biosensors

In recent years, there has been a rising demand for a highly sensitive yet rapid sensing platform for applications in disease diagnosis, drug screening and/or delivery, etc. Microcantilever sensors satisfy that need, but there are a few shortcomings currently that require further attention. Therefore, to expand and further develop microcantilever sensors into reliable platforms with widespread utilization requires the key challenges and gaps to be fulfilled as follows:

- Cost

  The cost challenges currently in the field of microcantilevers are due to the material and readout methods that are currently most widely used. Silicon based microcantilevers are expensive and time-consuming to fabricate and are extremely delicate to handle, in addition to being difficult to fabricate into large arrays. Current readout methods are expensive and bulky, and therefore are unsuitable for widespread adoption. Challenges in improving both costs remain.

- Readout

Microcantilevers have the potential to be utilized in highly multiplexed arrays for many assay applications. However, challenges arise from not only the fabrication of large arrays of cantilevers, but the readout methods required to monitor the deflection signals. Electronic readout schemes are fast but are too expensive to integrate individual electronic circuits for disposable applications. In order to realize the full capability of cantilevers as a sensing platform, further development has to be conducted for viable readout schemes such as optical methods for simultaneous monitoring of large numbers of cantilever sensors.

- Sensitivity

Sensitivity is another challenge for microcantilever sensors in liquid for cell analyses. Resonant mode cantilevers, while more sensitive in air and vacuum for cell growth monitoring, are limited in liquid environments with cell media due to the viscous and/or damping effects of liquid. While this may not be a large issue in all liquids, it can be detrimental in more viscous fluids. The downside to static mode cantilevers is their lower sensitivity compared to resonant mode cantilevers. Therefore, there needs to be methods of increasing the sensitivity of microcantilever sensors, operating in static mode, for cell experiments in liquid media.

2.8 Conclusions:

MEMS based sensors has unique advantages of being low cost, rapid, highly sensitive, and reliable sensing platform for detection of many analytes. Significant progress has been made in the past decade to enable microcantilever based biosensors to be a powerful platform for biomedical applications. Although high sensitivity and a wide range of biomolecular interactions have been demonstrated, further improvements on cost, fabrication, sensitivity, high-throughput signal readouts, and integration with microfluidic systems will be key areas for future research. Future efforts targeting the development of reliable and robust methods to interface with sensor arrays effectively while simultaneously allowing for scaling to large arrays will be key to successfully introducing new applications.

2.9 References

Abu-Lail, N., Kaholek, M., LaMattina, B., Clark, R.L., Zauscher, S., Micro-Cantilevers with End Grafted Stimulus-Responsive Polymer Brushes for Actuation and Sensing. *Sensors and Actuators B: Chemical*, **114(1)**, 371-378 (2006).

Agrawal, A., Zhang, C., Byassee, T., Tripp, R.A., Nie, S., Counting single native biomolecules and intact viruses with color-coded nanoparticles. *Anal Chem*, **78**, 1061–1070 (2006).

Alexei V., Nehal, I.A.L., Dong-Woo, L., Ashutosh C., Stefan Z., Micro-Cantilever Sensing and Actuation with End-Grafted Stimulus-Responsive Elastin-Like Polypeptides . *Langmuir*, **23(1)**, 339-344 (2007).

Alvarez, M., Carrascosa, L.G., Moreno, M., Calle, A., Zaballos, A., Lechuga, L.M., Martinez, A.C., Tamayo, J. Nanomechanics of the formation of DNA self-assembled monolayers and hybridization on microcantilevers. *Langmuir*, **20**, 9663–9668 (2004).

Alvarez, M., Tamayo, J., Optical sequential readout of microcantilever arrays for biological detection, *Sensors and Actuators . B: Chemical*, **106**, 687-690 (2005).

Antonik, M.D., D'Costa, N.P., Hoh, J.H., A biosensor based an micromechanical interrogation of living cells. *IEEE Engineering in Medicine and Biology Magazine*, **16(2)**, 66-72 (1997).

Arntz, Y., Seeling, J.D., Lang, H.P., Zhang, J., Hunziker, P., Ramseyer, J.P., Meyer, E., Hegner, M., Gerber, C., Label-free protein assay based on a nanomechanical cantilever array. *Nanotechnology*, **14**, 86-90 (2003).

Aubin, K.L., Huang, J., Park, S.M., Yang, Y., Kondratovich, M., Craighead, H.G., Ilic, B.R., Microfluidic encapsulated nanoelectromechanical resonators. *J Vac Sci Technol B*, **25**, 1171–1174 (2007).

Backmann, N., Christian, Z.C., Huber, F., Bietsch, A., Plückthun, A., Lang, H.P., Güntherodt, H.J., Hegner, M., Gerber, C., A label-free immunosensor array using single-chain antibody fragments. *Proc. Natl. Acad. Sci.*, **102**, 14587-14592 (2005).

Bailey, R.C., Kwong, G.A., Radu, C.G., Witte, O.N., Heath, J.R., DNAencoded antibody libraries: a unified platform for multiplexed cell sorting and detection of genes and proteins. *J Am Chem Soc*, **129**, 1959–1967 (2007).

Baselt, D.R., Fruhberger, B., Klaassen, E., Cemalovic, S., Britton, C.L., Patel, S.V., Mlsna, T.E., McCorkle, D., Warmack, B., Design and performance of a microcantilever-based hydrogen sensor. *Sensors and Actuators B*, **88**, 120-131 (2003).

Baselt, D.R., Lee, G.U., Hansen, K.M., Chrisey, L.A., Colton, R.J., A High- Sensitivity Micromachined Biosensor, *IEEE*, **85**, 672 (1997)

Berger, R., Delamarche, E., Lang, H.P., Gerber, C., Gimzewski, J.K., Meyer, E., Guntherodt, H.J., Surface Stress in the Self-Assembly of Alkanethiols on gold. *Science*, **276**, 2021-2024 (1997).

(a) Bietsch, A., Hegner, M., Lang, H.P., Gerber, C., Inkjet deposition of alkanethiolate monolayers and DNA oligonucleotides on gold: Evaluation of spot uniformity by wet etching, *Langmuir*, **20 (12)**, 5119-5122 (2004).

(b) Bietsch, A., Zhang, J., Hegner, M., Lang, H.P., Gerber, C., Rapid functionalization of cantilever array sensors by inkjet printing, *Nanotechnology*, **15**, 873–880 (2004).

Binnig, G., Quate, C.F., Gerber, C., Atomic force microscope. *Phys. Rev. Lett.*, **56**, 930-934 (1986).

Biswal, S.L., Raorane, D., Chaiken, A., Majumdar, A., Using a microcantilever array for detecting phase transitions and stability of DNA. *Clinics in Laboratory Medicine* **27(1)**, 163-171 (2007).

Braun, T., Ghatkesar, M.K., Backmann, N., Grange, W., Boulanger, P., Letellier, L., Lang, H., Bietsch, A., Gerber, C., Hegner, M., Quantitative time-resolved measurement

of membrane protein-ligand interactions using microcantilever array sensors. *Nat. Nanotechnol.*, **4**, 179–185 (2009)

Bryan, A.K., Goranov, A., Amon, A., Manalis, S.R., Measurement of mass, density, and volume during the cell cycle of yeast, *Proc Natl Acad Sci U S A.*, **10**, 1073 (2009).

Burg, T.P., Godin, M., Knudsen, S.M., Shen, W., Carlson, G., Foster, J.S., Babcock, K., Manalis, S.R., Weighing of biomolecules, single cells and single nanoparticles in fluid. *Nature* **446**, 1066–1069 (2007).

Burg, T.P., Godin, M., Knudsen, S.M., Shen, W.J., Carlson, G., Foster, J.S., Babcock, K., Manalis, S.R., Weighing of biomolecules, single cells and single nanoparticles in fluid, *Nature*, **446**, 1066-1069 (2007).

Calleja, M., Nordström, M., Álvarez, M., Tamayo, J., Lechuga, L.M., Boisen, A., Highly sensitive polymer-based cantilever-sensors for DNA detection, *Ultramicroscopy*, **105**, 215-22 (2005).

Calleja, M., Tamayo, J., Johansson, A., Rasmussen, P., Lechuga, L.M., Boisen, A., Polymeric cantilever arrays for biosensing applications, *Sensor Letters*, **1**, 1-5 (2003).

Calleja, M., Tamayo, J., Nordström, M., Boisen, A., Low-noise polymeric nanomechanical biosensors, *Applied Physics Letters*, **88,** 113901-3 (2006).

Campbell, G. A., Uknalis, J., Tu, S.I., Mutharasan, R., Detection of Escherichia coli O157:H7 in ground beef samples using piezoelectric excited millimeter-sized cantilever (PEMC) sensors. *Biosensors and Bioelectronics*, **22** (7), 1296-1302 (2007).

Caruso, F., Rodda, E., Furlong, D. N., Quartz crystal microbalance study of DNA immobilization and hybridization for nucleic acid sensor development. *Anal. Chem.* **69,** 2043–2049 (1997).

Cha, B.H., Lee, S.M., Park, J.C., Hwang, K.S., Kim, S.K., Lee, Y.S., Ju, B.K., Kim, T.S., Detection of Hepatitis B Virus (HBV) DNA at femtomolar concentrations using a

silica nanoparticle-enhanced microcantilever sensor. *Biosensors and Bioelectronics*, **25**, 130-135 (2009).

Das, M., Gregory, C., Molnar, P., Riedel, L.M., Wilson, K., Hickman, J., A defined system to allow skeletal muscle differentiation and subsequent integration with silicon microstructures. *Biomaterials*, **27**, 4374-80 (2006).

Das, W., Molnar, P., Hickman, J.J., Differentiation of skeletal muscle and integration of myotubes with silicon microstructures using serum-free medium and a synthetic silane substrate. *Nature Protocols*, **2(7)**, 1795-1801 (2007).

Duggan, D., Bittner, M., Chen, Y., Meltzer, P., Trent, J., Expression profiling using cDNA microarrays. *Nat. Genet. Suppl.* **21,** 10–14 (1999).

Fritz, J., Baller, M.K., Lang, H.P., Rothuizen, H., Vettiger, P., Meyer, E., Guntherodt, H.J., Gerber, C., Gimzewski, J.K., Translating Biomolecular Recognition into Nanomechanics. *Science*, **288**, 316-318 (2000).

Gammelgaard, L., Rasmussen, P.A., Calleja, M., Vettiger, P., Boisen, A., Microfabricated photoplastic cantilever with integrated photoplastic/carbon based piezoresistive strain sensor. *Appl. Phys. Lett*, **88**, 113508-113510 (2006).

Georgiadis, R., Peterlinz, K. P., Peterson, A. N., Kinetic control of hybridization in surface immobilized DNA monolayer films. *J. Am. Chem. Soc.* **122,** 3166–3173 (2000).

Gfeller, K. Y., Nugaeva, N., Hegner, M., Rapid biosensor for detection of antibiotic-selective growth of Escherichia coli. *Appl. Environ. Microbiol*., **71**, 2626–2631 (2005).

Ghatkesar, M.K., Barwich, V., Braun, T., Ramseyer, J., Gerber, C., Lang, H.P. Dreschler, U., Despont, M., Higher modes of vibration increase mass sensitivity in nanomechanical microcantilevers. *Nanotechnology*, **18**, 445502 (2007).

Giesfeldt, K.S., Connatser, R.M., De Jesus, M.A., Dutta, P., Sepaniak, M.J., Gold-polymer nanocomposites: studies of their optical properties and their potential as SERS substrates. *J Raman Spectrosc,* **36,** 1134–1142 (2005).

Grice, M.E., Politzer, P., Use of molecular stoichiometry to estimate vibrational energy. *Chemical Physics Letters*, **244**, 295-298 (1995).

Grogan, C., Raiteri, R., O'Connor, G.M., Glynn, T.J., Cunningham, V., Kane, M., Chariton, M., Leech, D., Characterisation of an antibody coated microcantilever as a potential immuno-based biosensor, *Biosensors & Bioelectronics*, **17**, 201-207 (2002).

Gupta, R., Akin, D., Bashir, R., Detection of bacterial cells and antibodies using surface micromachined thin silicon cantilever resonators. *J. Vac. Sci. Technol. B,* **22**, 2785–2791 (2004).

Hagan, M. F., Majumdar, A., Chakraborty, A. K., Nanomechanical Forces Generated by Surface Grafted DNA. *J. Phys. Chem. B,* **106**, 10163-10173 (2002).

Hansen, K.M., Ji, H.F., Wu, G., Datar, R., Cote, R., Majumdar, A., Thundat T., Cantilever-based optical deflection assay for discrimination of DNA single-nucleotide mismatches. *Anal. Chem*., **73**, 1567-71 (2001).

Helm, M., Servant, J.J., Berger, R., Read-out of micromechanical cantilever sensors by phase shifting interferometry, *Appl. Phys. Lett*. **87**, 064101 (2005).

Ho, Y.P., Kung, M.C., Yang, S., Wang, T.H., Multiplexed hybridization detection with multicolor colocalization of quantum dot nanoprobes. *Nano Lett*., **5**, 1693–1697 (2005).

Hosokawa, K., Sato, K., Ichikawa, N., Maeda, M., Power-free poly(dimethylsiloxane) microfluidic devices for gold nanoparticle- based DNA analysis. *Lab Chip*, **4,** 181–185 (2004).

Ilic, B., Czaplewcki, D., Zalalutdinov, M., Craighead, H.G., Campagnolo, C.,Batt, C., Single Cell Detection With Micromechanical Oscillators, *J. Vac. Sci. Technol., B*, **190 (6)**, 2825-2828 (2001).

Ilic, B., Czaplewski, D., Craighead, H.G., Neuzil, P., Campagnolo, C., Batt, C., Mechanical Resonant Immunospecific Biological Detector, *Appl. Phys. Lett.*, **77**, 450–452 (2000).

Ilic, B., Yang, Y., Aubin, K., Reichenbach, R., Krylov, S., Craighead, H.G., Enumeration of DNA Molecules Bound to a Nanomechanical Oscillator, *Nano Letters*, **5**, 925-929 (2005).

Johansson, A., Blagoi, G., Boisen, A., Strong broad C-band room-temperature photoluminescence in amorphous Er_2O_3 film. *Applied Physics Letters* **89**, 173505 (2006).

Kelling, S., Paoloni, F., Huang, J., Ostanin, V., Elliot, S., Simultaneous readout of multiple microcantilever arrays with phase-shifting interferometric microscopy. *Rev. Sci. Instrum*. **80**, 093101-093108 (2009).

Kim, J., Park, J., Na, K., Yang, S., Baek, J., Yoon, E., Choi, S., Lee, S., Chun, K., Park, J., Park, S., Quantitative evaluation of cardiomyocyte contractility in a 3D microenvironment. *Journal of biomechanics*, **41 (11),** 2396-401 (2008).

Kima, J., Park, J., Na, K., Yang, S., Baek, J., Yoon, E., Choi, S., Lee, S. Chun, K., Park, J., Park, S., Quantitative evaluation of cardiomyocyte contractility in a 3D microenvironment. *Europace*, **41**, 2396-2401 (2008).

Knowles, T.P.J., Shu, W., Huber, F., Lang, H.P., Gerber, C., Dobson, C.M., Welland, M.E., Label-free detection of amyloid growth with microcantilever sensors, *Nanotechnology*, **19**, 384007 (2008).

Krecmer, P., Moulin, A. M., Stephenson, R. J., Rayment, T., Welland, M. E., Elliott, S. R., Reversible Nanocontraction and Dilatation in a Solid Induced by Polarized Light. *Science*, **277**, 1799-1802 (1997).

Lang, H.P., Berger, R., Andreoli, C., Brugger, J., Despont, M., Vettiger, P., Gerber, C., Gimzewski, J.K., Ramseyer, J.P., Meyer, E., Guntherodt, H.J., Sequential position readout from arrays of micromechanical cantilever sensors. *Appl. Phys. Lett.*, **72**, 383–385 (1998).

Lang, H.P., Berger, R., Battiston, F., Ramseyer, J.P., Meyer, E., Andreoli, C., Brugger, J., Vettiger, P., Despont, M., Mezzacasa, T., Scandella, L., Guntherodt, H.J., Gerber, C., A chemical sensor based on a micromechanical cantilever array for the identification of gases and vapors. *Appl. Phys. A*, **66**, 61-64 (1998).

Lechuga, L.M., Tamayo, J., Alvarez, M., Carrascosa, L.G., Yufera, A., Doldan, R., Peralias, E., Rueda, A., Plaza, J.A., Zinoviev, K., Dominguez, C., Zaballos, A., Moreno, M., Martinez, C., Wenn, D., Harris, N., Bringer, C., Bardinal, V., Camps T, Vergnenegre C, Fontaine C, Diaz V, Bernad A., A highly sensitive microsystem based on nanomechanical biosensors for genomics applications. *Sens Actuators B Chem,* **118**, 2–10 (2006).

Lien, V., Vollmer, F., Microfluidic flow rate detection based on integrated optical fiber cantilever. *Lab on a Chip*, **7**, 1352-1356 (2007),

Lindblad-Toh, K., Tanenbaum, D. M., Daly, M. J., Winchester, E., Lui, W. O., Villapakkam, A., Stanton, S. E., Larsson, C., Hudson, T. J., Johnson, B. E., Low of heterozygosity analysis of small-cell lung carcinomas using single-nucleotide polymorphism arrays. *Nat. Biotechnol.* **18,** 1001–1005 (2000).

Liu, D., Balasubramanian, S., A proton fuelled DNA nanomachine. *Chem., Int. Ed.*, **42**, 5734–5736 (2003).

Liu, W.T., Zhu, L., Qin, Q.W., Zhang, Q., Feng, H., Ang, S., Microfluidic device as a new platform for immunofluorescent detection of viruses. *Lab Chip* **5**, 1327–1330 (2005).

Lucas, L.J., Chesler, J.N., Yoon, J.Y., Lab-on-a-chip immunoassay for multiple antibodies using microsphere light scattering and quantum dot emission. *Biosens Bioelectron*. **23,** 675–681 (2007).

MacBeath, G. & Schrieber, S. L., *Science* **289,** 1760–1763 (2000).

(a) Maraldo, D., Mutharasan, R., Preparation-free method for detecting Escherichia coli O157: H7 in the presence of spinach, spring lettuce mix, and ground beef particulates. *J Food Protect,* **70(11)**, 2651-2655 (2007).

(b) Maraldo, D., Mutharasan, R., 10-Minute Assay for Detecting Escherichia coli O157:H7 in Ground Beef Samples using Piezoelectric-Excited Millimeter-Sized Cantilever (PEMC) Sensors. *Journal of Food Protection*, **70(7)**, 1670-1677 (2007).

McKendry, R., Zhang, J., Arntz, Y., Strunz, T., Hegner, M., Lang, H.P., Baller, M.K., Certa, U., Meyer, E., Güntherodt, H.J., Gerber, C., Multiple label-free biodetection and quantitative DNA-binding assays on a nanomechanical cantilever array. Proc. Natl. Acad. Sci. USA, **15**, 9783-9787 (2002).

Medintz, I.L., Konnert, J.H., Clapp, A.R., Stanish, I., Twigg, M.E., Mattoussi, H., Mauro, J.M., Deschamps, J.R., A fluorescence resonance energy transfer-derived structure of a quantum dot-protein bioconjugate nanoassembly. *PNAS,* **101,** 9612–9617 (2004).

Mertens, J., Rogero, C., Calleja, M., Ramos, D., Martin-Gago, J.A., Briones, C., Tamayo, J., Label-free detection of DNA hybridization based on hydration-induced tension in nucleic acid films. *Nat Nanotechnol.*, **3**, 301-7 (2008).

Minne, S.C., Manalis, S.R., Quate, C.F., Parallel atomic force microscopy using cantilevers with integrated piezoresistive sensors and integrated piezoelectric actuators. *Appl. Phys. Lett*. **67**, 3918 (1995).

Moulin, A.M., O'Shea, S.J., Badley, R.A., Doyle, P., and Welland, M.E., Measuring Surface-Induced Conformational Changes in Proteins. *Langmuir*, **15 (26)**, 8776-8779 (1999).

Ndieyira, W.N., Watari, M., Donoso-Barrera, A., Vogtli, M. Batchelor, M., Zhou, D., Cooper, M., Strunz, T., Abell, C.A., Rayment, T., Aeppli, G., McKendry R.A., Nanomechanical detection of antibiotic mucopeptide interactions in a model for superbug drug resistance. *Nat. Nanotech.*, **3**, 691–696 (2008).

Nelson, B. P., Grimsrud, T. E., Liles, M. R., Goodman, R. M., Corn, R. M., Surface plasmon resonance imaging measurements of DNA and RNA hybridization adsorption onto DNA microarrays. *Anal. Chem.* **73,** 1–7 (2001).

Noeth, N., Keller, S.S., Boisen, A., Cantilever-based micro-particle filter with simultaneous single particle detection. *J. Micromech. Microeng*. **21**, (2011).

Nugaeva, N., Gfeller, K.Y., Backmann, N., Duggelin, M., Lang, H.P., Guntherodt, H.J., Hegner, M., An antibody-sensitized microfabricated cantilever for the growth detection of Aspergillus niger spores. *Microsc. Microanal*. **13**, 13–17 (2007).

Park, J., Kim, J., Roh, D., Park, S., Kim, B., Chun, K., Fabrication of 3D thin polymer structures for hybrid sensors and actuators, *Journal of Micromechanics and Microengineering*, **16**, 1614–1619 (2006).

Park, J., Ryu, J., Choi, S.K., Seo, E., Cha, J.M., Ryu, S., Kim, J., Kim, B., Lee, S.H., Real-Time Measurement of the Contractile Forces of Self-Organized Cardiomyocytes on Hybrid Biopolymer Microcantilevers. *Anal. Chem*., **77 (20)**, 6571–6580 (2005).

Park, J., Ryu, S.K., Kim, J., Cha, J., Jeongeun, B., Park, S., Kim, B., Lee, S.H., A three-dimensional model of fluid-structural interactions for quantifying the contractile force

for cardiomyocytes on hybrid biopolymer microcantilever. *Journal of biomechanics*, **40(13),** 2823-30 (2007).

Park, K., Jang, J., Irimia, D., Sturgis, J., Lee, J., Robinson, J.P., Toner, M., Bashir, R., Cantilever sensor detection of microorganisms and cell growth. *Lab on a Chip*, **8**, 1034-1041 (2008).

Park, T., Lee, S., Seong, G.H., Choo, J., Lee, E.K., Kim, Y.S., Ji, W.H., Hwang, S.Y., Gweon, D.G., Lee, S., Highly sensitive signal detection of duplex dye-labelled DNA oligonucleotides in a PDMS microfludic chip: confocal surface-enhanced Raman spectroscopic study. *Lab on a Chip* **5,** 437–442 (2005).

Peng, H., Soeller, C., Vigar, N.A., Caprio, V., Travas-Sejdic, J.T., Label-free detection of DNA hybridization based on a novel functionalized conducting polymer. *Biosens. Bioelectron*., **22**, 1868–1873 (2007).

Perez, J.M., Josephson, L., O'Loughlin, T., Hogemann, D., Weissleder, R., Magnetic relaxation switches capable of sensing molecular interactions. *Nat. Biotechnol*. **20**, 816–820 (2002).

Puleo, C.M., Yeh, H.C., Liu, K.J., Wang, T.H., Coupling confocal fluorescence detection and recirculating microfluidic control for single particle analysis in discrete nanoliter volumes. *Lab Chip* **8,** 822–825 (2008).

Quist, A., Chand, A., Ramachandran, S., Cohen, D., Lal, R., Piezoresistive cantilever based nanoflow and viscosity sensor for microchannels. *Lab Chip*, **6,** 1450–1454 (2006).

Raorane, D.A., Lim, M.D., Chen, F.F., Craik, C.S., Majumdar, A., Quantitative and label-free technique for measuring protease activity and inhibition using a microfluidic array. *Nano Letters* **8(9)**, 2968-2974 (2008).

Reed, J., Schmit, J., Han, S., Wilkinson, P., Gimzewski, J.K., Interferometric profiling of microcantilevers in liquid, *Optics and Lasers in Engineering*, **47**, 217-222 (2009).

Saiki, R. K., Scharf, S., Faloona, F., Mullis, K. B., Horn, G. T., Erlich, H. A., Arnheim, N., Enzymatic amplification of beta-globin genomic sequences and restriction site analysis for diagnosis of sickle cell anemia. *Science,* **230,** 1350–1354 (1985).

Sato, Y., Hosokawa, K., Maeda, M., Detection of non-cross-linking interaction between DNA-modified gold nanoparticles and a DNA-modified flat gold surface using surface plasmon resonance imaging on a microchip. *Colloids Surf B Biointerfaces* **62,** 71–76 (2008).

Savran, C.A., Knudsen, S.M., Ellington, A.D., Manalis, S.R., Micromechanical Detection of Proteins Using Aptamer-Based Receptor Molecules. *Anal. Chem.*, **76**, 3194–3198 (2004).

Shekhawat, G., Tark, S., Dravid, V., MOSFET-Embedded Microcantilevers for Measuring Deflection in Biomolecular Sensors. *Science*, **311**, 1592-1595 (2006).

Shephard, J.D., Varadam, D., Wang, W.X., Liu, Y., Parry, J.P., Hand, D.P., Shu, W., Direct writing large arrays of micro-cantilevers for bio-MEMS devices, *Proceedings of LAMP2009 5th International Congress on Laser Advanced Materials Processing, Japan*, (2009).

Shu, W., Microcantilever-based sensors and actuators, *VDM Verlag, Germany*, (2008).
Shu, W., Laue, E.D., Seshia, A. A. Investigation of Biotin-Streptavidin Binding Interactions using Microcantilever Sensors. *Biosensors & Bioelectronics*, **22**, 2003-2009 (2007).

Shu, W., Laurenson, S., Knowles, T.P., Ferrigno, P.K., Seshia, A.A., Highly specific label-free protein detection from lysed cells using internally referenced microcantilever sensors, *Biosens. Bioelectron*., **24**, 233–23 (2008).

Shu, W., Liu, D., Watari, M., Riener, C.K., Strunz, T., Welland, M.E., Balasubramanian, S., McKendry, R.A., DNA molecular motor driven micromechanical cantilever arrays. *J. Am. Chem. Soc.*, **127**, 17054–17060 (2005).

Southern, E., Mir, K., Shchepinov, M., Molecular interactions on microarrays. *Nat. Genet.* **21,** 5–9 (1999).

Stavis, S.M., Edel, J.B., Samiee, K.T., Craighead, H.G., Single molecule studies of quantum dot conjugates in a submicrometer fluidic channel. *Lab Chip* **5,** 337–343 (2005).

Su, M., Li, S. U., Dravid, V.P., Microcantilever resonance-based DNA detection with nanoparticle probes. *Apl. Phys. Lett*. **82**, 3562-3564 (2003).

Thaysen J., Marie, R., Boisen, A., *IEEE International Conference on Micro Electro Mechanical Systems, Technical Digest*, IEEE, New York, 401–404 (2001).

Thundat, T., Chen, G.Y., Warmack, R.J., Allison, D.P., Wachter, E.A., Vapor detection using resonating microcantilevers. *Anal. Chem*. **67(3)**, 519-521 (1995).

Thundat, T., Wachter, A., Sharp, S.L., Warmack, R.J., Detection of mercury vapor using resonating microcantilevers. *Appl. Phys. Lett*. **66(13)**, 1695-1697 (1995).

Thundat, T., Warmack, R.J., Chen, G.Y., Allison, D.P., Thermal and ambient-induced deflections of scanning force microscope cantilevers. *Appl. Phys. Lett*, **64**, 2894-2896 (1994).

Tortonese, M., Barrett, R.C., Quate, C.F., Atomic resolution with an atomic force microscope using piezoresistive detection. *Appl. Phys. Lett*. **62**, 834 (1993)

Turner, I., Wilson, G.S., Biosensors: Fundamentals and Applications. In: Oxford University Press, Oxford, 770 (1989).

Waggoner, P.S., Craighead, H.G., Micro- and Nanomechanical Sensors for Environmental, Chemical, and Biological Detection, *Lab on a Chip*, **7**, 1238-1255 (2007).

Wang, D. G., Fan, J., Siao, C., Berno, A., Young, P., Sapolsky, R., Ghandour, G., Perkins, N., Winchester, E., Spencer, J., Large-scale identification, mapping, and genotyping of single-nucleotide polymorphisms in the human genome. *Science* **280,** 1077–1082 (1998).

Wang, X., Lu, P., Dai, N., Liao, C., Wang, Y., Zheng, Q., Guo, X., Zhang, Q., Femtosecond laser direct fabrication of metallic microcantilevers for a micro-corrosion-fatigue test. *J. Micromech. Microeng*. **17** , 1307–1313 (2007).

Wilson, K., Molnar, P., Hickman, J., Integration of functional myotubes with a Bio-MEMS device for non-invasive interrogation. *Lab on a chip,* **7(7)**, 920-2 (2007).

Wu, G., Datar, R.H., Hansen, K.M., Thundat, T., Cote, R.J., Majumdar, A., Bioassay of prostate-specific antigen (PSA) using microcantilevers, *Nat. Biotechnol.*,**19**, 856–860 (2001).

Wu, G., Haifeng, J., Hansen, K., Thundat, T., Datar, R., Cote, R., Hagan, M. F., Chakraborty, A. K., Majumdar, A., Origin of nanomechanical cantilever motion generated from biomolecular interactions. *Proc. Natl. Acad. Sci*., **98**, 1560-1564 (2001).

Xi, J., Schmidt, J.J., Montemagno, C.D., Self-assembled microdevices driven by muscle, *Nat Mater,* **4 (2)**, 180-4 (2005).

Yeh, H.C., Simone, E., Zhang, C., Wang, T.H., Single bio-molecule detection with quantum dots in a microchannel. In: Micro electro mechanical systems, 17th IEEE International Conference on. (MEMS), 371–374 (2004).

Yi, J. W., Shih, W. Y., Mutharasan, R., Shih, W.H., In situ Cell detection Using Piezoelectric Lead Zirconate Titanate-Stainless Steel cantilevers. *J. Appl. Physics*., **93(1),** 619-625 (2003).

Yin, T.I., Zhao, Y., Lin, C.F., Tsai, H.H., Juang, Y.Z., Urban, G.A., Transducers'11, Beijing, China, (2011).

Yue, M., Lin, H., Dedrick, D.E., Satyanarayana, S., Majumdar, A., Bedekar, A.S., Jenkins, J.W., Sundaram, S., A 2-D microcantilever array for multiplexed biomolecular analysis. *Microelectromechanical Systems*, **13**, 290 – 299 (2004).

Yue, M., Stachowiak, J.C., Lin, H., Datar, R., Cote, R., Majumdar, A., Label free protein recognition 2D array using nanomechanical sensors. *Nano Letters*, **8(2)**, 520-524 (2008).

Zhang, Q., Zhu, L., Feng, H., Ang, S., Chau, F.S., Liu, W.T., Microbial detection in microfluidic devices through dual staining of quantum dots-labeled immunoassay and RNA hybridization. Analytica Chimica Acta **556(1)**, 171-177 (2006).

Zhang, X.R., Xu, X., Development of a biosensor based on laser-fabricated polymer microcantilevers, *Appl. Phys. Lett*. **85**, 2423-2425 (2004).

Zhou, F., Biesheuvel, P.M., Choi, E., Shu, W., Poetes, R., Steiner, U., Huck, W.T.S., Polyelectrolyte brush amplified electroactuation of microcantileversNano Lett., **8**, 725–30 (2008).

Zhou, F., Shu, W., Welland, M.E., Huck, W.T.S., Highly Reversible and Multi-Stage Cantilever Actuation Driven by Polyelectrolyte Brushes. *J. Am. Chem. Soc.*, **128**, 5326-5327 (2006).

Chapter 3 Experimental Details

3.1 Optical Beam Detection System

Significant portions of the experiments in this thesis were performed using a custom built single cantilever optical beam detection system. While later experiments were performed with a multi-array cantilever system, although a single cantilever system was still able to adapt to a wide range of different conditions in a liquid environment. Single cantilever systems have been shown to be able to detect a variety of interactions, including biomolecular binding interactions (Wu *et al.*, 2001), electrochemical (Brunt *et al.*, 1996), magnetic (Cowburn *et al.*, 1997), thermal (Berger *et al.*, 1998), and optical (Kreemer *et al.*, 1997) properties. Due to the inherent sensitivity of the device, the cantilevers can be vulnerable to external noises and other factors that have to controlled or canceled by utilizing an isolated environment with a combination of anti-vibration surfaces, temperature controls, and lighting controls.

An optical readout scheme similar to the conventional AFM (Binnig *et al.*, 1982) is used for the microcantilever detection setup. This is a static mode operation as opposed to the dynamic or resonant mode where the cantilevers are vibrated at a certain resonant frequency. In comparison, static mode is better suited towards liquid environments, which causes inherent damping problems for dynamic mode cantilevers. As shown in Figure 3-1a, the main components of the system consists of a flow cell chamber, position sensitive photodiode (PSD, Laser Components PSM 1-10), 5mW laser diode (532nm, ThorLab), fluid delivery/control system, temperature control system, data acquisition card (National Instruments BNC-2120), and computer with a LabVIEW programming environment.

As the laser beam is focused on the tip of the microcantilever, the gold coating on the surface of the cantilever reflects the laser. Through the reflection, the signal is detected by a PSD and the position data is then amplified and sent to the computer, whereby LabVIEW is used to analyze and record the signals. The liquid flow cell chamber was manufactured from polyether-ether-ketone (PEEK) for its known biocompatibility and resistance to chemicals and solvents that would be used in the system. The chamber consists of a flow channel with a polyimide cantilever chip mounted inside. The cantilever chip is secured inside with two identical shaped PEEK bindings and mounted

with a nylon M2 screw. There is a 5mm × 18mm channel with inlet and outlet fluid points to allow for liquid to pass through the system. The top of the chamber is sealed with a rubber O-ring and covered with a 25mm diameter round sapphire glass (which is more flexible than glass) in order to have a higher clamping force for a better seal with the O-ring. The polyimide cantilevers were fabricated from 25μm thick sheets (RS Components, UK) that were first coated with gold in either a thermal evaporator or electron beam physical vapor deposition (e-beam). 5nm of chromium was first deposited onto a sheet of polyimide in order to aid the adhesion of gold, followed by a deposition of 40nm of gold. Afterwards, the cantilever shape was laser fabricated with a nano- or pico- second laser, details can be found in section 3.4.

The basics of the functionality of an optical readout system can be seen in Chapter 2. The laser is focused to the optimal distance using an optical microscope to focus the laser spot to be the smallest size on the tip of the cantilever beam. The mounting and complete system can be seen in Figure 3-1b. The important areas of cantilever fabrication, temperature control, programming, and fluid control will be discussed in the next sections.

3.1.1 Microcantilever Fabrication

Microcantilevers were fabricated using a nano or pico-second laser. Polyimide was the material of choice because of its excellent electrical (non-conductive), physical (chemical resistant), and mechanical (soft and can be cut by laser) properties. Thicknesses of 7.8 μm, 12.5 μm, 25 μm, and 50 μm were tried, but the majority of the experiments were conducted with 25 μm thickness polyimide due to its already high sensitivity an ease of handling. Films thinner than 25 μm produced a non-uniform cantilever array even before experiments begin.

Polyimide films (RS Components, UK) were purchased in sheets, followed by a thorough cleaning with pure ethanol. After drying, the films were then coated with 5nm of chromium followed by 40nm of gold in a thermal evaporator. After the gold coating, the microcantilevers were one step fabricated using a nano or pico-second laser into the cantilever chips. Each chip required roughly 10 seconds through laser fabrication, and therefore was batch fabricated and stored until required use.

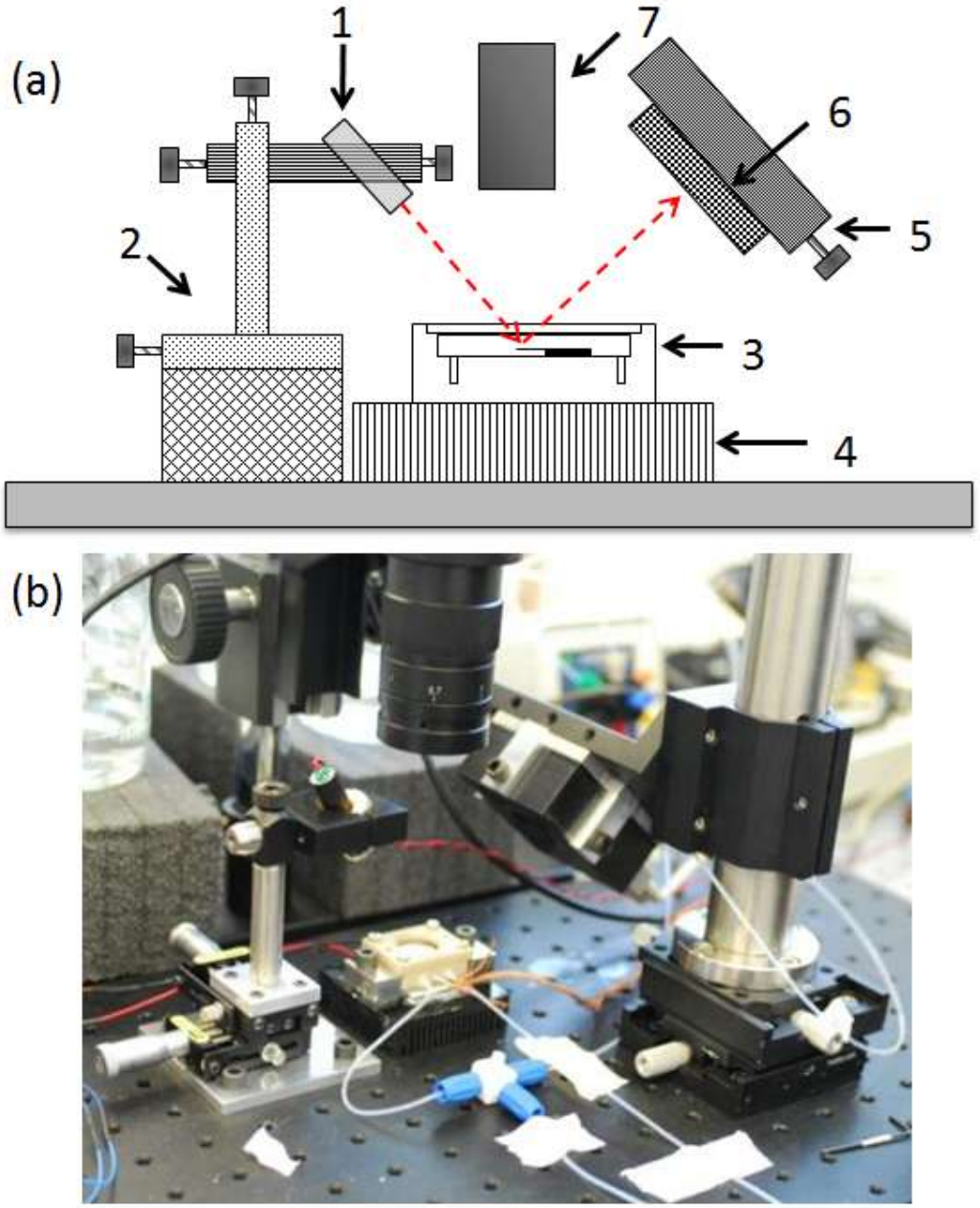

Figure 3-1: Schematic of the optical deflection cantilever system, which includes: (a) 1) Laser diode 2) Laser mount with X-Y stage 3) Cantilever holder liquid flow chamber 4) Heatsink with peltier 5) PSD holder with X-Y stage 6) PSD 7) Microscope (b) Image of actual setup in the laboratory.

3.1.2 Temperature control

The temperature control setup consists of a 30×30×3.2mm sized peltier device (33.4W, ΔT of 67℃, 3.9A maximum current, 85℃ maximum temperature, RS Components, UK) that was fitted directly underneath the liquid flow cell chamber. In order to ensure the best thermal conductivity between the peltier device and the reaction chamber, a thin layer of thermal paste was applied between them. The peltier was controlled with an H-

bridge circuit, fed through a 12V power supply, and controlled in LabVIEW using proportional, integral, and derivative (PID) algorithms with a generated pulse frequency from the digital I/O lines.

An L6203 DMOS full bridge driver (4A max current, 100kHz operating frequency) was used as the H-bridge circuit. An H-bridge is essentially a circuit that allows for a voltage to be applied across a load in either direction, thus allowing for either heating or cooling effects from the peltier. The H-bridge circuit is built from integrated solid-state switches within the L6203 chip. The control switches allows for current to flow in either direction, and is controlled by two standard 5V TTL voltage signals, which is sourced from the National Instruments Data Acquisition (DAQ) digital I/O board. Regardless of the current direction, the H-bridge passes the 12V signal and required current from the power supply directly to the peltier.

PID control was used as a feedback loop mechanism as it is able to calculate the error value between the desired set temperature and current temperature values. This calculation is then used to determine the amount of current forced through the peltier, allowing for a faster heating/cooling cycle when desired. The PID algorithm includes three separate parameters, and the schematic can be seen in FIGURE 3-2. For example in the control loop, it can be seen that each of the heating and cooling cycles of the peltier can be used to adjust the temperature of the liquid cell chamber to the desired set point temperature. As the thermocouple measures the actual temperature inside the chamber (feedback), the system then adjusts the heating and cooling until the temperature stabilizes at the desired set point value. The actual temperature from the thermocouple is the process variable, the desired temperature is the set point, and the heating/cooling stages of the process is the manipulated variable. The error (e) is thus the difference between the actual measured temperature and the set point.

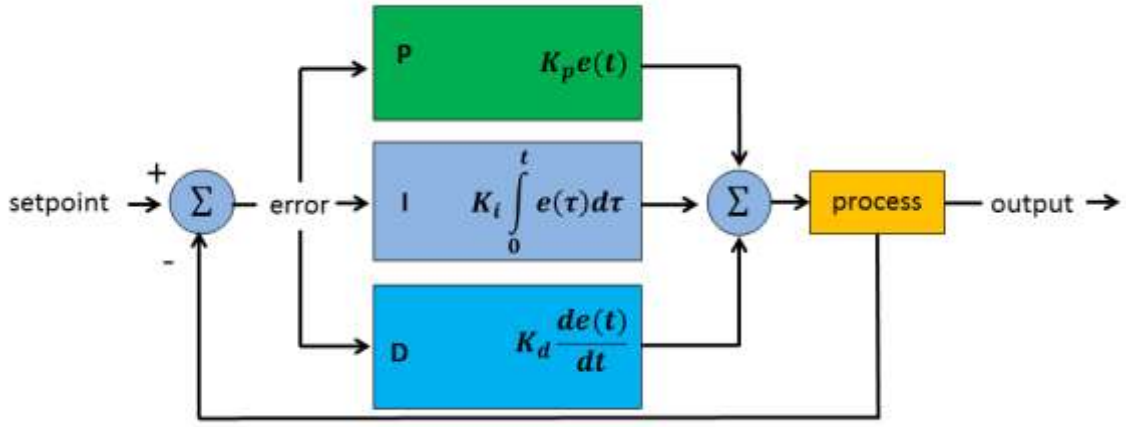

Figure 3-2: PID schematic with the formulas for control

For simplicity, the following description will describe a heating process for the chamber and PID control. Following the measurement of the actual temperature and then calculating the error, the PID system then determines how much to change the output, which can be seen as a valve with unlimited degrees of control, i.e., able to apply heat of various levels. When the PID controller first turns on or applies a current for heating the peltier, it may want to turn it on only slightly if the set point and actual temperatures are not too far apart, while it may turn to full heating current if the two values are very far apart. This is the proportional control aspect of the system. If the controller realizes that the heating is not increasing at a rapid enough pace, then it may try to open up the valve and increase the heating current more and more as time increases, and this is therefore the integral component of the system.

The major hurdle and difficulty in the fine tuning of the system is that when the change in heating is too large for the error value, the controller will lead to overshoot, where the temperature overshoots the desired set point value, thereby adjusting and providing a reverse current of cooling, overshooting, and then repeating nonstop. This creates an oscillating temperature around the desired set point with a constant, growing, or decaying sinusoidal type pattern. Therefore, to dampen the oscillations, the controller's adjustments have to be tempered through the derivative aspect of the control.

Many tuning methods were used, such as the well-regarded Ziegler-Nichols model from the 1940's, by adjusting the K_p, K_i, and K_d parameters which are constants seen in Figure 3-2. This method stated that K_i and K_d be set to zero, while only tuning the proportional K_p variable. Once the system has reached a stable oscillation, K_u (ultimate

gain of the proportional variable where the system oscillates) and the P_u (oscillation period) can be calculated to find the corresponding values for K_p, K_i, and K_d.

Table 3-1: Effects of increasing each of the K parameters on a PID system during tuning. (Ang *et al*, 2005, Zhong, 2006)

Parameter	Rise time	Overshoot	Settling time	Error	Stability
K_p	Decrease	Increase	Small change	Decrease	Decrease
K_i	Decrease	Increase	Increase	Large decrease	Decrease
K_d	Small decrease	Small decrease	Small decrease	No change	Improve

While the Ziegler-Nichols method of tuning provided a great starting point, it did not provide for an accurate and reliable temperature control for the system. The system would either continue to overshoot by a large amount, or undershoot whereby the temperature is never reached. Thus, custom manual tuning was used to complete the system. A table for the effects of increasing each of the Kp, Ki, and Kd parameters can be seen in Table 3-1. With the use of Table 3-1, the PID values were found, which provided an acceptable reaction time, followed by a small overshoot, and an immediate settling at the desired temperature. The temperature control was found to be accurate to ±0.05 ℃, with no degradation in quality over an extended period of time.

The last hurdle in the temperature control once PID tuning was completed was converting the PID output value into a digital I/O signal into the H-bridge circuit. The circuit control consists of two inputs (S0 and S1), whereby if S0 is on, and S1 is on, then heating would occur, and if S1 is on and S0 is off, then cooling would occur. Because the PID output was a value from -1 to 1 (max cooling to max heating), there was no direct method to convert that signal into a digital I/O output. Therefore, a LabVIEW program with a counter and pulse frequencies were used. It was found that a 40 pulses per second (40Hz) controlling signal produced the best results. The code generated a series of pulses corresponding to the PID value. For example a PID value of 1 (maximum heating) would generate a constant 5V output to the H-bridge, while a PID

value of 0.5 (medium heating) would generate pulses of on/off at equally spaced time periods so essentially the peltier would be heating half the time. Thus the pulse is able to switch on/off the digital I/O lines at a rapid rate, creating an output to the H-bridge from the PID values.

3.1.3 Temperature Calibration

The temperature control system was calibrated by monitoring the cantilever signal change with respect to the actual temperature change. A T-type thermocouple (copper/constantan, RS Components, UK) was used for its high sensitivity of ~43.0 μV/℃. As a calibration, temperature was changed in steps of 1.00℃ to validate the cantilever bending signals. Due to the gold coating on one side of the cantilever beam, thermal effects from raising the temperature create a compressive surface stress (downwards bending) of the cantilever, and vice versa for temperature decreases. From Figure 3-3, an upwards trending signal shows a downwards bending of the cantilever, as expected. It can be clearly seen that there is a direct correlation between the temperature change and the cantilever deflection signal, signaling that both the optical detection system and the temperature control system is fully optimized. The cantilever signal does not return fully to its original position due to inherent hysteresis of the material and properties of the cantilever beam.

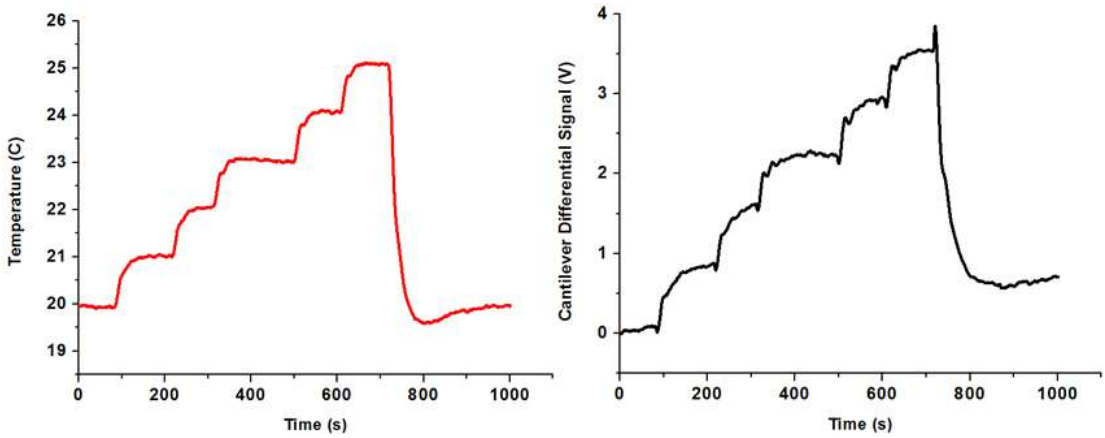

Figure 3-3: Temperature calibration data for the microcantilever system. Left shows the actual temperature monitored, and right is the signal change from the PSD in the cantilever.

3.1.4 Programming

LabVIEW 8.5 was used for all programming and controlling of the system. The inputs into LabVIEW include timings for fluid control, temperature, data acquisition

frequency, and miscellaneous control aspects. A LabVIEW state machine is a construct whereby a case structure is contained inside a while loop. The order and logic of execution of each particular case is determined by the output from the previous state, which is located in a shift register. When the output from one case is wired to the input of the case selector, the order of operation can then be determined.

The main advantage of using a state machine is that it allows for multiple steps to be linked in series so that there is no conflict between the executions of each step, which also allows for easier debugging. A string was used as the case selector, the advantage being that with the labeling of each case, the state machine in essence becomes self-documenting. In addition, this allows for the advantage of not being forced to include all cases in the first iteration of the program, whereby further cases can be easily implemented and added in the future. Although a disadvantage of this is that the string state can be misspelled creating numerous problems and becoming difficult to pinpoint which state is causing the problems.

Because there are so many aspects of the microcantilever system that requires constant control and monitoring, the program itself is extremely complicated. The front panel (Figure 3-4**)** that the user sees consists of 3 small XY graphs (temperature, differential, and sum) and 1 large XY graph (normalized cantilever signal). The top left of the front panel consists of the controls of fluid, and allows for programming the 6 channel fluid valve. This will be further discussed in the next section. Lastly, there are many parameters for temperature, file saving, and data acquisition frequency. File saving was initially performed by creating a very large array of all the data, and once the program was stopped, it would batch save the entire set of data into a text file in spreadsheet format. This obviously was not the best of ideas in case the program crashed or was stopped improperly, whereby the data would then not be saved. New versions of the file save would only take the new data points, and save into the same text file every time the while loop was processed, so this means that it would save once every 1-2 seconds or however frequently the program was set to capture data.

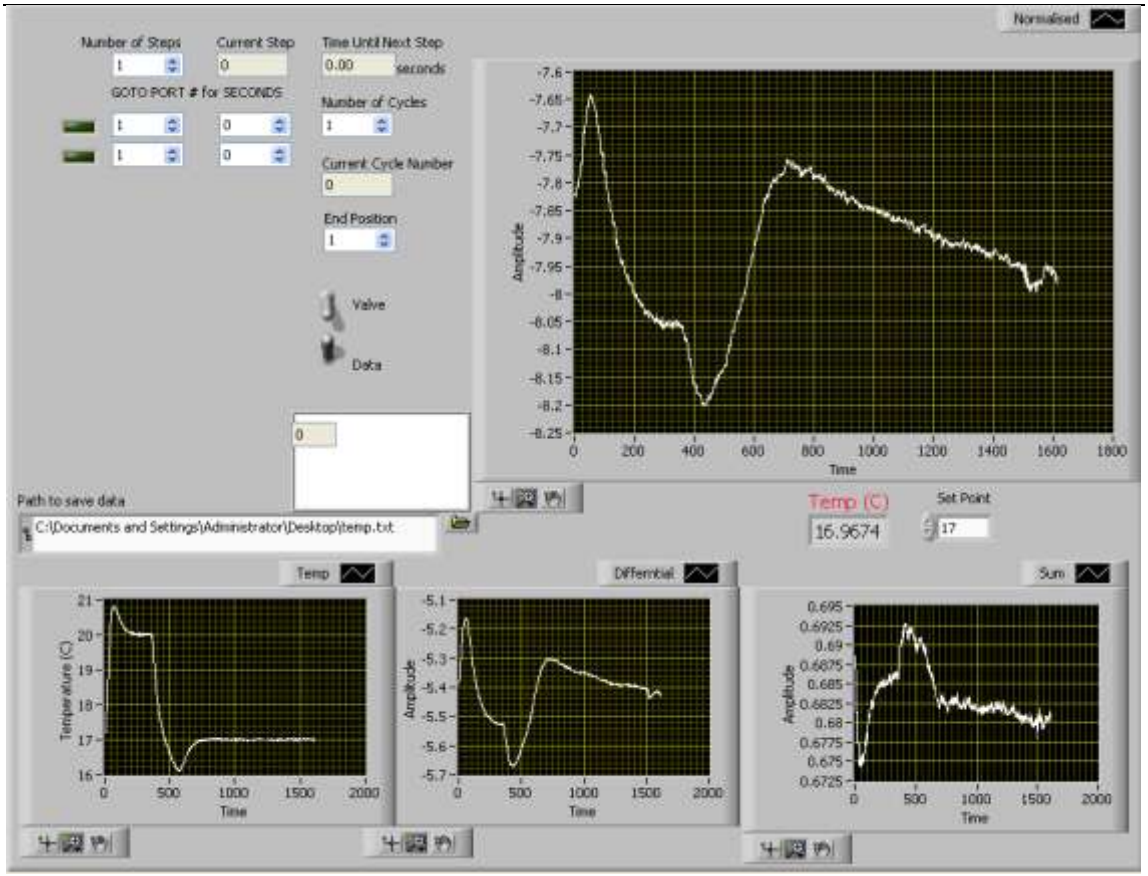

Figure 3-4: LabVIEW front panel for the optical readout system. This includes the fluid valve control, and values from the PSD and temperature.

For data acquisition, a standard DAQ system was used, with analog input running at continuous sampling, with the format of analog 1D waveform NChan NSamp. This means that the program would continuously run at the specified sampling rate, while placing the data points into a 1D waveform. The sampling rate is controlled by two variables: sampling rate, and samples to read at a time. Sampling rate is the frequency in Hz of the speed that the data should be acquired, while samples to read at a time determines how many data points should be read at once, before acquiring again. For example, a sampling rate of 10kHz with a samples to read at a time of 1,000, would provide 10 data points per second, because in order to reduce noise, the mean of the 1,000 samples is taken (down sampling) to increase the noise to signal ratio. Due to the relatively slow and long lasting response of the microcantilevers, a sampling rate of 10kHz and a samples to read of 10k was used, providing 1 data point per second, while giving the opportunity to take the mean of 10k points to reduce the noise dramatically.

3.1.5 Fluid Control

Fluid delivery into the chamber was controlled by a 6-way valve (Hamilton Modular Valve Positioner, Hamilton Bonaduz AG), a schematic of which can be as seen in Figure 3-5. The valve is able to rotate and take any of the 6 inputs to connect with the output. After control commands were determined, programming had to be performed to control the valves. As discussed earlier, the LabVIEW program consists of multiple inputs for the user so that the input number from valve, time, and sequence of inputs can be controlled. The functions required a series of separate controls within LabVIEW, using its built-in Visual Instrument Software Architecture (VISA) to control the valve through a standard RS-232 serial port (Baud 9600, Parity Odd, Data bits 7, Stop bits 1, Start Bits 1). The valve required an initialization before performing any commands, and required all the commands to be sent at once in order to function (list of commands in APPENDIX 1).

Much confusion occurred at this stage, as sending each of the commands required to operate the valve in series incurred no response. Therefore, the solution was to write all the commands together into a text file, and push all the commands through to the valve with VISA. Logic was also implemented to determine the shortest path from one input to another. This was a simple if-then logic of which direction to turn the valve. This was required to reduce the amount of turning the valve undergoes, to limit the amount of contamination or erroneous events from other inputs to the valve when it was switching. As the valve control was a separate function inside the LabVIEW program, a pause function was simply added to stop further commands for the user specified period of time. This allowed for automation of fluid injection into the system, which greatly enhances the capabilities of using multiple reagents.

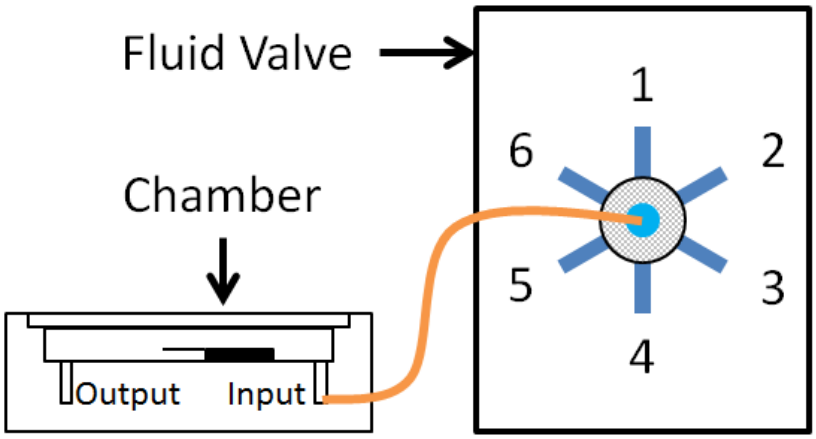

Figure 3-5: Fluid control valve with 6 rotary positions to control the liquid sample being injected into the flow cell chamber.

3.1.6 Cantilever Readout Systems

In order to utilize the signal from the PSD, there requires a method to quantify the data into an actual cantilever deflection. The microcantilever system uses a PSD to detect the reflection of the laser from the cantilever tip. The laser is focused and aligned with the tip of the cantilever, and as the cantilever bends, the reflective signal is then captured through the PSD, simultaneously measuring laser position and light intensity. PSD's works similar to a standard photo diode, having a diode that when exposed to the laser spot causes the local resistance and thus the electron flow to change (Wallmark, 1957). As the active surface area of the PSD comes in contact with light, the photocurrents that flow change direction and flow towards the p and n areas, but unlike a photodiode, the PSD distributes the current among the electrical contacts according to the position of the laser beam. The PSD consists of an n-type silicon substrate incorporating two resistive layers that are separated with a p-n junction. The contacts are placed at opposite ends of the p-type resistive layer on the front side, and if the PSD is two dimensional, there is an additional two contacts on the rear side on a n-type resistive layer. When the light spot of the laser hits the silicon, photocurrent is generated and flows from the laser point to the resistive layers of the electrodes. Because the resistive layers are extremely uniform, the current at each electrode can be seen as inversely proportional to the distance between the electrode and the light spot. The electrodes carrying current is then modified and the position can then be determined.

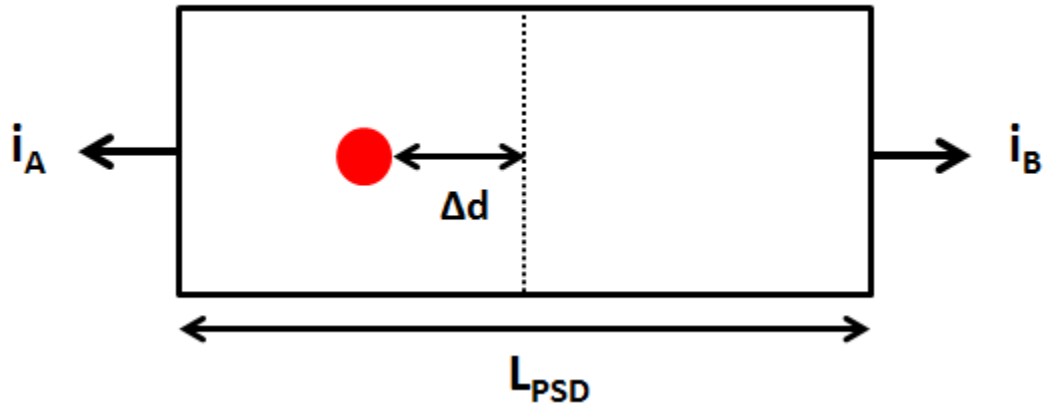

Figure 3-6: Schematic of the currents generated by the PSD when the laser spot is altered through cantilever deflections.

The PSD that is used is linear, i.e. it directly and linearly converts the laser spot into two currents (i_A and i_B) from its two ends as shown in Figure 3-6. The currents can then be outputted into an amplifier, which take the photocurrent from the electrodes and process the signals in a way that can be measured, i.e. X, Y, and SUM (light intensity, I_A+I_B) outputs. For a one dimensional PSD that is used, the position can be calculated by:

$$\boldsymbol{Y = \frac{L_{PSD}}{2}\left(\frac{I_A - I_B}{I_A + I_B}\right)} \qquad \textbf{(3.1)}$$

Where L_{PSD} is the length of the PSD area, and I_A and I_B are the currents in opposite directions.

As the laser spot reflection moves due to the changes in cantilever deflection, the positional change in Y can be determined to be:

$$\boldsymbol{Y = \frac{L_{PSD}}{2}\left(\frac{\Delta(I_A - I_B)}{I_A + I_B}\right)} \qquad \textbf{(3.2)}$$

The output from the PSD amplifier is then connected to the DAQ device. As the initial cantilever system utilizes a one dimensional PSD, the only inputs that are necessary are the Y and SUM signals, which are converted from a voltage equation after translating the currents. A major problem that caused many discrepancies was the misinterpretation of the data. It was assumed that the differential signal outputted from the amplifier

needed to be normalized by the SUM signal. Thus a normalized cantilever bending signal was then calculated within the LabVIEW program to normalize the discrepancies from the voltage, because as the light intensity varies (from ambient room lighting, sapphire glass reflection, and variations in cantilever reflection), the Y signal can change as well as the currents in the photodiode would be constantly changing with the light intensity. Therefore, the signal was normalized by taking Y and dividing by the SUM signal.

$$\Delta \boldsymbol{z} = \frac{\boldsymbol{L}\times\boldsymbol{L_{PSD}}}{\boldsymbol{8s}}\left(\frac{\Delta(\boldsymbol{A}-\boldsymbol{B})}{\boldsymbol{A}+\boldsymbol{B}}\right) \quad \textbf{(3.3)}$$

This turned out to be incorrect, as the PSD amplifier that was used outputted the same range of differential signals regardless of the intensity of the light. Therefore, the signals were normalized automatically internally, and thus the cantilever deflection can be directly determined by calculating the distance that the laser spot moves on the PSD, followed by translating the distance to the deflection of the cantilever itself through the equation:

$$\Delta \boldsymbol{x} = \frac{\boldsymbol{l}\times\Delta\boldsymbol{d}}{\boldsymbol{4s}} \quad \textbf{(3.4)}$$

Where Δx is the cantilever deflection, l is length of cantilever, Δd is the distance the laser spot on the PSD moved, and s is the distance from the cantilever tip to the PSD. Therefore, the cantilever deflection of Δx can then be calculated.

For calibration of the system, the laser beam is required to focus on the very tip of the cantilever beam, to maximize the readout signal as the tip is where the most deflection occurs. The system is adjusted by moving the laser until it is centered on the cantilever tip, and at the same time, the PSD is used to ensure that there is a reflective signal. Once a signal is achieved by realizing a positive SUM signal, then the laser is further adjusted to create a balance having the maximum SUM signal while still focused on the tip of the cantilever. While it is impossible to achieve the maximum sum signal while the laser is focused at the very tip of the cantilever, a signal of >50% of the maximum sum signal can be achieved at the tip of the cantilever, creating enough reflectivity signal to sustain signal quality. Lastly, the Y position (X and Y for the multiple cantilever arrays) of the

laser should be centered to 0 to allow for maximum possible signal change, although it is not required as the signal change is not large enough to reach the full ±10V swing that is possible.

3.2 Laser Scanning Multiple Cantilever Array Readout System

Optical readout systems offer an easy to use, reliable, and highly sensitive method to monitor cantilever deflection. But the main limitation in the use of this readout scheme is the difficulty in interpreting the signals from arrays of cantilever sensors. One method is to employ an array of laser beams and focus them sequentially on the cantilever sensors (Archibald *et al.*, 2007). However, the disadvantages of this approach include the difficulty in alignment, the need of multiple laser diodes or optical fibers, and higher cost and complexity for the system. Therefore, in order to develop and implement an all in one, fully automated, and user friendly system, the second version of the microcantilever system, based on Martinez *et al.*, (2010), utilizes a scanning laser beam to essentially "scan" across multiple cantilevers, with the subsequent beam reflections being monitored through a two-dimensional PSD. How the system works can be seen in Figure 3-7.

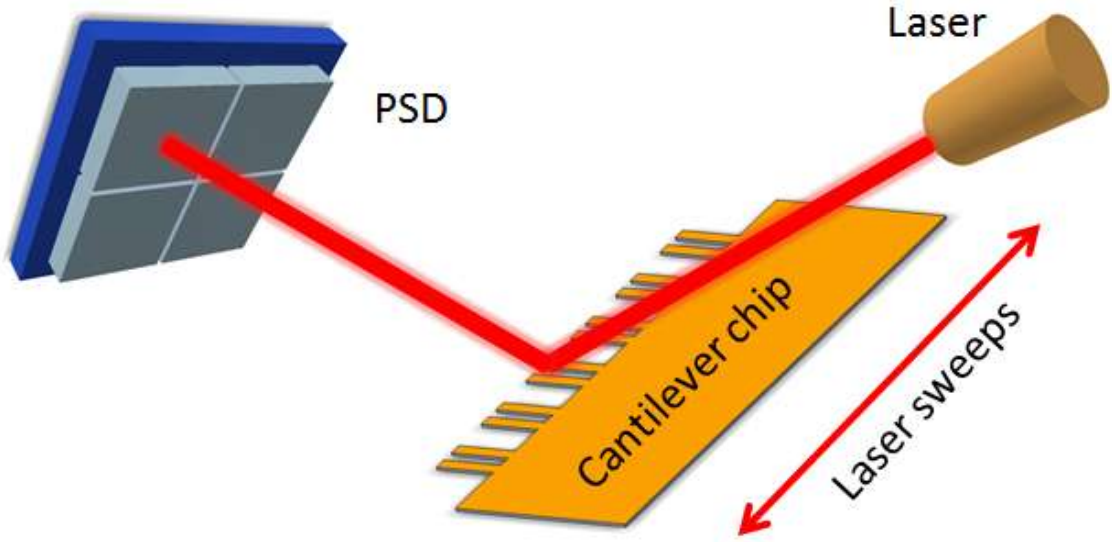

Figure 3-7: Laser scanning multiple cantilever readout system

The major difference between the laser scanning multiple cantilever detection version compared to the single cantilever version of the system is the addition of a linear

actuator (SMAC LASW20, USA). This allows for a laser to be mounted on top of the actuator, performing a scanning motion to sweep the laser beam across multiple microcantilevers. The workings of the linear actuator involve a piston that rides on a linear bearing carriage, and this slides on a linear guide rail. There is a copper coil that is mounted on the piston, and the coil resides inside a magnet. As current is injected through the coil, a force is produced creating motion to the piston along the guide. While there are bumpers on the ends of the piston travel to prevent excessive impact force, there are also flags mounted on the piston to active limit switches before the end of the travel distance is reached. There is also an optical encoder, so that the distance travelled can be read as the piston is moved. The linear actuator requires a controller and communicates with the computer through a standard RS-232 serial port with a +24V power supply. A schematic demonstrating the system with the actual lab setup can be seen in Figure 3-8.

The system consists of a controller, cable, and actuator. The controller first generates movement of the actuator as is commanded by the software, and the position of the actuator is constantly fed back from the encoder, while simultaneously being monitored by the controller. The controller automatically attempts to minimize the error of movement through PID control variables that are set (default PID values were used as they were sufficient for this application, but can be programmed if stringent requirements are necessary).

Before programming can occur, there is a set of acceleration and velocity values that need to be calculated. For velocity, a test at 5mm/s was performed initially, but it was found that 2.5mm/s provided slower but more stable results. In order to set the controller to a certain speed, the encoder update period has to be calculated. This can be seen through an example of a desired velocity of 10mm/s with a 5 micron encoder, where the update period would be 200us. So

10mm/s × 200 (counts/mm) = 2000 encoder counts/s
2000/5000 (update period/s) = 0.4 encoder counts per update period
0.4×65536 (internal constant) = SV26214 (Set velocity to 26214 = velocity of 10mm/s)

A similar calculation can be performed for acceleration, for example of having a desired acceleration of 100mm/s^2:

100mm/s^2 × 200 (counts/mm) = 20000 counts/s^2

20000/5000^2 (update periods/s^2) = 0.0008 counts/update period^2

0.0008 ×65536 (internal constant) = SA52 (Set acceleration to 52 = acceleration of 100mm/s^2

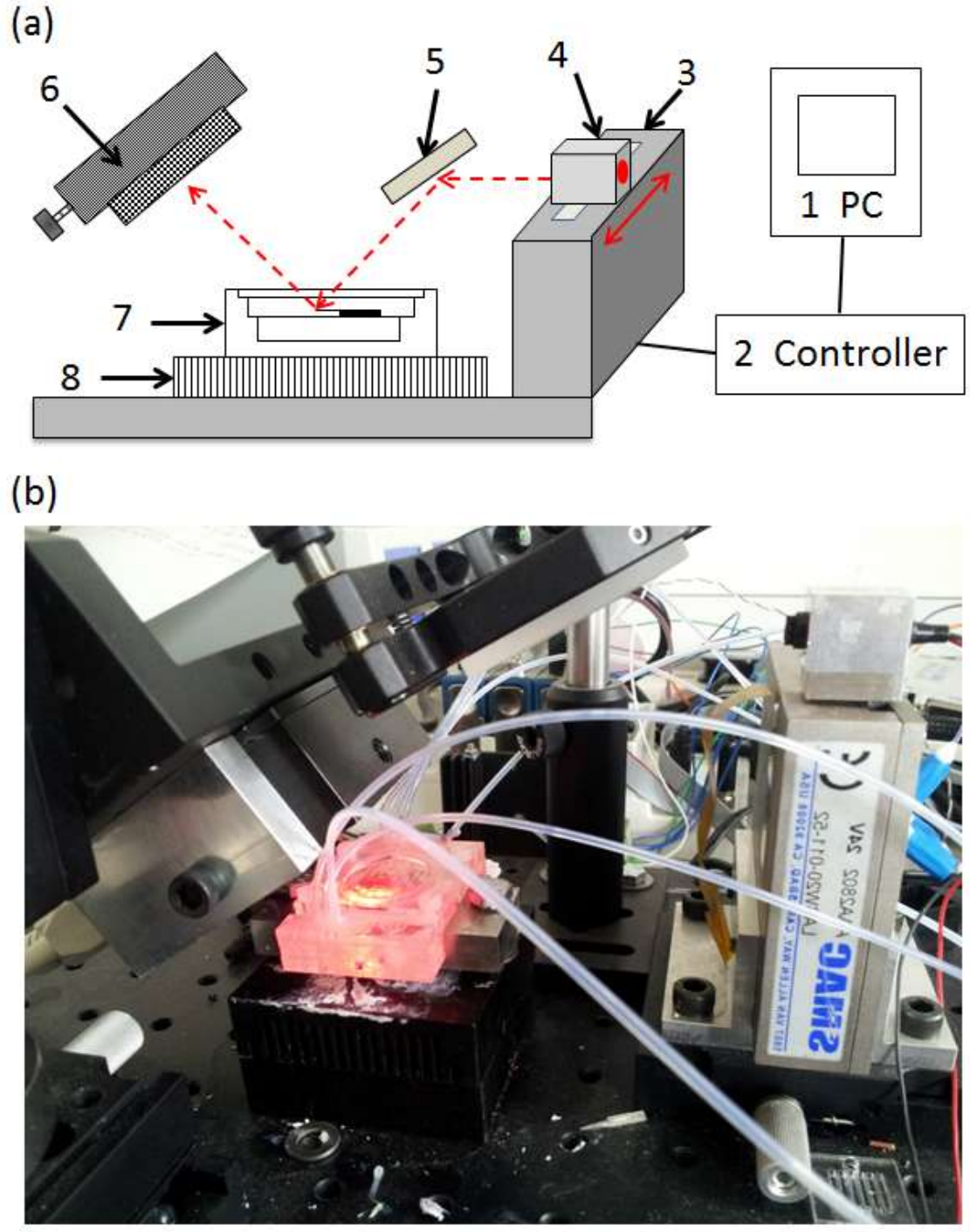

Figure 3-8: a) Schematic of the control of the laser scanning microcantilever readout system which includes: 1) Computer 2) Linear actuator controller 3) Linear actuator 4) Laser diode 5) Mirror 6) PSD 7) Liquid flow cell housing with microcantilever array 8) Heatsink. b) Actual setup in the lab.

3.2.1 Programming

The scanning microcantilever system has many similar properties to the initial static system. While the readout features are the same, the lack of a fluid control that requires pausing for user inputs can be disregarded, and therefore the state machine is not used in

this system. The scanning system though, because of its use of a linear actuator required extensive programming to synchronize the scanning of the laser to the data acquisition of the system.

The first challenge was to program the linear actuator to perform a sweeping motion scanning across the microcantilever array. The SMAC controller utilizes a programming language similar to that of assembly code. The code is stored in non-volatile RAM inside the controller, and consists of a two-letter command followed by a number. There are three methods of controlling the actuator. The first is the Force mode where it is open loop, receiving no feedback from the encoder, whereby actual position is still monitored, but has no effect on the output. The second is Position mode, where the actuator can be moved to various positions along the distance of the piston. It uses acceleration, velocity, and force settings to move to either an absolute or relative position. Lastly, there is the Velocity mode, where it allows the actuator to be moved with a given velocity, acceleration, force, and direction. Position mode was selected to move the laser across the cantilevers to a given position, moved back to the original position, moved across the cantilevers again, etc.

Commands to the linear actuator are through standard ASCII characters with a carriage return, but without linefeeds. There is also a requirement for a 250ms gap period in between each command that is sent, to prevent the interface from ignoring or missing the sent commands. In order to initialize the actuator to begin usage, a series of commands are sent, which are stored in a text file and each line is read 250ms apart by LabVIEW's VISA architecture and sent to the actuator. The initialization file can be seen in APPENDIX 1.

Designing the program to synchronize the laser scanning process with the data acquisition in addition to recording only the data points where the laser was focused on the very tip of the cantilever was a challenging task. The first method that was used was to do an initial scan over the cantilever tips. When the laser was focused on the center of a cantilever, the SUM signal from the PSD would naturally be at its highest intensity due to the most reflected light from the cantilever beam. Therefore, in a 12 cantilever array that was used for experiments, there would be 12 peaks or highest SUM values after the initial scan. The data points on the initial scan were saved into an array and the

position of the peaks were then determined and saved as well. After the initial scan, each following scan would only take the saved positions of the initialization scan into account. While this system theoretically sounds like an efficient and accurate way of acquiring the signals, there was a fundamental problem to this solution. The peaks or maximum SUM positions in the array would change over time. For example, if the initial scan acquired that the first SUM signal peak was at array position 100, after an hour, that array position may have moved to array position 110, but the program would still be reading array position 100, therefore acquiring the incorrect data value. This created a constant drift in the signal, which would be completely unsuitable for use in experiments. The reason for this drift is probably due to the fact that while the linear actuator encoder is very accurate, there is always a slight difference in the positions that it is asked to move to, and thus after every successive move, the start and end positions would alter slightly, expounding the difference after a longer period of time.

The solution to this problem was a simple one, which was to scan the entire cantilever array and find the peak SUM signals after each scan, which would reflect the location of the cantilever tip (Figure 3-9). Although this was more calculation demanding and slower, it allowed for more consistent signals over a long period of time. While the linear actuator is sweeping the laser across the cantilevers, LabVIEW is programmed to simultaneously capture the X, Y, and SUM data from the two-dimensional PSD. Each of the X, Y, and SUM data points are saved into their respective arrays. Using an X-Y peak detector algorithm, the peaks within the SUM array can be found, using necessary parameters such as minimum peak height and width of peak (i.e. number of data points the peak must contain). The array positions for the peaks that are found are then saved, and the found positions are used to extract the peak positions from the X and Y arrays, providing the X and Y data points for the cantilevers. There was an issue with the peak detector, as there were sometimes random noises or unexplained smaller peaks that occur during the scanning, which also gets picked up by the peak detector algorithm. The solution to this problem was to do an initial scan, manually locate the peaks, and separate them into different regions for the peak detector algorithm. For example, if there are peaks at array position 1000, 2000, 3000, and 4000, then the regions would be set from 500-1500, 1500-2500, etc. Then, limiting the peak detector algorithm to detect only one peak of the highest magnitude in that region, it allows for consistent array position tracking of the highest SUM values. Once the array position for the peaks are

determined, then it is simple to select the points in the X and Y arrays with the same array positions, and use only those data points and plot the signals on the LabVIEW front panel shown in Figure 3-9.

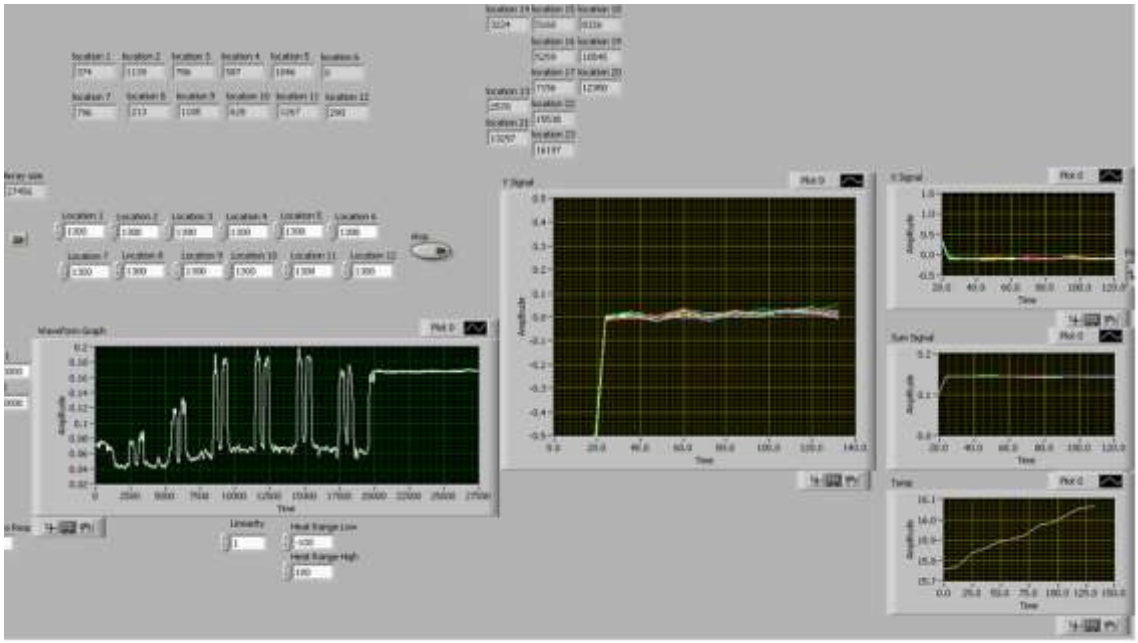

Figure 3-9: LabVIEW front panel for laser scanning cantilever array system. This includes the peaks detection along with data from the PSD and temperature.

Synchronization of moving the linear actuator with data acquisition was achieved by sending the commands for the required movement to the actuator controller. Because the controller needs a "GO" command to begin movement, data acquisition and the "GO" command were started simultaneously, and data acquisition was stopped after 5 seconds (time can be calculated from knowing the speed and distance of movement). Time was once again calculated by a timer function outside the main WHILE loop, with a separate timer within the while loop that resets after each iteration of the loop. Taking the inner timer and subtracting the outer timer gives a real-time calculation of operation time, which is used to save data in addition to plotting on X-Y plots.

After testing, it was found that a scanning speed of 2.5mm/s, with a sampling frequency of 5kHz, generated 10k data points which was sufficient to perform peak analysis and to obtain stable results over a long period of time. The linear actuator was set to move relative to its current position, moving 50,000 (10mm) encoder counts in one direction, followed by moving back -50,000 encoder counts to its original position. While it was possible to capture data moving both back and forth, unless the range of movement was

centered exactly over the cantilevers, it would have required extra calibration and initial region setup. Therefore it was decided that data capture would only occur during movement in one direction only, as experiments do not require such fast data capture speeds.

3.2.2 Scanning Live Cell Culture Chamber Design

The scanning chamber design is similar to the one in the single microcantilever design, but there are many fundamental changes and enhancements that have been adopted. The biggest challenge for this chamber is the addition of a method to expose the liquid inside of the chamber to 5% CO_2 gas, without leaking or external interference, in order to make the chamber suitable for culturing cells. Therefore, a gas permeable membrane was used as a barrier between the gas and liquid, which does not introduce bubbles into the system, only exposing the liquid to the extremely low pressure CO_2 as needed. Teflon membranes (Katco, EU) was found to be highly gas permeable, particularly at low thicknesses, therefore 12.7 µm Teflon sheets were used as the boundary layer between the gas and the liquid sections of the chamber. Typical cell culturing methods in an incubator store the cells and media inside a gas permeable flask or petri dish, but with a cantilever system that requires both optical transparence and being self-contained, that was not an option. The only option was to use a gas permeable membrane that seals off liquid, but also allows the correct concentration of CO_2 to pass through and expose the media.

The initial cantilever chamber design consisted of 7 layers of 1mm and 2mm thick Poly(methyl methacrylate) (PMMA), constructed together through the use of double sided tape (3M, 50 µm). The bottom is a base layer, followed by a thermocouple layer, a cantilever holder layer, liquid flow layer, gas flow layer, liquid exit layer, and a top cover to seal the chamber. The base layer is the layer that would be in contact with the metallic holder, with no entrances on its surface. The second thermocouple layer, when sandwiched between the base layer and the cantilever holder layer, allows a thermocouple to be inserted to monitor the temperature of the chamber, crucial for cell culture studies. Both the thermocouple and cantilever holder layer have M2 tapped screw holes to allow for mounting of the cantilever along with the holders. The fourth layer is the liquid flow layer, whereby liquid cell culture media is injected utilizing a curled design to elongate the distance the liquid would travel to increase its exposure to

CO_2 gas. On top of the liquid flow layer is the Teflon permeable membrane, followed by the gas flow layer. On the top section of the gas layer, 5% CO_2 gas is flowed through, whereby exchanging gas into the liquid media when the media is injected into the cantilever chamber. The next liquid exit layer is where the liquid would exit. The exit layer was placed on top to enhance the ability to extract bubbles that naturally float on the surface of the chamber. Lastly, the uppermost layer consists of a cutout for the glass optical piece, which is sealed to the chamber through a silicon O-ring. The design can be seen in Figure 3-10.

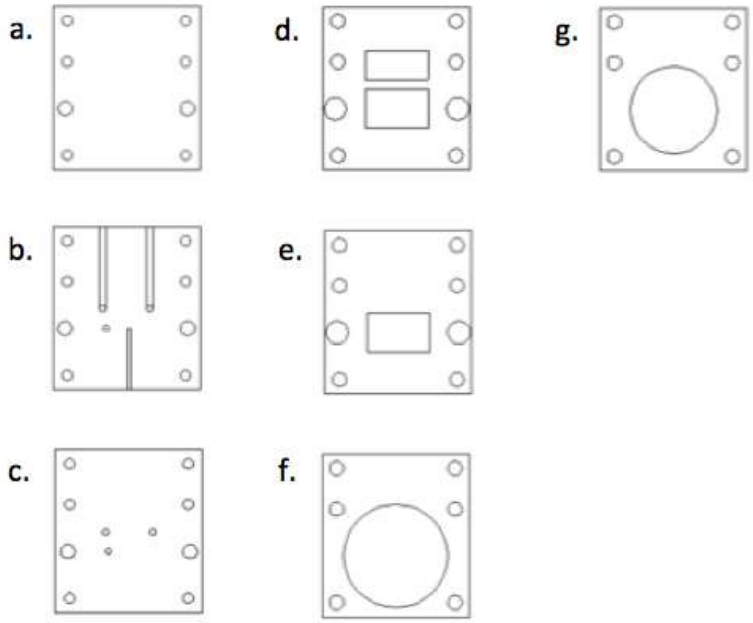

Figure 3-10: Scanning flow cell chamber design. a) Bottom base layer. b) Liquid input layer with slot for thermocouple. c) Liquid input layer to allow bottom liquid channels to connect with the chamber liquid well. d) Layer to separate gas and liquid flow. e) Cover up gas layer while only exposing liquid chamber area. f and g) Cover to fit in 25mm sapphire glass to seal the chamber.

While this design was sufficient as an initial first step, it was soon realized that there is a major design fault in the gas exchange system. The only liquid that is exposed to gas is during the injection phase, and not in the actual chamber itself where the liquid is contained. Therefore, because experiments do not constantly inject new media, in addition to the small channel for the liquid entrance, means that there is insufficient gas permeability or diffusion into the liquid media. When the chamber is sealed and after the initial media is injected, there is absolutely no flow or movement inside the

chamber, which never allows the area of liquid that was exposed to gas to mix with the rest of the liquid. Therefore this design was changed to a new version.

The new version of the cantilever chamber is similar, except for expanding the area where gas and liquid can exchange. The overall design remains the same, aside from the added layer to expand the cantilever holder layer to a larger size that encompasses both the original liquid section in addition to the gas section. (Figure 3-11) This means that the liquid inside the cantilever chamber, not just the injection area, would be constantly exposed to gas through the gas permeable membrane. This design is the final design that is used for all successive experiments, and no design flaws have been found. For all the designs, epoxy is used to seal the tubing at the inlets and outlets, to prevent air bubbles from entering the system.

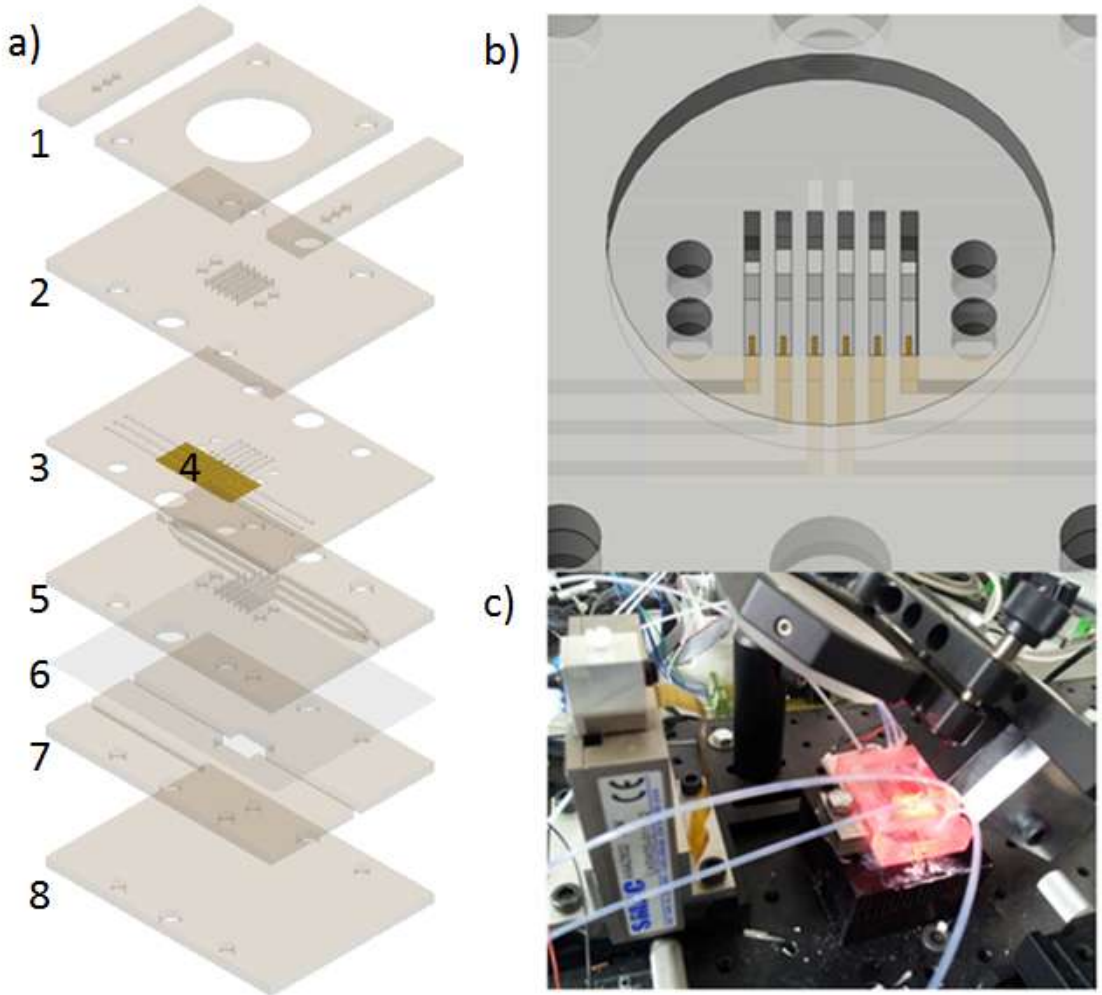

Figure 3-11: Microcantilever system setup integrated microfluidics. a) 1) Top cover with tubing connectors. 2) Layer with channels only to mate with cover. 3) Input channels. 4) Polyimide microcantilever array chip. 5) Output channels. 6) Gas permeable membrane. 7) Gas flow layer with slot for thermocouple. 8) Bottom base plate. b) Top view of the microcantilever sensor array mounted in the chamber. c) Actual chamber and system in the lab with scanning laser, temperature control, microfluidic channels, and PSD.

3.2.2.1 CO2 Laser Fabrication of PMMA

Carbon dioxide lasers (CO_2) was invented in 1964, and are the highest power continuous wave lasers, which is particularly useful with their high efficiency and ease of construction. Their gases (CO_2, N_2, and He) are mixed and led into a discharge tube with a few torr of pressure. The gases travel through the tube in one second and is pumped out of the other end with a mechanical forepump, with an electric discharge that is maintained at the ends of the discharge tube. The left full mirror is fully reflective, and the right mirror is partially transmitting, therefore creating a laser that radiates at 10.6 microns.

The Speedy 300 laser by Trotec is utilized, with a 120W maximum power and a large workspace area. The main advantages of this system are the ease of use with all CAD drawings and maintenance free designs. PMMA sheets can be easily laser machined into the proper specifications required for the chambers that were used in the scanning cantilever array experiments. The best parameters that were found for the cutting of 2mm PMMA was 25% power (30W) with a cutting speed of 1cm/s and 3 passes. This was found to give cleaner cuts than a higher power and/or slower speed with 1 pass.

3.3 Portable Microcantilever Detection System

Microcantilever readout schemes using piezoresistive methods work by detecting changes in the resistivity of the material in the cantilever as stress is applied (Minne *et al.*, 1995, Tortonese *et al.*, 1993). When a piezoresistive material such as doped silicon incurs a strain, its resistivity changes and can then be measured by external electronics. Because cantilever biosensors were derived from AFMs, piezoresistive cantilevers were also first used as an alternative readout method for AFMs instead of the optical

detection method (Tortonese *et al.*, 1991). Piezoresistive cantilevers have been demonstrated to be able to perform chemical (Yang *et al*, 2003), magnetic (Yuan *et al.*, 1994), gas (Su *et al.*, 2002), tactile (Noda *et al.*, 2006), and mass (Jin *et al.*, 2006) sensing experiments. One of the main advantages of piezoresistive readouts is that the readout electronics can be integrated onto the same chip and also that they work in liquid media of any opacity. Disadvantages include more built in noise from the electronics, affecting the sensitivity and resolution of the detection scheme (Yu *et al*, 2002).

3.3.1 Design and fabrication

While silicon or polyimide microfabrication of custom sensors is currently a very viable option, it is not cost effective for mass production of devices. Therefore, off the shelf commercial piezoresistive strain gauges were used as the sensor device. Its basic transduction property through resistance change can be defined as:

$$\boldsymbol{R = \frac{\rho l}{A}} \qquad \textbf{(3.5)}$$

Where R is the resistance, ρ is the resistivity, l is the length, and A is its cross-sectional area. From the equation, as the strain gauge undergoes tension, resistance increases and vice versa.

Polyimide strain gauges with dimensions of 1.6×2.5mm with a thickness of 40μm were sandwiched in between polyimide film. The commercial strain gauges were supplied in a single row of 16 gauges connected in serial as shown in Figure 3-12. Conversion of the strain gauges into cantilever sensors required laser micromachining to cut the surface along the gauge active area. The area of the strain gauge itself was 200 μm wide by 1mm long. In order to reduce the cantilever dimensions to the smallest possible, precise alignment had to be used to minimize the border of the cantilevers. In the first process, a mask on a piece of paper was cut with the laser to the size and shape of the entire cantilever array, and stuck to the laser platform. Then, manually by eye and hand, the array was placed as best as possible to fit perfectly into the mask that was previously cut. This was the alignment, and the cantilevers were cut with the laser along the edges of the strain gauge elements. This was a massive failure, as the <50 μm border was not

possible to align by this method. At best, this provided a few hundred μm of alignment. A better approach had to be developed.

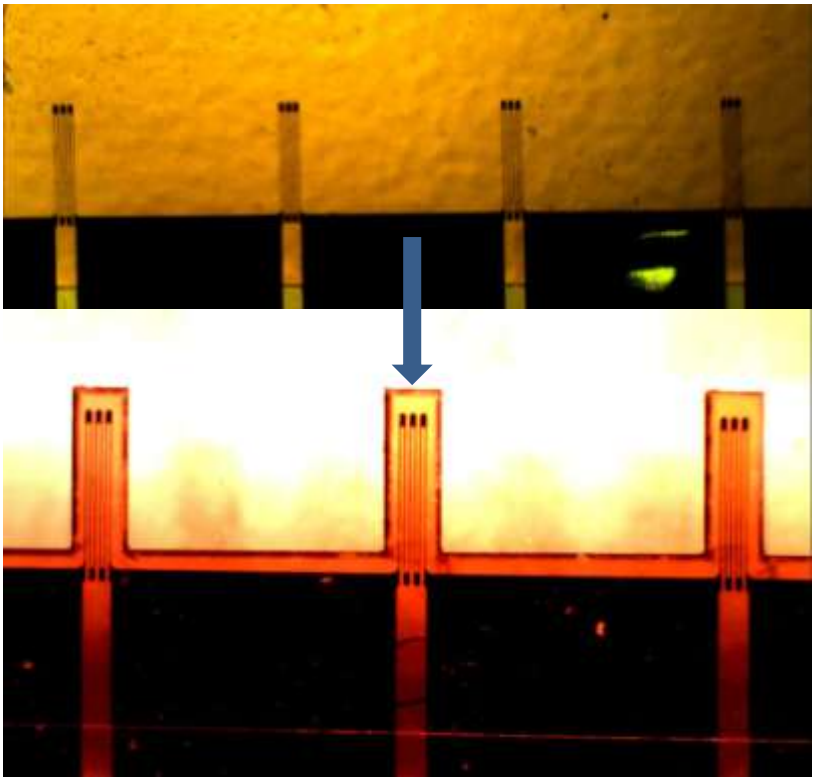

Figure 3-12: Strain gauges commercially sourced, and strain gauges after laser micromachining into piezoresistive cantilever sensors.

The solution was similar to the previous method, but instead of cutting out the entire shape of the cantilever array, only the cantilevers were cut onto the piece of paper that was first stuck onto the laser platform. So the process proceeds as follows.

1) Tape a piece of paper that is larger than the required cut onto the laser platform table.
2) Determine the lowest possible power output and/or fastest speed for the laser to give the smallest spot size and least amount of burning of the edges and cut the outline of the cantilevers on the piece of paper.
3) Place the strain gauge array on top of the paper.
4) Use a miniature microscope (a 200X zoom miniature microscope was used, Veho, UK) to align the strain gauges within the outline of the cantilever on the piece of paper.

5) Without moving the aligned strain gauges, use weights to weigh down the strain gauge array to prevent any movement.
6) Remove the microscope and laser machine the cantilevers onto the strain gauge array.

With this solution, an alignment within 25 μm on each side could be achieved reliably, although not quickly. Because this fabrication did not require large batches of sensors, this method was suitable due to its accuracy and lack of a more refined solution, and thus was used extensively during many future laser micromachining processes, results of which can be seen in Figure 3-12.

3.3.2 Piezoresistive Readout Scheme

A Wheatstone bridge setup was used as the electronic readout system as any signal from the strain gauges is so miniscule that they require large amplification in order to be read. Wheatstone bridges are the most common electrical circuits for the readout of piezoresistive sensors. They are used to measure the small resistance changes in devices such as strain gauges that would otherwise be very difficult to detect by any other means. The schematic of a Wheatstone bridge can be seen in Figure 3-13.

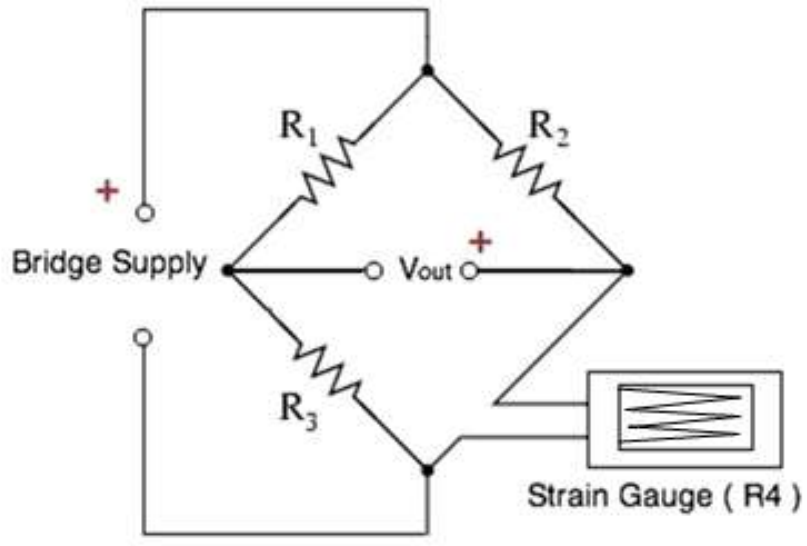

Figure 3-13: Wheatstone bridge schematic

A Wheatstone bridge consists basically of two voltage divider circuits. When the following equation is satisfied,

$$\frac{R_1}{R_3} = \frac{R_2}{R_4} \quad \textbf{(3.6)}$$

The bridge becomes balanced and V_{out} = 0. Three precision resistors are used in conjunction with the strain gauge to balance the bridge. Moreover, as a single strain gauge was used purely for testing purposes in this quarter bridge setup, it can easily be made to accept half bridge or full bridge setups with 2 or 4 strain gauges in the Wheatstone bridge being read simultaneously. When the strain gauges undergo tension or compression, the output voltage will change as the bridge becomes unbalanced as shown by this equation:

$$V_{out} = \left(\frac{R_4}{R_2+R_4} - \frac{R_3}{R_1+R_3}\right) V_{bridge} \quad \textbf{(3.7)}$$

Since a 120Ω strain gauge typically only experiences a 0.2Ω change per micro-strain, amplification is needed in order to see measurable changes.

A readily available commercial strain gauge amplifier that incorporates a Wheatstone bridge was used as the amplifier platform. (RS Components, UK) Due to low changes in resistance, strain gauge amplifiers require large amounts of common mode rejection ratio. The output of V_{out} before amplification with a 5V bridge supply could be less than 1mV. This strain gauge amplifier satisfies the need for a high common-mode rejection ratio (CMRR) by controlling the bridge supply precisely, removing any common mode voltages. It was then set up to produce a gain of 1000, providing outputs in the range of a few volts so that the system can be easily read on a computer. LabVIEW 8.5 was used as the data acquisition software to read the changes in the strain gauge sensors. Sensor arrays are able to plot a detailed special distribution of the hand. Because of the amplification, peak-to-peak voltages of over 3V were achieved, allowing for very precise detection of any strain that was placed on the sensors.

Any force applied on the sensors creates either a tensile or compressive stress on the strain gauges. A tensile force results in a positive voltage change while a compressive force produces a negative change in voltage. Experimental testing was limited to two Wheatstone bridge amplifiers, allowing for a maximum of 8 sensors to be detected

simultaneously. In addition, the use of Wheatstone bridges allows for compensation sensors, that is, using one sensor in the bridge as a reference sensor to compensate for any external forces that would act on all of the sensors, or to disregard strain changes due to temperature variations. This leads to a highly increased signal-to-noise ratio, allowing for more precise measurements.

As the Wheatstone bridge requires to be fully balanced, the resistors and sensor devices have to be incredibly precisely fabricated to be at least within 1Ω of each other. Additionally, the effects lead wires and connector impedances also come into consideration. If all the elements are not identical, a Wheatstone bridge becomes unbalanced as the equations discussed earlier shows, thereby greatly reducing its sensitivity and usefulness as a platform for monitoring changes in the sensors, and in some cases, will stop functioning completely. This leads to another problem if a Wheatstone bridge were used. Fabricating piezoresistive sensors with better than 0.1% resistance tolerance requires high levels of controls, costs, and repeatability, which may not be possible for some applications due to high costs, especially if it were to be mass produced for commercial uses. The strain gauges that were used were commercially sourced in an array of 16 strain gauges on one row. All the gauges are connected in serial with each other, meaning that one broken gauge disconnected the entire system. Also, the manufacturer had problems with reliably fabricating the gauges without massive amounts of rejected or unusable gauges from either broken connections somewhere in the array, or unsatisfactory tolerances where the gauge would not be within $120 \pm 1\Omega$.

Using analog multiplexers could solve broken gauges along the serial connection, but analog multiplexers cannot be used for Wheatstone bridge sensor arrays. Analog multiplexers, when turned on, produce a built in R_{on} resistance, which makes the bridge highly unbalanced. This is not factoring in the problem where R_{on} varies each time a different sensor is multiplexed. Another problem that arises is that if a full bridge of 4 sensors were used, it is not possible to determine which of the 4 sensors is undergoing strain..

3.4 Laser Micromachining

Laser micromachining has been an essential process in the design, development, and fabrication of all three cantilever detection systems.

3.4.1 Nanosecond Laser

In the beginning, there was only access to the nanosecond laser by Inazuma, a schematic of which can be seen in Figure 3-14. It is a solid state q-switched that can be operated in three wavelengths, 1064nm (IR), 532nm (Green), and 355nm (UV). The fundamental wavelength of 1064nm can be doubled to 532nm and tripled to 355nm. The pulse duration is 30ns, and an average power in IR wavelength of 30W, although the pulse energy depends strongly on the repetition rate. The power is 30W at 15kHz, therefore making it 2mJ pulse energy. Each wavelength has a separate output aperture, creating three independent beam paths, whereby each beam is expanded and focused into the scan head, which consists of two beam steering mirrors. Precise focusing was performed to be within 0.1mm of the optical distance, by performing 1 cut at each distance, as the best focus would produce the smallest laser spot size and highest energy. Therefore the focus distance that provided the smallest cut line width and cleanest cut was chosen as the best focus.

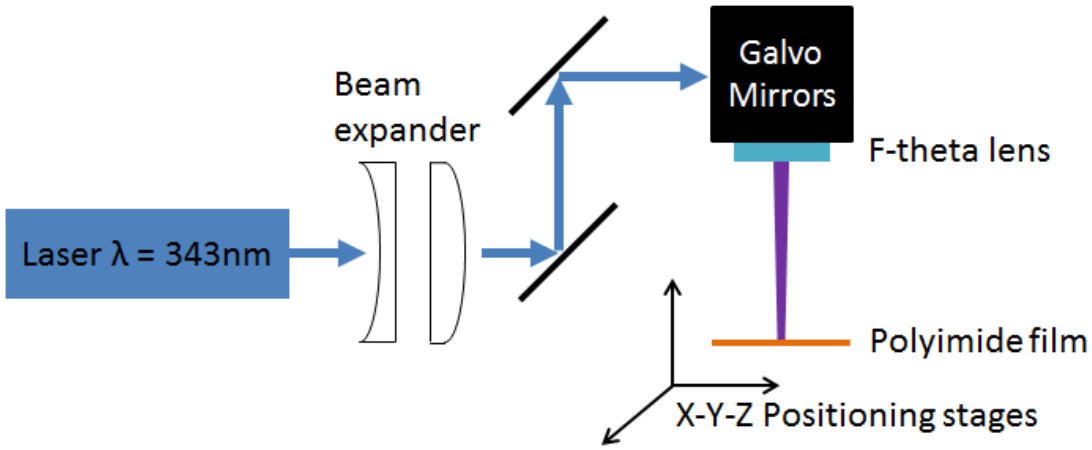

Figure 3-14: Schematic of a nano- and pico- second laser

The Inazuma laser as a solid state laser used a crystalline rod that is doped with ions to provide the energy states that are required. The population inversion, which means that the molecules are in a state where there are more members in an excited state rather than lower energy states, is steady in the dopant. Q-switching is the method used for the laser to produce a beam that is pulsed. This method compared to mode-locking creates lower pulse repetition rates, higher pulse energies, and pulse durations that are longer. As most laser micromachining was performed for laser ablation, which is removing the material from a solid surface with the laser, lower repetition rates and higher pulse durations create events that are unfavorable. For example, as seen in Figure 3-15, while

these cantilevers were fabricated with the picosecond laser for better results, the edges along the edge of the cantilever beam is still black, due to too much energy required to remove the material, thus charring or burning the edges in the heat affected zone. These were unfixable regardless of using a lower power or higher scan head speed.

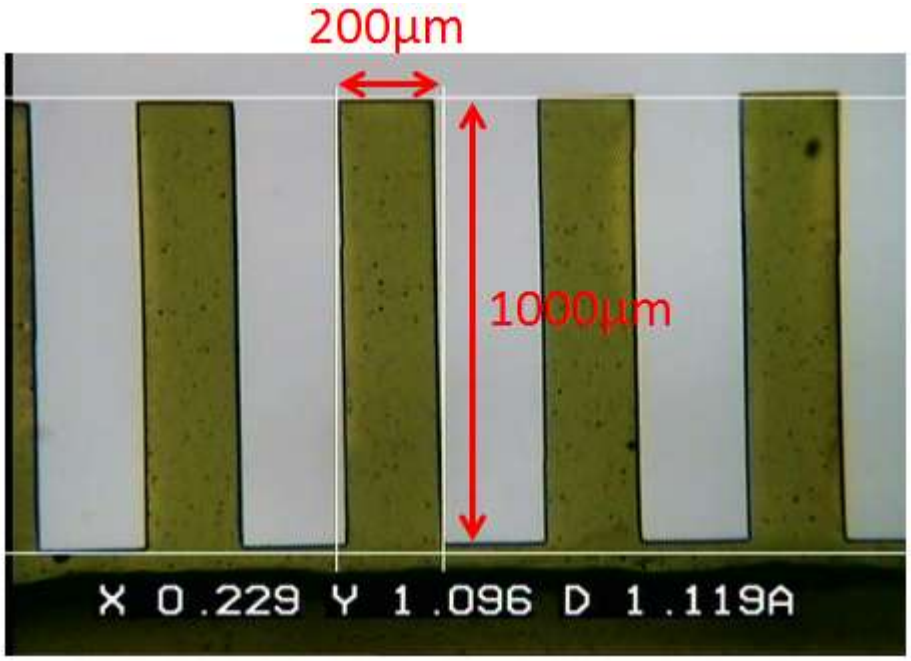

Figure 3-15: Cantilever array with dimensions of 1mm x 0.2mm fabricated with a picosecond laser.

3.4.2 Picosecond Laser

The new picosecond laser is a Trumpf TruMicro 5x50 (Figure 3-16), a solid state laser that is an oscillator that is mode-locked with an amplifier and diode pumped with a thin-disk laser. The maximum pulse energy in IR is 125 µJ through all repetition rates. The max repetition rate is 400kHz therefore creating a 50W average power. In the green wavelength range, the maximum power is 30W making it 75 µJ pulse energy. In the UV range, the maximum power is 14W with 35 µJ pulse energy. All of these are maximum values and can be modified, as the modification takes place in the software, which is pre-configured for the IR, and providing the percentage of output power that is required. Each wavelength has a separate output with three completely independent beam paths. The UV beam is expanded by a factor of 2.8, while green and IR are expanded by a factor of 2. The expansion factors were chosen to match the beam diameter to the aperture of the scan heads, which include two steering mirrors and an f-theta lens. Focusing techniques were the same as the nanosecond laser, but spot size was much

reduced due to lower heat absorption by the material, and cuts of ~10 µm wide was achieved. Therefore, there was significantly less burning around the cantilever edges due to higher repetition rates and lower pulse durations as opposed to the nanosecond laser.

Mode locking is the technique employed by the picosecond laser, instead of q-switching, creating a pulsed laser that is capable of pulses with extremely short duration, hence the name picosecond. The technique uses a fixed phase relationship between the modes of the laser's resonant cavity. Afterwards, interference between these modes causes the laser to become pulses that are of extremely short duration. Lastly, a disk laser structure is based on using a cooled disk media with a large surface area to volume ratio. This allows for more efficient cooling of the laser media, which then turns into a higher average power. This is as opposed to the popular rod based laser, which is less efficient at cooling, and therefore is unable to produce the sustained high average power of the disk based laser.

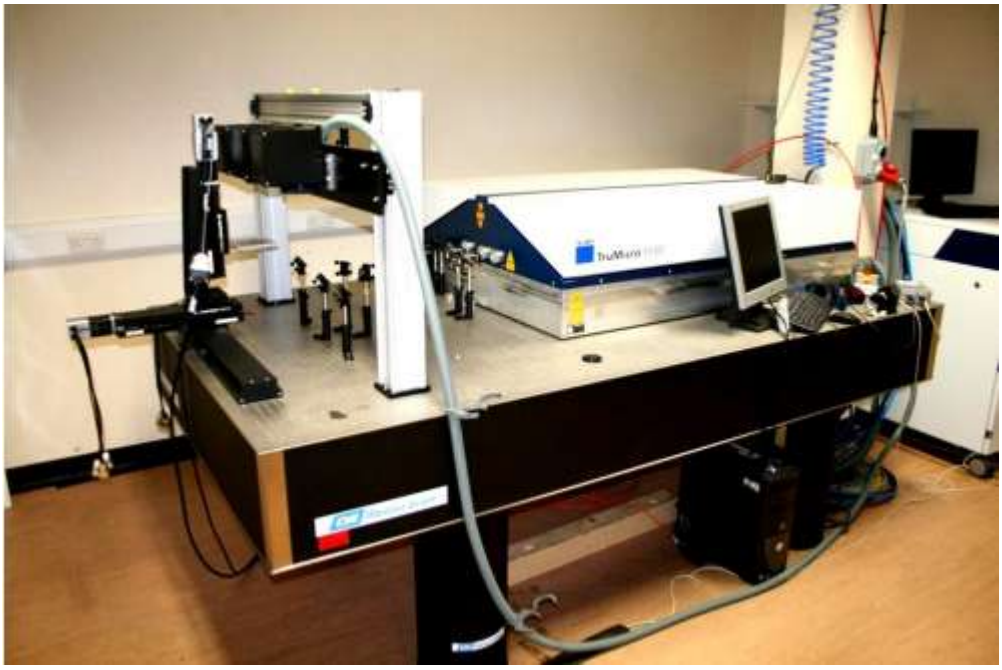

Figure 3-16: Trumpf TruMicro picosecond laser

The work piece can be positioned using three axis linear stages (Aerotech) and are controlled via a software interface where programs can be written to perform movements in a specific order, however the precision of the stages is limited, so is the smoothness of the movement. The stages move on ball bearings and are driven by a screw and a servo motor this causes disadvantages in precision but is a far cheaper

choice compared to the more accurate air bearing stages. The accuracy is limited to ±6μm in Z-axis; ±8μm in Y-axis, and ±16μm in X-axis. However the stages offer a resolution of 0.5 μm enabling high enough resolution to position the samples very precisely. The scan heads also offer the advantage of being quicker as they can perform movements at speeds as fast as 3000 mm/s and are therefore ideal for complex shapes that would otherwise require a long time to manufacture involving the stages. The scan heads are the main manufacturing tool accessed via the laser software. However the repetition rate and the wavelength cannot be changed within the program.

3.5 Conclusions

- Microcantilever sensors can be monitored using different techniques, such as optical or electrical methods. All parameters such as temperature and fluidic control can be integrated and precisely controlled during the experiments. An array of up to 16 or 32 microcantilever sensors can be simultaneously measured.

- Both a single and scanning optical beam detection systems were constructed, integrating elements such as temperature control, calibration, and readout systems.

- Cantilever sensor arrays can be rapidly fabricated through the nano- or pico-second laser system. The deflection of the cantilever can be easily calculated to provide values for surface stress or other forces behind cantilever bendings.

- Tests were performed to validate the feasibility of the cantilever array measurement system. A unique cantilever array chamber was designed to provide cells with a natural environment, incorporating gas delivery functions.

- Portable microcantilever sensors were developed with a novel method to allow for highly multiplexed measurement systems.

3.6 References

Ang, K.H., Chong, G.C.Y., Li, Y., PID control system analysis, design, and technology. *IEEE Trans Control Systems Tech*, **13(4),** 559-576 (2005).

Archibald, R., Datskos, P., Devault, G., Lamberti, V., Lavrik, N., Noid, D., Sepaniak, Dutta, P., Independent component analysis of nanomechanical responses of cantilever arrays. *Analytica Chimica Acta,* **584 (1),** 101-105 (2007).

Berger, R., Lang, H.P., Gerber, C., Gimzewski, J.K., Fabian, J.H., Scandella, L., Meyer, E., Guntherodt, H.J., Micromechanical thermogravimetry. *Chemical Physics Letters* **294(4-5)**, 363-369 (1998).

Binning G., Rohrer, H., Gerber, C., Weibel, E., Surface studies by scanning tunneling microscopy. *Physics Review Letters* **49**, 57-61 (1982).

Brunt, T.A., Rayment, T., O'Shea, S.J., Welland, M.E., Measuring the surface stresses in an electrochemically deposited metal monolayer: Pb on Au. *Langmuir* **12(24)**, 5942-5946 (1996).

Cowburn, R.P., Gray, S.J., Bland, J.A.C., Multijump magnetic switching in in-plane magnetized ultrathin epitaxial Ag/Fe/Ag films. *Phys. Rev. Lett*. **79**, 4018 (1997).

Jin, D., Li, X., Liu, J., Zuo, G., Wang, Y., Liu, M., Yu, H., High-mode resonant piezoresistive cantilever sensors for tens-femtogram resoluble mass sensing in air. *J. Micromech. Microeng*. **16(5)**, 1017, (2006).

Kracmer, P., Moulin, A.M., Stephenson, R.J., Rayment, T., Welland, M.E., Elliot, S.R., Reversible nanocontraction and dilatation in a solid induced by polarized light. *Science* **277**, 1799-1802 (1997).

Martinez, N.F., Kosaka, P.M, Tamayo, J., Ramirez, J., Ahumada, O., High throughput optical readout of dense arrays of nanomechanical systems for sensing applications. *Rev. Sci. Instrum*, **81**, 125109 (2010).

Minne, S.C., Manalis, S.R., Quate, C.F. Parallel atomic force microscopy using cantilevers with integrated piezoresistive sensors and integrated piezoelectric actuators. *Appl. Phys. Lett*. **67**, 3918 (1995).

Noda, K., Hoshino, K., Matsumoto, K., Shimoyama, I., A shear stress sensor for tactile sensing with the piezoresistive cantilever standing in elastic material. *Sensors and Actuators A: Physical* **127(2)**, 295-301 (2006).

Renteria, A.S.M., MecWins, S.L., http://sine.ni.com/cs/app/doc/p/id/cs-12212, Date unknown. Retrieved 2011-08-28

Su, Y., Evans, A.G.R., Brunnschweiler, A., Ensell, G., Characterization of a highly sensitive ultra-thin piezoresistive silicon cantilever probe and its application in gas flow velocity sensing. *J. Micromech. Microeng*. **12(6)**, 780 (2002).

Tortonese, M., Barrett, R.C., Quate, C.F., Atomic resolution with an atomic force microscope using piezoresistive detection. *Appl. Phys. Lett*. **62**, 834 (1993).

Tortonese, M., Ginzton E., Yamada, H., Barrett, R.C., Quate, C.F., *Solid-state Sensors and Actuators*, 448-451 (1991).

Wallmark, J.T., A new semiconductor photocell using lateral photoeffect. *Proceedings of the IRE* **45**, 474-483 (1957).

Wu, G., Haifeng, J., Hasen, K., THundat, T., Datar, R., Cote, R., Hagan, M.F., Chakraborty, A.K., Majumdar, A., Origin of nanomechanical cantilever motion generated from biomolecular interactions. *Proc. Natl. Acad. Sci*. **98**, 1560-1564 (2001). kraemer moulin science 277 1997

Yang, M., Zhang, X., Vafai, K., Ozkan, C.S., High sensitivity piezoresistive cantilever design and optimization for analyte-receptor binding. *J. Micromech. Microeng*. **13(6)**, 864 (2003).

Yu, X., Thaysen, J., Hansen, O., Boisen, A., Optimization of sensitivity and noise in piezoresistive cantilevers. *J. Appl. Phys*. **92**. 6296 (2002).

Yuan, C.W., Batalla, E., Zacher, M., de Lozanne, A.L., Kirk, M.D., Tortonese, M., Low temperature magnetic force microscope utilizing a piezoresistive cantilever. *Applied Physics Letters* **65(10)**, 1308-1310 (1994).

Zhong, J., URL: http://saba.kntu.ac.ir/eecd/pcl/download/PIDtutorial.pdf, (2006). Retrieved 2012-04-04.

Chapter 4 Monitoring Yeast Cell Growth and Drug Interactions by the Bending of Viscoelastic Polymer Microcantilever Biosensors

4.1 Introduction

The ability to monitor cell proliferation precisely is fundamental to many biomedical applications including infectious diseases, drug discovery and testing, and public health applications, such as food and water quality. Current methods to monitor cell growth including optical (Chang *et al*., 2004), fluorescent (Walkup *et al*., 2000), and electrical (Xiao *et al*., 2002) measurements are indirect and inevitably introduce external interference into the systems. Typical cell screening techniques require labeling and have focused on drug discovery (Drews, 2000), or the detection of specific biological cells, often aiming towards single cell detection limits (Ilic *et al*., 2001). In addition to being time consuming (5-14 days), advanced taxonomic skill is required to identify the correct cell strain (Hoog de *et al*., 2000). Other tests such as radioimmunoassay (RIA, Wide *et al*., 1996), enzyme-linked immunosorbent assay (ELISA) (Pizza *et al*., 2000), fluorescent antibody methods (Stygen *et al*., 1995), polyimidease chain reaction (PCR, Hermanson, 1996), and Western blot technique (Burnette, 1981) are able to identify cell strains without the need for culturing, but are still limited by the inability for real-time cell growth monitoring capabilities.

The use of microcantilevers for cell studies provides many advantages, such as being highly sensitive, selective, label-free, real time, and provides in-situ detection methods. The enhanced sensitivity of polymer microcantilevers has been reported previously, although not for cell studies but instead for applications such as AFM (Gaitas *et al*., 2006), DNA (Zhang *et al*., 2004b), temperature/pH (Montserrat *et al*., 2006), and optical imaging (Wang *et al*., 2005). Cantilevers have been shown to possess a mass resolution in the region of pico to femptogram ranges in both air (Lang *et al*, 1999, Gupta *et al*, 2004) and liquid (Hosaka *et al*., 2006, Braun *et al*., 2005). Therefore, single cell detection and monitoring on the cantilever surface has been reported previously (Park *et al*., 2008, Bryan *et al*., 2009, Burg *et al*., 2007, Godin *et al*., 2010). Cell growth detection has been demonstrated by monitoring resonance frequency changes of microcantilevers as the mass increases from immobilized fungal spores on the surface of the cantilevers in humid air (Nugaeva *et al*., 2005). The typical low sensitivity

experienced by cantilevers in liquid environments due to damping effects have been bypassed by trapping cells on the cantilever tip and filling the cantilevers with liquid, demonstrating the ability to monitor single cells (Lee *et al*., 2010). Although the method is extremely sensitive and useful in studying the features and mechanisms of individual cells, it is so far limited in studying non-adherent cell growth and requires complex microcantilever devices and instruments.

The static bending mode of cantilever biosensors has been utilized previously to detect the presence of bacteria, leading to small deflection signals typically below 200nm (Dhaval *et al*., 2006, Weeks *et al*., 2006, Zhang, 2004a). However, they have all been focused towards direct detection of whole organisms (*E. coli, Bacillus subtilis, Salmonella*) through binding of cells on the cantilever surface, rather than real-time growth monitoring. While detection of bacterial cells is undoubtedly essential for applications such as biological threats, to our best knowledge, there have been no studies demonstrating the ability to monitor live cell growth using simple bending mode microcantilevers. On account of the many similarities of cell division and DNA repair systems to human cells, the well-established eukaryotic model organism (Nickoloff *et al*., 1998, Goffeau *et al*., 1996, Petranovic *et al*., 2010), *Saccharomyces cerevisiae* yeast cells was chosen to study cell growth on microcantilever sensors.

In this chapter, the first example of growth-induced surface stress bending of polymer cantilevers for real-time yeast cell growth measurement is reported, expanding the applications of simple bending mode microcantilevers as a powerful cell screening tool for cell-based assays as well as providing new fundamental insights into drug-cell interactions. A new strategy for highly sensitive, label-free and real-time monitoring the growth of yeast cells and the growth inhibition through its interaction with drugs using simple bending-mode of polymer microcantilever biosensors is demonstrated. *S. cerevisiae* strains YN94-1 and YN94-19 were deposited onto microcantilever sensor surfaces and the growth curves corresponding to the bending were investigated under different culture conditions. The real-time polymer based microcantilever bending signal revealed distinct growth characteristics of cells cultured in SC±uracil and SC+5'-fluororotic acid media, which are indiscernible using conventional screening methods. Large bending signals of up to ~7μm from polymer based cantilever were observed,

which were attributed to the surface stress changes of 5.66 N/m arising from the yeast cells' growth. When compared to the signal from silicon nitride microcantilevers, polymer based cantilevers exhibited at least one order of magnitude increase in terms of sensitivity. The enhanced signal was attributed to the viscoelastic properties of polymer materials. This new method of enhanced sensitivity in static mode microcantilever monitoring of cell growth opens new opportunities of polymer microcantilevers for biomedical applications in the fields of disease diagnosis and cell-based assays for drug screening.

4.2 Project Background

The project was performed in collaboration with Dr. Lilian Schweizer and Prof. Michael Schweizer from the School of Life Sciences at Heriot-Watt University. *Saccharomyces cerevisiae* cells were provided at a concentration of $2.5x10^6$ cells/mL. All cell culturing was provided by them, in addition to the various different cell media types used in the following experiments. In addition, experimental design was aided by them to determine suitable experiments to validate our findings, followed by insight into cell mechanics and behaviors once experiments were completed. The ultimate goal of the experiments was to determine if the single cantilever detection system is capable of detecting and monitoring cell growth in real-time, in order to determine the growth and death characteristics of yeast cells that would otherwise be unable to be detected at a macro cell culture level.

4.3 Experimental Details

The main series of experiments were carried out using specially-fabricated polyimide microcantilevers, where growth was followed for two strains of *S. cerevisiae* (YN94-1 and YN94-19), which were deposited onto the microcantilever sensor surfaces. Growth was initiated by injection of one of three Synthetic Complete (SC) medium; SC alone, SC with uracil and SC with 5'-fluororotic acid (FOA) and the bending signal followed over a period of up to 24 hours. An additional experiment was carried out for the YN94-1 cultured in SC with uracil, using both the new cantilevers and a commercially available Si_3N_4 microcantilever.

4.3.1 Microcantilever sensors and test cell

Polymer microcantilever sensors were used instead of conventional silicon or silicon nitride-based microcantilevers. While silicon based cantilevers were used as a control

reference, polymer cantilevers are able to bypass the high cost and multi-step manufacturing process while retaining higher sensitivity without sacrificing other benefits. In addition to ease of fabrication, polymer microcantilevers can be easily manufactured into large arrays, allowing multiplexed detection of many substances simultaneously. Laser micromachining methods were used to microfabricate polymer film into the cantilevers with the dimensions of 25μm in thickness, 200μm in width, and 1000μm in length. Then a thin film of gold (40 nm) with 5 nm of chromium as adhesion layer was coated on one side of the cantilever to provide a reflective coating for optical beam measurement.

The cantilever chip was mounted in a liquid flow cell chamber with a volume of 250μL, and bending was monitored through an optical measurement system, consisting of a 5mW laser diode with a wavelength of 680 nm and PSD. Temperature of the liquid chamber was precisely controlled to 28±0.05 °C using a thermoelectric module under the chamber, which is the optimal temperature for yeast cell growth.

The commercially sourced V-shaped silicon nitride cantilevers (Veeco Instruments Inc.) are 140μm in length, 18μm in width, and 0.55μm in thickness. They are purchased pre-coated with 45 nm of gold on one side of the cantilever surface.

For both cases, cantilever deflections in nm were calculated from the voltage output of the PSD amplifier, and converted to nm using the dimensions of the system (Zhou *et al.*, 2006).

4.3.2 Cell Culture and Detection Using Microcantilever Sensors

S. cerevisiae cells were grown aerobically either in liquid media at 28-30°C with shaking at 200 rpm or at 30°C in solid media. The strains were maintained on solid media at 4°C, while subcultures were created every six weeks. When there was need for long-term storage of the cells, 1 mL of early-stationary phase culture was mixed with 1 mL of 30% (v/v) sterilized glycerol solution and stored at -70°C.

To use the yeast, a microcantilever chip was placed into the sterilized (with ethanol) flow cell chamber, and 20μL of either strain at an initial concentration of ~$2x10^8$

cells/mL, was pipetted onto the gold-coated face of the chip and allowed to rest for 1 min. to ensure that the cells had settled onto the surface. Afterwards, the chamber was filled with deionized water to prevent any cell growth as the polyimide cantilevers require a period of time to allow the material to adjust to the liquid, so any future bending could be confirmed to be from cell behavioral changes on the surface of the cantilever. The system was left to stabilize overnight or until the system reached steady state equilibrium where the PSD voltage would remain constant. During this process, the temperature was controlled precisely to 28°C. Future work would include observations into how cells adhere to the surface of the microcantilever itself and how to specifically target a single side of the cantilever, as this is currently unknown.

After the baseline of the microcantilever sensors was achieved, culture media allowing growth of the yeast cells was then injected into the flow cell at a rate of ~1 mL/min. Cell culture media used included Yeast Extract Peptone Dextrose (YEPD) media (10 g yeast extract, 20 g bacteriological peptone, 20 g glucose dissolved in a final volume of 1 liter dist. H_2O, autoclaved for 15 min at 121 $^{\circ}$C at 1 atm.) and SC+- uracil media (SC = Synthetic Complete ±uracil and SC+5'-FOA media is prepared as described by Marden *et al*. (2006) The system was allowed to rest while the cantilever bending (Figure 4-1) information was collected in real-time until yeast cell growth or death has ceased, causing a second steady state voltage signal from the PSD. SEM images in Figure 4-2 confirm the presence of yeast cells on the surface of the cantilever after a completed growth experiment. Each experiment was repeated multiple times to ensure consistent, accurate, and reproducible cantilever bending growth curves. The measurement precision of the microcantilever resolution had been found to be ~5nm from earlier work.

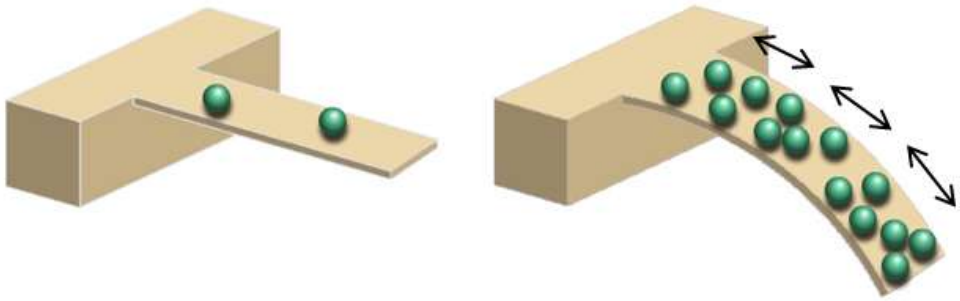

Figure 4-1: Schematic of loading of cells on a microcantilever surface. As cells reproduce and increase numbers on the cantilever surface, it creates a downwards bending motion of the cantilever beam.

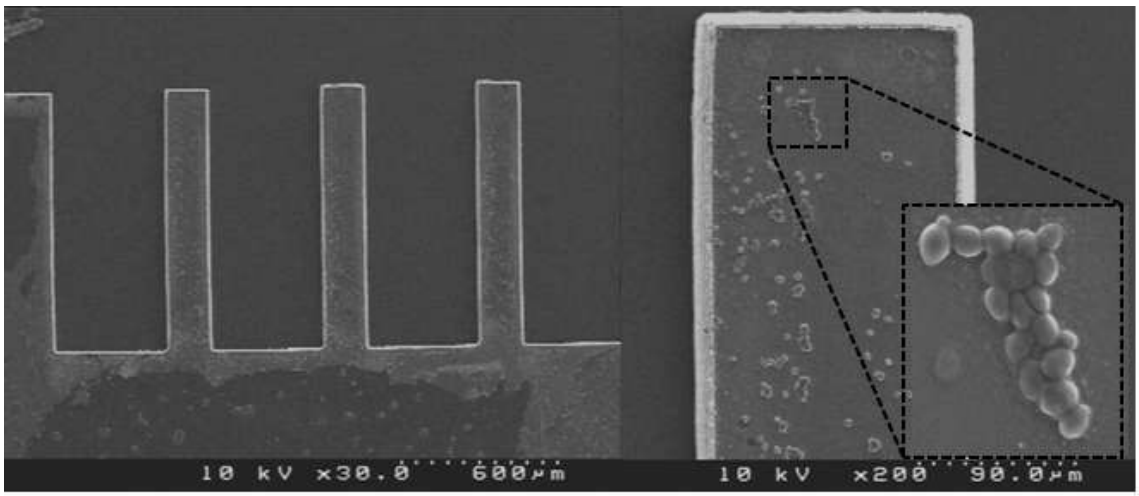

Figure 4-2: SEM images of the microcantilevers after the completion of a growth experiment, confirming the presence of only yeast cells on the surface that creates the downwards bending motion.

4.4 Challenges

Throughout the period of study, it was not unmet with many challenges that caused a plethora of failed experiments. While results were very positive at first, there was a sudden period where the cantilever sensors experienced minimal deflection while simultaneously producing noisy and/or unreliable signals. The first example of which was for a typical growth experiment (regardless of growth media type), seen in Figure 4-3.

It can be seen that after equilibrium and the injection of a growth media, there appears to be an initial period of growth, but after 2 hrs., the growth slowed down dramatically and the signal continues to fluctuate for over 20 hrs. Another example of such a failed experiment is shown in Figure 4-4. The experiments were repeated several times, but similar slow or even no growth curves were continually observed. Further investigation was carried out by changing the concentrations of growth media as shown in Figure 4-4.

In this instance, the attempt was to perform a growth condition with three varying concentrations of media. Although this signal clearly demonstrates a small amount of downwards cantilever deflection, it can be seen that the bending is again of very small magnitude in addition to no distinguishable difference between the three media growth concentrations.

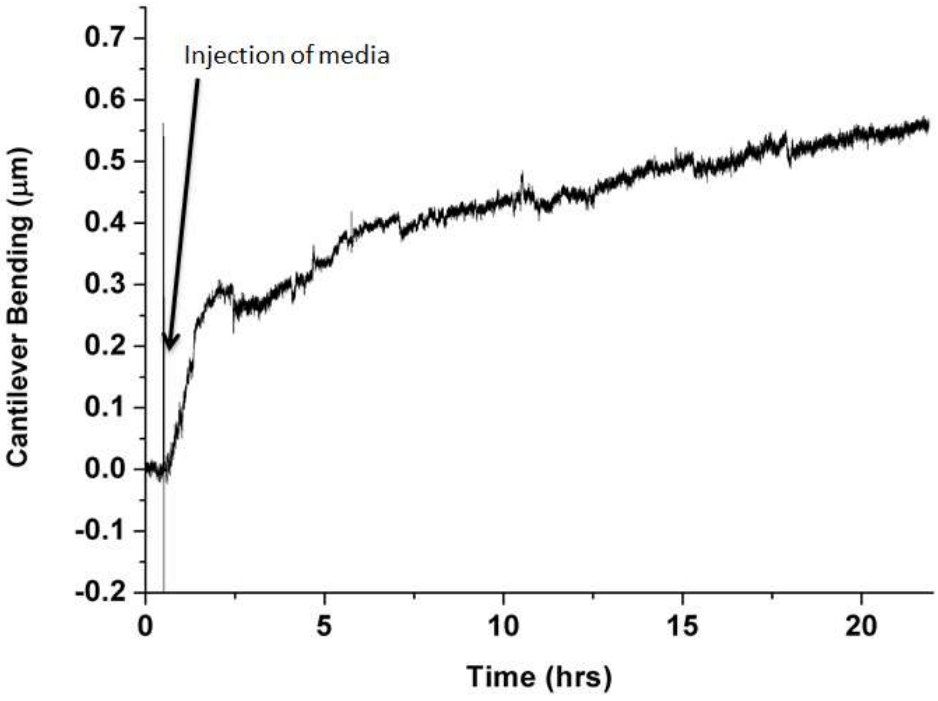

Figure 4-3: Failed yeast growth experiment due to blockage of tubing.

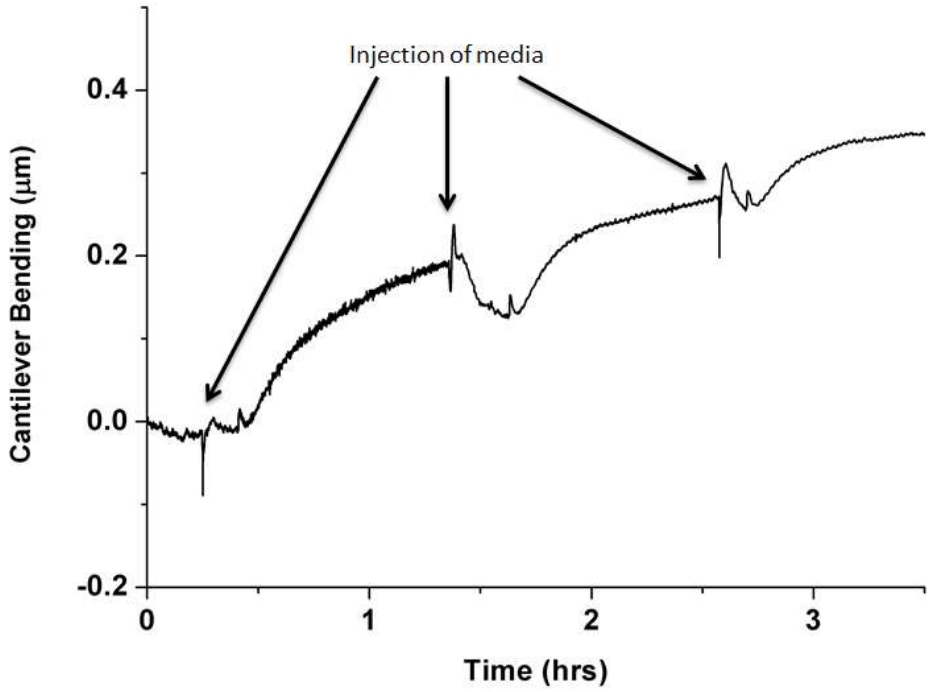

Figure 4-4: Failed yeast growth experiment with varying concentrations of media due to blockage of tubing.

After much deliberation and careful observations, the cause of these failed experiments was finally identified. While all tubing from the automated valve and fluid control system was flushed with pure ethanol (99.9%) prior to all experiments, residue build up from both cells and media from experiments still occurred and partially blocked all the tubing. Once the tubing was replaced with new ones, yeast cell growth reverted back to normal growth conditions and the problem was solved. One hypothesis of the reason is due to the flow chamber design. Because the media was injected into the system using gravity only, the flow rate was very slow. This combined with the partially blocked tubing caused the flow rate to slow down even further. The liquid enters the flow cell from the bottom surface, and an extremely slow flow rate would cause the growth media that was injected to not mix or push out and replace the existing liquid inside the flow cell chamber. Thus the yeast cells were not able to be exposed to the new media, hence the low levels of growth and unstable cantilever deflection signals. This was not the only problem, as other times, there were cases of possible bacterial contamination, improper handling of the cantilevers, or the yeast cells simply did not reproduce due to unknown reasons. But after the main issue of tubing blockage was solved, experiments were carried out successfully for the following results.

4.5 Results and Discussion

4.5.1 Growth and Control

Yeast cells on the surface of the microcantilever sensor were subjected to both growth and non-growth conditions. YN94-MATa yeast strains were used in the first instance with YEPD medium to confirm the ability for the microcantilever sensors to monitor cell growth and Figure 4-5 shows the growth curves of yeast vs. control by monitoring growth continuously over a 24 hr. period. After the injection of growth media into the system, the microcantilever sensors bend downwards and continuously over the 24 hr. period, corresponding to a rapid and exponential cell growth. The trace of the cantilever bending replicates the characteristics of a growth curve for yeast cells obtained by optical density measurement: a short initial lag phase of approximately 2 hrs. followed by an exponential phase of approximately 12 hrs. at which time the cells have entered stationary phase. Careful calibrations using control sensors without any cells attached on the surface but exposed to identical media conditions showed a negligible bending in an opposite direction, eliminating the possibility of sensor signals caused by non-specific interactions between the gold-coated surface and different media. Extremely large downwards bending signals of ~7μm was observed in the growth conditions compared to non-growth or control conditions. For all experiments, there was a slight dip in the signal during the injection of media, this was due to both the flow of liquid causing the cantilever sensors to bend and also the thermal effects due to temperature differences between the old (28℃ controlled) and new (room temperature) media. Future work would include pre-heating the new media before injection to minimize the thermal effects.

Following this demonstration of principle, further experiments were performed using YN94-1 and YN94-19 yeast strains chosen because they respond differently to different growth medium (SC alone, SC with uracil, and SC with 5'-fluororotic acid (5'-FOA)) [Boeke *et al.*, 1987]. In this way, the changes in sensor response due to the effects of withholding vital nutrition and/or adding toxins could be studied. Growth characteristics of the two yeast strains on the various media correlate to the theoretical growth characteristics listed in Table 1. All conditions where yeast growth was expected from

macro-scale cell cultures produced a downward bending of the cantilever beam on a micro-scale. Differences between growth and non-growth measurements were seen within 1 hr. after injection of media. In addition, when compared with normal growth states, the non-growth conditions provided a clear distinction in the bending signal of the cantilevers, allowing for strain or media differentiation within the initial hour.

Table 4-1: Expected responses for the strains of yeast to the medium used. (Boeke *et al.*, 1987)

Strain/Medium	SC with uracil	SC without uracil	SC with 5'-FOA
YN94-1	increased growth	no growth	increased growth
YN94-19	increased growth	increased growth	no growth

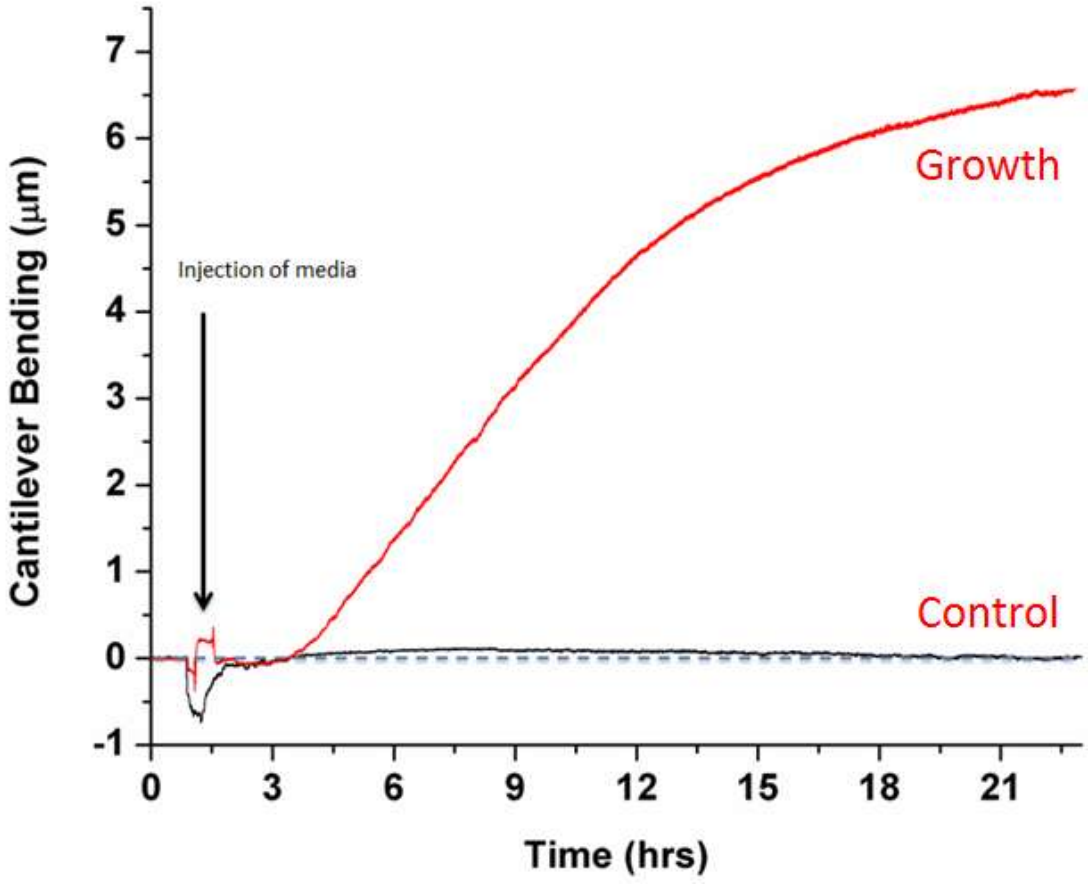

Figure 4-5: Growth vs. control curves of yeast growth on the cantilever surface. The growth curve signaled a significant downward bending of the cantilever beam, as opposed to the control experiment without cells, eliminating any possible effects.

4.5.2 Effect of Cell-Drug Interactions

In order to study the effects of drug interactions on different genotypes, a chemical toxin 5'-FOA in the culture media was used, which promotes cell death in yeast strains that are uracil prototrophs (e.g. YN94-19). On the other hand, 5'-FOA should not inhibit cell growth of the yeast strain, which is an uracil auxotroph (e.g. YN94-1). As illustrated in Figure 4-6, the cantilever exhibited maximal downwards bending of ~6μm. Rather than producing a flat or downward-trending curve (indicating stable or upwards bending of the cantilever), 5'-FOA media produced a short period of exponential growth, reaching peak growth after 5 hrs. with a downwards cantilever bending of ~1.5μm. The reason for this is that 5'-FOA is metabolized to 5'-fluoro-uracil, which is toxic to an uracil prototrophic strain (YN94-19).

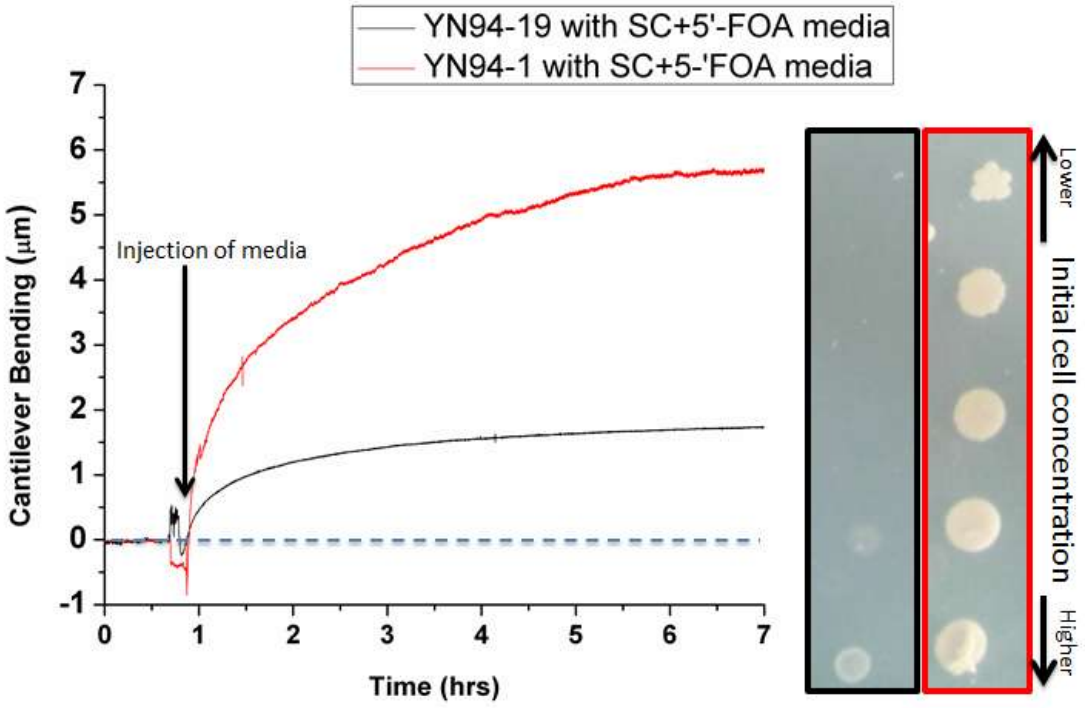

Figure 4-6: Growth curves of YN94-1 and YN94-19 yeast cells in 5'-FOA media, with comparison to the cell culture at a macro level.

In addition, in order to study the effects of withholding nutrition from the cells, YN94-1 was cultured in SC-uracil media. Growth was expected to be non-existent according to macro-level cell cultures in Figure 4-7. The relatively smaller downward bending (~0.25μm) of the microcantilever observed with the YN94-19 strain with SC-Uracil media can be explained by the initial growth caused by the separation of committed

daughter cells from the mother cells. Conversely, the YN94-1 strain with SC-Uracil media replicated as normal signified once again by the ~6μm of downwards direction cantilever bending.

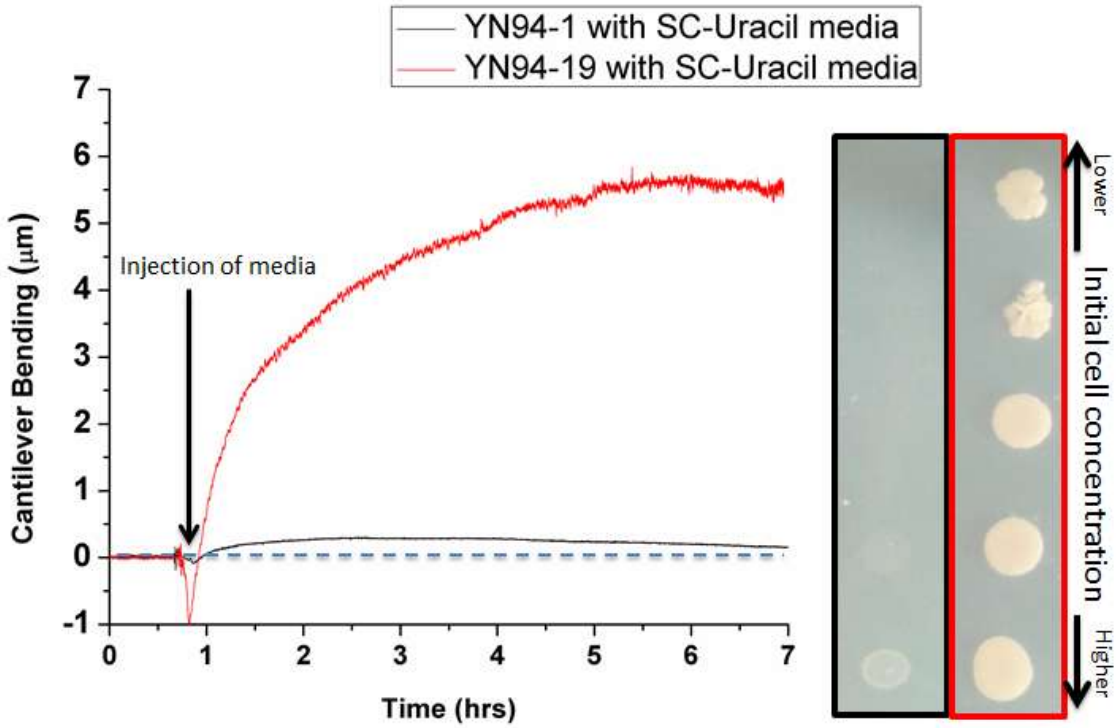

Figure 4-7: Growth curves of YN94-1 and YN94-19 yeast cells in SC-Uracil media, with comparison to the cell culture at a macro level.

4.5.3 Comparison of Results

Interestingly, there is a considerable difference between the growth characteristics illustrated by the cantilever bending of the two conditions where cells were not expected to grow, although there were no differences between them on solid media. **(**Figure 4-8**)** The presence of the toxin in the media did not kill the cells immediately but permitted slight growth as described above, followed by cells continuing to remain on the surface of the cantilever, with a stable downwards cantilever bending of ~1.5μm. With a lack of key nutrients in the media (SC-Uracil), the cells replicated initially, but quickly started to die, decrease in surface stress, and detach from the surface of the cantilever, even producing an upwards bending of the cantilever in the end. These events show that this system is ultra-sensitive compared to traditional cell culturing at the macro-level, as differentiation between toxins and lack of nutrition can be revealed within 30 min. after introduction of culture media. This demonstrates that it would be possible to test

reactions or interactions with regards to a new drug or vaccine by being able to differentiate between different cell strains and their behavior towards different drugs.

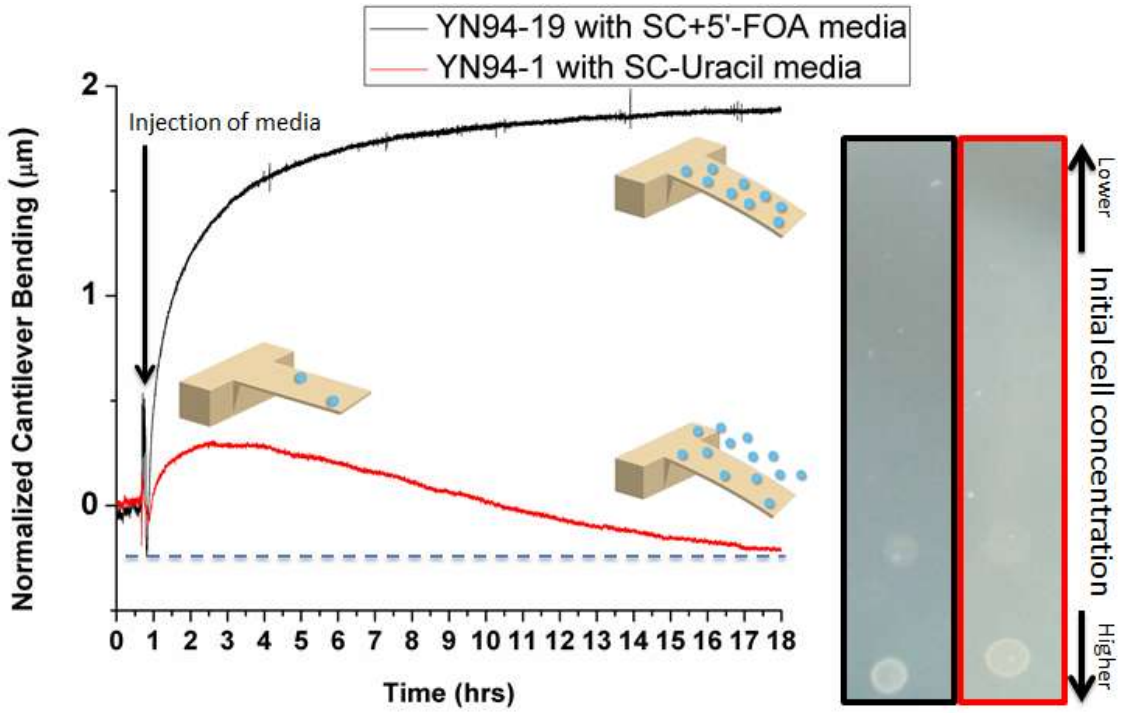

Figure 4-8: Growth curves of YN94-1 and YN94-19 yeast cells in non-growth conditions. Cantilever bending scaling was enlarged in order to demonstrate the differences that would otherwise be difficult to differentiate, with a comparison to the cell culture at a macro-level that shows no difference.

4.5.4 Growth Induced Bending Signals

The static bending caused by the binding or adsorption of biomolecules to microcantilever sensors can be explained by the change of surface stresses (Fritz, 2008, McKendry *et al*., 2002). The static bending mode of cantilever biosensors has been utilized previously to detect the presence of bacteria, leading to small deflection signals typically below 200nm (Dhaval *et al*., 2006, Weeks *et al*., 2006, Zhang, 2004a). Liang *et al*. (2008) confirmed cell-substrate interaction induced surface stress changes through the use of quartz crystal microbalance. In contrast, cell growth induced microcantilever bending has not been reported previously but it is likely that the bending induced by cell

proliferation on the microcantilever substrate are mainly caused by changes in surface stress as well.

The physical origin of the surface stress changes is complex (Fritz, 2008). Dependent on different materials and molecular systems, the surface stress change may be caused by different sources including intermolecular interactions (Van der Waals and Pauli exclusion) (Stachowiak et. al., 2006), hydrophobic or entropic interactions (Fritz, et. al., 2000, Wu *et al*., 2001), electrostatic forces (Ibach, 1997, Watari *et al*., 2007, Godin et. al., 2010) and hydration forces (Mertens *et al*. 2008). Therefore, the plausible explanations for cell growth induced surface stress change can come from cell-substrate interactions and cell-cell interactions. The growth of yeast cells on the cantilever substrate increase the amount of membrane proteins interacting with the cantilever surfaces. Electrostatic forces between the charged membrane proteins and gold surface will continue to increase with the cell growth. On the other hand, with the amount of cell increase within the well-defined cantilever area, the cell-cell interaction from budding cells including electrostatic forces and hydration forces is likely to increase and generate repulsive forces among cells, leading to a compressive stress on the microcanitlevers, similar to the surface stress changes from protein-protein interaction reported by Moulin *et al*. (2000).

The surface stress from cell growth induced bending can be esimated from the Stoney equation (Stoney, 1909):

$$\boldsymbol{\delta = \frac{3\sigma(1-v)}{E}\left(\frac{L}{t}\right)^2} \qquad \textbf{(4.1)}$$

Where δ is the cantilever deflection, σ is the surface stress, L is the beam length, t is the cantilever thickness, and v and E are Poisson's ratio and Young's modulus of the substrate, respectively. The effective surface stress on the polymer cantilevers with the bending signal of 6.0 μm is 5660 mN/m using a generally accepted moduli E = 2.5GPa and v = 0.34 (Dupont). It might be noted in passing that the dimensions of surface stress involve m^{-1} rather than m^{-2} to avoid the need to specify the thickness of the surface film.

SEM images of removed cantilever chips after completed experiments show less than 1,000 yeast cells per cantilever. Optical method readout schemes such as the one that was used for the cantilever sensors have a typical sensitivity of ~5nm. Given that the 6μm of bending signal corresponds to a maximum cell count of <1000 cells, the sensitivity of the cantilever sensors corresponds to the activity of a single yeast cell.

Growth experiments were also conducted with media concentrations of 1:50 (1 part media to 50 parts water), 1:10 (standard concentration used in previous experiments), and 1:1 (pure media). (Figure 4-9) It can be seen that there is a distinct difference in the amount of cantilever bending with the varying media concentrations, with the lowest amount of bending from the most diluted media, and the highest amount of bending from the highest concentration media. This correlates positively with expected results, and the comparison to the control experiment (no cells, 1:10 concentration media) still shows a significant amount of cell growth and cantilever bending even with highly diluted media, and further demonstrates the high sensitivity of the static polymer cantilevers for yeast cell growth.

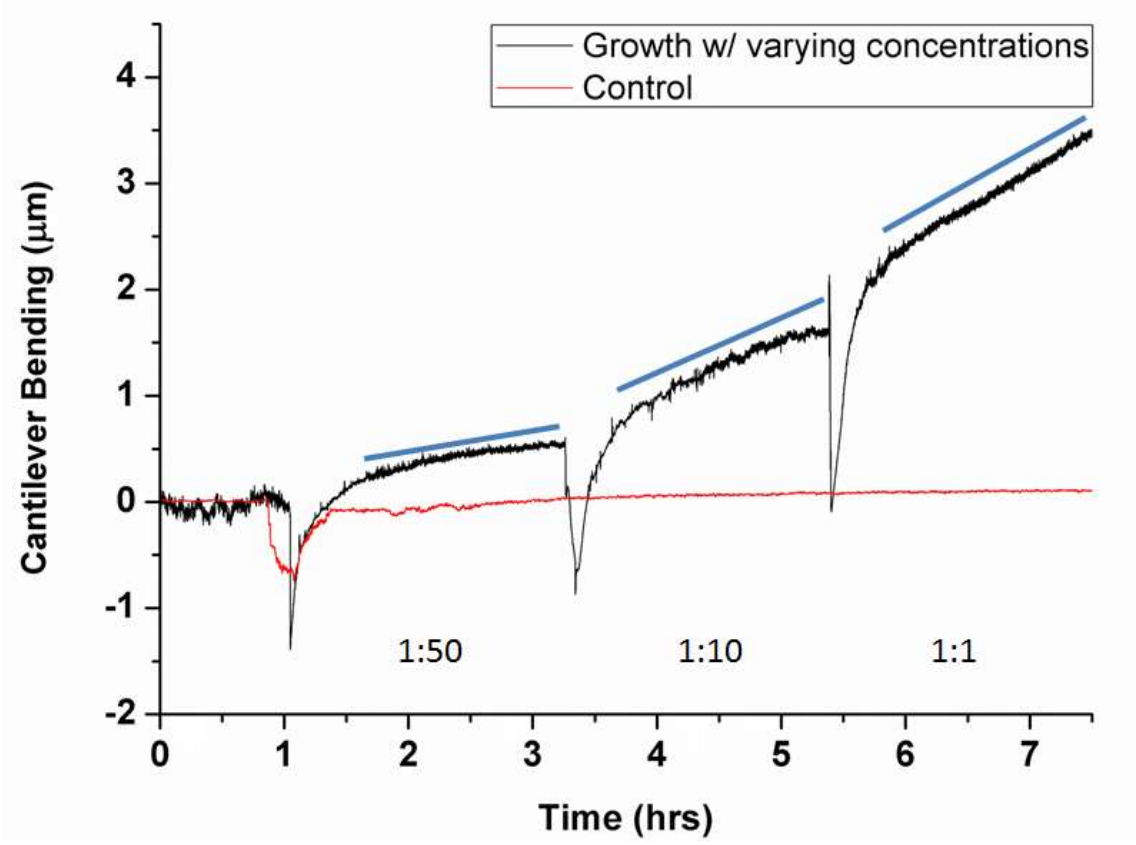

Figure 4-9: Growth curve of experiment with varying media concentrations. This includes 1:50 (1 part media to 50 parts water), 1:10 (original media concentration),

and 1:1 (pure media). After comparison to the control curve with no cells but 1:10 concentration media, even 1:50 media concentrations produced significant cell growth.

4.5.5 Effect of Viscoelastic Polymer Cantilevers

It should be noted that the cell growth induced polymer cantilever surface stress of 5660 mN/m is larger than the maximum reported surface stress changes of cantilever biosensors in liquid environments (Fritz, 2008). In order to determine the possible reasons for this large surface stress, a control experiment using silicon nitride cantilevers was performed to compare the effects of the different materials. Figure 4-10 illustrates the growth characteristics of YN94-1 yeast strain with SC+Uracil media grown on the surface of a gold-coated silicon nitride cantilever. The growth bending curves were converted into the surface stress changes through Stoney equation. Similar to the response on the polymer cantilever, the cell growth on silicon nitride cantilevers exhibited exponential type growth followed by a slowing period until reaching a steady state signal where growth has stopped. However, in contrast to polymer cantilevers, silicon nitride cantilevers exhibited a much lower bending signal or surface stress changes of 440 mN/m, approximately 13 times smaller than the 5660 mN/m as observed by the polymer cantilever. This finding agrees well with the analysis of Wenzel *et al*. (2009), who calculated that SU-8 polymer cantilevers would exhibit a 50% longer response time but with a ten-fold increase in sensitivity, which they attribute to the lower modulus.

The significant enhanced sensitivity recorded by polymer cantilever sensors may be due to the viscoelastic effect from the polymer materials. A recent theoretical study has predicted that viscoelastic polyimide cantilever will exhibit at least one order of magnitude greater in the bending signal than cantilevers made of elastic materials (e.g. silicon or silicon nitride) (Wenzel *et al*., 2009), which is consistent with our finding of 13-times enhanced sensitivity. **(**Figure 4-10**)** The study further predicts that although polymer cantilevers will provide a much larger degree of sensitivity, it comes with the cost of a lower response rate. From the results in Figure 3, there is a clear difference in their response time constants (i.e. polyimide cantilever of 1.3 hrs., silicon nitride cantilever of 0.87 hrs.).

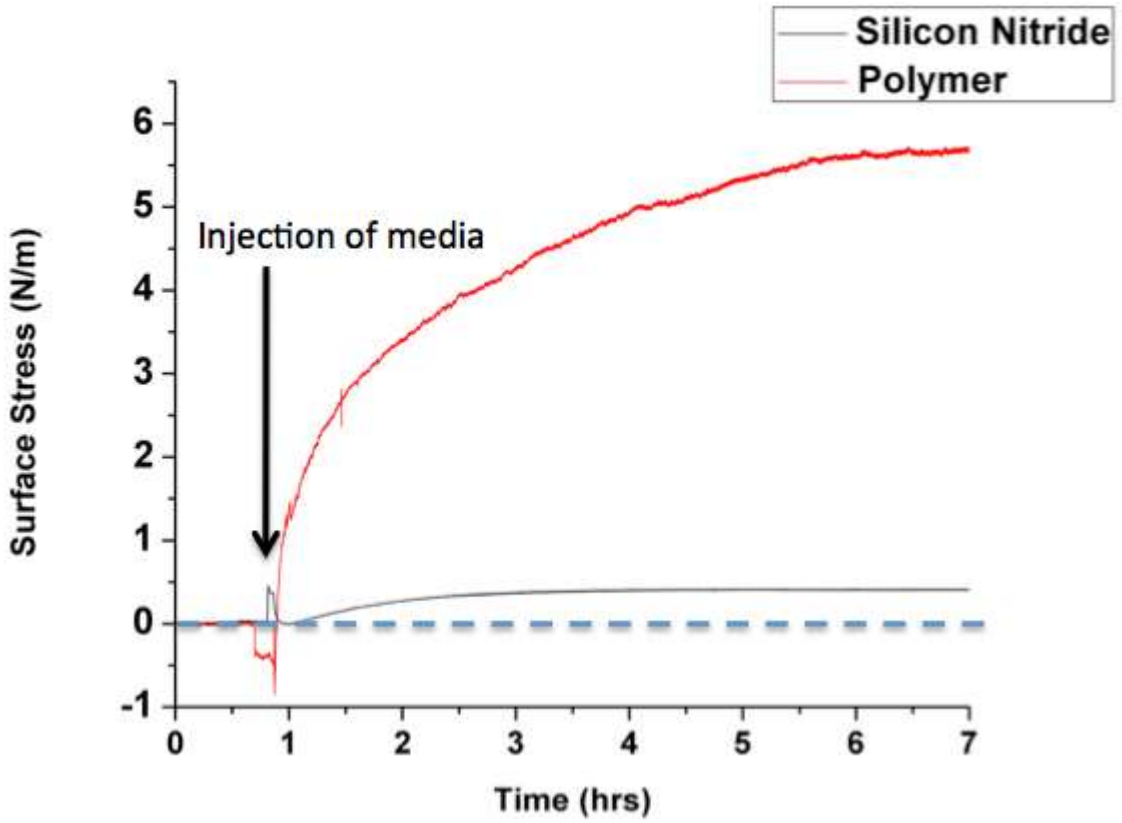

Figure 4-10: YN94-1 yeast strain with SC+Uracil media grown on the surface of a silicon nitride compared to polymer cantilevers. Surface stress is used as the amplitude due to the differences in size between the two cantilevers. The noise levels of the polymer cantilevers are due to the reflective coating's inconsistencies on the cantilever surface, as opposed to commercially sourced silicon nitride cantilevers with more uniform reflective coatings.

Wenzel *et al.'s* analysis considers the polymer to behave as a standard linear solid (SLS) for which the constitutive equation is:

$$\eta\dot{\sigma} + E_1\sigma = \eta\left(E_1 + E_2\right)\dot{\varepsilon} + E_1E_2\varepsilon$$

Such materials require two elastic moduli (E_1 and E_2) and a viscous modulus (η) to characterize their stress-strain-time behavior and require extensive testing at a variety of strain rates in order to determine the three moduli. Unfortunately, published data rarely, if ever, give viscoelastic data in terms of viscoelastic models and the only published information related to polyimide that could be found (SII NanoTechnology Inc.)

indicates a storage modulus, $E'' = 7.3 \times 10^7 Pa$ and a loss modulus, $E' = 3 \times 10^9 Pa$ at 28℃ obtained from testing over the frequency range of 0.5 and 10Hz. Wenzel *et al.* recognized that viscoelastic polymers generally (not just the SLS) exhibit two extremes of elastic modulus: a "rubbery" modulus over short timescales (slow loading), and a "glassy" modulus over longer timescales (rapid loading). The rubbery modulus of polyimide appears to be about 40 times lower than the glassy modulus, so that two values of the quasi-static bending stiffness of the cantilever can be calculated (assuming end loading) of 0.057 N/m and 2.34 N/m. Under similar loading conditions, the static stiffness of the V-shaped Si_3N_4 cantilever can be calculated using an equation due to Sader (Sader, 1995) as 0.13N/m. (Full calculations can be seen in APPENDIX 2) Thus, at best, it might be expected that the particular polymer cantilever used here would be about twice as sensitive as the commercial Si_3N_4 cantilever on the basis of the mechanical properties of the substrate. The Stoney equation takes into account the width of the cantilever, so the remaining factor (of ~7) must be associated with the surface interaction depth between the polymer and the Si_3N_4, which is inherently assumed to be the same for both substrate materials. It seems likely that a polymer, especially one that absorbs water, such as polyimide (Arlon Inc.), will exhibit surface interactions with a growing biological community that go some way below the surface. Precise resolution of this issue will require testing with different polymeric cantilever materials showing different water absorption and viscoelastic properties.

4.6 Conclusions

- In this project, the first example of growth-induced surface stress bending of polymer cantilevers for real-time yeast cell growth measurement has been characterized. Two different *S. cerevisiae* yeast strains were utilized with polymer cantilevers, which were found to be highly sensitive in differentiating the effects of both withholding essential nutrients and also drug interactions with yeast cells.

- Yeast cell growth on the surface of the polymer cantilevers yielded a large bending signal, likely related to the surface stress due to cell-cell and cell-substrate interactions. Further investigation on probing the origin of the bending signal induced by cell growth will be needed in the future.

- The polymer cantilevers demonstrated a much greater sensitivity than silicon nitride cantilevers, and this enhanced sensitivity could only be partly attributed to the rubbery modulus of the polyimide used. It seems likely that the additional sensitivity is associated with the interaction depth of the biological activity on the polymer surface.

- This new method of enhanced sensitivity in static mode microcantilever monitoring of cell growth opens new opportunities of polymer microcantilevers for biomedical applications in the fields of disease diagnosis and cell-based assays for drug screening.

4.7 References

Arlon Inc. Application Note. Moisture absorption of polyimide MCBs, available at http://www.arlon-med.com/Moisture_Pickup_Drying_Poly.pdf, accessed December 2012

Boeke, J.D., Trueheart, J., Natsoulis, G., Fink, G.R., 5-fluoroorotic acid as a selective agent in yeast molecular genetics. *Methods Enzymol* **154**, 164-175 (1987).

Braun, T., Barwich, V., Ghatkesar, M.K., Bredekamp, A.H., Gerber, C., Hegner, M., Lang, H.P., Micromechanical mass sensors for biomolecular detection in a physiological environment. *Phys. Rev. E* **72**. (2005).

Bryan, A.K., Goranov, A., Amon, A., Manalis, S.R., Measurement of mass, density, and volume during the cell cycle of yeast. *PNAS* **107 (3)**, 999-1004 (2009).

Burg, T.P., Godin, M., Knudsen, S.M., Shen, W., Carlson, G., Foster, J.S., Babcock, K., Manalis, S.R., Weighing of biomolecules, single cells and single nanoparticles in fluid. *Nature Letters* **446**, 1066-1069 (2007).

Burnette, W.N., Western blotting: electrophoretic transfer of proteins from sodium dodecyl sulfate-polyacrylamide gels to unmodified nitrocellulose and radiographic

detection with antibody and radioiodinated protein A. *Analytical Biochemistry* **112(2),** 195-203 (1981).

Calleja, M., Javier, T., Nordstrom, M., Boisen, A., Low-noise polymeric nanomechanical biosensors. *Applied Physics Letters*, **88 (11)**, 113901-113903 (2006).

Carter, A.T., Beiche, F., Hove-Jensen, B., Narbad, A., Barker, P.J., Schweizer, L.M., Schweizer, M., PRS1 is a key member of the gene family encoding phosphoribosylpyrophosphate synthetase in Saccharomyces cerevisiae. *Mol.Gen. Genet.* **254 (2)**, 148-156 (1997).

Chang, M.C.Y., Pralle, A., Isacoff, E.Y., Chang, C.J., A selective, cell-permeable optical probe for hydrogen peroxide in living cells. *J. Am. Chem. Soc.*, **126 (47)**, 15392-15393 (2003).

Dhayal, B., Henne, W.A., Doorneweerd, D.D., Reifenberger, R.G., Low, P.S., Detection of bacillus subtilis spores using peptide-functionalized cantilever arrays. *J. Am. Chem. Soc.*, **128**, 3716-3721 (2005).

Drews, J., Drug discovery: a historical perspective. *Science* **17**, 287, 1960-1974 (2000).

Engvall, E, Perlman, P., Enzyme linked immunosorbent assay (ELISA) quantitative assay for immunoglobulin. *Immunochemistry* **8(9)**, 871-874 (1971).

Feibelman, P.J., D-electron frustration and the large fcc versus hcp binding preference in O adsorption on Pt. *Phys. Rev. B* **56**, 2175-2182 (1997).

Fritz, J., Baller, M.K., Lang, H.P,, Rothuizen, H., Vettiger, P., Meyer, E., Gu □ntherodt H.J., Gerber, C., Gimzewski J.K., Translating biomolecular recognition into nanomechanics. *Science* **288,** 316–8 (2000).

Fritz J., Cantilever biosensors. *Analyst*, **133**, 855-863 (2008).

Gaitas, A., Gianchandani, Y.B., An experimental study of the contact mode AFM scanning capability of polyimide cantilever probes. *Ultramicroscopy* **106 (8-9)**, 874-880 (2006).

Godin, M., Delgado, F.F., Son, S., Grover, W.H., Bryan, A.K., Tzur, A., Jorgensen, P., Payer, K., Grossman, A.D., Kirscher, M.W., Manalis, S.R., Using buoyant mass to measure the growth of single cells. *Nature Methods* **1452**, 1-4 (2010).

Goffeau, A., Barrell, B.G., Bussey, H., Davis, R.W., Dujon, B., Feldmann, H., Galibert, F., Hoheisel, J.D., Jacq, C., Johnston, M., Louis, E.J., Mewes, H.W., Murakami, Y., Philippsen, P., Tettelin, H., Oliver, S.G., Life with 6000 genes. *Science* **274 (5287)**, 563-567 (1996).

Gupta, A., Akin, D., Bashir, R., Single virus particle mass detection using microresonators with nanoscale thickness. *Appl. Phys. Lett*. **84 (11)**, 1976-1978 (2004).

Haddad, S.A., Lindegren, C.C., A method for determining the weight of an individual yeast cell. *Appl. Microbiol.* **1(3)**, 153-156 (1953).

Hermanson, G.T., *Bioconjugate Techniques*. Academic Press (1996).

Hoog de, G.S., Guarro, J., Gene, J., Figueras, M.J., Atlas of Clinical Fungi. In: Centraalbureau voor Schimmelcultures, second ed. Universitat Rovira i Virgili, Reus, Utrecht (2000).

Hosaka, S., Chiyoma, T., Ikeuchi, A., Okano, H., Sone, H., Izumi, T., Possibility of a femtogram mass biosensor using a self-sensing cantilever. *Current Applied Physics* **6 (3),** 384-388 (2006).

Ibach, H., The role of surface stress in reconstruction, epitaxial growth and stabilization of mesoscopic structures. *Surf. Sci. Rep.* **29**, 193 (1997).

Ilic, B., Czaplewski, D., Zalalutdinov, M., Craighead, H.G., Neuzil, P., Campagnolo, C., Batt, C., Single cell detection with micromechanical oscillators. *J. Vac. Sci. Technol. B* **19**, 2825 (2001).

Lang, H.P., Baller, M.K., Berger, R., Gerber, Ch., Gimzewski, J.K., Battiston, F.M., Fornaro, P., Ramseyer, J.P., Meyer, E., Guntherodt, H., A cantilever array-based artificial nose. *J., Anal. Chem. Acta* **393**, 59-65 (1999).

Lee, J., Shen, W., Payer, K., Burg, T. P., Manalis, S.R., Toward attogram mass measurements in solution with suspended nanochannel resonators. *Nano Letters* **10 (7)**, 2537-2542 (2010).

Marden, A., Walmsley, R.M., Schweizer, L.M., Schweizer, M., Yeast-based assay for the measurement of positive and negative influences on microsatellite stability. *M. FEMS Yeast Res* **6 (5)** 716-725 (2006).

Mertens, J., Rogero, C., Calleja M., Ramos, D., Mart ń-Gago, J.A., Briones, C., Tamayo, J., Label-free detection of DNA hybridization based on hydration-induced tension in nucleic acid films. *Nature Nanotechnology*, **3(5)**, 301–307 (2008).

McKendry, R., Zhang, J., Arntz, Y., Strunz, T., Hegner, M., Lang, H.P., Baller, M.K., Certa, U., Meyer, E., Gu ntherodt, H.J., Gerber. C., Multiple label-free biodetection and quantitative DNA-binding assays on a nanomechanical cantilever array. *Proc. Natl. Acad. Sci. U.S.A.* **99 (15)**, 9783 (2002).

Nickoloff, J.A., Hoekstra, M.F., DNA Damage and Repair: DNA Repair in Higher Eukaryotes (1998).

Nugaeva, N., Gfeller, K.Y., Backmann, N., Lang, H.P., Duggelin, M., Hegner, M., Micromechanical oscillators as rapid biosensor for the detection of active growth of Escherichia coli. *Biosensors and Bioelectronics* **21**, 849-856 (2005).

Park, K., Jang, J., Irimia, D., Stugis, J., Lee, J., Robinson, P., Tonerd, M., Bashir, R., Living cantilever arrays for characterization of mass of single live cells in fluids. *Lab on a Chip* **8**, 1034-1041 (2008).

Petranovic, D., Tyo, K., Vermuri, G.N., Prospects of yeast systems biology for human health: integrating lipid, protein and energy metabolism. *J. FEMS Yeast Res* **10 (8)**, 1046-1059 (2010).

Pizza, M. Scarlato, V., Masignani, V., Giuliani, M.M., Arico, B., Comanducci, M., *et. al.*, Identification of vaccine candidates against serogroup B meningococcus by whole-genome sequencing. *Science*, **287(5459)**, 1816-1820 (2000).

Sader, J. E., Method for the calibration of atomic force microscope cantilevers. *Rev. Sci. Instrum.*, **66**, 4583 (1995).

Schneiter, R., Carter, A.T., Hernando, Y., Zellnig, G., Schweizer, L.M., Schweizer, M., The importance of the five phosphoribosyl-pyrophosphate synthetase (Prs) gene products of Saccharomyces cerevisiae in the maintenance of cell integrity and the subcellular localization of Prs1p. *Microbiology* **146 (12)**, 3269-3278 (2000).

Stachowiak, J.C., Yue, M., Castelino, K., Chakraborty, A. Majumdar, A., Chemomechanics of surface stresses induced by DNA hybridization. *Langmuir* **22**, 263–8 (2006).

Stoney, G.G., *Proc. R. Soc. Lond.*, **A82**, 172 (1909).

Stygen, D., Goris, A., Safrati, J., Latge, J.P., A new sensitive sandwich enzyme-linked immunosorbent assay to detect galactofuran in patients with invasive aspergillosis. *J. Clin. Microbiol.*, **33**, 497-500 (1995).

Walkup, G.K., Burdette, S.C., Lippard, S.J., Tsien, R.Y., A new cell-permeable fluorescent probe for Zn2. *J. Am. Chem. Soc.*, **122 (23)**, 5633-5645 (2000).

Wang, Y., Bachman, M., Li, G.P., Guo, S., Wong, B.J.F., Chen, Z., Low-voltage polymer-based scanning cantilever for in vivo optical coherence tomography. *Optics Letters*, **30 (1)**, 53-55 (2005).

Watari, M., Galbraith, J., Lang, H.P., Sousa, M., Hegner, M., Gerber, C, Horton, M.A., McKendry, R., investigating the molecular mechanisms of in-plane mechanochemistry on cantilever arrays. *J. Am. Chem. Soc.* **129**, 601–9 (2007).

Weeks, B.L., Camarero, J., Noy, A., Miller, A.E., De Yoreo, J.J., Stanker, L., A microcantilever-based pathogen detector. *Scanning*, **25(6)**, 297-299 (2006).

Wenzel, M.J., Josse, F., Heinrich, S.M., An analytical model for transient deformation of viscoelastically coated beams: Applications to static-mode microcantilever chemical sensors. *Journal of Applied Physics* **105**, 064903 (2009).

Wide, L., Radioimmunoassay of proteins with the use of Sephadex-coupled antibodies. *J. Biochem Biophys Acta* **30**, 257-260 (1996).

Wu, G.H., Ji, H.F., Hansen, K., Thundat, T., Datar, R., Cote, R., Hagan, M.F., Chakrabory, A.K., Majumdara, A., Origin of nanomechanical cantilever motion generated from biomolecular interactions. *Proc. Natl Acad. Sci. USA*, **98** 1560–4 (2001).

Xiao, C., Lachance, B., Sunahara, G., Luong, J.H.T., Assessment of cytotoxicity using electric cell-substrate impedance sensing: concentration and time response function approach. *Anal. Chem*., **74 (6)**, 1333-1339 (2002).

Zhang, J., Ji, H.F., Third-generation biosensors based on the direct electron transfer of proteins. *Analytical Sciences*, **20**, 585-587 (2004).

Zhang, R.X., Xu, X., Development of a biosensor based on laser-fabricated polymer microcantilevers. *Applied Physics Letters*, **85 (12)**, 2423-2425 (2004).

Zhou, F., Shu, W., Welland, M.E., Huck, W.T.S., Highly reversible and multi-stage cantilever actuation driven by polyelectrolyte brushes. *J. Am. Chem. Soc*. **128**, 5326-5327 (2006).

"Dupont Kapton Polyimide Film General Specifications, Bulletin GS-96-7". http://www.dupont.com/kapton/general/H-38479-4.pdf

SII NanoTechnology Inc. Application Brief, DMS no.11, August 1991

Chapter 5 Integrated microfluidics with Microcantilever Biosensor Arrays for Real-time Nanotoxicity Measurements

5.1 Introduction

The unique properties exhibited by nanoparticles (NPs) have encouraged their exploitation within diverse applications across many sectors. This is exemplified by the use of NPs for diagnostic sensing (Medintz *et al*., 2005), photodynamic therapy (Caruthers *et al*., 2007), drug treatments (Tan *et al.,* 2009), drug delivery (Gao *et al*., 2004) and antibacterials (Jones *et al*., 2010). The anticipated increase in exposure to NPs through greater use and production makes it necessary to assess the risks posed by NPs to human health and the environment. Despite the fact that this challenge has been recognized for some time (Maynard *et al*., 2006, Tsuji *et al*., 2006, Colvin, 2003); limited progress has been made within the assessment of NP safety, which derives, in part, from a lack of standardized approaches to evaluate NP toxicity.

The huge diversity of NPs under development means that it is not possible to only use *in vivo* models to assess NP safety. Instead, *in vitro* systems, that are alternatives to animal testing, are essential to assess the toxicity of NPs due to time, financial and ethical considerations. *In vitro* models are often criticized for their inability to truly mimic the *in vivo* conditions, and so there are concerns surrounding their ability to predict NP safety. However, *in vitro* systems are very useful when screening the toxicity of NPs and comparing the toxicity of different types NPs at different target sites in the body. Assessment of the ability of NPs to elicit cytotoxicity is often the starting point for *in vitro* studies as they allow identification of inhibitory concentrations (IC) of NPs such as the IC_{50} (or similar) that can be used for benchmarking and regulatory purposes whilst also determining sub-lethal concentrations of NPs that can be used in mechanistic studies. There are currently many methods of performing cell viability or cytotoxicity assays, the most popular of which are the chemically labeled assays such as the MTT (3-(4,5-Dimethylthiazol-2-yl)-2,5-diphenyltetrazolium bromide, Lewinski *et al*., 2008) and MTS (3-(4,5-dimethylthiazol-2-yl)-5-(3-carboxymethoxyphenyl)-2-(4-sulfophenyl)-2H-tetrazolium, Xu *et al*., 2004), Alamar Blue (Weisberg *et al.,* 2005), lactate dehydrogenase (LDH, Atarashi *et al.,* 2008), 4-[3-(4-iodophenyl)-2-(4-nitrophenyl)-2H-5-tetrazolio]-1,3-benzene disulfonate (WST-1, Ishiyama *et al.,* 1996),

Trypan Blue (Tennant, 1964) and adenosine triphosphate based assays (ATP, Atarashi *et al*., 2008). These labeled techniques are unable to provide real-time cell behavior monitoring following cell exposure to NPs. (Koppenhofer *et al.,* 2012). In addition, interference of NPs with these assays can compromise their usefulness, due to the appearance of false positive or negative results (Worle-Knirsch *et al.,* 2006). Other techniques to monitor cell viability include optical (Chang *et al*., 2004), fluorescent (Walkup *et al*., 2000), and electrical (Prakesh, 2007) approaches, which possess the same disadvantages to the chemically labeled methods, in that they introduce external interference into the system. This external interference can affect the cell response, and are therefore unable to provide cell viability tests in a clean and non-disturbed cell growth environment (Scudiero *et al*., 1988). Typical cell screening techniques require labeling and have focused on drug discovery (Drews, 2000), or the detection of specific biological cells, often aiming towards single cell detection limits (Park *et al.,* 2008).

This *in vitro* study investigated the impact of NPs on the C3A human hepatoblastoma derived liver cell line using real-time label-free microcantilever biosensor arrays in a microfluidic cell culture chamber. Using microcantilever sensors as a platform for cell cytotoxicity tests allowed for the determination of cell behavior and kinetics during the entire duration of the assay. The use of microcantilever biosensors for cell studies provides many advantages such as being highly sensitive, selective, label-free, and allows monitoring of the cell response in real-time. Single cell detection and monitoring on the cantilever surface has been reported previously (Park *et al.,* 2008, Bryan *et al*., 2009, Burg *et al*., 2007, Godin *et al*., 2010) due to the high mass resolutions of cantilever sensors. Cell growth detection has been demonstrated by monitoring resonance frequency changes of microcantilevers as the mass increases from immobilized fungal spores (Nugaeva *et al*., 2005) and bacteria (Gfeller *et al.,* 2005) on the surface of the cantilevers in humid air. Although the methods currently demonstrated are sensitive and useful in studying the mechanisms of a cell, they have been limited in studying non-adherent cell growth. In addition, in comparison to large-scale assays, the throughput of a single cantilever system prevents rapid determination and testing of varying cells and/or media. Therefore, for practical applications, mammalian cell growth detection has not been reported previously using microcantilever sensors. In this chapter, we not only present the first practical example

of mammalian cell growth monitoring using low-cost polymer microcantilever sensors operating in static mode, but also demonstrate the use of a microfluidics based microcantilever array for simple real-time cell growth measurement for cell-based assays and the ability of the system to assess the cellular toxicity of NPs.

5.2 Project Background

The project was performed in collaboration with Prof. Vicki Stone and Dr. Nilesh Kinase from the School of Life Sciences at Heriot-Watt University. C3A liver cells were provided at a concentration of $1x10^6$ cells/mL. All cell culturing was performed by them, in addition to the various different cell media types used in the following experiments. Furthermore, the experiments were designed with their knowledge to determine suitable experiments to validate our findings, followed by insight into cell mechanics and behaviors once experiments were completed. After the experiments were completed, Dr. Kinase provided C3A cells stained with fluorescent dye, in order to culture cells on the surface of cantilever sensors to validate the results. The goal of the experiments was to determine if the scanning cantilever array detection system with microfluidics is capable of detecting and monitoring cell growth in real-time, while supporting the intricacies of highly vulnerable liver cell culturing on the surface of microcantilever sensors.

5.3 System Design and Methodology

A scanning microcantilever system with incorporated microfluidic channels, gas delivery system, and temperature control was used with an array of twelve gold-coated polymer microcantilevers on one chip. (Figure 5-1b, 1d) The scanning microcantilever sensor system is similar to Martinez *et al.*, (2010, Figure 5-1a), and consists of a linear actuator, which scans a laser across the array of cantilevers, allowing for real-time monitoring of cells with static mode cantilevers. Polymer cantilevers were fabricated into arrays through laser micromachining and have a thickness of 25μm and dimensions of 1mm x 200μm. 5nm of chromium followed by 40nm of gold were then coated on one side of the cantilever to provide a reflective coating for the laser beam. Six microfluidic channels fabricated with PMMA hold two cantilevers in each channel allowing for simultaneous delivery and monitoring of six independent experiments with varying cell and/or media types. This means that six different experiments are performed

simultaneously, with a duplicate of each experiment. CO2 for cell growth was delivered through a permeable membrane in the flow chamber well, whereby the membrane separates the liquid from the gas, allowing a 5% CO2 mixture to permeate and be exposed to the media. (Figure 5-1c) Temperature was precisely controlled to 37±0.5℃, the optimal temperature for C3A cell growth.

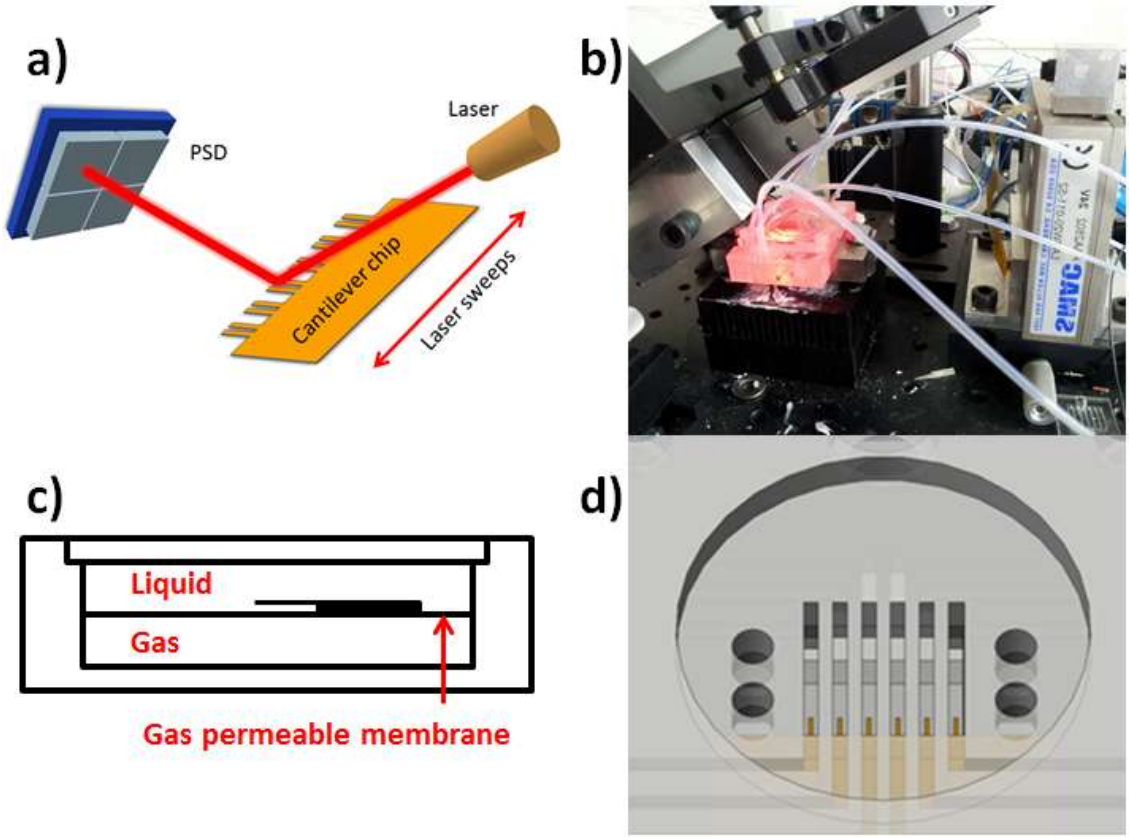

Figure 5-1: a) Schematic of the scanning cantilever system. b) Actual setup in the lab. c) Schematic of the flow cell chamber, with a gas permeable membrane separating the liquid and gas sections. d) 3D rendering of the microfluidic channels with cantilevers inside each channel.

The entire cantilever chamber was first flushed with highly diluted bleach (1%) for disinfection, followed by a thorough rinsing with deionized water to remove all traces of bleach. Phosphate buffered solution (PBS) was then injected into the chamber, allowed to rest for 15 minutes, and flushed with PBS at least 3 times to prepare the chamber for cell culturing. 10 µL of the C3A cells ($1x10^6$ cells/mL or 100 cells) were placed onto each of the microcantilever sensors. The cells adhered onto the cantilever surface (5 min.), and then cell culture growth medium was injected into the system. A

baseline growth model was obtained over a 3 hr period, and NPs were then injected (in cell culture media at varying concentrations; 0.5-128 μg/mL) for 18 hrs.

Silver NPs (Ag, < 20nm polyoxylaurat Tween 20 capped) were selected as the main particle of interest, due to its high toxicity towards C3A cells (Kermanizadeh *et al*. 2011). Silver NPs exhibit strong antibacterial activity and are therefore currently used in textiles, plastics, implants, contraceptives, water disinfectant, etc (Chen *et al*., 2008). Due to Ag NPs being used regularly for applications such as disinfecting water or preserving food, it is highly likely that some particles may be consumed by humans. It has been reported that after ingestion, Ag NPs are able to translocate to secondary target sites (Buzea *et al*., 2007, Gaiser *et al*., 2009, Takenaka *et al*., 2001). NPs have been observed to preferentially accumulate in the liver where they may exhibit toxicity (Takenaka *et al*., 2001, Hussain *et al*., 2005, Carlson *et al*., 2008, Chen *et al*., 2008). Hepatocytes constitute the main cell population in the liver, thus the C3A hepatocyte cell line is a relevant model to assess the liver response to NPs.

In addition, titanium dioxide NPs (TiO_2 rutile, anatase thermal 7 nm) were studied, due to their widespread use by many industries (Weir *et al*., 2012) such as paints, papers, plastics, food additives/colours, pharmaceuticals, and cosmetics (Jin *et al*., 2008). In particular, TiO_2 NPs have widespread use in sunscreen products and window coatings, due to their ability to absorb UV light with limited scattering (Jin *et al*., 2008). Studies have concluded that after ingestion of TiO_2 NPs, the particles tend to accumulate in the liver (Geiser *et al*., 2010), and the consequences of liver exposure to TiO2 needs to be evaluated.

Triton-X100 (a detergent – 0.01%) was used as a positive control to induce cell death. In addition, control experiments without cells, but with high doses of NPs were completed to disregard any non-specific or weight interferences from large amounts of nanoparticles and the cantilever sensors.

5.4 Challenges

The most significant challenge during the course of experiments was the chamber setup for the microcantilever sensors. As it can be seen in Figure 5-2, at least 50% of the

experiments first performed with the scanning cantilever array resulted in failures due to leaking from the chamber. This is due to the uneven pressure from the sapphire glass cover to the 1mm thick silicone layer when sealing the chamber. The silicone layer is quite soft, and in particular, the middle channels to not have constant pressure to prevent cross contamination in addition to leaking outwards. The solution was to seal the chamber by removing the silicone layer. Since the chamber itself is a single use design, double sided tape was used instead to fully seal the sapphire cover to the channels. Double sided tape was stuck to both sides of a 1mm thick layer of PMMA. This piece was cut to the same shape of the microfluidic channels just like the silicone layer, creating a chip with channels and double sided tape on both sides. This piece was aligned with the main chamber, followed by sticking the sapphire cover on top, creating a semi-permanent seal that prevented any further leakage from occurring. This solution minimized the failure rate of the experiments from channel leakage.

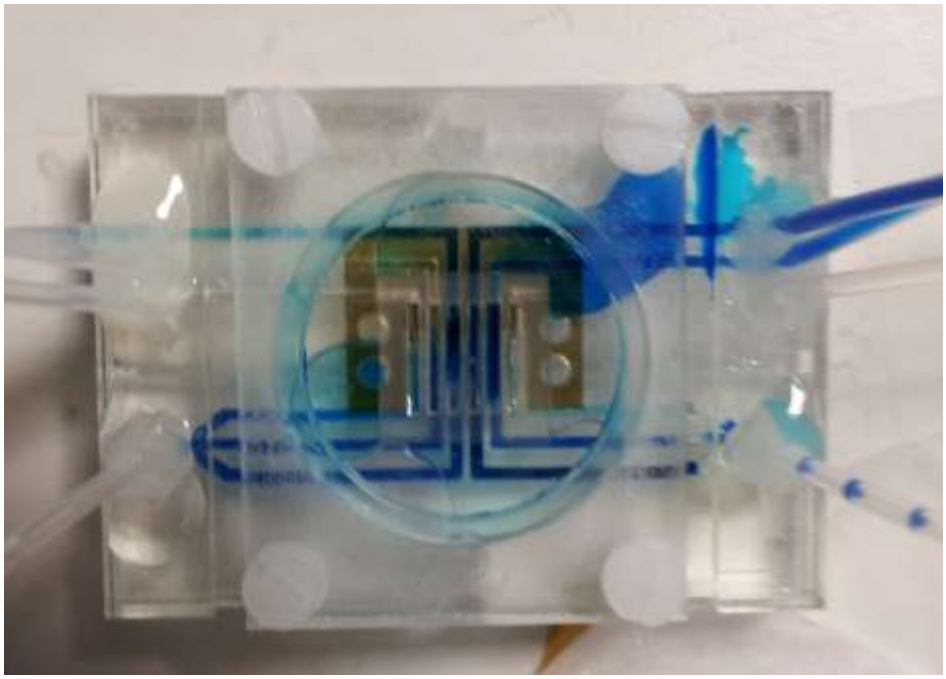

Figure 5-2: Flow cell chamber for the microcantilever array. Leakage can be seen through the use of blue food coloring.

The second main reason for experimental failure in the beginning was due to the injection of media. As seen in Figure 5-3, from the initial experimental start, there was a slow and steady leakage of the cantilever chamber. It was decided to continue with the experiment as new cells were not available immediately for a replacement experiment.

After the injection of media with NPs at the 3 hr. mark, large spikes occurred and air bubbles formed in the middle of the microfluidic channels, creating data that was unusable. This was due to too rapid of an injection speed for the media, causing a large disturbance of the cantilever beams. Because the media is injected into the system using a series of syringes, a syringe pump was instead used to control the exact injection flow rate. Rather than hand pumping the syringe at a speed of 2mL in a few seconds, the syringe pump injected the media at a slow and steady pace of 2mL in 10 min. This minimized the disturbance of the cantilevers and also solved the problem of air bubbles by reducing the pressure inside the microfluidic channels. Other experimental failures all arose from human error due to improper handling of cells or other procedures. Following the proper sealing of the chamber, the following results were successfully obtained.

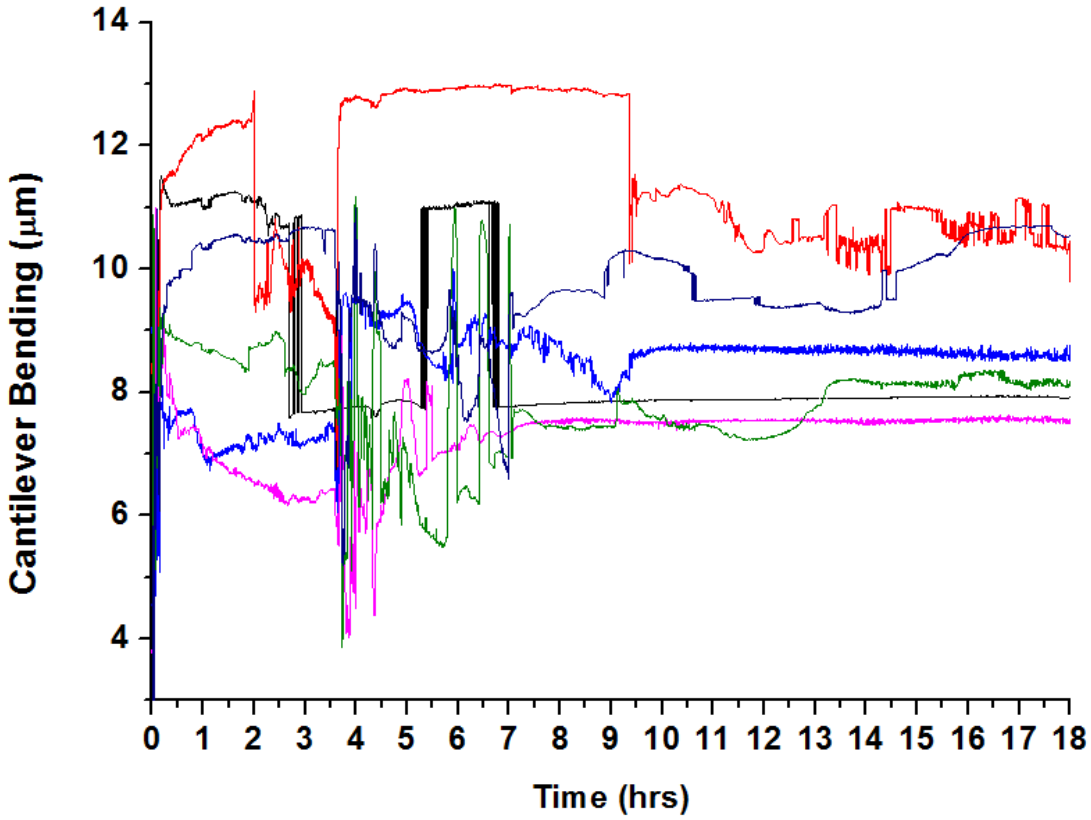

Figure 5-3: Failed experiment due to too rapid of injection of media after slight leakage from initial sealing of chamber.

5.5 Results and Discussion

C3A cells on the surface of the microcantilever sensor were subjected to a wide variety of growth and non-growth conditions. Differences in cantilever bending, signify

different quantities of remaining viable cells. Figure 5-4a shows the growth curves of C3A cells with a pure growth media, six varying concentrations of Ag NPs, Triton-X100, and a medium and NP control with no cells. After the injection of growth media into the system, the cell growth curve demonstrated a rapid and exponential growth. This was indicated by an extremely large downwards cantilever deflection (~4μm) which was recorded for the baseline growth condition, and subsequent lower growth conditions produced downwards bending from ~1-4μm. All conditions where C3A cells were expected to grow produced a downwards bending of the cantilever.

The cantilever bending signals show that all concentrations of Ag NPs produce a temporary pause in cell growth for ~2 hr. followed by continued but subdued growth. The impact of Ag NP exposure on cantilever bending was concentration dependent. Higher concentrations of Ag caused less bending signifying a fewer number of viable cells and hence lower amount of growth. Each experiment with different NP concentrations was repeated three times.

The results correlate with the results obtained by Kermanizadeh *et al*., (2011), whereby Ag NPs exhibited significant toxicity towards the cells using conventional cytotoxicity assays. Following the injection of the Ag NPs, there was a clear and distinct difference in the growth of the cells. A dose dependent inhibition of cell growth was induced by silver NPs; so that an increasing concentration of silver NPs increased their toxicity. Higher concentrations of Ag produced a lower amount of cell growth, while lower concentrations of Ag produced a larger amount of cell growth. Regardless of the nanoparticle concentration, all cells noticed a 2.5 hr. recovery period after the initial injection of NPs, as they maintained their current cell characteristics before recovering and followed by continued growth. TiO_2 NPs seen in Figure 5-5a demonstrated extremely similar results to those of silver NPs, with a brief period of growth followed by a reaction phase after initial injection of the NPs, ending with significant growth starting from 2 hr. after injection. It should be noted that noise levels and chip to chip variations inherent to polymer microcantilever chips are constantly present, and therefore all tests require an internal reference sensor to eliminate these effects.

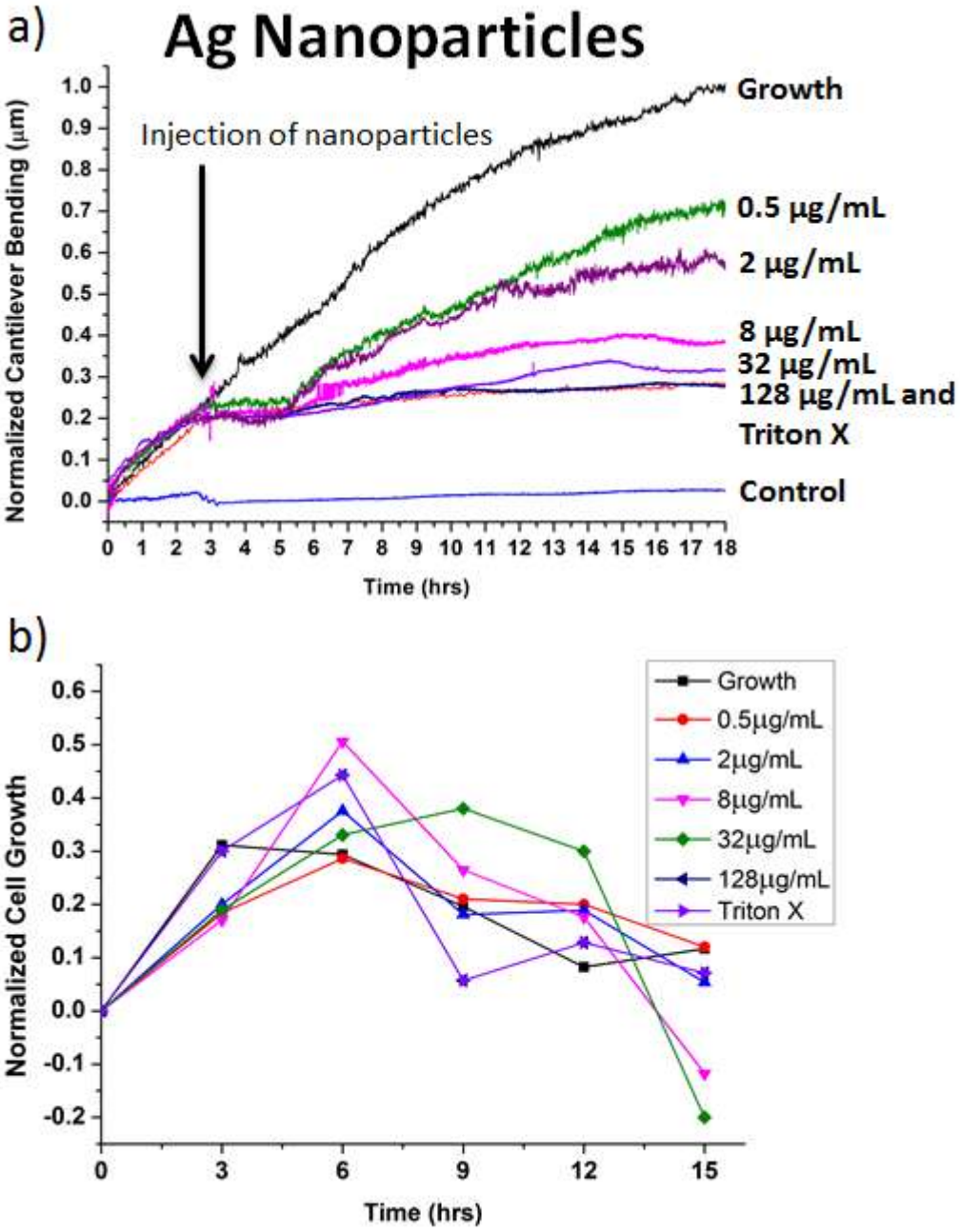

Figure 5-4: a) Cantilever bending signals with respect to varying Ag nanoparticle concentrations. b) Normalized cell growth rates over time with Ag nanoparticles, shown as a percentage of total growth. The control experiments were performed with the highest concentration of Ag NPs (128 µg/mL) and no cells, to determine if the NPs had any direct effects on the microcantilever sensors.

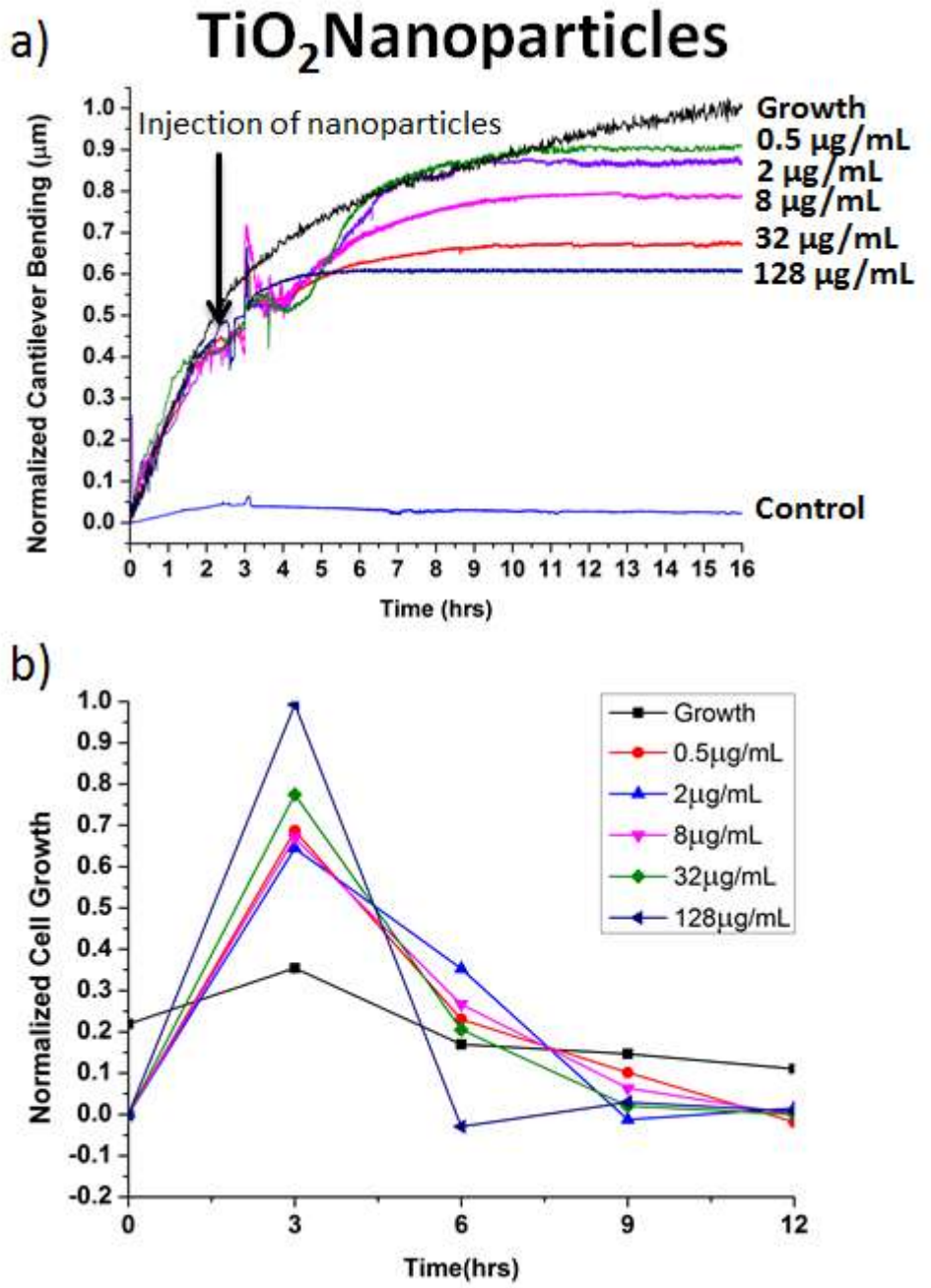

Figure 5-5: a) Normalized cantilever bending signals with respect to varying TiO_2 nanoparticle concentrations. Control signifies no cells on cantilever surface. b) Normalized cell growth rates over time with TiO_2 nanoparticles, shown as a percentage of total growth. The control experiments were performed with the highest concentration of Ag NPs (128 µg/mL) and no cells, to determine if the NPs had any direct effects on the microcantilever sensors.

The results are consistent with studies demonstrating that identical Ag NPs are more toxic to cells than TiO_2 NPs (Kermanidazeh *et al.*, 2011). Ag NP results correlate to

those of previous studies where 0.5 μg/mL demonstrated toxicity to liver cells (Kawata *et al*. 2009, Park *et al*., 2010). The reasons for this are unknown, as Chen *et al*. (2008) showed that silver particles of a nano-scale size demonstrate peculiar physical, chemical, and biological properties. TiO_2 NPs were found to demonstrate relatively low levels of toxicity towards C3A liver cells, compared to Ag NPs. (Kermanizadeh *et al*., 2011) Other studies support those results, as another cell line was found to demonstrate no toxicity towards TiO_2 NPs (Jin *et al*., 2008).

It can be seen from the results that in the case of the experiments comparing Ag to TiO_2 NPs on microcantilever sensors, the curves are dissimilar. For the Ag NPs, after the period of non-growth after the injection of the NPs, the cells continue to replicate causing a continual downwards bending of the cantilever beam over the 15 hr. period.

Conversely, the results of the TiO_2 NPs show that the cells on the cantilever surface only reproduce for a short period of time after the injection of the NPs, followed by a steady state whereby no more cantilever deflection occurs. The reason for this is in the difference of how the experiments were performed. In the case of Ag NPs, the results obtained were from a single cantilever system with temperature and gas control. The experiments were performed one at a time. This required a long period of time to conduct and also reproduce the results, and thus for the TiO_2 NP experiments, it was run utilizing the multiple cantilever scanning array system with microfluidic channels. Therefore, comparing the normalized cell growth rates as a percentage of total growth in Figures 5-4b and 5-5b**,** it can be seen that TiO_2 NP growth peaks much earlier at 3 hr. compared to Ag NP growth at 6 hr.

While the cantilever array system allowed for a much higher throughput (6 vs. 1) compared to the single cantilever system, the results differ slightly. The reason behind this is thought to be caused by the microfluidic channels. As the cells proliferate, they require nutrients from the growth media to sustain continued growth. But with the microfluidic channel, the cell culture "well" inside each channel was significantly smaller compared to the single cantilever system where the entire cantilever is mounted into a very large well (volume of 1000 times larger). Therefore, the cells are unable to sustain growth in the microfluidic channels for an extended period of time as opposed to

the cells inside the single cantilever system are able to. It is more clearly seen in the difference between the full growth states of both the deflection curves.

In addition, aside from the lower concentrations of NPs (<8 μg/mL), these results do not correlate to the previous studies where TiO_2 NPs were shown to be less toxic to C3A cells compared to Ag NPs. While this may also be an unknown factor due to the microfluidic channels, another possible reason that studies have shown that TiO_2 NPs do not cause toxicological damage to mammalian cells under dark conditions (Koeneman *et al*., 2010). Conventional toxicity experiments are performed in an incubator, which is a dark condition, possibly affecting the toxicity of TiO_2 NPs. But in the case for microcantilever sensors, the scanning laser is constantly directed at the cantilevers where the cells are being cultured. Therefore, with the constant light, it may be possible that it increases the toxicity of the TiO_2 NPs, which may not have been noticed in conventional cell assays in a dark environment.

It should be noted that cell growth induced polymer cantilever surface stresses from the micron range of bending is larger than the maximum reported surface stress changes of cantilever biosensors in liquid environments (Fritz, 2008). The significant enhanced sensitivity recorded by polymer cantilever sensors may be due to the viscoelastic effect from the polymer materials. A recent theoretical study has predicted that viscoelastic polyimide cantilever will exhibit at least one order of magnitude greater in the bending signal than cantilevers made of elastic materials (e.g. silicon or silicon nitride) (Wenzel *et al*., 2009).

In order to validate the experiments, and to confirm that cells are able to survive and be cultured on microcantilever surfaces, staining experiments were performed in addition to SEM images after the experiments in Figure 5-6.

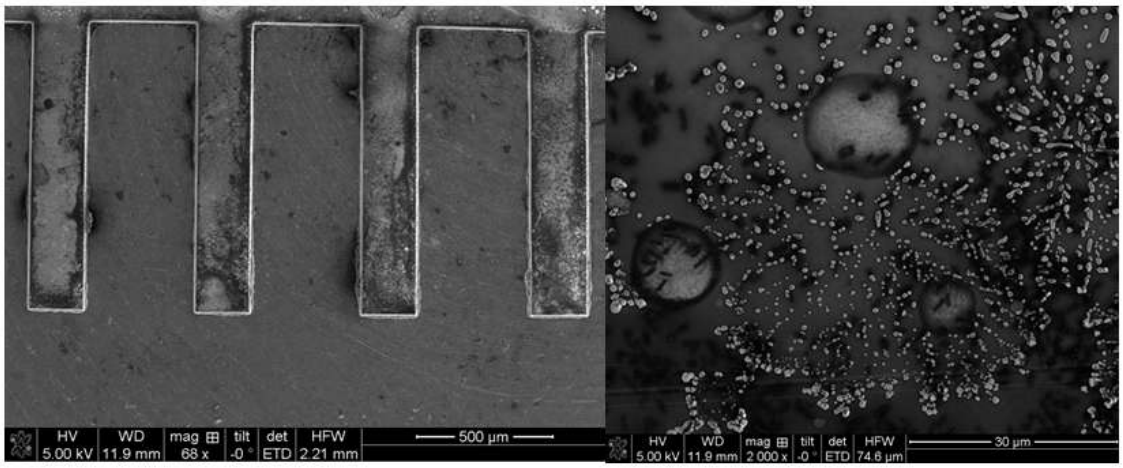

Figure 5-6: SEM images of the cantilever array after completed experiment with Ag NPs.

SEM imaging of the cantilevers proved to be relatively inconclusive. There appeared to be cells on the surface of the cantilever, and it appeared that the NPs were actually able to penetrate the cell and remain inside (as seen by the black dots in the middle of the cells. But there also seemed to be an excessive amount of residue forming all over the cantilever, and it was not possible to determine the origins and cause of them.

Afterwards, further experiments were conducted by just staining the C3A cells and culturing them on the surface of the cantilever to determine if the cantilever surfaces were viable for cell culturing. Phalloidin-TRITC dye was used to stain actin fibers (entire cell) except the nucleus and has an excitation at 557nm wavelength with emission at 576nm (red), while the nucleus was stained with Pseudo DAPI dye (blue), all of which was performed by Dr. Kinase. The resulting images can be seen in Figure 5-7.

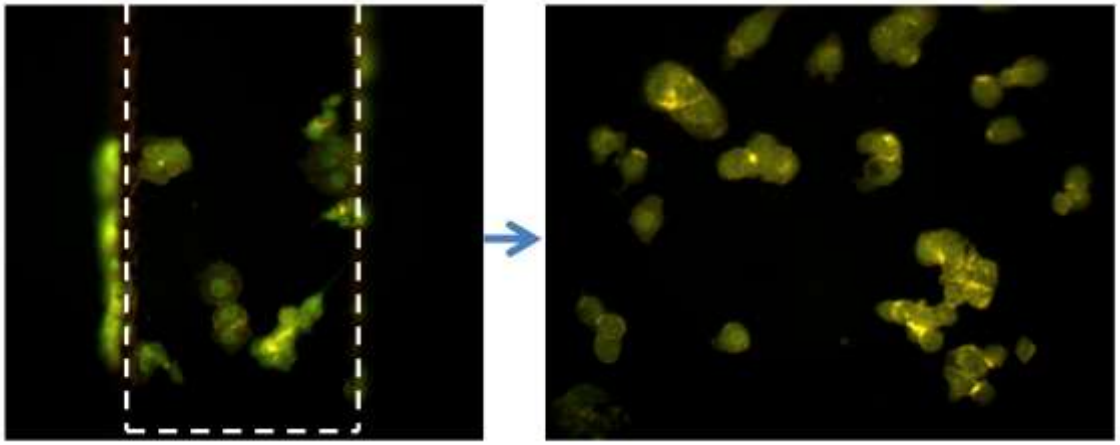

Figure 5-7: Fluorescent microscope images of cells attached to a microcantilever sensor.

Furthermore, Diff-Quick was used as a staining agent for its simplicity in staining the cells on the cantilever surface. Results can be seen below in Figure 5-8 and 5-9.

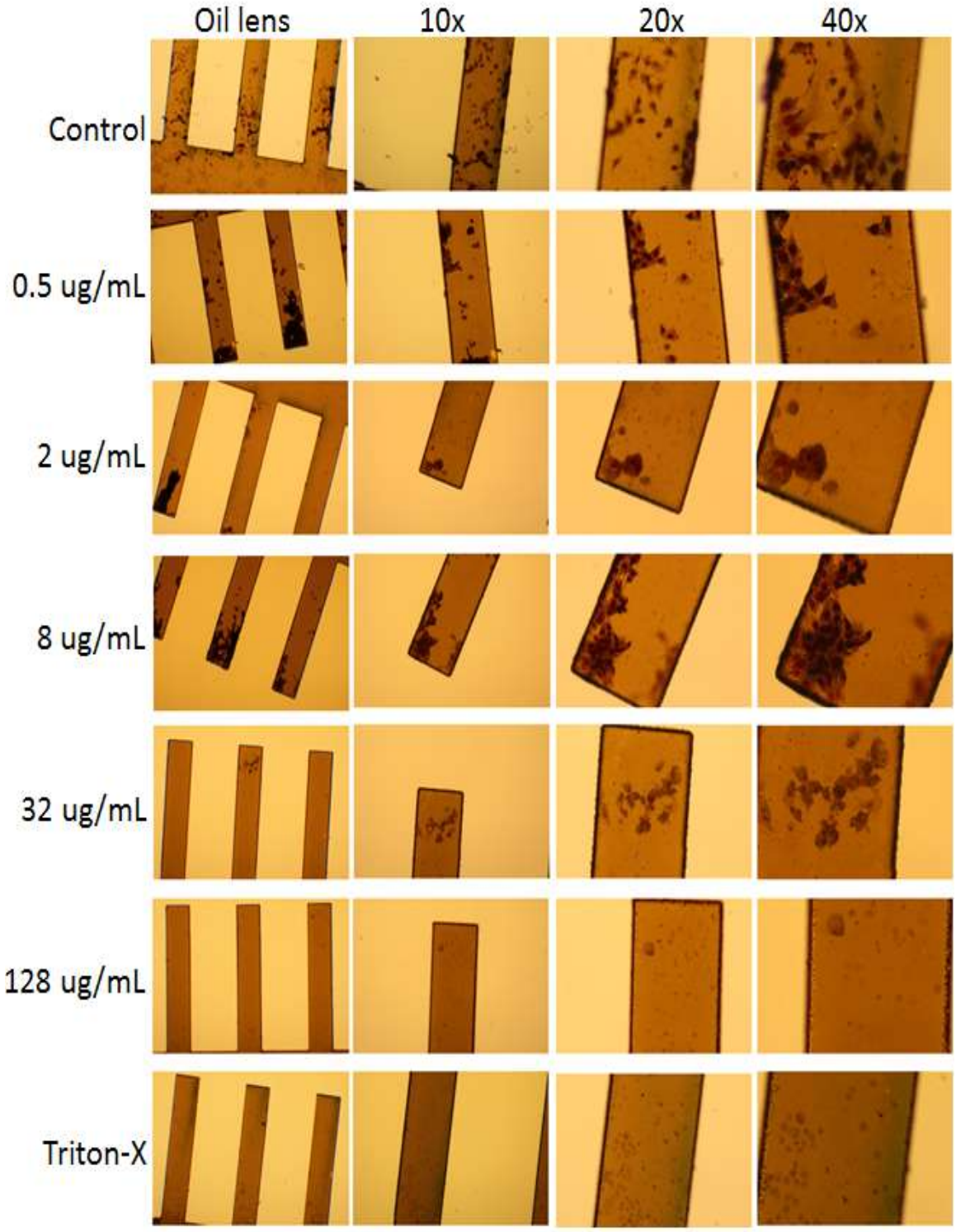

Figure 5-8: Microscope images of a microcantilever array with C3A cells treated with different concentrations of Ag NPs (y-axis) under varying magnification levels (x-axis).

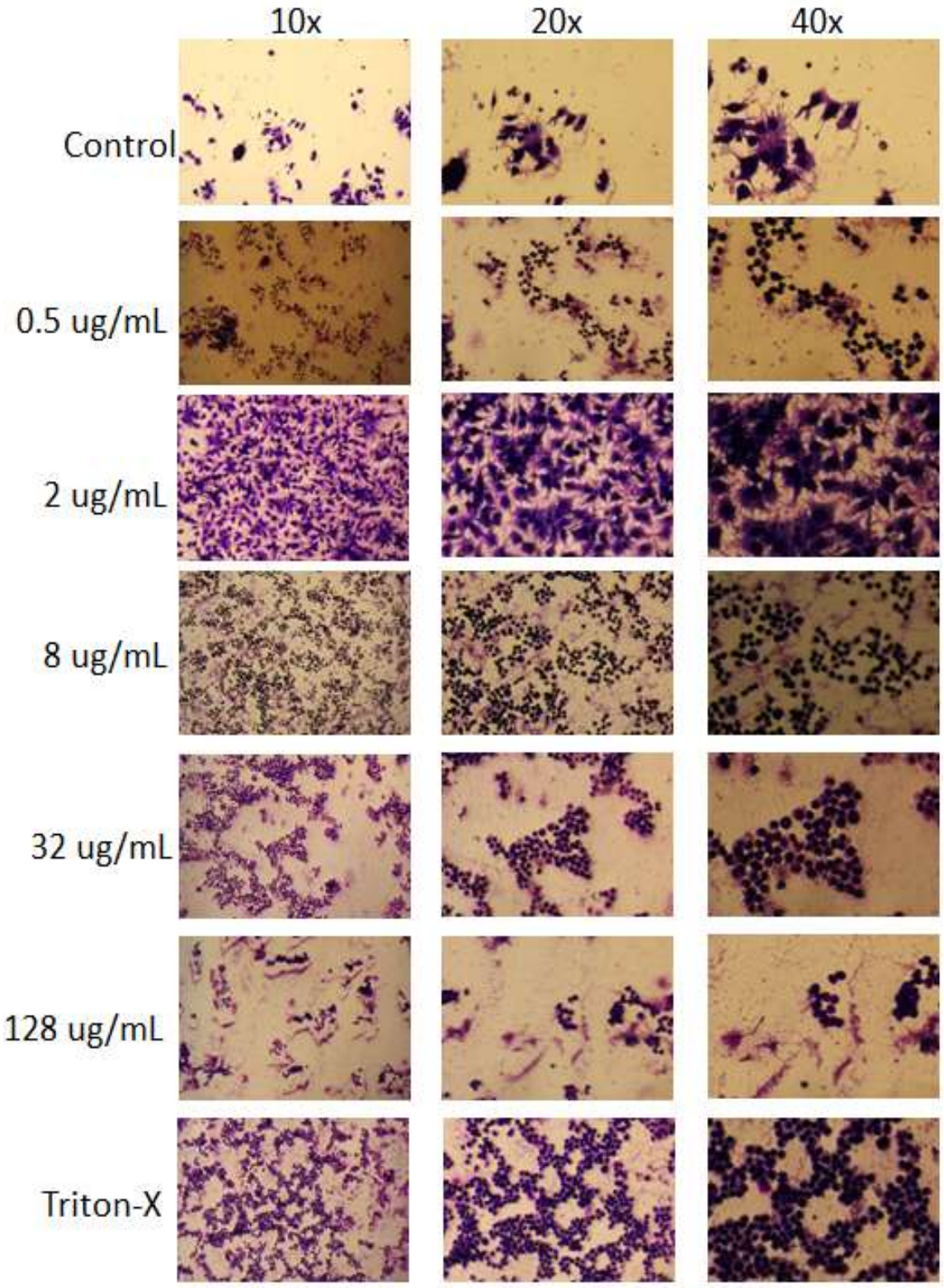

Figure 5-9: Fluorescent microscopy images of a microcantilever array with C3A cells stained with Diff-Quick before being treated with different concentrations of Ag NPs (y-axis) under varying magnification levels (x-axis).

From those results, it can easily be seen that higher concentrations of Ag NPs create the lowest number of viable cells, although differences may be small. This is because the number of cells used in the microcantilever experiments were extremely small compared to traditional cell culture assays, which translated into difficulties and inconsistencies. In order to attempt to fully compare the microcantilever system to conventional assays, a lactate dehydrogenase (LDH) assay was used. These assays measure the LDH levels for each cell culture, which is produced when cell membranes break down and LDH is able to move from inside the cells to its surrounding media. Unfortunately, the assay is not possible due to the low cell numbers used in the cantilever sensor experiments (0.1 million cells per treatment). Due to the large wells required for the assay, there were only ~20-30 cells per cantilever, which caused extremely low LDH release from cell damage. This may indicate that the colorimetric LDH assay is not sensitive enough when measuring a low number of cells, which the microcantilever sensors have been demonstrated above to easily monitor.

5.6 Conclusions

- A microcantilever array of static mode polymer microcantilever sensors with an integrated cell culture chamber and gas delivery system was developed to provide simple, higher throughput real-time assessment assays for measuring cytotoxicity.

- Human hepatoblastoma derived liver cell line C3a cells were exposed to silver and titanium dioxide nanoparticles. Results indicate that the polymer cantilevers combined with microfluidic channels provide a high throughput method for performing real-time cytotoxicity assays, without introducing any external interference into the system, allowing cells to behave as they would in real life.

- The sensors displayed distinct cell kinetics over a 24 hr. period, and could pave the way for exciting new possibilities for further study into the effects of cytotoxicity, cell screening, drug development, and nanoparticle health safety. It is now necessary to evaluate the wider applicability of the findings to more diverse types of NPs and cells. Such high throughput systems for screening NP

toxicity are urgently required due to the diversity of NPs whose safety requires assessment.

5.7 References

Atarashi, K., Nishimura, J., Shima, T., Umesaki, Y., Yamamoto, M., Onoue, M., Yagita, H., Ishii, N., Evans, R., Honda, K., Takeda, K., ATP drives lamina propria TH17 cell differentiation. *Nature* **455**, 808-812 (2008).

Braun, T., Barwich, V., Ghatkesar, M.K., Bredekamp, A.H., Gerber, C., Hegner, M., Lang, H.P., Micromechanical mass sensors for biomolecular detection in a physiological environment. *Phys. Rev. E* **72** (2005).

Bryan, A.K., Goranov, A., Amon, A., Manalis, S.R., Measurement of mass, density, and volume during the cell cycle of yeast. *PNAS* **107 (3)**, 999-1004 (2009).

Burg, T.P., Godin, M., Knudsen, S.M., Shen, W., Carlson, G., Foster, J.S., Babcock, K., Manalis, S.R., Weighing of biomolecules, single cells and single nanoparticles in fluid. *Nature Letters* **446**, 1066-1069 (2007).

Buzea, C., Pacheco, I.I., Robbie, K., Nanomaterials and nanoparticles: sources and toxicity. *Biointerpahses* **2**, 18-67 (2007).

Carlson, C., Hussain, S.M., Schrand, A.M., Braydich-Stolle, L.K., Hess, K.L., Jones, R.L., Schlager, J.J., Unique cellular interaction of silver nanoparticles: size-dependent generation of reactive oxygen species. *Journal of Physical Chemistry* **112**, 13608-13619 (2008).

Caruthers, S.D., Wickline, S.A., Lanza, G.M., Nanotechnological applications in medicine . *Curr Opin Biotech*, **18,** 26-30 (2007).

Chang, M.C.Y., Pralle, A., Isacoff, E.Y., Chang, C.J., A selective, cell permeable optical probe for hydrogen peroxide in living cells. *J. Am. Chem. Soc*., **126(47)**, 15392-15383 (2004).

Characterising the potential risks posed by engineered nanoparticles: a first UK government research report. Edited by Department for Environment FaRA (2005).

Chen, C., Zhang, P., Hou, X., Chai, Z., Subcellular distribution of selenium and Se-containing proteins in human liver. *Biochemica et Biophysica Acta* **1427**, 205-215 (1999).

Chen, X., Schluesener, H.J., Nanosilver: a nanoproduct in medical application. *Toxicology Letters* **176**. 1-12 (2008).

Colvin, V.L., The potential environmental impact of engineered nanomaterials . *Nat Biotechnol*. **21,** 1166-1170 (2003).

Daley, G.Q., Callahan, L., Catley, L., Cavazza, C., Mohammed, A., Neuberg, D., Wright, R.D., Gilliland, D.G., Griffin, J.D., Characterization of AMN107, a selective inhibitor of native and mutant Bcr-Abl. *Cancer Cell* **7(2)**, 129-141 (2005).

Drews, J., Drug Discovery: a historical perspective, *Science* **287(5460)**, 1960-1964 (2000).

Gao, X., Cui, Y., Levenson, R.M., Chung, L.W.K., Nie, S., In vivo cancer targeting and imaging with semiconductor quantum dots. *Nat Biotechnol*., **22,** 969-976 (2004).

Fritz, J., Cantilever biosensors. *Analyst*, **133**, 855-863 (2008).

Geiser, M., Kreyling, W.G., Deposition and biokinetics of inhaled nanoparticles. *Particle and Fibre Toxicology* **7**, 2-19 (2010).

Godin, M., Delgado, F.F., Son, S., Grover, W.H., Bryan, A.K., Tzur, A., Jorgensen, P., Payer, K., Grossman, A.D., Kirscher, M.W., Manalis, S.R., Using buoyant mass to measure the growth of single cells. *Nature Methods* **1452**, 1-4 (2010).

Gupta, A., Akin, D., Bashir, R., Single virus particle mass detection using microresonators with nanoscale thickness. *Appl. Phys. Lett.* **84 (11)**, 1976-1978 (2004).

Hansen, K.M., Ji, H.F., Wu, G., Datar, R., Cote, R., Majumdar, A., Thundat, T., Cantilever based optical deflection assay for discrimination of DNA single nucleotide mismatches, *Anal. Chem*, **73(7)**, 1567-1571 (2001).

Hosaka, S., Chiyoma, T., Ikeuchi, A., Okano, H., Sone, H., Izumi, T., Possibility of a femtogram mass biosensor using a self-sensing cantilever. *Current Applied Physics* **6 (3)**, 384-388 (2006).

Hussain, S.M., Hes, K.L., Gearhart, J.M., Geiss, K.T., Schlager, J.J., Toxicity evaluation for safe use of nanomaterials: recent achivements and technical challenges. *Toxicology in vitro* **19**, 975-983 (2005).

Ilic, B., Czapiewski, D., Zalalutdinov, M., Craighead, H.G., Neuzil, P., Campagnolo, C., Batt, C., Single cell detection with micromechanical oscillators, *J. Vac. Sci. Technol. B* **19**, 2825 (2001).

Ishiyama, M., Tominaga, H., Shiga, M., Sasamoto, K., Ohkura, Y., Ueno, K., A combined assay of cell viability and in vitro cytotoxicity with a highly water-soluble tetrazolium salt, neutral red and crystal violet. *Biological & Pharmaceutical Bulletin*, **19(11)**, 1518-1520 (1996).

Jin, C.Y., Zhu, B.S., Wang, X.F., Lu, Q.H., Cytotoxicity of titanium dioxide nanoparticles in mouse fibroblast cells. *Chemical Research in Toxicology* **21**, 18781-1877 (2008).

Johansson, A., Polymeric cantilever-based biosensors with integrated readout. *Applied Physics Letters* **89(17)**, 173505-173508 (2006).

Kawata, K., Osawa, M., Okabe, S., In vitro toxicity of silver nanoparticles at noncytotoxic doses to HepG2 human hepatoma cells. *Environmental Science and Technology* **43**, 6046-6051 (2009).

Koeneman, B.A., Zhang, Y., Westerhoff, P., Chen, Y., Crittenden, J.C., Capco, D.G., Toxicity and cellular responses of intestinal cells exposed to titanium dioxide. *Cell Biology and Toxicology* **26**, 225-238 (2010).

Kumar, C. (Ed), Nanomaterials for Medical Diagnosis and Therapy. Weinheim: Wiley-VCH, (2007).

Lang, H.P., Baller, M.K., Berger, R., Gerber, Ch., Gimzewski, J.K., Battiston, F.M., Fornaro, P., Ramseyer, J.P., Meyer, E., Guntherodt, H., A cantilever array-based artificial nose. *J., Anal. Chem. Acta* **393**, 59-65 (1999).

Lee, J., Shen, W., Payer, K., Burg, T. P., Manalis, S.R., Toward attogram mass measurements in solution with suspended nanochannel resonators. *Nano Letters* **10 (7)**, 2537-2542 (2010).

Martinez, N.F., Kosaka, P.M, Tamayo, J., Ramirez, J., Ahumada, O., High throughput optical readout of dense arrays of nanomechanical systems for sensing applications. *Rev. Sci. Instrum*, **81**, 125109 (2010).

Maynard, A.D., Aitken, R.J., Butz, T., Colvin, V., Donaldson, K., Oberdorster, G., Philbert, M.A., Ryan, J., Seaton, A., Stone, V., Safe handling of nanotechnology. *Nature* **444**, 267-269 (2006).

Medintz, I.L., Uyeda, H.T., Goldman, E.R., Mattoussi, H., Quantum dot bioconjugates for imaging, labeling and sensing. *Nat Mater*., **4,** 435-446 (2005).

Nanoscience and nanotechnologies: opportunities and uncertainties. Edited by The Royal Society, Royal Academy of Engineering, (2004).

Nugaeva, N., Gfeller, K.Y., Backmann, N., Lang, H.P., Duggelin, M., Hegner, M., Micromechanical cantilever array sensors for selective fungal immobilization and fast growth detection. *Biosensors and Bioelectronics* **21**, 849-856 (2005).

Park, E.J., Yi, J., Kim, Y., Choi, K., Park, K.I., Silver nanoparticles induce cytotoxicity by a Trojan-horse type mechanism. *Toxicology In Vitro* **24**, 872-878 (2010).

Park, K., Jang, J., Irimia, D., Stugis, J., Lee, J., Robinson, P., Tonerd, M., Bashir, R., Living cantilever arrays for characterization of mass of single live cells in fluids. *Lab on a Chip* **8**, 1034-1041 (2008).

Prakesh, S.B., On-chip capacitance sensing for cell monitoring applications. *Sensors Journal IEEE* **7(3)**, 440-447 (2007).

Renteria, A.S.M., Developing an automated bionanomechanical sensing platform for DNA hybridization detection in advanced genetic analysis applications, MecWins S.L., from NI.com case study

Scudiero, D.A., Shoemaker, R.H., Paull, K.D., Monks, A., Tierney, S., Nofziger, T.H., Currens, M.J., Seniff, D., Boyd, M.R., Evaluation of a soluble tetrazolium/formazan assay for cell growth and drug sensitivity in culture using human and other tumor cell lines, *Cancer Research*, **48**, 4827 (1988).

Takenaka, S., Karg, E., Moller, W., Roth, C., Ziesenis, A., Heinzmann, U., Scharamel, P. Heyder, J., Pulmonary and systemic distribution of inhaled ultrafine silver particles in rats. *Environmental Health Perspectives* **4**, 547-551 (2001).

Tennant, J.R., Evaluation of the trypan blue technique for determination of cell viability. *Transplantation*, **2(6)**, (1964).

Tsuji, J.S., Maynard, A.D., Howard, P.C., James, J.T., Lam, C., Warheit, D.B., Santamaria, A.B., Research strategies for safety evaluation of nanomaterials, Part IV: Risk assessment of nanoparticles. *Toxicol Sci* **89,** 42-50 (2006).

Twentyman, P.R., Luscombe, M., A study of some variables in a tetrazolium dye (MTT) based assay for cell growth and chemosensitivity, *Br J Cancer* **56(3)**, 279-285 (1987).

Walkup, G.K., burdette, S.C., Lippard, S.J., Tsien, R.Y., A new cell permeable fluorescent probe for Zn2+. *J. A. Chem. Soc*., **122**, 5644-5645 (2000).

Weir, A., Westerhoff, P., Fabricius, L., Hristovoski, K., Von Goetz, N., Titanium dioxide nanoparticles in food and personal care products. *Environmental Science Technology* **46(4)**, 2242-2250 (2012).

Weisberg, E., Manley, P.W., Breitenstein, W., Bruggen, J., Cowan-Jacob, S.W., Ray, A., Huntly, B., Fabbro, D., Fendrich, G., Hall-Meyers, E., Kung, A.L., Mestan, J., *et al.*, Characterization of AMN107, a selective inhibitor of native and mutant Bcr-Abl. *Cancer Cell*, **7(2)**, 129-141 (2005).

Wenzel, M.J., Josse, F., Heinrich, S.M., *Journal of Applied Physics* **105**, 064903 (2009).

Worle-Knirsch, J.M., Pulskamp, K., Krug, H.F., Opps they did it again! Carbon nanotubes hoax scientists in viability assays. *Nano Lett*. **6(6)**, 1261-1268 (2006).

Xu, C.Y., Inai, R., Kotaki, M., Ramakrishna, S, Aligned biodegradable nanofibrous structure: a potential scaffold for blood vessel engineering. *Biomaterials* **25(5)**, 877-886 (2004).

Chapter 6 Readout Methods of Microcantilever Arrays

6.1 Introduction

In previous chapters, all work was carried out using optical microcantilever readout systems. While the scanning microcantilever array system allowed for rapid and simultaneous measurements of up to twelve cantilevers simultaneously, larger arrays would have been difficult and inefficient. In particular, using an optical laser based readout method provides a bending signal that is relative. This means that any movement or disturbance in the system would produce results that are not repeatable in real-time as it possesses no "memory". This is as opposed to an absolute measurement system; where the cantilever array chip can be removed, further processed, and reattached while still providing reproducible results. Therefore, in this chapter, research was conducted into new readout methods for large arrays of microcantilever sensors, which would allow for greatly increased throughput for biosensing applications.

6.2 DNA Microarrays

DNA microarrays are now one of the most powerful tools in molecular biology, particularly for DNA sequencing and diagnostics. While there have been sequencing techniques such as sequencing by hybridization (Wallace *et al*., 1979), the most significant advancement was DNA arrays and sensors. (Fodor *et al*., 1991, Southern *et al*., 1992) DNA arrays solved the problems of low hybridization efficiency and slow and labor intensive procedures. DNA analysis aspects of interest are its applications for disease diagnosis, such as being used for viral infection and mutation detection, in addition to determining if a gene is upregulated or downregulated (Yershov *et al*., 1996, Drobyshev *et al*., 1997, Healey *et al*., 1997).

Even though every single cell in the human body possesses the same genetic material, only specific genes are active in different cells. The key to understanding how the cells function is to determine which genes are active or inactive in a particular cell. DNA microarrays allow for simultaneous experiments on thousands of genes, enhancing the ability to understand the fundamentals behind different diseases and illnesses. For example, cancers were previously classified solely on the organ that they affected, but after further examination, it was concluded that cancers could be classified by the patterns of gene activity in the tumor cells (Golub *et al*., 1999).

There are many downsides to this process of genetic study. DNA microarrays require pre-labeling before the experiment of the DNA, typically with fluorescent tags, which is both time consuming and costly. In addition, the equipment necessary to perform the technique is a limiting factor, including costs from preparation of DNA strands, or the ability for the robotics to handle the scanning for the fluorescent tags. Therefore, an alternative approach to DNA microarrays has been developed with the use of large arrays of microcantilever sensors. The new method is high throughput, label-free, and could potentially lead to a viable and alternative method to DNA microarrays. In this section, the details of the experiments will be presented and discussed.

6.2.1 Chip Functionalization by Printing

In order to precisely functionalize large arrays of microcantilever sensors with cells, a more efficient and effective method such as cell printing is required. There are currently many methods for constructing cellular patterns on a surface, including soft lithography (Zhang *et al.*, 1999, Kane *et al*., 1999, *Tan et al.*, 2003), laser based cell writing (Odde *et al.*, 2000)), photolithography (Bhatia *et al*., 1992, Liu *et al.*, 2002), dip-pen nanolithography (Piner et al., 1999, Lee *et al*., 2002, Wilson *et al*., 2001), and inkjet printing (Roth *et al.*, 2003). Soft lithography patterning includes microcontact printing and flow patterning with microfluidic channels (Tan *et al*., 2003). The benefit of soft lithography is the ability for high resolution features from 2-500μm (Kane *et al*., 1999). Laser based cell writing involves guiding the cells down hollow fibers with an infrared laser (Odde *et al*., 2000) and is useful to study cell attachment applications. Photolithographic patterning activates photosensitive groups on a substrate by UV irradiation with a patterned mask (Liu *et al.*, 2002). Lastly, dip-pen nanolithography uses AFM techniques to pattern cells down to a dimension of 30nm (Wilson *et al*., 2001). While all these techniques have their advantages, they all suffer from disadvantages such as low throughput or being time consuming.

Inkjet printing on the other hand combined with CAD techniques have already been utilized for applications such as biosensor development (Newman *et al.*, 1992), biochips (Xu *et al.*, 2004), DNA arrays (Allain *et al.*, 2001, Schena *et al.*, 1998), DNA synthesis (Blanchard *et al.*, 1996), and microdeposition (Roda *et al.*, 2000). Inkjet printing using standard commercially sourced inkjet heads provide minimal excitation to the cells, allowing for high cell viability in addition to precise control over the target. Because

cells are quite fragile and difficult to print, DNA was used as a proof of concept for this study.

The first microcantilever array was fabricated on 25μm polyimide sheets, with a cantilever size of 250μm in length and 50μm in width. On a chip with a $1cm^2$ area, ~800 cantilevers were one step laser fabricated using the nanosecond laser in the UV range. Initial results were unsatisfactory, and further testing showed that the laser scanning head did not move with sharp edges creating a cantilever that was not straight. A layer of 5nm titanium was first coated to aid the adhesion of the subsequent coating of 40nm of platinum. Platinum was used rather than gold because of its interaction with the DNA printing steps that took place at Duke University in collaboration with Prof. Jingdong Tian and Dr. Ishtiaq Saaem.

DNA was printed onto the microcantilevers through a modified inkjet printer. The inkjet printer used a piezoelectric material behind a nozzle, rather than other methods such as thermal heating elements. Thermal heating methods incorporate a heater, and in order to print a droplet, a pulse of current is injected into the heating element, causing an intense vaporization of the ink, creating a bubble that increases pressure, forcing the ink out. In a piezoelectric inkjet printer, in order to print a liquid out of the nozzle, a voltage is applied and the piezoelectric material alters its shape, creating a pressure pulse in the fluid chamber, which then forces a drop of ink out of the nozzle. The key advantages to the piezoelectric method over the thermal method are that there are no volatile components and they do not suffer with buildup of ink residue. The inkjet printing head was removed from an Epson printer, the ink chambers were replaced by custom flasks containing DNA, and control was done through C programming language. The inkjet printer head was mounted on a CNC machine, controlling the X-Y-Z directions.

The methods for printing DNA onto the cantilever started with determining how the printing was going to cover the entire surface of the rectangular shaped cantilevers. Two methods were used, which included overlapping multiple droplets, or using a mask to make the background to the cantilever hydrophilic whereby the liquid would naturally spread across the cantilever surface only. These methods can be seen in Figure 6-1.

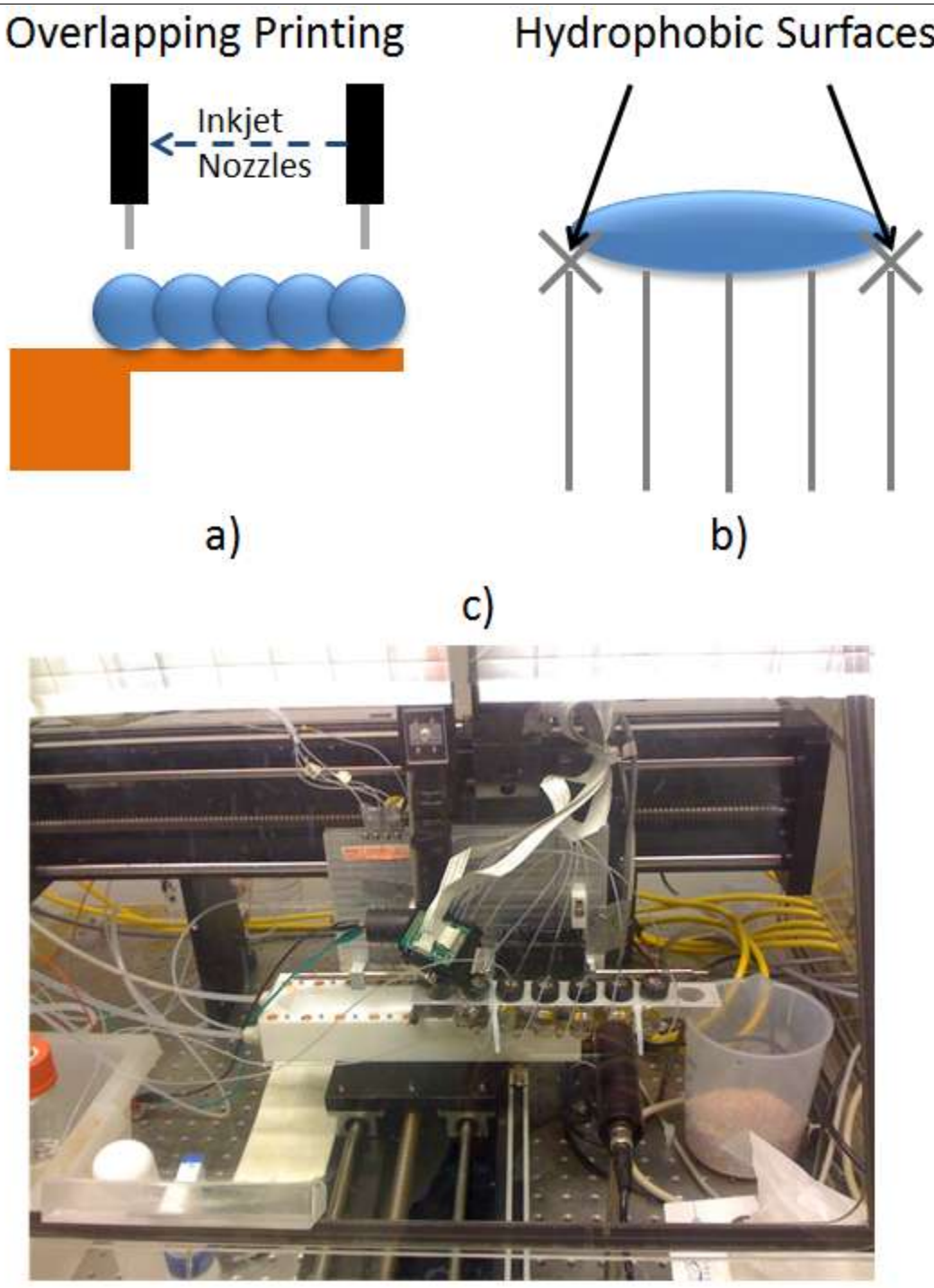

Figure 6-1: DNA printing methods and equipment using inkjet technology. a) Inkjet nozzles printing overlapping droplets. b) Hydrophobic edges so droplet will remain only on cantilever surface. c) Actual setup in the lab at Duke University.

Both methods required the surface of the cantilever to be modified into a hydrophilic surface, to enhance the distribution of the DNA liquid. In order to achieve that, steps were taken to fabricate a mask from photoresist which covers the cantilever array. Blacked out sections for the mask included the rectangular shaped cantilevers only, and

with the use of a positive photoresist, whereby the cantilevers would have a layer of photoresist on the surface. Next, the entire chip was soaked in hydrophobic saline (Heptadecafluoro-1,1,2,2,tetra-hydrodeayltrimethooxysilane). After rinsing, the resist was removed to expose the cantilevers, followed by soaking in 3-Triethoxysilylpropyl-4-hydroxybutyramide to make the cantilevers hydrophilic.

Once the chips were prepared, printing of the DNA was performed layer by layer on top of the cantilever surface seen in Figure 6-2. At this stage, many problems arose and forced the discontinuation of the experiments. A major problem was the alignment under the print head. Because the microcantilever chips were on a piece of polyimide without any alignment markings, it was almost impossible to align them at a perfect right angle to the print head movement, causing a drift in the printing. Next, due to unknown reasons, the platinum coating on the microcantilevers disappeared after an extended amount of printing, due to the washing process that occurs after each DNA base layer is printed. A theory as to why this occurred was that the platinum coating for the chips that were used were not properly coated, as the e-beam system failed to reach vacuums levels of 10^{-6} Pa, possibly causing uneven and non-uniform coating of the platinum. Another reason could be that laser fabrication occurred after the coating of the platinum. This may cause laser ablation to the edges of the polyimide, which then allowed liquid to slowly enter the underside of the coating, washing it off.

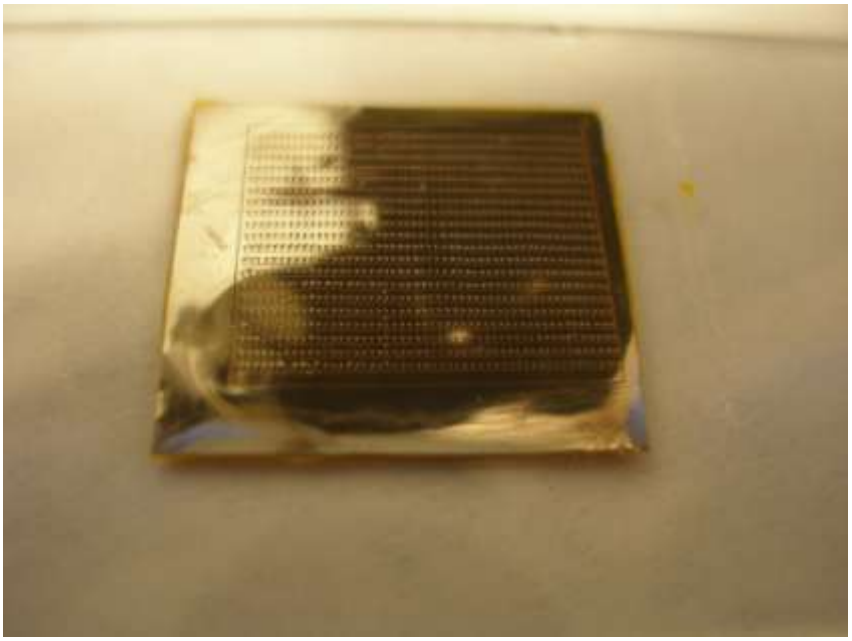

Figure 6-2: Large cantilever array with DNA printed on, bright spots indicate a liquid spot where DNA is located.

6.3 Readout Methods

6.3.1 Interferometry (in collaboration with UCLA)

Initial tests were performed at the University of California – Los Angeles with Dr. Jason Reed in an attempt to simultaneously readout a large array of microcantilever sensors. A commercial VEECO white light interferometry system was used to scan a cantilever array of 25 cantilevers in one row, each with a size of 250 μm in length, and 50 μm in width. An interferometer splits the light from a source with a beam splitter in order to follow two separate optical paths, ending in a recombination of the light at the detector. The recombination of the beams, which splits into different directions, creates fringes or patterns that depend on the differences between the two optical paths. This path difference is the difference in the distance that is travelled by the reference and sample beams, which then creates a phase difference between them. The typical reference surface is an extremely flat surface that is precisely aligned to be perpendicular to the source beam. After fringes are detected, analytical software is used to reconstruct and profile the sample.

Due to the "softness" of the cantilever sensors at a rest state, the cantilevers are always deflected by a small amount. This meant that the interferometer was required to "scan" a large distance in order to produce fringes on the entire cantilever. Depending on the number of cantilevers being scanned simultaneously, it required ~20s. per scan. In addition, the system produced high noise levels, possibly due to the difficulty in creating a custom mount to the system, as the interferometer was a commercial system. Tests were performed and successfully demonstrated the monitoring of cantilever beams from changing the temperature. Results can be seen below in Figures 6-3 to 6-6.

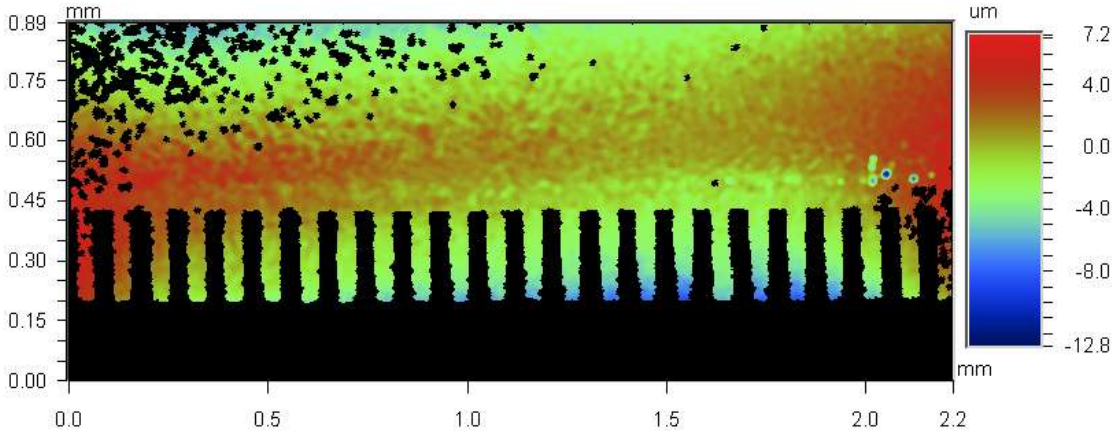

Figure 6-3: Interferometer cantilever bending readout (2D)

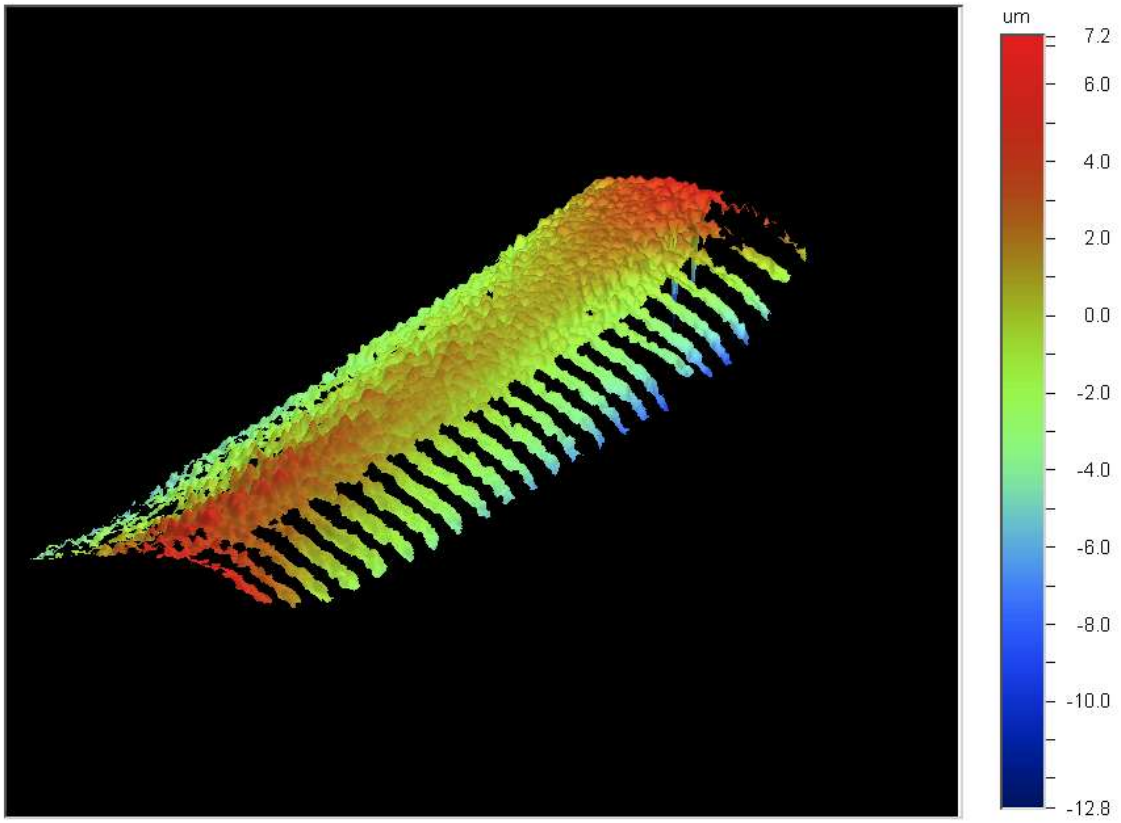

Figure 6-4: Interferometer cantilever bending readout (3D)

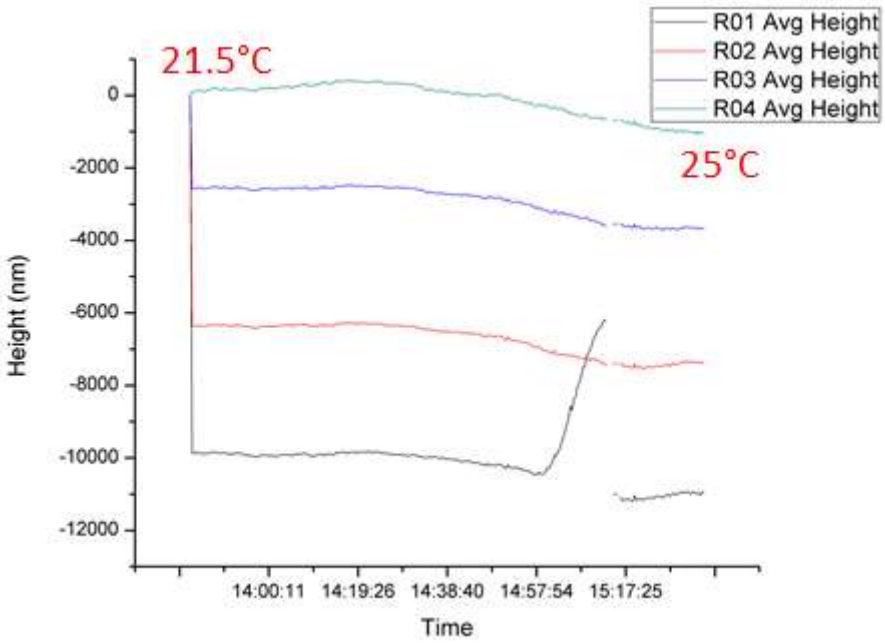

Figure 6-5: Temperature test 1 of 4 cantilevers bending from 21.5 to 25 °C.

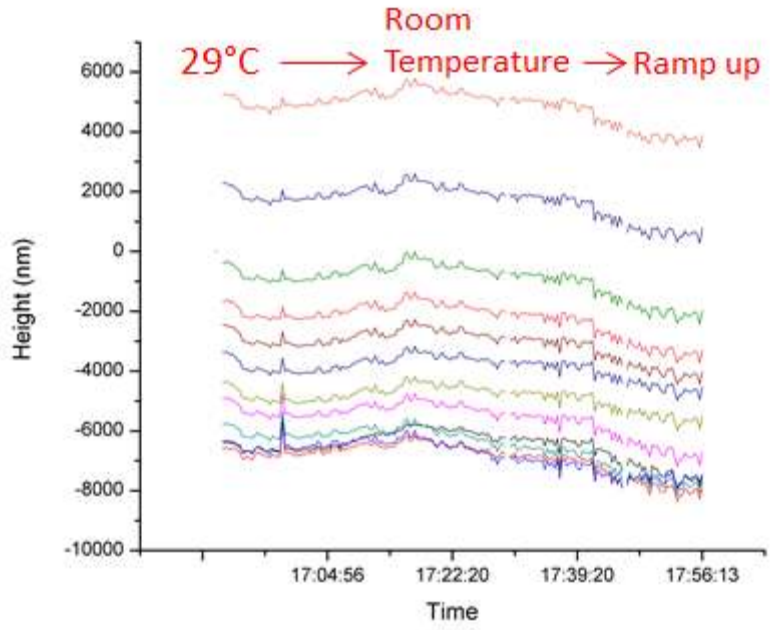

Figure 6-6: Temperature test 2 of 12 cantilevers bending from 29 ° C to room temperature to constantly ramping up temperature.

6.4 Modified Chip Design

Due to the problems with the previous experiments, a collaboration was created with Prof. Andrew Moore and Dr. Jesus Valera at Heriot-Watt University. Instead of a commercial interferometer system, a custom built system was used to simultaneously readout multiple cantilevers. The readout system consists of a Michelson interferometer, which is the most common configuration of interferometry and can be seen in Figure 6-7. It is the same as a standard interferometer setup as described above, with two polished mirrors M1 and M2. The source emits a light (laser) that hits point C. The mirror M is only semi-reflective; so one beam is transmitted to A while the other goes to B, essentially dividing the source beam into two beams that are equal in intensity. Both beams then recombine at point C' whereby an interference pattern can be detected and visible to the detector at point E. Essentially, the detector would see the two images stacked on top of each other.

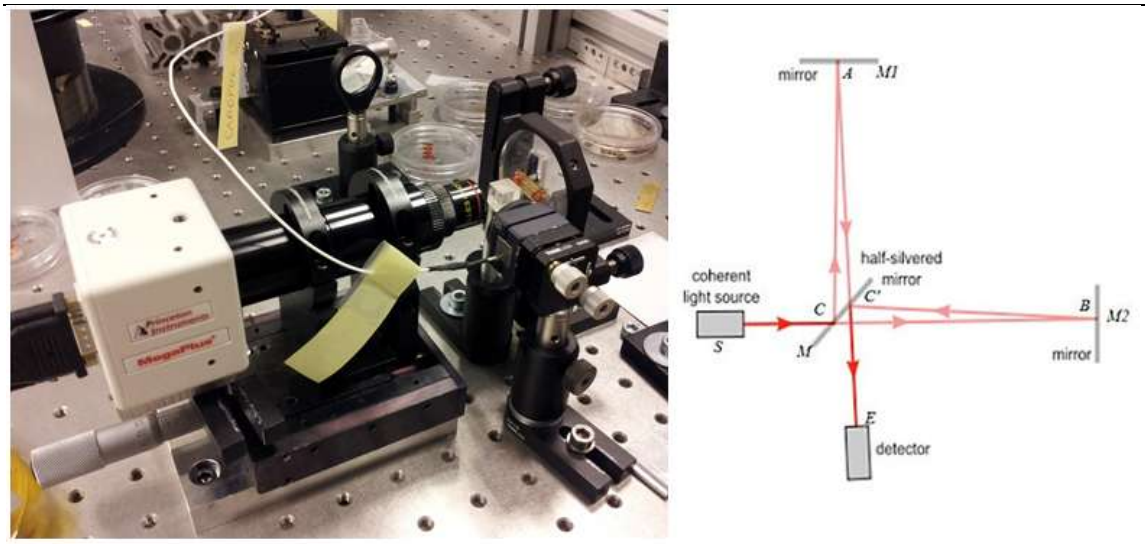

Figure 6-7: Setup of the Michelson interferometer and the light path the laser takes.

The problem with this setup is that the cantilevers were not very uniform in their flatness. In addition, many cantilevers produced a large bending in the order of microns even when in a steady rest phase. This is the reason for VEECO's interferometer setup to "scan" the distance of the cantilever in the Z direction, in order to read out the entire bending curvature of the cantilever beams. Because of this drawback, a flatter and more uniform cantilever array had to be fabricated.

The first idea was to use a thicker polyimide layer as the backing substrate, to hold and support the thinner cantilever polyimide layer. In theory, this coupled with individual supporting "windows" for the cantilevers would create a flat and rigid enough surface for the interferometer setup to be used. Therefore, a 50 µm polyimide layer was used as the substrate, followed by double sided tape (3M, 50 µm) to bind the two polyimide layers together. The method was to first laminate the double sided tape onto the thicker polyimide sheet. Running it through a roll laminator increases the uniformity and adhesive qualities of the double sided tape. This combined layer is then placed under the nanosecond laser, cutting "windows" into an array. After this was completed, the thinner 25 µm polyimide layer was then laminated on top of the substrate with doubled sided tape on it. This creates a 3 layer chip with windows that support each section of the thinner polyimide sheet. The entire chip then undergoes another round of laser fabrication with the nanosecond laser using the alignment technique discussed in the earlier chapter, cutting cantilevers onto the thinner polyimide sheet in the middle of the

windows on the substrate. This creates a chip that has the thicker polyimide layer providing support and added rigidity to the thinner polyimide cantilevers, hopefully increasing its flatness and uniformity.

Unfortunately, as seen by the results of the readout shown in Figure 6-8, surface flatness was not greatly improved with this method. One reason for this may be due to the lamination process. The laminator roller is not a smooth surface. It consists of "fingerprint" style lines in its soft pliable material, and those patterns transfer onto the double sided tape when it is rolled through the machine. In addition, the 50 μm polyimide layer as the substrate was found not to be much more rigid than the 25 μm layer, thus not improving the situation greatly. The next idea was to use a much more rigid material as the substrate for the chip and also to replace the double sided tape with a flatter adhesive.

A stainless steel substrate was chosen for its rigidity and photoresist was chosen as the adhesive layer. Etched stainless steel chips were sourced from Photofab UK, with an array of 13 rows by 18 columns worth of "windows" for support allowing for 234 cantilevers on an area of $1cm^2$. Dry film photoresist was chosen for its suitability as an adhesive layer for its smooth surface and ability to be easily laminated. Elga's Ordyl SY300 20 μm thick dry film resist was chosen for its wide availability in Europe. Dry film photoresist is typically used in etching circuit boards, having properties that are heavily resistant to chemicals and good adhesion properties.

The resist is first laminated on top of the stainless steel substrate. A lamination temperature of 105 °C and a speed of 4mm/s were chosen by its recommendation from the data sheet. The high temperature allows for the resist to slightly melt, providing solid adhesion to many materials. The surface of the substrate was first cleaned thoroughly with ethanol and blown dry with nitrogen to remove any dust particles that may be present. After the resist has been laminated to the metal substrate, windows of the same size and location were cut with the nanosecond laser in the green wavelength (532nm) as using the UV (355nm) wavelength would expose the photoresist, causing it to develop. This is followed by the lamination of the polyimide layer for cantilevers on top at the other side of the photoresist. After thorough cleaning of the polyimide sheet, it was once again rolled through the laminator at 105 °C but at a slower speed of 2mm/s.

It was found that a faster speed was required for the metal substrate lamination as opposed to a lower speed for the polyimide lamination. Once the 3 layer chip was completed, the cantilevers were aligned and laser cut by the picosecond laser in the UV range with dimensions of 250μm in length by 50μm in width. The last step for the fabrication of the chips was to coat the surface of the polyimide with a gold layer. For some reason, significant amounts of laser ablation residue was found to be on the surface of the cantilevers, causing non-reflective patches under the interferometer. Therefore, plasma treatments were used (Diener Electronic Zepto, Germany) along with thorough cleaning by ethanol before the gold coating was required. 5nm of chromium followed by 40nm of gold was then subsequently coated onto the chip, completing the fabrication process.

Results obtained through this method also ended up being relatively poor, extremely similar to those in Figure 6-8, as the cantilevers were of a very small size, thus only a few pixels from the CCD camera in the interferometer setup was on each cantilever. In addition, surface flatness was not much improved through this method. These drawbacks coupled with the fact that these new chips were significantly more difficult to fabricate due to the very precise alignment required by the small windows, yet another cantilever array chip design was chosen for its design simplicity along with possibly its ability to be of acceptable surface uniformity to proceed with some initial experiments.

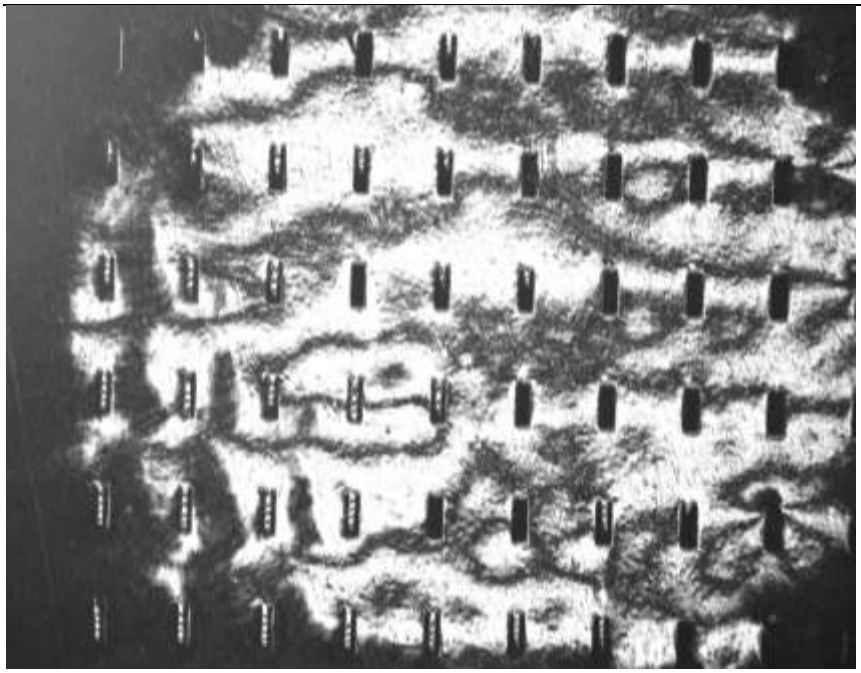

Figure 6-8: Image from the interferometry readout system of an entire cantilever array. It can be seen that the chip surface is not smooth and not all cantilevers are visible at the same time.

6.5 Final Cantilever Array Design

From the problems that have risen above, it was clear that a more simplified cantilever array with relatively decent surface flatness qualities were needed. After reviewing the previous results, it was found that the initial cantilever arrays (used with the VEECO system) gave the best overall uniformity but because of the design where the cantilever rows were facing each other, both rows were unable to be read out simultaneously.

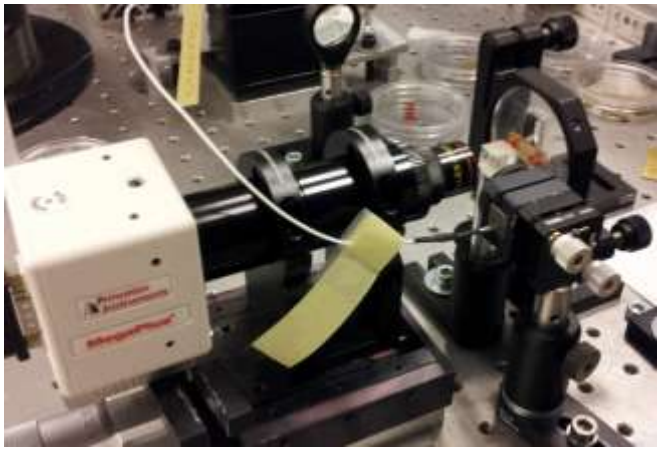

Figure 6-9: Interferometer readout setup with cantilever chip mounted

Therefore, the final cantilever array design consists of a 1mm PMMA substrate with a layer of double sided 3M tape. This substrate was first CO_2 laser machined with screw holes and a middle large window cut-out. A 25μm film of polyimide was then laminated on top. The cantilevers were then cut with the picosecond laser with dimensions of 1mm in length by 200μm in width, with spacing between them of 200μm, in an array of 25 cantilevers in a single PMMA substrate window. Finally, an identical piece of PMMA substrate was then placed on top so when the entire chip is screwed down into the holder, the two substrates would essentially press together, hopefully creating a more uniform and flat surface. The entire chip mounted in the interferometer setup can be seen in Figure 6-9 with the subsequent fringes in Figure 6-10 and bending readout of 4 cantilevers in Figure 6-11. The fringes seen are standard interfermetric fringes, with the data from Figure 6-10 being translated into real-world bending in Figure 6-11.

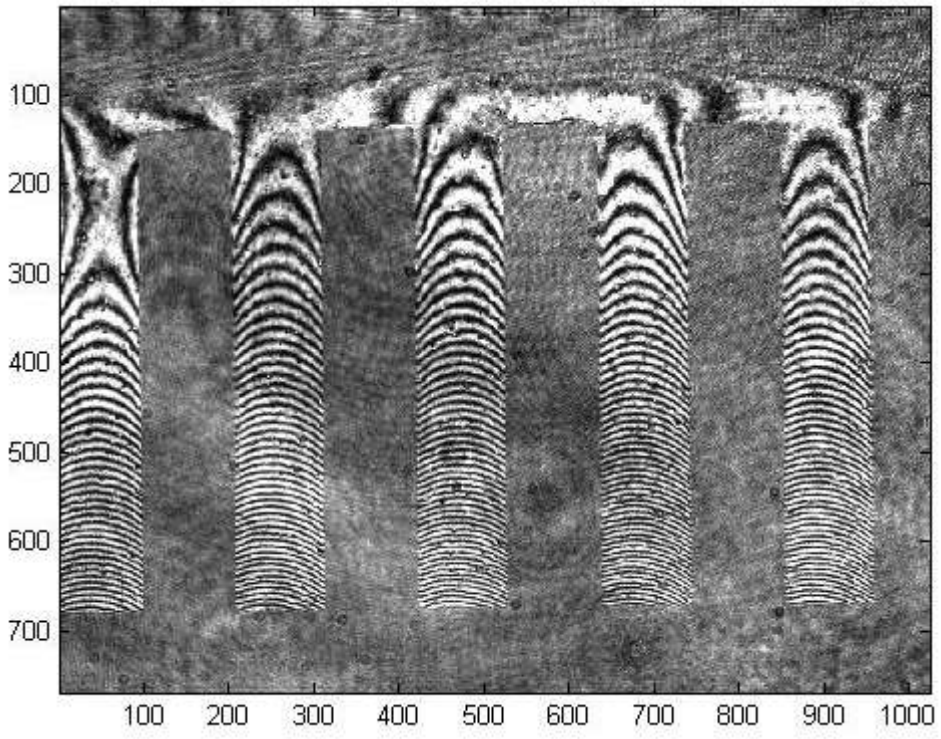

Figure 6-10: Interferometer readout of the cantilever chip, showing the fringes

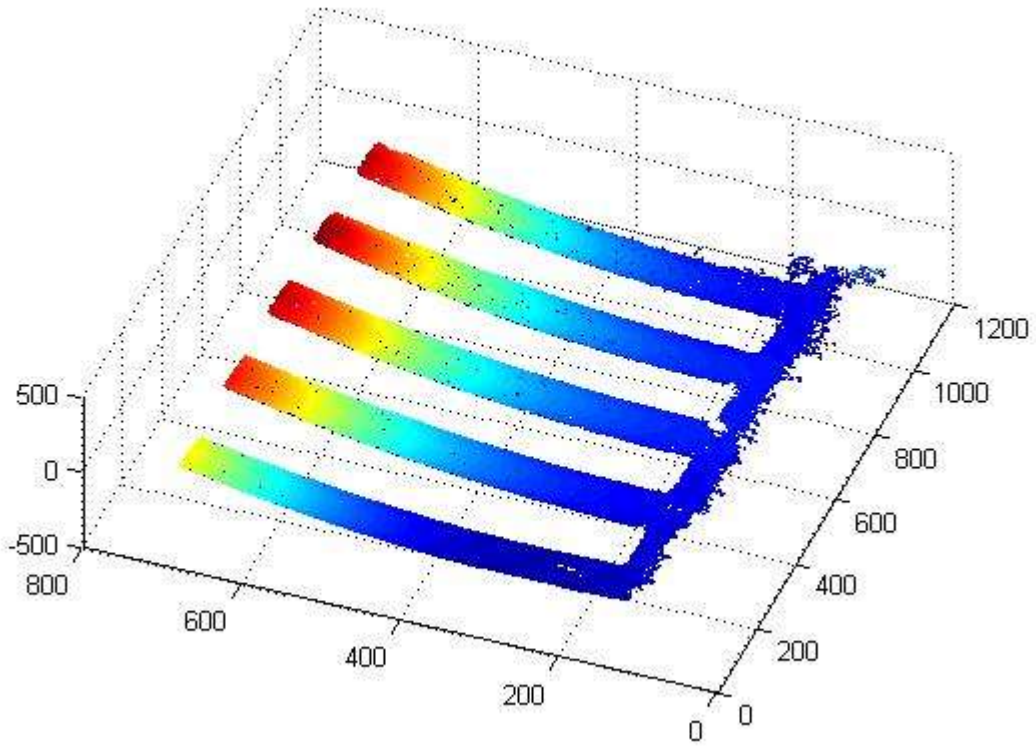

Figure 6-11: Sample image of the cantilever deflection readout as a result of the fringes from the interferometer cantilever readout system.

6.6 Magnetic Beads Enhanced Bending

Due to the difficulties in the fabrication and read out of the cantilever array chips, an alternative and simpler experiment was discussed to validate the design and use of the cantilever arrays. As discussed in previous chapters, microcantilever sensors are highly capable of label-free detection of biomolecules without the need for pre-labeling with fluorescent or radioactive dyes (Lang *et al*., 2005). But in order to dramatically enhance the sensitivity of the microcantilever sensors, there is a need to find a method to dramatically amplify the amount of cantilever bending, while also addressing the downsides of cantilever based sensors, which is that they are susceptible to temperature variations and other external factors (Shu *et al*., 2006). Therefore, magnetic beads were chosen as the solution to greatly enhance the amount of cantilever deflection. As the reagents bind onto the surface of the cantilever, a powerful neodymium magnet (25mm x 25mm, first4magnets UK) is gently moved underneath the cantilever, generating a magnetic field, pulling the magnetic beads of the bound substance, increasing the amount of bending normally seen in surface stress induced bending only. This section

will describe the results of a biotin-streptavidin study with magnetic beads attached. Biotin-streptavidin was chosen as the model system because they have been well studied in order to gain a perspective on the feasibility of such a magnetic bead enhanced cantilever sensor system. In addition, multiple concentrations of the G-quadruplex-Thrombin protein detection experiments were successfully carried out to provide a very rough estimate of detection limits.

6.7 Cantilever preparation

6.7.1 Biotin-streptavidin

After the entire cantilever array chip is assembled, the chip was rinsed thoroughly with ethanol and blown dry by nitrogen gas. 1mM of biotin thiol (Nanoscience Instruments, USA) is then coated onto the gold surface, and allowed to bind at least overnight. The biotin was purchased already self-assembled. This is then followed by gently rinsing the cantilevers with ethanol to remove any unbound biotin particles. Magnetic particle (10 μm size, >1000 pmol/mg) bound streptavidin (Sigma-Aldrich, UK) is then deposited onto the cantilevers, and allowed to rest and bind for a period of 30 minutes. A final gentle rinse of the cantilevers with ethanol removes any unbound streptavidin particles to allow for accurate readouts. In order to simplify the experiment and to remove the need for a real-time binding of the substances, all the cantilevers were fully functionalized prior to the testing, with the only variable being with or without the magnetic field. Non-specific interactions could have been reduced with the addition of bovine serum albumin (BSA) or polyethylene glycol (PEG) but were not included in this short study.

6.7.2 Thrombin

For thrombin detection, magnetic particles were used as well to enhance the bending signal. To begin with, the cantilever was once again coated with a thin 40nm gold surface. The cantilevers are then rinsed with deionized water and blown dry with nitrogen. Then the first layer of the primary anti-thrombin aptamer G-quadruplex DNA (DNA all purchased from IBA, Germany) sequence of 5'-SH-(CH2)6-TT TTT TTT TTG GTT GGT GTG GTT GG-3' was pipetted onto the surface for immobilization. Next, human thrombin protein was added to the system and lastly a second binding aptamer of 5'-biotin-GGT TGG TGT GGT TGG-3' with magnetic beads coated streptavidin was hybridized with the primary aptamer. As before with the biotin-

streptavidin tests, rather than using a real-time fluid system, for simplicity the entire process was performed before the experiment and the only variable was the magnet being inserted and taken out.

6.7.3 Results and Discussion

Due to the high demands of surface uniformity and flatness from the in house interferometry systems, all results were obtained through collaboration with Zeta Instruments (San Jose, CA), with their commercial white light interferometer system on the final design of the cantilever array chip. Because the biotin-streptavidin experiment is only used a validation of the system, the particle concentration was not altered throughout the tests. Results can be seen in Figure 6-12.

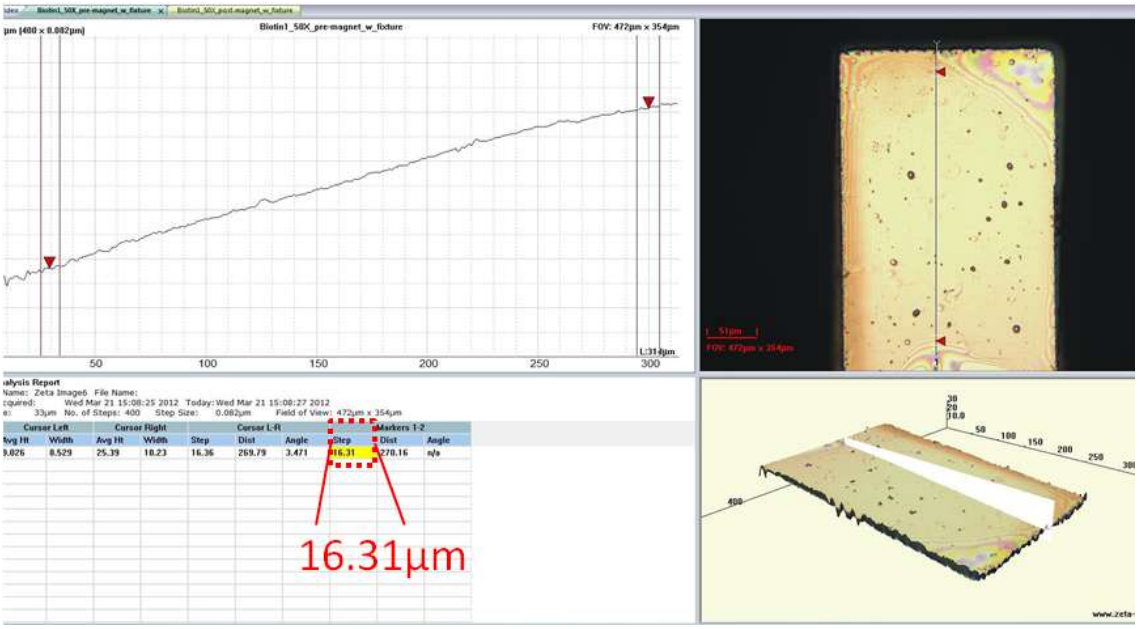

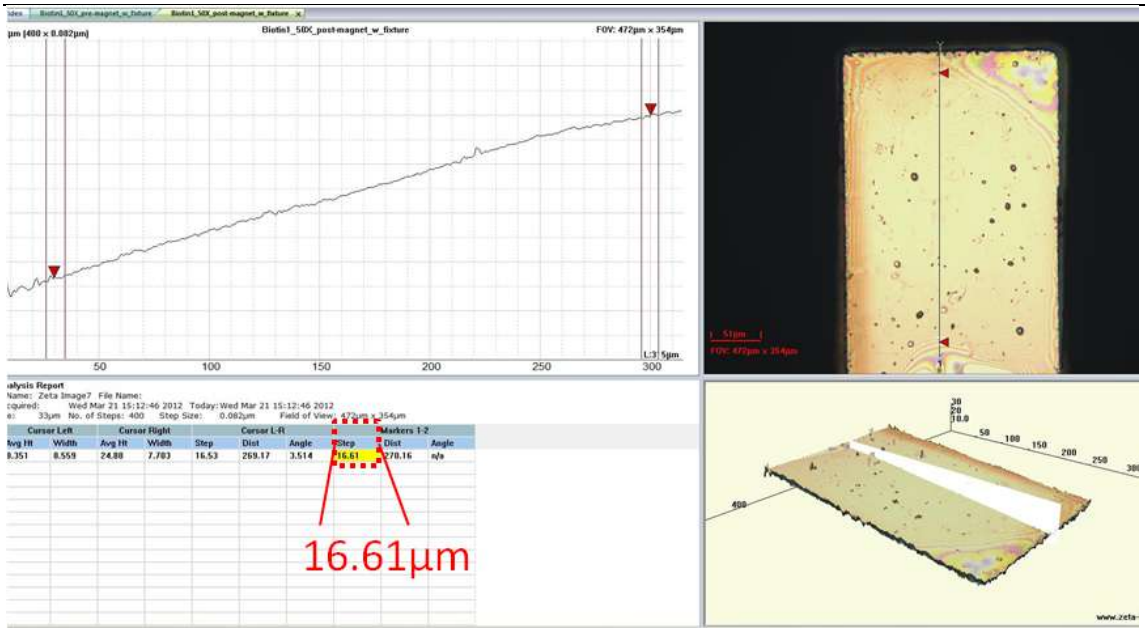

Figure 6-12: Bending signals of the cantilever before and after the insertion of a magnet with a biotin-streptavidin magnetic bead enhanced cantilever. Signal increases from 16.31µm to 16.61µm, signaling a 300nm increase in cantilever deflection.

From the yellow highlighted cell, it can be seen that the pre and post magnet biotin-streptavidin with magnetic particle enhanced sensors produced a ~300nm bending. Similarly, with the thrombin experiments, a 10x concentration of thrombin produced ~230nm of bending, while a 1x concentration of thrombin produced ~150nm of bending. Graphs and full data can be found in APPENDIX 3. Although the data shows only 1 cantilever being read out at a time, multiple cantilevers could have been easily readout simultaneously as shown in Figure 6-13.

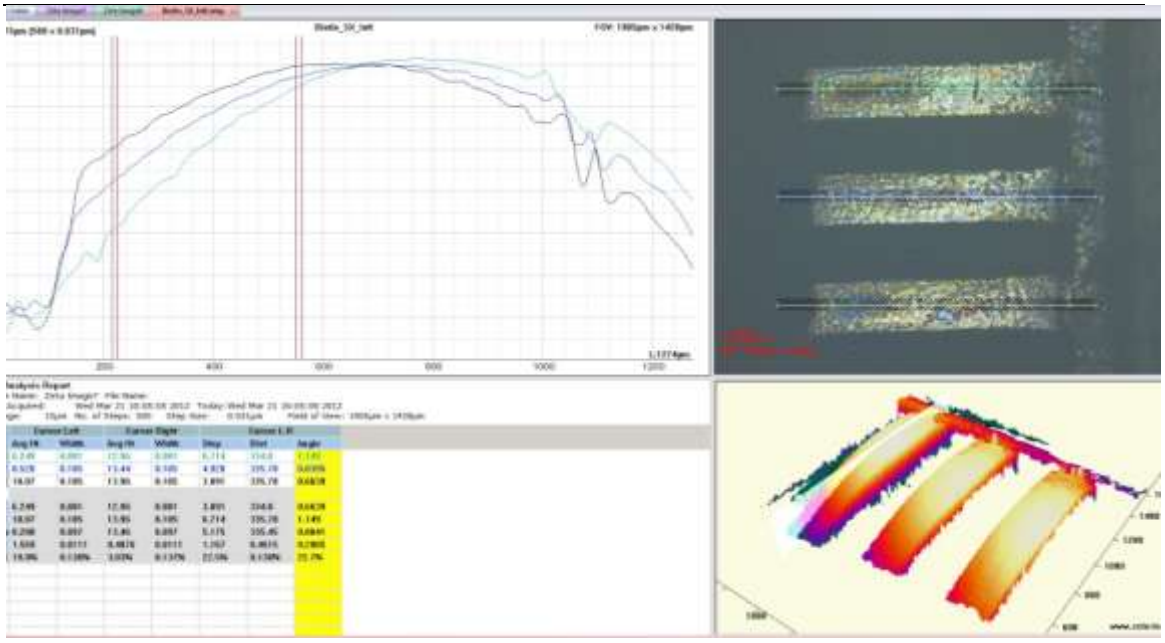

Figure 6-13: Sample image of multiple cantilever readout through interferometer.

In order to further validate these results, as the functionalization of these chips were not performed immediately before the experiments, tests were conducted with the single cantilever optical readout method for comparison. From Figure 6-14, it can be seen that extremely similar results were noticed during these experiments, signifying that the cantilever array experiments are fully capable of being analyzed. In addition, this shows that utilizing a magnet to enhance the sensitivity of the cantilever sensors can be a viable method of detecting small concentrations of substances. From Shu *et al*., (2006), the maximum amount of cantilever deflection for biotin-streptavidin binding (with silicon based cantilever sensors) was found to be ~30nm, from surface stress induced bending alone. The fully repeatable bending of ~300nm from polyimide based cantilever sensor arrays with magnetic beads indicates that there is a significant increase in cantilever bending, although the origin of the large bending cannot be differentiated between the more sensitive polyimide material or the magnetic particles.

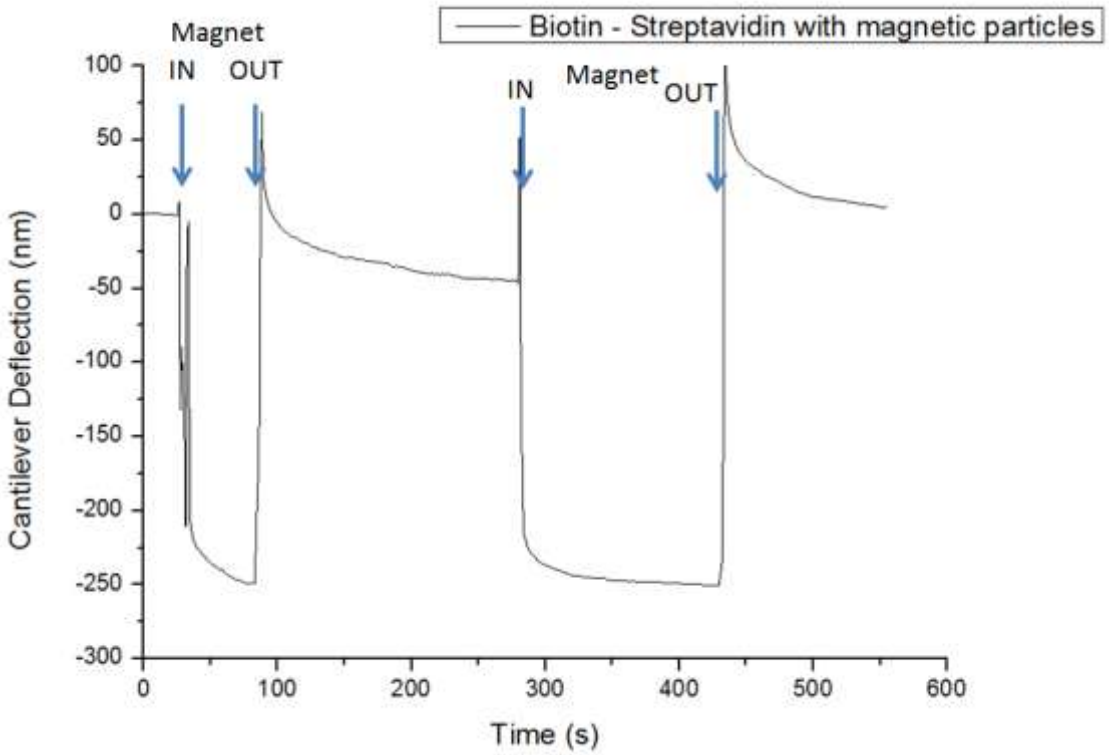

Figure 6-14: Magnetic particle enhanced biotin-streptavidin experiment results using a single cantilever optical readout scheme.

6.8 Conclusions

- These results are significant in the fact that the observed deflection of the cantilever sensors is only due to the magnetic effects of the experiment. This is in addition to the inherent surface stress in the order of tens of microns that would have been experienced by the cantilever had the experiment been performed in a real-time liquid environment.

- Work is currently still on going to successfully use the in-house interferometer system to allow to real-time liquid environment binding experiments while utilizing the enhanced bending of the magnetic particles. Detection limits of the cantilever sensors will also be demonstrated for both biotin-streptavidin and thrombin detection experiments.

- In theory, with the additional deflection caused by magnetic forces, these cantilever arrays should be highly sensitive, and could allow a new generation of microcantilever biosensor arrays.

6.9 References

Allain, L.R., Askari, M., Stokes, D.L., Vo-Dinh, T., Microarray sampling-platform fabrication using bubble-jet technology for a biochip system. *J. Anal. Chem*. **371(2),** 146–50 (2001).

Bhatia, S.K., Hickman, J.J., Ligler, F.S., New approach to producing patterned biomolecular assemblies. *J. Am. Chem. Soc*. **114(11)**, 4432–4433 (1992).

Blanchard, A.P., Kaiser, R.J., Hood, L.E., High-density oligonucleotide arrays. *Biosensors Bioelectronics*, **11(6–7),** 687–90 (1996).

Drobysehv, A., Mologina, N., Shik, V., Probedimskaya, D., Yershov, G., Mirzabekov, A., Sequence analysis by hybridization with oligonucleotide microchip: identification of B-thalassemia mutations. *Gene* **188(1)**, 45-52 (1997).

Fodor, S.P., Read, J.L., Pirrung, M.C., Stryer, L., Lu, A.T., Solas, D., Light-directed, spatially addressable parallel. *Science* **251(4995)**, 767-773 (1991).

Golub, T.R., Slonim, D.K., Tmayo, P., Huard, C., Gaasenbeek, M., Mesirov, J.P., Coller, H., Loh, M.L., Downing, J.R., Caligiuri, M.A., Bloomfield, C.D., Lander, E.S., Molecular classification of cancer: class discovery and class prediction by gene expression monitoring. *Science* **286-5439**, 531-537 (1999).

Healey, B.G., Matson, R.S., Walt, D.R., Fiberoptic DNA sensor array capable of detecting point mutations. *Analytical Biochemistry* **251(2)**, 270-279 (1997).

Kane, R.S,, Takayama, S., Ostuni, E., Ingber, D.E., Whitesides, G.M., Patterning proteins and cells using soft lithography. *Biomaterials* **20(23-24)**, 2363-2376 (1999).

Lang, H.P., Hegner, M., Gerber, C., Cantilever array sensors. *Mater. Today* **8**, 30 (2005).

Lee, K.B., Park, S.J., Mirkin, C.A., Smith, J.C., Mrksich, M., Protein nanoarrays generated by dip-pen nanolithography. *Science* **295(5560),** 1702–5 (2002).

Liu, V.A., Jastromb, W.E., Bhatia, S.N., Engineering protein and cell adhesivity using PEO-terminated triblock polymers. *J. Biomed. Mater. Res*. **60(1)**, 126–134 (2002).

Newman, J.D., Turner, A.P.F., Marrazza, G., Ink-jet printing for the fabrication of amperometric glucose biosensors. *Anal. Chim. Acta*. **262(1),** 13–7 (1992).

Odde, D.J., Renn, M., Laser-guided direct writing of living cells. *J., Biotechnol. Bioeng*. **67(3)**, 312–318 (2000).

Piner, R.D., Zhu, J., Xu, F., Hong, S.H., Mirkin, C.A., Dip-pen nanolithography. *Science* **283(5402),** 661–3 (1999).

Roda, A., Guardigli, M., Russo, C., Pasini, P., Baraldini, M., Protein microdeposition using a conventional ink-jet printer. *Biotechniques* **28(3),** 492–6 (2000).

Roth, E.A., Xu, T., Das, M., Gregory, C., Hickman, J.J., Boland, T., Inkjet printing for high-throughput cell patterning. *Biomaterials* **25**, 3707-3715 (2004).

Schena, M., Heller, R.A., Theriault, T.P., Konrad, K., Lachenmeier, E., Davis, R.W., Microarrays: biotechnology's discovery platform for functional genomics. *Biotechnol*.**16(7),** 301–6 (1998).

Shu, W., Laue, E.D., Seshia, A.A., Investigation of biotin-streptavidin binding interactions using microcantilever sensors. *Biosensors and Bioelectronics* **22(9-10)**, 2003-2009 (2005).

Souther, E.M., Maskos, U., Elder, J.K., Analyzing and comparing nucleic acid sequences by hybridization to arrays of oligonucleotides: evaluation using experimental models. *Genomics* **13(4)**, 1008-1017 (1992).

Tan, W., Desai, T.A., Evaluation of nanostructured composite collagen-chitosan matrices for tissue engineering. *Tissue Eng*. **9(2)**, 255–267 (2003).

Wallace, R.B., Shaffer, J., Murphy, R.F., Bonner, J., Hirose, T., Itakura, K., Hybridizaztion of synthetic oligodeoxyribonucleotides to 174 DNA: the effect of single bas pair mismatch. *Nucleic Acids Research* **6(11)**, 3543-3558 (1979).

Wilson, D.L., Martin, R., Hong, S., Cronin-Golomb, M., Mirkin, C.A., Kaplan, D.L., Surface organization and nanopatterning of collagen by dip-pen nanolithography. *Proc. Natl. Acad. Sci. USA* **98(24),** 13660–4 (2001).

Xu, T., Petridou, S., Lee, E.H., Roth, E.A., Vyavahare, N.R., Hickman, J.J., Boland, T., Construction of high-density bacterial colony arrays and patterns by the ink-jet method. *Biotechnol. Bioeng.*, **85(1),** 29–33 (2004).

Yershov, G., Barsky, V., Belgovskiy, A., Kirillov, E., Kreindlin, E., Ivanov, I., Parinov, S., Guschin, D., Drobishev, A., Dubiley, S., Mirzabekov, A., DNA analysis and diagnostics on oligonucleotide microchips. *PNAS* **93(10)**, 4913-3918 (1996).

Zhang, S.G., Yan, L., Altman, M., Lassle, M., Nugent, H., Frankel, F., Lauffenburger, D.A., Whitesides, G.M., Rich, A., Biological surface engineering: a simple system for cell pattern formation. *Biomaterials* **20(13)**, 1213–1220 (1999).

Chapter 7 Development of Autonomous Microfluidic and Portable Sensor Systems

7.1 Microfluidics

Microfluidics typically includes technologies that are used to control the flow of miniscule amounts of liquids or gases. The use of microfluidics allow for automated biological and chemical handling in order to decrease the chances of human error and cross contamination. There have been significant research into microfluidic platforms for biological automation (Lee *et al*., 2010, Wu *et al*., 2009, Balagadde *et al*., 2005). Amounts of nanoliters to milliliters make microfluidic systems highly adaptable to many applications. Other advantages over macro size devices include quicker diffusion in mixing, lower cost, higher sensitivity, lower energy consumption, less waste, and easier temperature control because of the size. Due to the size of the current microcantilever flow cell, a few milliliters of liquid is needed to be injected into the system. On the surface, it may seem like a very small amount, but comparing that to the size of cells or other small biomolecules, it is quite a large amount. Therefore, microfluidic channels or devices can be incorporated into the microcantilever sensor setup to flow tiny amounts of liquids to the cantilever beams for analysis. It can be seen in Figure 7-1 that the cantilever beams can be wedged and sealed inside microfluidic channels, which allows for precise delivery of droplets of liquids onto the cantilever beams for analysis. Use of a few droplets of blood or other liquids make detection of analytes easier for more efficient, and could lead to other lab on a chip platforms.

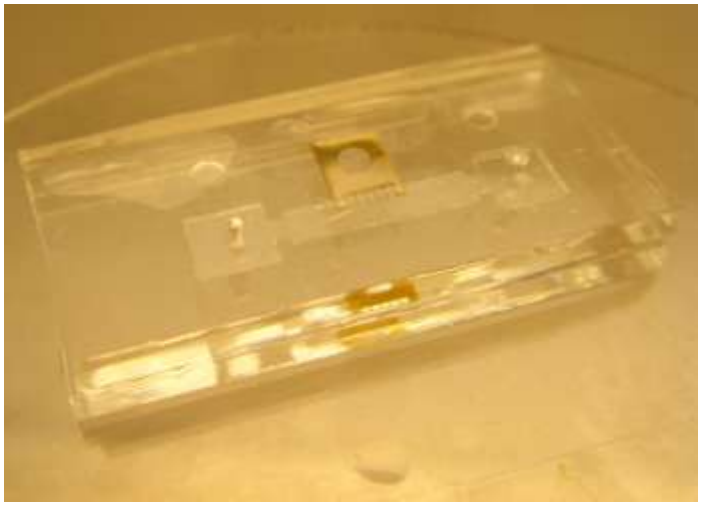

Figure 7-1: Microcantilever chip sandwiched in between two PDMS microfluidic channels.

Recently, a new type of microfluidic device was developed, which is a micropump as seen in Figure 7-2 that consists of two valves and a single pump in the middle.

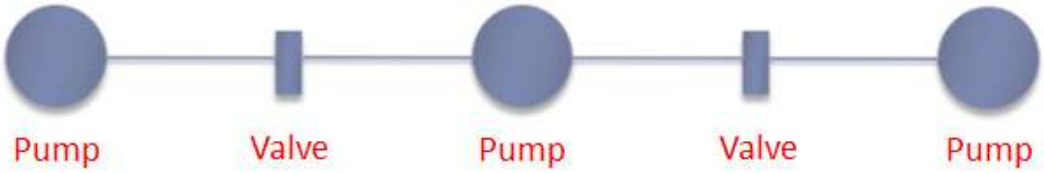

Figure 7-2: Micropump schematic with 3 pumps and 2 valves for microfluidic manipulation.

Compressed air inlets are connected to the valves and pump, requiring under 5 psi of pressure to actuate the pumping mechanism. The structure is built on a glass wafer in the clean room using SU8-50, which is an epoxy based photoresist. The SU-8 is first spin coated onto the wafer using parameters that creates a thickness of roughly ~175μm. After the spin coating process, it must be soft baked on a hot plate to evaporate the solvent. After the soft bake, it is then exposed to a certain wavelength of light with a patterned mask, whereby making the exposed patterns insoluble in the liquid solvent. Next, it must be placed back onto the hotplate for a post exposure bake, followed by placing the wafer in EC Solvent, which removes the non-exposed portions of the pattern.

The biggest problem when creating devices on SU-8 involves the pre- and post- bake times. According to the official SU8-50 datasheet, it recommends 10 minutes at 65° C and 30 minutes at 95° C for the pre bake followed by a post bake of 1 minute at 65° C followed by 10 minutes at 95° C and a 350-400nm exposure. When these parameters were first attempted, none of the patterns were dissolved in the solvent, signaling that the baking times were very far from optimal.

After much experimenting, new parameters of 10 minutes at 65° C followed by 10 minutes at 95°C for the prebake, 950nm exposure, and 2 minutes at 65° C created decent results. The SU-8 pattern would dissolve and fully develop in the solvent solution. While these parameters are probably still not optimal, they were sufficient to create the microfluidic devices, as further optimization of the parameters would take too much time and effort for little gain.

A silicone membrane was then bonded on the micropump device, allowing to a pumping movement or actuation from the compressed air. A full device can be seen in Figure 7-3 and the sizes can be configured to pump different amounts of liquids per actuation. Each pump is capable of pumping different amounts of liquid depending on the diameter and depth of the pumping circle. Because SU-8 is capable of creating channel depths of a few micrometers up to a few hundred micrometers, each pump actuation has the ability to pump from the order of nanoliters to milliliters. The current setup that is used has pump dimensions of 6mm diameter and ~175 μm. After calculations, this works out to ~5 μL per pump. The pumping system was fully controlled through a LabVIEW algorithm, and allows for pump cycles of under 1ms, although at such high speeds the device is limited by the resonant frequency of the membrane. In testing, the maximum rate of pumping cycles was found to be 10 ms with the current silicone membrane of ~60 μm in thickness. This device has great potential to be used as drug delivery systems, micromixers, microdispensers, heat exchangers, microreactors, flow controllers, inkjet print heads, cell analysis, etc.

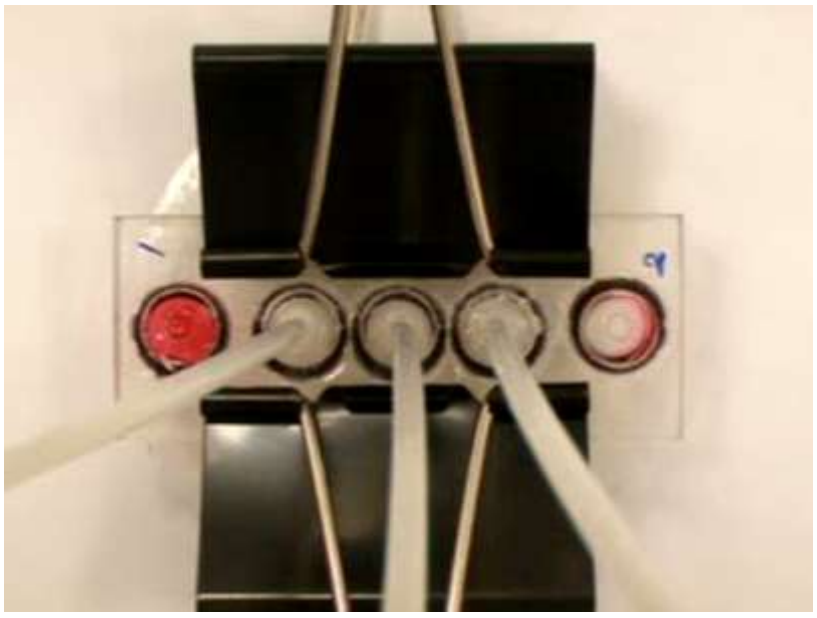

Figure 7-3: Full setup of micropump device. Each valve and pump is attached to a compressed air tube. The pieces for this initial study were simply clamped together.

7.2 Portable Microcantilever Sensors

Microfabricated biosensors have enormous potential to deliver highly sensitive, small size, highly portable, and reliable sensor devices for a wide range of biomedical

applications. However, commercial devices of this type are severely hindered by its high cost, multistep, and silicon based manufacturing processes. In addition, it is difficult and costly to functionalize the tiny sensor arrays after the device is manufactured; therefore, most of the current technologies are limited to detect one substance per sensor chip. A portable sensor array was developed (Figure 7-4), using a polymer substrate instead of silicon, which provides benefits such as lower costs, higher sensitivity, ease of use, and multiplex detection. Studies were performed for haptics, stem cell growth, and also the detection of cryptosporidium parvum (pathogen).

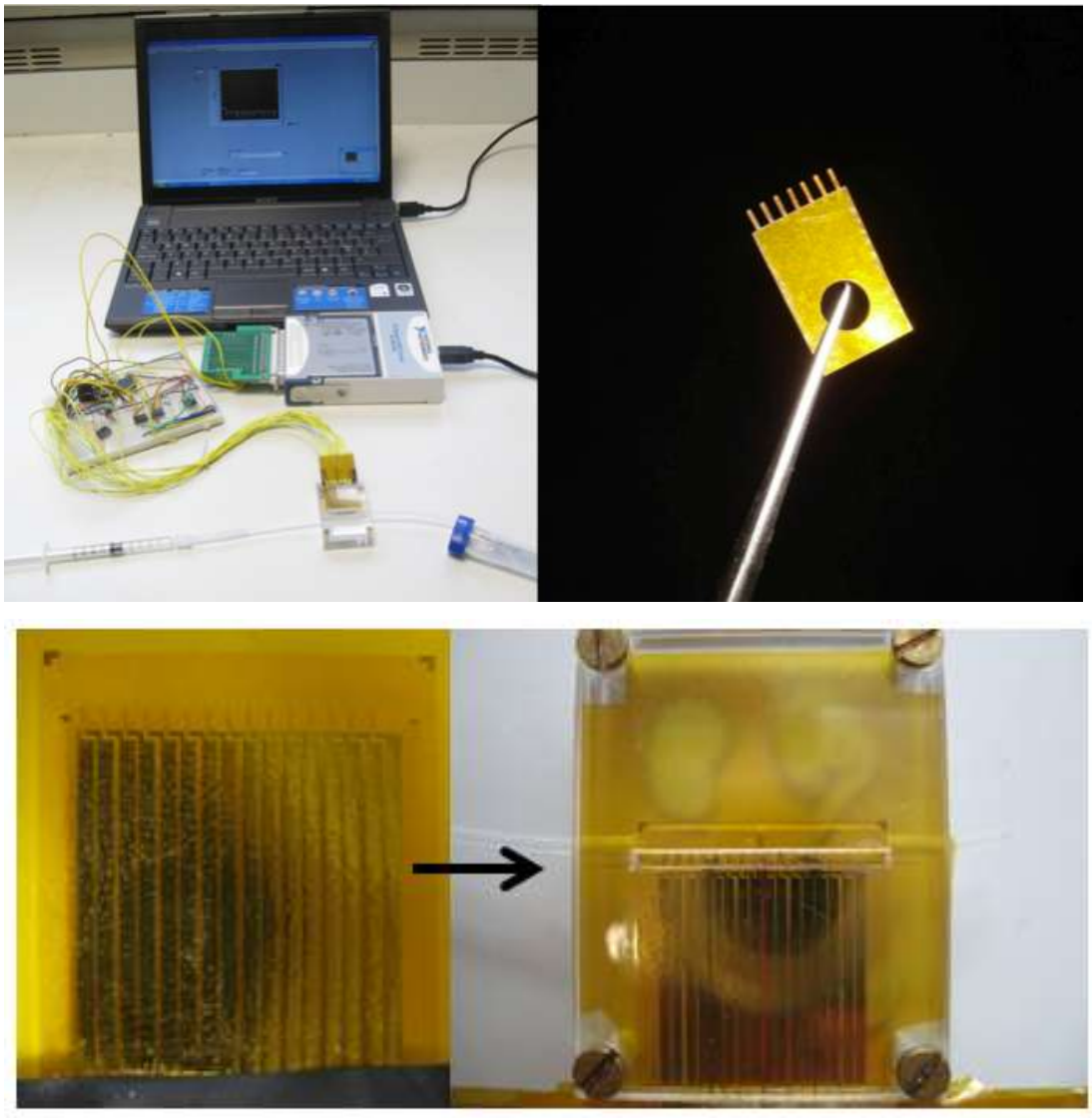

Figure 7-4: Portable cantilever system only requires a laptop, data acquisition, and a circuit board.

The sensor chips themselves are explained in detail in section 3.3. In order to enable specificity and to increase the overall effectiveness and reliability of the sensors, there

needs to be as many sensors in an array as possible. This creates many unforeseen problems that arise once arrays get into hundreds or even thousands of sensors that operate concurrently. Wheatstone bridges are fine if used for arrays of smaller number of sensors, but once the numbers start to grow, many problems arise.

As a substitute for a Wheatstone bridge, an Anderson Loop is instead used to allow for simultaneous readouts from multiple strain gauges. The Anderson loop was developed over 10 years ago by NASA as a substitute for Wheatstone bridges (Anderson, 1998). One of the main elements that make the Anderson unique is its use of an active dual-differential subtractor. The subtractor basically takes two input potentials, and amplifies them by a gain, which taking into account any common potential differences. Using an active subtractor instantly removes the problem of lead wire or connector impedances (Anderson 1997). A schematic of the Anderson loop can be seen in Figure 7-5.

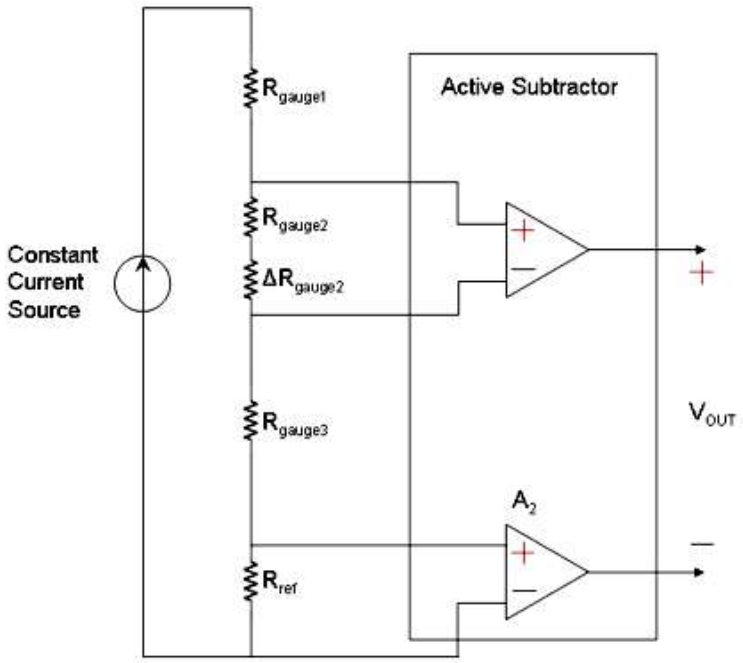

Figure 7-5: Schematic of Anderson Loop readout scheme

From the schematic, it is seen that there are numerous instrumentation amplifiers that are used to amplify the voltage signal due to the change of strain gauge sensors. Because a separate amplifier is used for each sensor element, this removes the major problem of Wheatstone bridges, that is, it is costly and difficult to maintain identical resistances for each sensor element. This design eliminates the need for identical

resistors as each sensor can utilize any desired resistance. This allows for massive arrays of sensor elements, without the need for countless circuits for the readout of signals.

The biggest barrier overall currently is still due to the readout scheme. As discussed earlier, Wheatstone bridges have trouble in this application due to the varying resistances of the strain gauges, causing unbalanced bridges. Because the Anderson loop is patented, there is a lack of literature and detailed information on the exact construction of the circuit. It was determined that the active subtractor section can be built using two instrumentation amplifiers and one high gain differential amplifier. An instrumentation amplifier is a type of differential amplifier, but they include input buffers that remove the effects of input impedance. They also offer low DC offsets, drift, and noise while offering high gain, common-mode rejection ratios, and input impedances. The strain gauges are fed by a custom current source using a LM334 IC to provide either 10, 100, or 1000 μA. Currents are kept low to reduce the heating and thermal drift effects that are intrinsically built into strain gauges. The subtractor circuit shown in Figure 7-6 takes the voltage drop across the variable strain gauge sensor into one instrumentation amplifier, the voltage drop of the reference sensor into the second instrumentation amplifier, and then subtracts the reference signal from the variable sensor signal, producing an output of only the voltage differences between the two.

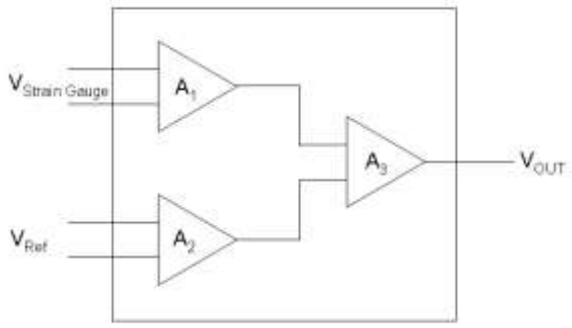

Figure 7-6: Anderson loop active dual subtractor circuit.

Because the difference is very small, a very high gain differential amplifier is required to output a measurable signal in the computer through LabVIEW. From purely theoretical calculations, the gauges should be able to have an output swing of ±5V which is more sensitive than a Wheatstone bridge while using a considerably less amount of power.

The sensitivity of an Anderson loop is double that of a Wheatstone bridge. In the case of an array utilizing 4 sensor elements, the increased sensitivity allows for extremely low power consumption, as it only requires only one-fourth of the supply current required in a Wheatstone bridge for an output amplitude equivalent to the bridge setup. Costs are reduced as well, due to the cost of Anderson subtractors being under $10. In addition to fixing the problems from the Wheatstone bridge, an Anderson loop allows for fewer wiring connections and built in temperature compensation and calibrations for sensitive environments.

In theory, the number of gauges that could be read in real-time is infinite. A multiplexer was used to switch between the gauges, reducing the number of amplifiers needed. This allows for the use of only two amplifiers in total, as the multiplexer output wires directly to the first amplifier, while a control gauge wires to the second. Simultaneous readout was achieved by switching the multiplexer, instead of the 1:1 ratio of strain gauges to amplifiers used by the original Anderson loop, lowering costs and complexity of the circuit. Each end of every individual strain gauge is connected to a multiplexer, whereby the required input to the multiplexer could be controlled. Therefore, the resistance from the strain gauge is measured one by one as the multiplexer switches between the inputs. One strain gauge at the end of the array was then used as the "control," whereby each active strain gauge would subtract the control gauge to measure the difference between them.

As the DAQ cards could not read resistance directly, a constant current source was set up to provide a constant current through the system in order for voltage to be read. By using a standard LM334 3-terminal adjustable current source that provides excellent current regulation and wide voltage range, the current could be controlled through a change in resistors. Finally, the last problem the circuit suffered from was increased noise, possibly due to the multiplexers or the floating electrical interference from the circuitry. Therefore, a simple low-pass filter was placed as the output of the final amplifier, with a resistor connected to V_{in}, a capacitor connected to ground, and Vout is the point in between the resistor and capacitor. Any choice of many combinations of resistors and capacitors could have been used, but a combination was chosen to be as close to 0Hz as possible for the low pass, as the only signal that the output should be is

DC, which has no frequency. Noise was significantly reduced, particularly useful because the change in signal from the system was quite small to begin with.

7.3 Calibration as a Tactile Haptics Sensor

The circuit was once again fully controlled and read through LabVIEW 8.5. For calibration, one of the most complex interactions between humans and the external world is through touch and feel. Even though it is one of the five basic human senses, it is relatively under-researched compared to other senses such as audio and visual technologies. External inputs are captured as the skin acts as a large sensor to the surrounding environment. Therefore, creating artificial skins with the same level of sensitivity and interaction of humans are extremely challenging, and has been a topic of focus for over a decade. Machines, robots, buildings, and humans would all benefit from advancement in tactile sensors that successfully mimic that of a human's skin (Vladimir et al., 2004). The only other mechanical device developed to date for force feedback is the Haptic device. However, these devices do not convey nor receive multipoint kinesthetic information.

Human skin does not operate like an on-off switch. Instead, it operates like a very high-resolution flexible and stretchable sensor. Therefore, smart skins need to emulate this type of interaction and operation by using large arrays of sensors. Artificial smart skins are not limited to any one specific industry or field, and have endless possibilities such as sensors for virtual reality, gaming, physiotherapy, robotics, surgeries, catheters, etc.

MEMS tactile sensors offer many advantages over conventional sensors such as small size, high sensitivity, low power consumption, and the potential for massive multiplexing. Piezoresistive materials for the detection of strains has been studied extensively, (Rajanna et al., 1987, 1988, Sanpath et al., 1986, Tamborin et al., 1997) and is typically preferred over capacitive (Shimojo, 1997), piezoelectric (Benes et al., 1995), and optical methods (Begej, 1988). While most MEMS tactile sensors are microfabricated from silicon, its cost is still quite high and therefore is unsuitable for most low-cost commercial applications (Wisitoraat et al., 2007). Additionally, silicon is known to be brittle and could break under heavy pressures (Engel et al., 2006). Only recently has the commercial sector seen mass-produced products such as the Nintendo Wii, which utilizes such sensors devices incorporating force interactions.

Many considerations for the types of sensors for artificial smart skins had to be considered. The sensors must be able to react to natural body movements, as there could be highly uneven surfaces or irregular stresses applied to them. Secondly, because of the sheer amount of skin that needs to be replicated, the sensors need to be cost effective in addition to being able to be massively multiplexed to function and be analyzed simultaneously. Lastly, the sensors will be placed in close proximity to actual skin, therefore the materials and any other reactions must be compatible and non-harmful to ensure long-term use and safety.

While there have been many successfully demonstrated tactile sensors (Park et al., 2009, Mei et al., 2000, Rossi et al., 2005), they all employ microfabrication techniques that are time consuming and costly. In this section, we have developed a low-cost artificial smart skin glove using integrated microsensor arrays for the detection of hand movements. As the finger is bent up and down, the sensors at the knuckle joints would read the amount of deflection in the area and therefore the voltage output would adjust accordingly. The advantage of a strain gauge array is that as they are mounted across the entire joint, each gauge would output different signal amplitudes due to the differences in bending across the joint. This means that the sensor on the very top of the joint experiences the largest change while the ones towards the edges experience a small change. As these eight sensors are all simultaneously monitored in real-time in Figure 7-7, a 3-D graph can be made which shows the actual bending of the finger, shown in Figure 7-8**.** The eight plots each represent a different sensor, due to the bending of the finger. The first 3-D plot represents the sensor readouts when the finger is straight and unbent. The Z-axis is the voltage readout, Y-axis is time, and the X-axis indicates the 8 different sensors, as they are aligned on the glove. After bending the finger, the 3-D plot changes to reflect the amplitude of bending sensed by each of the gauges. The middle gauge incurs the largest amount of deflection while the gauges at the end incur the least. Sensors at each end do not produce a linear voltage change because they are mounted on the side of the finger joint, making them almost perpendicular to the middle sensor.

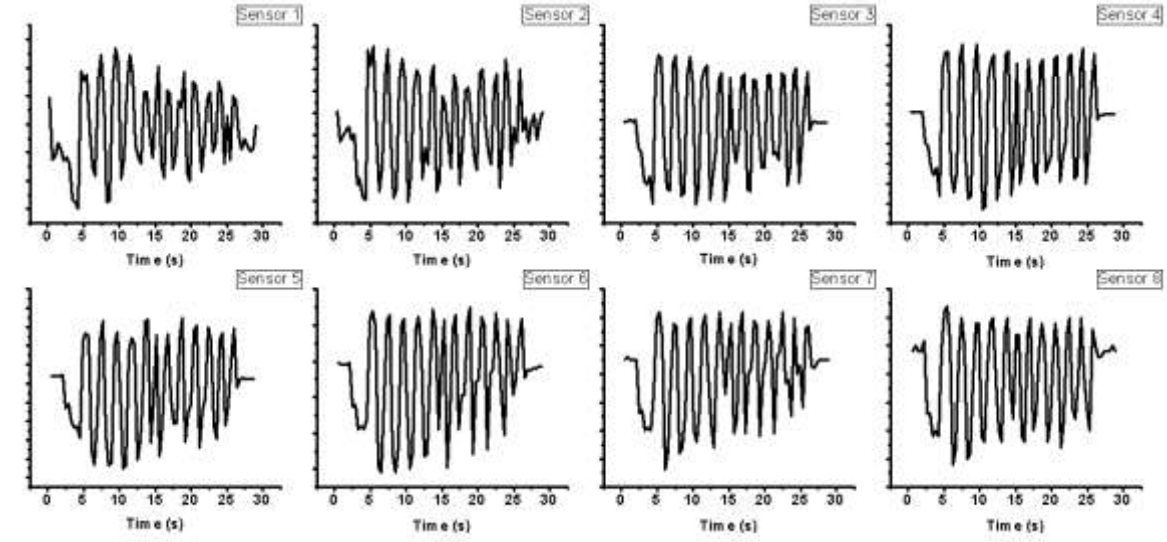

Figure 7-7: Simultaneous readout data of 8 sensors in real-time

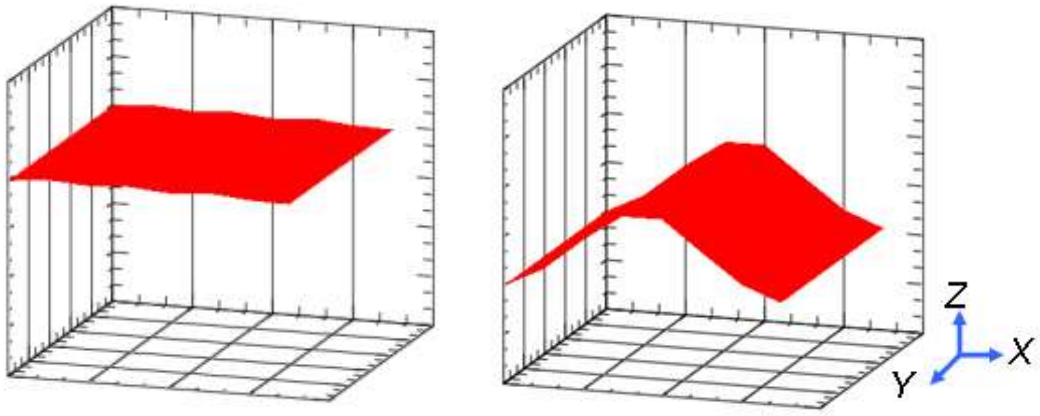

Figure 7-8: Data from sensors converted into 3D plot

Future applications of this kind are endless. The health care industry could benefit greatly, using these sensors for minimally invasive surgeries or catheter probes, which could limit the effects of human error. Therefore, the development of low-cost and sensitive MEMS sensor arrays will greatly benefit all aspects of future research and development.

7.4 Stem Cell Growth Monitoring

Measurement of the proliferation of human embryonic stem cells using microcantilever sensors was attempted. The aim of the study was to test the possibility and potential of culturing hESc on microcantilevers and to measure the growth of stem cells in the culture media. A collaboration with Roslin Cellab (Edinburgh, UK) showed that the

stem cell line RCM-1 will attach and grow on microcantilevers coated in commercially available matrix, CellSTART, in StemPRO media from Invitrogen. The microcantilever chamber was sterilized using ethanol washes, and the culture maintained sterility throughout the experiment.

7.4.1 Stem Cell Preparation

Because stem cells are very vulnerable and susceptible to external interferences such as bacteria and mishandling, a thorough procedure was developed to provide the best environment for cell growth. Experiments were performed at Roslin Cellab. The first stage was the full sterilization of the microcantilever chambers. Each chamber was fully separated and submerged in 100% ethanol and allowed to dry in a laminar flow hood, followed by 2 more repeats. Before use, the chamber was once again wiped with ethanol and allowed to air dry. Next, the microcantilevers had to be coated with cell matrix. CellStart matrix was prepared as per manufacturer's instructions (1:50 dilution), and 3mL was applied to the chamber. The chamber was placed in a petri dish and was incubated at 37^{o} C for 1 hr. Once done, the chamber was removed, and matrix solution was aspirated and replaced with media and/or cell suspension. The hESc culture was subjected to a ROCK inhibitor at a concentration of 10 µM followed by 1 hr. incubation. Single cell suspension was washed and harvested using 1mL Accutase for 2-3 min. at 37^{o} C, followed by using a pipette to gently triturate into single cells. The cell suspension was collected in a tube containing 4mL of media. This was followed by a centrifuge to pellet the cells, at 1300rpm for 3 minutes. The supernatant was aspirated and the cell pellet was re-suspended in 500 µL media. Using a pipette, 1 µL of cell suspension was carefully placed on each cantilever of interest. The chamber was placed onto a petri dish and into the incubator for 1 hr. to allow it to fully settle. Finally, the chamber was filled with 3mL of media and placed back into the incubator to monitor for growth changes. (Figure 7-9, full set of images in APPENDIX 4)

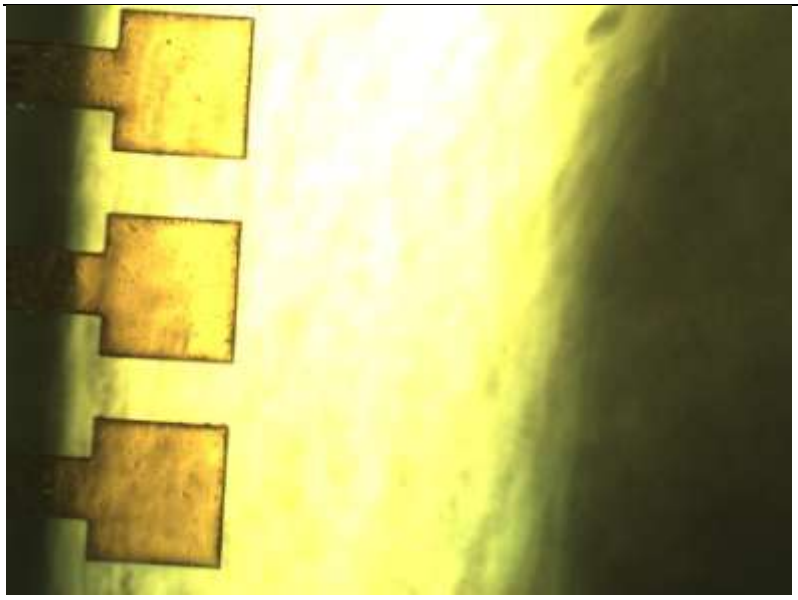

Figure 7-9: Control cantilever (center cantilever in image) at 2.5x magnification. No cells on the surface and image taken 24 hours after initial setup of experiment.

7.4.1.1 Results and Discussion

From Figure 7-10, it can be seen that there is a considerable downwards deflection of the cantilever beams. The spikes at each ~24 hr. interval indicates the chamber being removed from the incubator for a media change. After the media change, it can be seen that the cantilever beams require a period of time for stabilization, before the cells continue to proliferate and cause the cantilever beams to move in a downwards direction. All these signals are a differential signal, in that the original signal automatically subtracts a control signal of a cantilever beam with no cells on the surface. This reduces the noise and any external interference that may arise in the experiments. What is unknown is the reasoning behind the cantilever deflection, as these cantilever beams are not coated with a gold layer, and therefore the reasoning behind large cantilever deflections due to cell surface stress shown in the previous chapters cannot be used. Further experiments can be performed to demonstrate whether or not the cantilever sensors are indeed bending downwards from cell growth, such as monitoring a few control cantilevers, or by coating the cantilevers with gold to determine if the deflections are indeed larger due to surface stress interactions. Conclusions are that microcantilever sensors can be successfully coated with commercial cell matrix for culture and that hESc adapted to CellSTART matrix will grow on the microcantilevers, and display a normal hESc morphology from outgrowths subjected to single cell suspension. While these tests were not a complete success, it

demonstrates the ability for stem cells to proliferate on a polyimide based cantilever surface. In addition, with the initial study, there may be an indication that the electronic portable cantilever array system is able to successfully detect and monitor stem cell growth in real-time, allowing for new areas of study in the future for areas such as disease and drug discovery and testing.

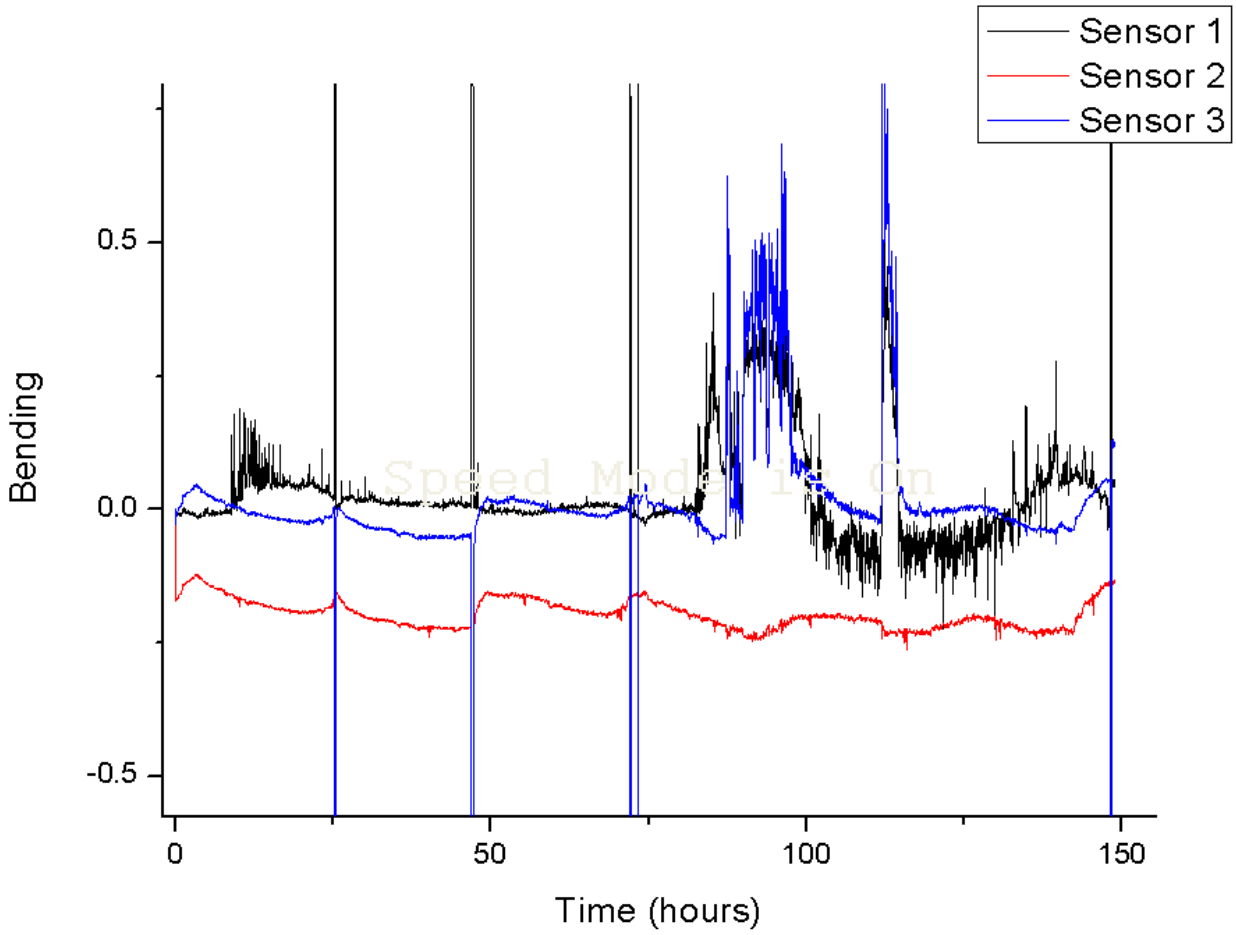

Figure 7-10: **The microcantilever sensor bending curve monitoring the stem cell growth. There are three active sensors, all signals are relative signal by subtracting a reference signal. The curve has overall downwards trend, which shows the cantilever bending down due to cell growth. The three sensors were read-out simultaneously in real-time, and differences between them are due to the variations between the cantilevers.**

7.5 Cryptosporidium Pathogen Detection

Cryptosporidium parvum protozoa is a global issue with regards to the contamination of water supplies. The pathogen has the ability to cause severe diarrhea and can sometimes

be fatal for infants and young children along with immune compromised adults. It is estimated that 250-500 million cases of cryptosporidium infections occur in developing countries every year (Snelling *et al*., 2007). Because the pathogen is immune to many conventional water treatment methods, outbreaks are still possible even in the developed world, causing health and economic problems, such as through the loss of productivity (King *et al*., 2007). Current methods of cryptosporidium detection relies on immune-magnetic separation, which requires labeling and staining with fluorescent dyes along with manual examination and identification. This process typically requires 3 days, and does not include testing for the type of species or viability. This is crucial as this long period of time allows for a contamination of water supplies that would reach the mass population, causing an outbreak. In addition, current methods are highly expensive and requires specialized scientists and technicians. Therefore, an easier method to detect cryptosporidium in addition to cell viability are crucial.

This study was performed in collaboration with Dr. Helen Bridle and Ann Shinshee Walker from the University of Edinburgh, UK. Cells were provided by them and all experiments were performed at Heriot-Watt University.

7.5.1 Procedure

Portable microcantilever sensors were utilized in order to provide a platform that allows for rapid and inexpensive testing, in addition to the ability to perform experiments at the water supply itself. Physioabsorption (Poltras et al., 2009) of an antibody anti-C.parvum of 10 µg/ml solution in PBS was used to soak the cantilevers with 40nm of gold on the surface. The flow rate of the solution was 50 µl/min, after which it was allowed to rest for 60 min., followed by a rinse cycle with PBS for 20 min. to remove any unbound antibody. The cantilevers were then exposed to a suspension of C. parvum for 20 min. with a flow of 50 µl/min, followed by 60 min. of resting. A rinse with PBS for 20 min. ensured any unbound C. parvum was removed. During this period, the cantilever would deflect if any C. parvum bound to the surface. For this experiment, dead C. parvum was used as it is a containment level 2 category pathogen, and was treated for 30 min. at 45 ° C before use.

In order to reduce any non-specific binding, the cantilevers were exposed with 10mg/ml solution of BSA in PBS for 20 min. at a flow rate of 50 µL/min, followed by a 60 min.

rest period and a PBS rinse cycle to remove any unbound BSA. After the readings from the cantilevers, SEM images were taken to observe the surface and count oocysts. This included a rinse with PBS after the experiment, and to expose the cantilevers to osmium tetraoxide or MeOH for 1 hr. to fix the cells to the surface. This was followed by a thin coating of Au to create a conductive surface for SEM imaging (Guntupalli et al., 2007).

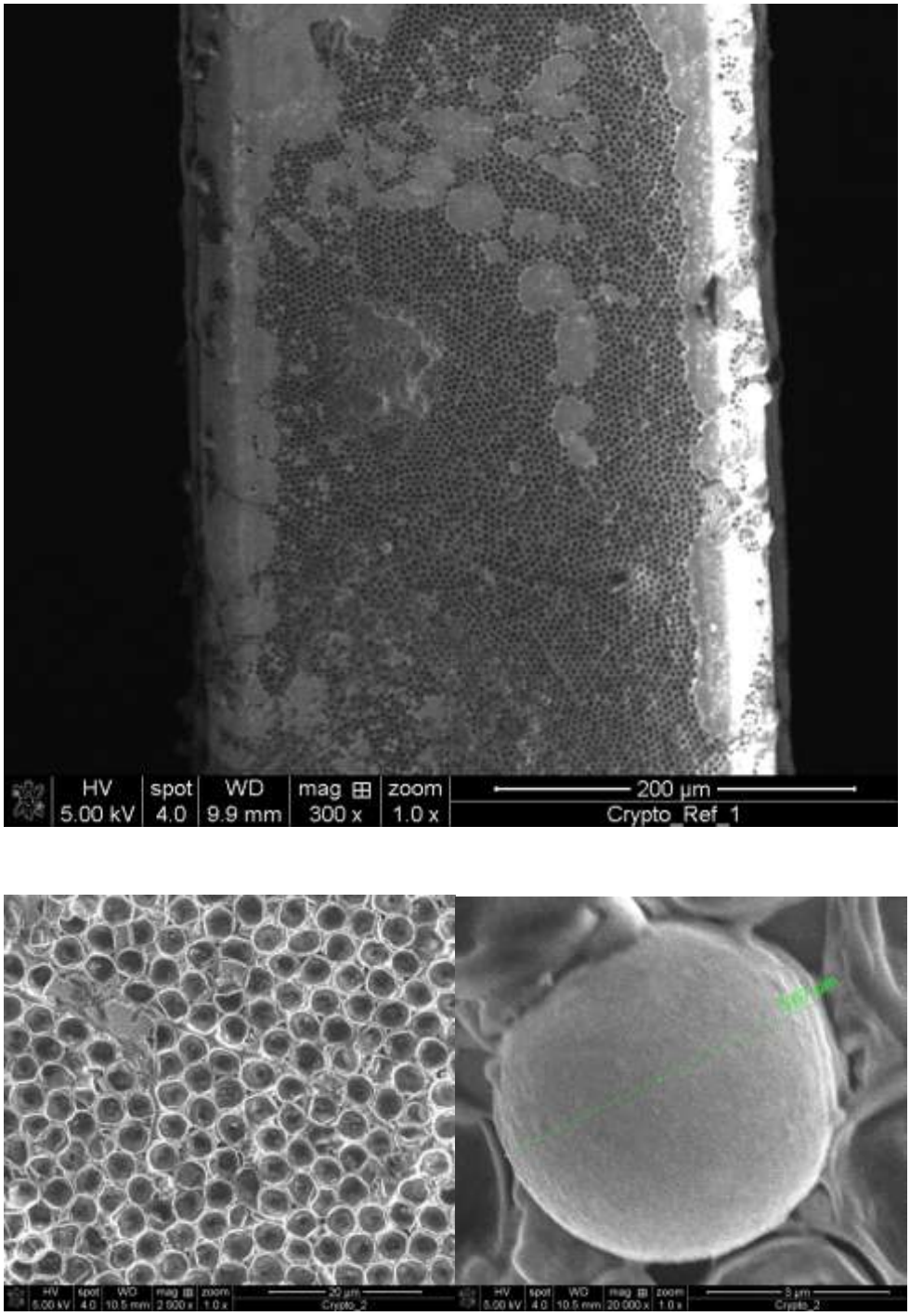

Figure 7-11: SEM images of cryptosporidium cells after experiment. It can be seen that the majority of cells seem to have "deflated."

From Figure 7-11, it show the cells bound to the surface of the cantilever at a higher zoom level. The cells have collapsed, i.e. they all seem to have a depression in the center in a deflated pattern. This may be due to cell dehydration from not performing the SEM immediately after the experiment was completed.

7.5.2 Results and Discussion

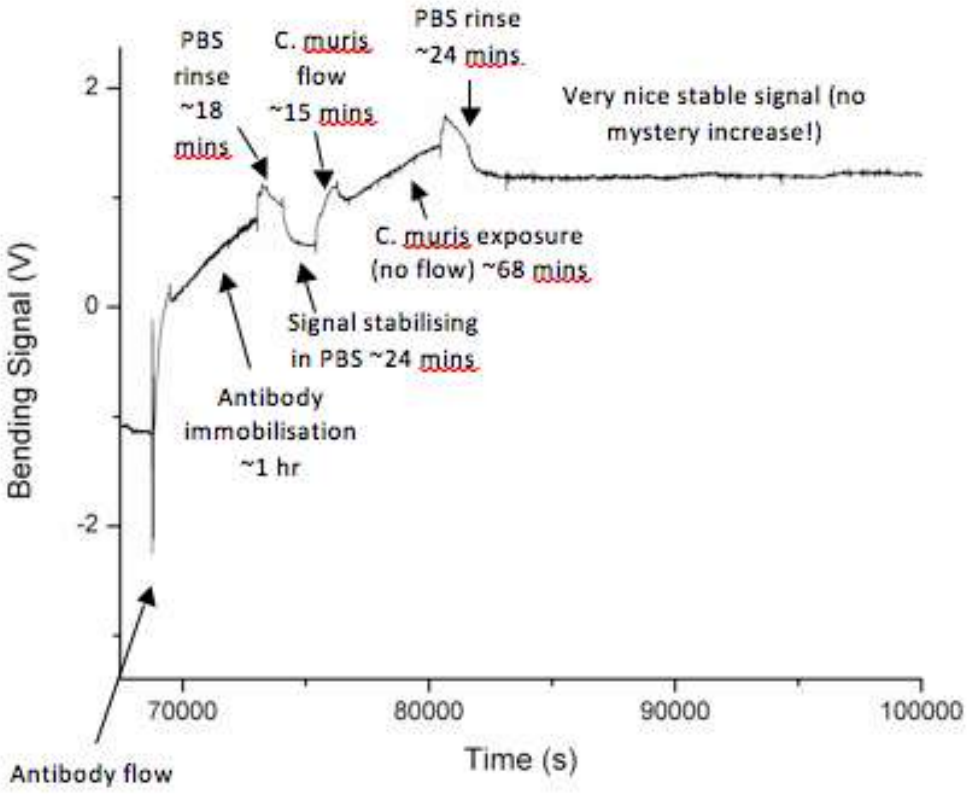

Figure 7-12: Signal of cryptosporidium detection. $3.2x10^5$ C. muris and 10µg/mL cryp-a-glo antibody was used. After exposure to the antibody, there was an upwards bending signal, and further bending after the injection of C.muris.

In the first experiment, no BSA was used, with a $3.2x10^5$ C. muris and 10µg/mL cryp-a-glo antibody. Following flow of antibody, a 0.76V differential signal change was observed (after rinsing, 0.48V increase). Upon addition of C. muris, a 0.52V increase in signal was observed (0.28V after rinsing). It can also be seen that after rinsing the C. muris solution that had been added, the signal dropped to a slightly lower voltage. This suggests that there may have been cells that were sitting on the surface of the cantilever,

but that was not actually bound to the surface. Therefore, following the flow of PBS, the signal dropped as some unbound cells was rinsed away.

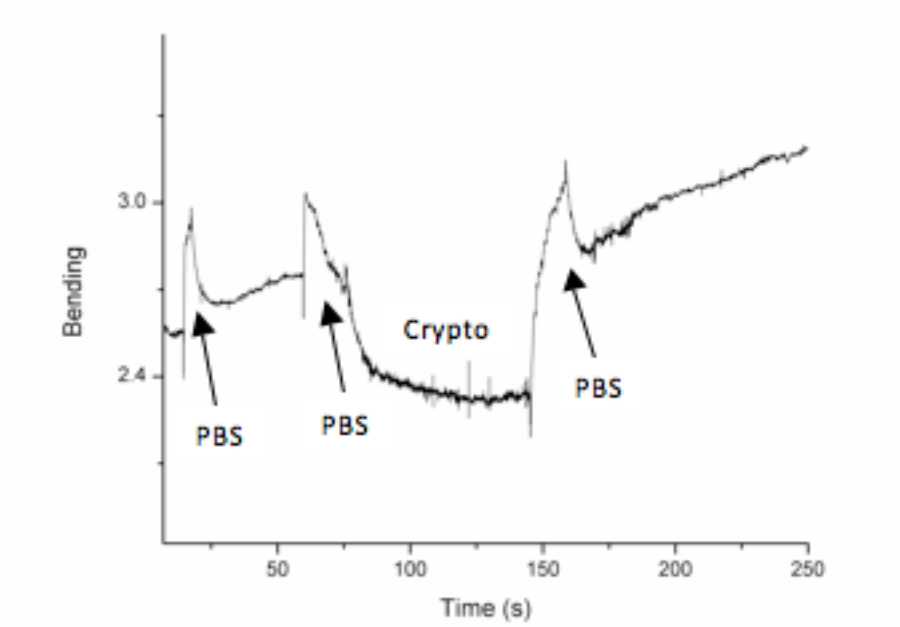

Figure 7-13: Signal of cryptosporidium detection where the cantilever surface was functionalized before placing it in the test chamber. **$3.2x10^5$ C. muris was used, but the stabilization period caused the experiment to fail.**

In the subsequent experiment, the cantilever surface was functionalized with antibody before allowing the cantilever to equilibrate in the chamber. Unfortunately, the stabilization period in deionized water was for 24 hr., which may have upset the antibodies that were present. Therefore, this in addition to the use of BSA, has resulted in the lack of crypto cell binding signals. After recording, there is again an unexplained ~0.4V increase in the signal.

There may be a couple of possibilities for the lack of a cantilever deflection signal. Either the lack of signal increase could be because BSA is blocking the surface, or blocking the antibody, although this should not be the case according to Poitras *et al*., (2009). Alternatively, it could be because the antibody was denatured or damaged in the equilibrium stage with deionized water, and therefore there was nothing to bind the cells.

In this brief study, a highly portable, low cost, and easy to use cantilever biosensor system has been demonstrated for the detection of cryptosporidium cells. Although the current sensitivity of the sensors is unknown, it demonstrates promise through the ability to detect the waterborne pathogen, and if further studies are conducted, may be highly successful in detecting other pathogens and diseases as well.

7.6 Conclusion

- A microfluidic pump design was successfully validated for microfluidic manipulation. This can be used in future development for cell studies, or many other disease diagnosis applications.

- Microcantilever arrays were shown to be able to sustain stem cell growth on the surface without contamination, followed by real-time monitoring of stem cell growth. Results indicated a positive correlation between the signal and cell proliferation. This could lead to advanced developments in the stem cell research field.

7.7 References

Wisitoraat, A., Patthansasetakul, V., Lomas, T., Tuantranont, A., Low cost thin film based piezoresistive MEMS tactile sensor. *Sensors and Actuators A* **139**, 17-22 (2007).

Anderson, K.F., *IEEE Instrumentation and Measurements Magazine* **1**, (1998).

Anderson, K.F., *Measurement Science Conference*, (1997).

Balagadde, F.K., You, L., Hansen, C.L., Arnold, F.H., Quake, S.R., Long-term monitoring of bacteria undergoing programmed population control in a microchemostat. *Science* **309(137)**, 65 (2005).

Begej, S., Planar and finger-shaped optical tactile sensors for robotic applications. *IEEE J. Robot Automat*. **4**, 472-494 (1988).

Benes, E., Groschl, M., Burger, W., Schmid, M., Sensors based on piezoelectric resonators. *Sensors and Actuators A* **48**, 1-21 (1995).

Engel, J., Chen, J., Liu, C., Polymer micromachined multimodal tactile sensors. *Appl. Phys. Lett*. **89**, 50-61 (2006).

Guntupalli, R., Hu, J., Lakshmana, R.S., Huang, T.S., Barbaree, J.M., Chin, B.A., A magnetoelastic resonance biosensor immobilized with polyclonal antibody for the detection of Salmonella typhimurium. *Biosens Bioelectron* **22**, 1474 (2007).

Hong, J.W., Quake, S.R., Integrated nanoliter systems. *Nature Biotechnology*, **10**, 1179 (2003).

King, B. J., Monis, P. T., Critical processes affecting Cryptosporidium oocyst survival in the environment. *Parasitology* **134**, 309-323 (2007).

Lee, C.C., Snyder, T.M., Quake, S.R., A microfluidic oligonucleotide synthesizer. *Nucleic Acids Research* **38**, 2514 (2010).

Lee, C.C., Sui, G., Elizarov, A., Shu, C.J., Shin, Y.S., Dooley, A.N., Huand, J., Daridon, A., Wyatt, P., Stout, D., Kolb, H.C., Witte, O.N., Satyamurthy, N., Heath, J.R., Phelps, M.E., Quake, S.R., Tseng, H.R., Multistep synthesis of a radiolabeled imaging probe using integrated microfluidics. *Science* **310**, 1793 (2005).

Mei, T., Lee, W.J., Ge, Y., Chen, Y., Ni, L., Chan, M.H., An integrated MEMS three-dimensional tactile sensor with large force range. *Sensors and Actuators* **80**, 155-162 (2000).

Park, C.S., Park, J., Lee, D.W., A piezoresistive tactile sensor based on carbon fibers and polymer substrates. *Microelectronic Engineering* **86**, 1250-1253 (2009).

Poitras, C., Fatisson, J., Tufenkji, N., Real-time microgravimetric quantification of Cryptosporidium parvum in the presence of potential interferents. *Water Research* **43**, 2631 (2009).

Rajanna, K., Mohan, S., Studies on meandering path thin-film strain gauge. *Sensors and Actuators A* **15**, 297-303 (1988).

Rjanna, K., Mohan, S., Strain-sensitive property of vacuum evaporated manganese films. *J. Mater. Sci. Lett*. **6**, 1027-1029 (1987).

Rossi, D.R., Carpi, F., Scilingo, E.P., Polymer based interfaces as bioinspired smart skins. *Adv. In Colloid and Int. Sci*. **116**, 165-178, (2005).

Sanpath, S., Ramaniah, V., Behaviour of Bi-Sb alloy thin films as strain gauges. *Thin Solid Films* **137**, 199-205 (1986).

Shimojo, M., Mechanical filtering effect of elastic cover for tactile sensor. *IEEE Trans. Robot. Automat*. **13**, 128-132 (1997).

Snelling, W. J., Xiao, L., Ortega, G., Lowery, C.J., Moore, J.E., Rao, J.R., Smyth, S., Millar, B.C., Rooney, P.J., Matsuda, M., Kenny, F., Xu, J., Dooley, J.S.G., Cryptosporidiosis in developing countries. *J. Infect. Dev. Ctries.* **1**, 242-56 (2007).

Tamborin, M., Piccinini, S., Prudenziati, M., Morten, B., Piezoresistive properties of RuO based thick-film resistors: the effect of RuO grain size. *Sensors and Actuators A* **58**, 159-164 (1997).

Wu, A.R., Hiatt, J.B., Lu, R., Attema, J.L., Lobo, N.A., Weissman, I.L., Clarke, M.F., Quake, S.R., Automated microfluidic chromatin immunoprecipitation from 2,000 cells. *Lab On Chip* **60(9)**, 1365 (2009).

Chapter 8 Conclusions and Recommendations for Future Work

8.1 Research Assessment

The initial object of this research was to develop microcantilever sensors for cell studies. However, as the research progressed, further applications were included as well. With this aim, the main objectives were to use microcantilever biosensors for probing disease biomarkers, DNA, cell drug interactions, and cell nanoparticle interactions. One of the main goals was to investigate whether cell proliferation can be monitored in real-time on the surface of microcantilever sensors. Furthermore, another goal was to develop large scale cantilever arrays for assay experiments, including portable sensor arrays and multiplexed readout schemes. Experiments were performed to implement and carry out validations of the developed biosensor systems.

8.2 Conclusions

In this research, the objective to develop microcantilever sensors for a wide variety of applications has been successfully achieved. The main results can be summarized as follows:

- Cells (yeast, liver, and stem) has been shown to successfully proliferate on the surface of the microcantilever sensors. In addition, cell proliferation has been demonstrated to be monitored in real-time.

- Cell kinetics that would have otherwise been unnoticed through conventional cell culturing techniques can be differentiated by microcantilever sensors within a few hours. Furthermore, the sensors are able to differentiate between different types of cell medias, and also the different reactions that cells have towards different toxins and/or drugs.

- When the research on cell proliferation started, it was assumed that bending in static mode of microcantilever sensors from cell growth was due to mass loading, but it has been shown that it is due to a combination of yet unknown cell to cantilever surface stresses in addition to the added sensitivity of the polymer based cantilevers.

- Microcantilever arrays have been demonstrated through various different methods. This includes the fabrication and readout methods. Successful readout methods for microcantilever sensor arrays include optical, piezoresistive, and interferometry.

- The same microcantilever arrays have been integrated with microfluidics, to create a higher throughput liquid natural liquid environment for cell or general biological experiments.

- Other applications for sensing using microcantilevers have been confirmed. These include haptics tactile sensors, stem cell growth monitoring, and pathogen detection.

8.3 Recommendations for Future Work

With regard to future work, the following is recommended:

- Further studies using yeast cells as a base for drug-cell interactions. This is because yeast cells are extremely robust and similar to animal cells. The added sensitivity from the polymer based microcantilever sensors offers a viable platform for further development.

- Based on the results from the C3A liver trials, there are many other possible paths for further development. This is not only limited to drug-cell interactions, but also the study of many other nanoparticles, toxins, etc. This would allow for an highly sensitive approach to cell assays that may be more rapid and sensitive than conventional methods.

- The cantilever readout methods can all be further developed. The scanning array can easily be implemented into much larger arrays with either less spacing between cantilevers, or a larger PSD area size. Other areas to consider would be to enhance the sensitivity of the portable piezoresistive cantilever sensors, and to enhance the speed and reliability of interferometry based methods.

- There are many other applications using any type of the microcantilever sensors that were developed. These could include the study of cancers, infectious diseases, effects of drugs/toxins/nanoparticles, and the detection of other substances such as pathogens, and many other types of disease diagnosis.